PEAK TO AVERAGE POWER RATIO ANALYSIS AND REDUCTION OF COGNITIVE RADIO SIGNALS

Sajjad Hussain

N° d'ordre : 3977

Thèse

présentée devant
l'UNIVERSITÉ DE RENNES I

pour obtenir le grade de
Docteur de l'Université de Rennes I
Mention : *Traitement du Signal et Télécommunications*

par
Sajjad HUSSAIN

Équipe d'accueil : Institut d'Electronique et de Télécommunications de Rennes
École doctorale : Matisse
Composante universitaire : S.P.M.

Peak to Average Power Ratio Analysis and Reduction of Cognitive Radio Signals

Soutenue le 21 October 2009 devant la commission d'examen

Composition du jury

Rapporteurs
M. Michel TERRE — Professeur, CNAM, Paris
M. Mischa DOHLER — Chercheur, CTTC, Barcelone

Examinateurs
M. Gérard FAUCON — Professeur, Université de Rennes 1, Rennes
M. Jacques PALICOT — Professeur, IETR/Supélec, Rennes
M. Yves LOUËT — Maître de Conférences, IETR/Supélec, Rennes

Contents

List of Acronyms and Abbreviations

ADC	**A**nalog to **D**igital **C**onvertor
ADSL	**A**symetric **D**igital **S**ubscriber **L**ine
BER	**B**it **E**rror **R**ate
BPSK	**B**inary **P**hase **S**hift **K**eying
BPF	**B**and **P**ass **F**ilter
BS	**B**ase **S**tation
CCDF	**C**omplementary **C**umulative **D**istribution **F**unction
CDMA	**C**ode **D**ivision **M**ultiple **A**ccess
CF	**C**rest **F**actor
CR	**C**ognitive **R**adio
CVX	Convex Optimization toolbox
DAB	**D**igital **A**udio **B**roadcasting
DAC	**D**igital to **A**nalog **C**onvertor
DMT	**D**iscrete **M**ulti-**T**one
DSA	**D**ynamic **S**pectrum **A**ccess
DVB	**D**igital **V**ideo **B**roadcasting
DFT	**D**iscrete **F**ourier **T**ransform
EDGE	**E**nhanced **D**ata rate for **G**SM **E**volution
EPF	**E**ffective **P**eak **F**actor
FFT	**F**ast **F**ourier **T**ransform
GMSK	**G**aussian **M**inimum **S**hift **K**eying
GSM	**G**lobal **S**ystem for **M**obile communications
HIPERLAN	**HI**ig **PE**rformance **R**adio **L**ocal **A**rea **N**etwork
HPA	**H**igh **P**ower **A**mplifier
IBO	**I**nput **B**ack **O**ff
IDFT	**I**nverse **D**iscrete **F**ourier **T**ransform
IFFT	**I**nverse **F**ast **F**ourier **T**ransform
LO	**L**ocal **O**scillator
LNA	**L**ow **N**oise **A**mplifier
LP	**L**inear **P**rogramming
PTS	**P**artial **T**ransmit **S**equence
QAM	**Q**uadrature **A**mplitude **M**odulation
MC-CDMA	**M**ulti-**C**arrier **C**ode **D**ivision **M**ultiple **A**ccess
OBO	**O**utput **B**ack **O**ff
OFDM	**O**rthogonal **F**requency **D**ivision **M**ultiplexing
PAPR	**P**eak to **A**verage **P**ower **R**atio

PDF	**P**robability **D**ensity **F**unction
PEP	**P**eak **E**nvelop **P**ower
PMEPR	**P**eak to **M**ean **E**nvelope **P**ower **R**atio
PR	**P**ower **R**atio
PRC	**P**eak **R**educing **C**arrier
PSD	**P**ower **S**pectral **D**ensity
QPSK	**Q**uadrature **P**hase **S**hift **K**eying
RC	**R**aised **C**osine
RF	**R**adio **F**requency
SDR	**S**oftware **D**efined **R**adio
SI	**S**ide **I**nformation
SOCP	**S**econd **O**rder **C**one **P**rogramming
SRRC	**S**quare **R**oot **R**aised **C**osine
SSPA	**S**olid **S**tate **P**ower **A**mplifier
SLM	**S**e**L**ected **M**apping
SWR	**S**oft**W**are **R**adio
TI	**T**one **I**njection
TR	**T**one **R**eservation
TWTA	**T**ravelling **W**ave **T**ube **A**mplifier
UMTS	**U**niversal **M**obile **T**elecommunications **S**ystem
WLAN	**W**ireless **L**ocal **A**rea **N**etwork
ZP	**Z**ero **P**adding

Mathematical notations

x	Scalar
x^*	Conjugate of x
$\mathbf{x}$	Time domain vector
$\mathbf{X}$	Frequency domain vector
$\mathbf{x}^T$	Transpose of $\mathbf{x}$
$\tilde{\mathbf{x}}$	Clipped/Modified form of vector $\mathbf{x}$
$E\{\mathbf{x}\}$	Mathematical expectation of random vector $\mathbf{x}$
$\lvert\mathbf{x}\rvert$	Module of the vector $\mathbf{x}$
$\lVert\mathbf{x}\rVert$	Norm of the vector $\mathbf{x}$
$\lVert\mathbf{x}\rVert_2$	Euclidean norm of the vector $\mathbf{x}$
$\lVert\mathbf{x}\rVert_\infty$	Infinite norm of the vector $\mathbf{x}$

Résumé français

Introduction

La multiplication des standards de télécommunications fait apparaître la nécessité de disposer de terminaux multistandard et reconfigurables. Ces nouvelles fonctionnalités trouvent leurs réponses dans le domaine de la radio logicielle. De tels terminaux ne sont pas encore réalisables pour des raisons technologiques liées à la complexité nécessaire à leur réalisation (convertisseurs ultra rapides, processeurs reconfigurables, antennes et amplificateurs très large bande, ...). En se basant alors sur une véritable technologie radio logicielle, la radio intelligente va encore plus loin dans la prospective en dotant le terminal de capteurs qui lui permettront de s'adapter et de réagir vis à vis de son environnement. La radio devient alors décentralisée et flexible se détachant de la notion de standards et transmettant de façon opportuniste une communication dans une bande qui aura été détectée comme libre.

Ce travail de thèse s'inscrit dans le contexte présenté ci-dessus en se focalisant sur les conséquences de l'amplification de puissance d'un signal multistandard. En effet, l'amplification de puissance est un étage fondamental de tout système radio et certaines précautions doivent être prises avant d'amplifier un signal. En effet, les amplificateurs ont des caractéristiques non linéaires et de faibles rendements nécessitant un traitement du signal à amplifier afin de limiter d'une part les distorsions non linéaires et d'autre part la consommation des terminaux. Les signaux caractérisant les systèmes multistandard ayant des caractéristiques proches de celle d'un signal OFDM (connu pour les problèmes liés à l'amplification de puissance), ce travail apporte des réponses sur :

- les niveaux de puissance d'un signal multistandard
- les méthodes à développer pour en minimiser les fluctuations de puissance
- les conséquences de l'accès opportuniste au spectre sur les fluctuations de puissance dans un contexte de radio intelligente

1 Le PAPR des systèmes à porteuses modulées

1.1 Les systèmes à porteuses modulées

1.1.1 Les modulations OFDM

Contrairement aux systèmes de transmission de type série où le spectre de chaque symbole émis occupe toute la bande utile, les systèmes à transmission de type parallèle permettent

de partager la bande entre toutes les données. L'OFDM (Orthogonal Frequency Division Multiplexing) est ainsi un schéma de transmission où chacun des spectres des symboles de données émis occupe une portion de la bande utile, ces spectres ne se perturbant pas mutuellement, respectant la condition d'orthogonalité.

Plus précisément, un flux de N symboles utiles (issus d'un codage binaire à symbole quelconque) est dans un premier temps passé à travers un convertisseur série/parallèle. En supposant que les symboles c_k ont une durée initiale de $\frac{T}{N}$, après conversion série-parallèle, leur durée est T. Chaque symbole c_k vient alors moduler une porteuse f_k ($k = 0, ..., N-1$). L'espace séparant deux porteuses adjacentes est alors égal à $\frac{1}{T}$.

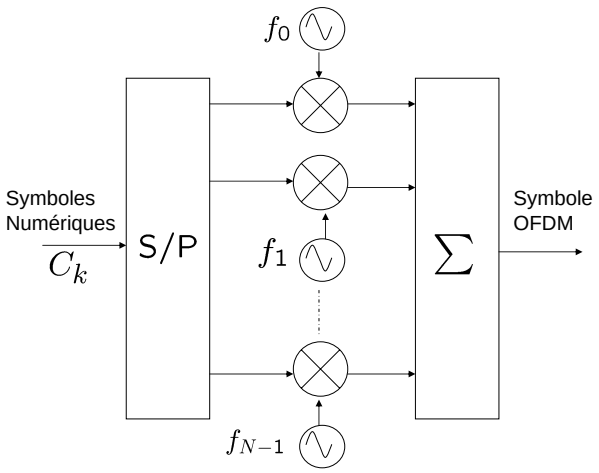

Figure 1: Réalisation analogique d'un modulateur OFDM

L'enveloppe complexe générée $s(t)$ est alors donnée par :

$$s(t) = \sum_{k=0}^{N-1} c_k e^{2j\pi f_k t}, \quad t \in [0, T]. \tag{1}$$

Le signal $s(t)$ est alors de durée T. On parle alors de symbole OFDM. Le spectre résultant est donc une combinaison linéaire de sinus cardinaux centrés autour des porteuses f_k. On parle d'orthogonalité entre les porteuses (le O de OFDM) dès lors que la valeur du spectre pour $f = f_k$ vaut c_k. Cette condition est réalisée en supposant que l'espace inter-porteuse entre f_{k+1} et f_k vaut exactement $\frac{1}{T}$. Cette condition permet en outre d'obtenir une efficacité spectrale optimale.

La réalisation intuitive de l'Equ.1 est illustrée sur la Fig.1 : il s'agit de mettre en parallèle N modulateurs analogiques et de sommer chacune de leurs sorties. Cependant, ceci est beaucoup trop complexe à mettre en oeuvre surtout lorsque N est grand. Une solution numérique a alors été proposée dans [1]. L'idée est d'utiliser les opérateurs de transformées de Fourier discrètes. Une version discrète à la fréquence symbole de l'Equ.1 est alors donnée par :

$$s(n) = \sum_{k=0}^{N-1} c_k e^{2j\pi \frac{kn}{N}}, \quad 0 \leq n \leq N-1. \tag{2}$$

Le paramètre N est généralement une puissance de deux afin d'appliquer les algorithmes de transformées de Fourier rapides. Le schéma de transmission est alors représenté sur la Fig. 2.

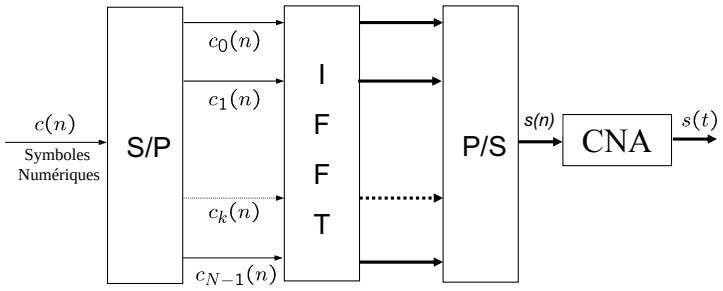

Figure 2: Réalisation numérique d'un modulateur OFDM

1.1.2 Des systèmes multiporteuse aux systèmes multistandard

La multiplication actuelle des services de télécommunications (voix, données, image, vidéo) amène les acteurs du marché à repenser les architectures des émetteurs/récepteurs pour pouvoir répondre à la flexibilité croissante demandée par les utilisateurs que nous sommes, à savoir, recevoir tout, partout et avec une qualité de service acceptable. Derrière cette contrainte forte se cache d'immenses challenges technologiques visant à concevoir un terminal mobile universel supportant plusieurs standards avec lequel le réseau sera transparent à l'utilisateur. On parle alors de terminal multistandard. Le domaine de la radio logicielle a ainsi pour objectif d'apporter des réponses à cela tant sur le plan de la convergence des réseaux, l'accès à de multiples interfaces air et la flexibilité des systèmes de traitement tant logiciels que matériels.

En 1995, Jo Mitola [2], [3] jeta les principes de la radio logicielle en proposant une architecture dite idéale : une antenne large bande suivie d'un convertisseur analogique/numérique à très haute fréquence d'échantillonnage permettant de traiter tout signal de façon numérique, à condition que les processeurs soient extrêmement rapides. Le terminal multistandard prend alors tout son sens si les processeurs sont dits reconfigurables (ou reprogrammables) par téléchargement de logiciels associés à la norme sur laquelle se base la télécommunication à passer. Les architectures sont alors entièrement pilotées par le logiciel et les traitements uniquement effectués en numérique . Dans la cas de la radio logicielle idéale, la conversion analogique numérique est alors directement effectuée en radio fréquence, juste après l'antenne. Cela rend ainsi le traitement numérique d'une bande de fréquence très grande et assouplit la réalisation d'un terminal multistandard. Le passage d'un standard à un autre est alors possible à condition que les processeurs de traitement du signal soient

reconfigurables par téléchargement des logiciels associés aux normes des standards. La Fig. 3 illustre ce principe.

Les obstacles technologiques sont cependant très grands, comme par exemple la réalisation de convertisseurs analogique/numérique ultra rapides, de processeurs à très forte puissance de calcul et à faible consommation ou d'amplificateurs de puissance et d'antennes très large bande.

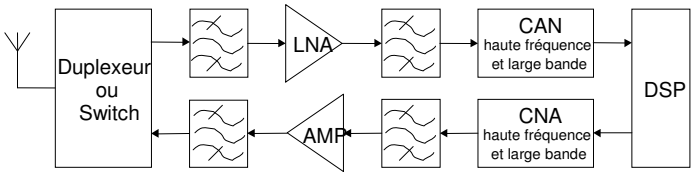

Figure 3: Schéma d'un émetteur-récepteur radio logicielle idéale

L'intérêt de la radio logicielle réside dans la possibilité de pouvoir démoduler une grand nombre de standards, rendant alors les systèmes multistandard. La notion de multiporteuse vue précédemment pour l'OFDM est alors étendue. Une illustration d'un signal multistandard peut être donnée par la Fig. 4. Chacun de ces standards peut être mono ou multiporteuse.

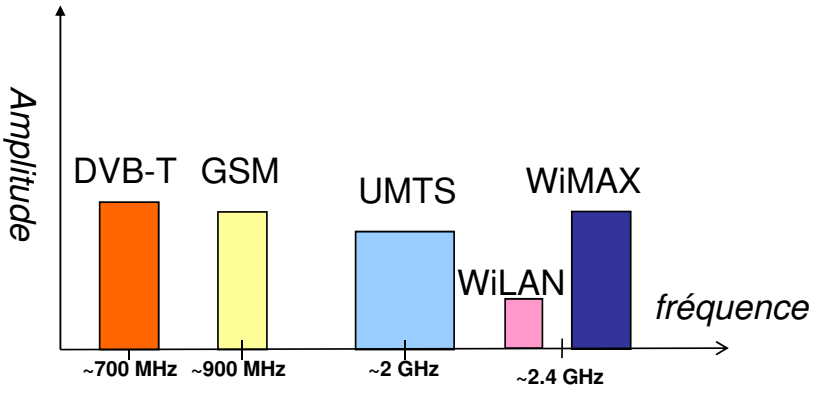

Figure 4: Un exemple de signal multistandard

La réalisation pratique d'un système radio logicielle étant aujourd'hui en partie limitée par les performances des convertisseurs analogiques-numériques, on parle alors de radio logicielle restreinte. Le principe est alors d'effectuer la conversion en fréquence intermédiaire, c'est à dire à des fréquences plus basses.

1.1.3 Evolution des systèmes multistandard vers la radio intelligente

La radio intelligente est une extension de la radio logicielle. Elle repose sur une radio logicielle (restreinte éventuellement) à laquelle on associe des capteurs et des organes d'analyse et de prise de décision. Les moyens sensoriels peuvent être en lien direct avec la radio (propagation...) ou le système de communication (consommation de puissance...) mais aussi avec l'environnement sociétal (localisation...) ou le comportement de l'utilisateur (réunion...). La radio intelligente vise à ajuster les fonctionnalités du système de communication au contexte d'utilisation sous toutes ses formes. La définition de la radio intelligente apportée par Jo Mitola est la suivante [3]:

"A radio or system that senses, and is aware of, its operational environment and can dynamically and autonomously adjust its radio operating parameters accordingly."

Un des capteurs les plus étudiés en ce moment est le capteur spectre dont l'objectif est de déterminer la ressource spectrale disponible afin de profiter des bandes libres pour alors transmettre un communication dite "opportuniste". Cette bande sera à nouveau libérée dès la communication terminée. Cette gestion souple du spectre est entièrement décentralisée (au niveau de la station de base et/ou du terminal). Cela n'est pas sans conséquence sur le signal multistandard à émettre : en effet l'ajout opportuniste d'un signal de communication ne doit pas détériorer les caractéristiques attendues du signal vis à vis des étages analogiques d'émission et de réception, comme par exemple les amplificateurs de puissance ou les filtres radio fréquence. Cette thèse aborde les conséquences de cet accès opportuniste au spectre sur le niveau de puissance du signal multistandard à émettre. Ce niveau est décrit à travers le Peak to Average Power Radio (PAPR) faisant l'objet de la partie suivante.

1.2 Le PAPR des systèmes OFDM

1.2.1 Expression

Le PAPR décrit les fluctuations de puissance d'un signal relativement à sa puissance moyenne. Pour un signal $x(t)$ définit sur un horizon temporel $[0, T]$, il est défini par :

$$\mathrm{PAPR}(x(t)) = \frac{\max\limits_{t\in[0,T]} |x(t)|^2}{\frac{1}{T}\int_0^T |x(t)|^2 dt}. \tag{3}$$

Le PAPR peut se décliner pour des signaux analogiques, numériques, à supports finis ou infinis. Il a été montré qu'une borne supérieure du PAPR pour les modulations OFDM à N porteuses et travaillant avec des symboles issus d'une modulation de type MAQ à M états est donnée par

$$PAPR_{max,M-MAQ} = 3N\frac{\sqrt{M}-1}{\sqrt{M}+1}. \tag{4}$$

Cependant cette borne est beaucoup trop large et ne reflète pas la réalité au plus près des fluctuations du signal OFDM. Il faut alors considérer une approche probabiliste en faisant l'hypothèse que les N échantillons du signal OFDM discret $\mathbf{x}$ suivent une loi gaussienne en vertu du théorème de la limite centrale. En se plaçant à échantillonnage critique ($L = 1$), c'est à dire en calculant le PAPR sur les N échantillons temporels, On obtient la fonction de répartition suivante :

$$Pr\Big[\text{PAPR}\{\mathbf{x}\} > \gamma\Big]_{L=1} \approx 1 - (1 - e^{-\gamma})^N. \tag{5}$$

Le PAPR doit être alors considéré comme une variable aléatoire.

Depuis une douzaine d'années, de très nombreux travaux se sont attachés à décrire le PAPR et ceci principalement dans le contexte de l'OFDM. En effet, dès lors que des porteuses sont sommées entre elles (comme c'est le cas par construction de l'OFDM), le signal résultant présente des pics d'amplitude pouvant atteindre des valeurs très grandes. Ce point est très important à prendre en compte au niveau de l'amplification de puissance.

1.2.2 Conséquences d'un fort PAPR pour l'amplification de puissance

Le fait qu'un signal donné ait un fort PAPR se conjugue avec les caractéristiques clés d'un amplificateur de puissance, à savoir son gain et son rendement. En effet, le gain d'un amplificateur est caractérisé par une zone linéaire puis une zone où le gain s'écarte de la linéarité jusqu'à saturer. Cette caractéristique est à relier au rendement de l'amplificateur qui est très faible dans la zone où justement le gain est constant et maximum lorsque le gain chute. Ceci est illustré sur la Fig.5. Le gain et le rendement sont respectivement définis comme $\frac{P_s}{P_e}$ et $\frac{P_s}{P_{dc}}$.

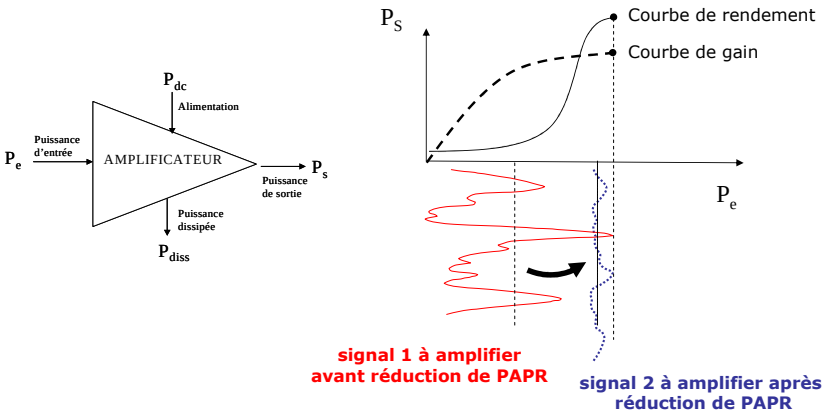

Figure 5: Bilan de puissance d'un amplificateur de puissance et courbes de gain/rendement

L'amplification de puissance d'un signal doit donc tenir compte de ces deux caractéristiques. Ce signal à amplifier n'est pas toujours à enveloppe constante et présente des fluctuations comme le montre la Fig.5 (signal 1) et un recul doit être obligatoirement pris de façon à ne pas saturer le signal amplifié. La conséquence de cela est que l'amplification est effectuée dans une zone où le rendement de l'amplificateur est faible. D'où l'idée de réduire ces fluctuations de puissance afin d'amplifier le signal (signal 2 sur la Fig.5) dans une zone où le rendement est maximum. Ceci n'a cependant de sens que si l'amplificateur est linéarisé, c'est à dire ayant une caractéristique de gain quasiment linéaire, faisant suite à un traitement spécifique. Cette réduction de fluctuations est appelée "réduction du

PAPR". Il existe un nombre très important de méthodes de réduction du PAPR. Le paragraphe suivant en détaille quelques unes.

1.2.3 Présentation de quelques méthodes de réduction du PAPR dans le contexte de l'OFDM

Il existe une quantité très importante de méthodes de réduction du PAPR pour l'OFDM, toutes proposées depuis une douzaine d'années. Présentant toutes des avantages et des inconvénients et au delà de la réduction du PAPR qui les caractéris toutes, il est nécessaire de bien regarder les points suivants :

- est ce que la méthode développée à l'émetteur nécessite une modification du récepteur?
- est ce que la méthode développée dégrade le taux d'erreur binaire?
- est ce que la méthode développée nécessite la transmission d'information extrinsèque?
- est ce que la méthode développée augmente la puissance moyenne globale du signal émis?
- quelle est la complexité de la méthod?

Des synthèses ont été proposées [4] ainsi qu'une classification [5] dans le but de regrouper les méthodes par catégorie. Le lecteur pourra se réferer à ces deux travaux pour de plus amples détails. Cependant voici développés succinctement trois types de méthodes très utilisées à ce jour.

La solution la plus intuitive pour limiter les fluctuations de puissance du signal à amplifier est de les saturer délibérément. Cette méthode est connue sous le nom de "clipping" [6]. Cette méthode dégrade malheureusement le taux d'erreur binaire et augmente la remontée des lobes secondaires en dehors de la bande utile. Cette technique ne nécessite pas de traitements en réception.

Les techniques connues sous le nom de "représentations multiples" sont d'autres façons efficaces de réduire le PAPR, au prix de complexités élevées. Elles sont connues sous le nom "Partial Transmit Sequence" (PTS) [7] et "Selective Mapping Technique" (SLM) [8]. L'idée est de sélectionner parmi un large choix de signaux à transmettre celui qui a le PAPR le plus faible. Ces techniques nécessitent en général la transmission d'informations additionnelles entre l'émetteur et le récepteur pour retrouver l'information originale transmise. Cela implique alors la modification du récepteur.

Une autre technique, largement utilisée dans cette thèse, est celle de l'ajout de signal. L'idée est d'ajouter un signal de correction c à un signal utile x à fort PAPR de façon à ce que le signal final $x + c$ ait un PAPR plus faible que celui de x. Cette approche a été largement décrite dans [9] où le signal est ajouté dans le domaine fréquentiel sur des porteuses dites réservées. Ceci a aussi été décrit dans le domaine temporel [10]. Ce signal

de correction c, qu'il soit temporel ou fréquentiel, est issu d'un algorithme d'optimisation souvent complexe et les gains de réduction de PAPR sont par contre importants. Le taux d'erreur et l'efficacité spectrale restent cependant des paramètres à étudier de près de façon à s'assurer qu'ils ne soient pas dégradés.

1.3 Les objectifs de la thèse

Dans la logique de ce qui a été présenté précédemment, les objectifs de la thèse sont multiples. Les finalités restent cependant les suivantes : d'une part décrire analytiquement le PAPR d'un système multistandard basé sur le concept de radio intelligente et d'autre part en proposer des méthodes de réduction efficaces.

Ce double objectif se décline en plusieurs sous points :

- établir analytiquement le PAPR d'un signal OFDM continu radio fréquence pour faire ensuite le lien avec un signal multistandard qui est par définition radio fréquence
- montrer l'équivalence entre l'OFDM et les signaux multistandard pour appliquer des méthodes similaires de réduction de PAPR
- étudier des méthodes de réduction du PAPR d'un signal multistandard en utilisant les bandes libres pour transmettre les porteuses de correction
- étendre la notion de capteurs de la radio intelligente au PAPR dans un contexte d'accès opportuniste au spectre

2 Etude théorique sur le PAPR d'un signal OFDM continu radio fréquence

2.1 Etat de l'art du PAPR d'un signal OFDM discret bande de base

Comme vu précédemment à travers l'Equ.5, l'approche probabiliste pour décrire le PAPR est incontournable. Cependant, l'Equ.5 n'est valable qu'à l'échantillonnage critique (facteur d'échantillonnage $L = 1$), c'est à dire pour exactement N points et ne reflète donc pas le comportement du PAPR d'un signal continu. De la fonction de répartition complémentaire décrite par l'Equ.5, il est alors possible de déduire les deux premiers moments du PAPR (moyenne m et variance σ^2)[11] :

$$m_{L=1} \approx lnN + \zeta, \tag{6}$$

(ζ est la constante d'Euler ($\zeta \approx 0.577$)) et

$$\sigma^2_{L=1} \approx \frac{\pi^2}{6}. \tag{7}$$

Afin d'extrapoler les résultats ci-dessus au cas continu, il faut alors suréchantillonner le signal d'un facteur $L > 1$ et faire tendre L vers l'infini. La Fig.6 illustre les simulations obtenues de la fonction de répartition complémentaire du PAPR pour différents facteurs de suréchantillonnage. On constate clairement qu'à partir de $L = 4$, les courbes n'évoluent plus [12]. Il est alors généralement admis que le PAPR d'un signal continu peut alors être obtenu en suréchantillonnant simplement le signal OFDM d'un facteur $L = 4$.

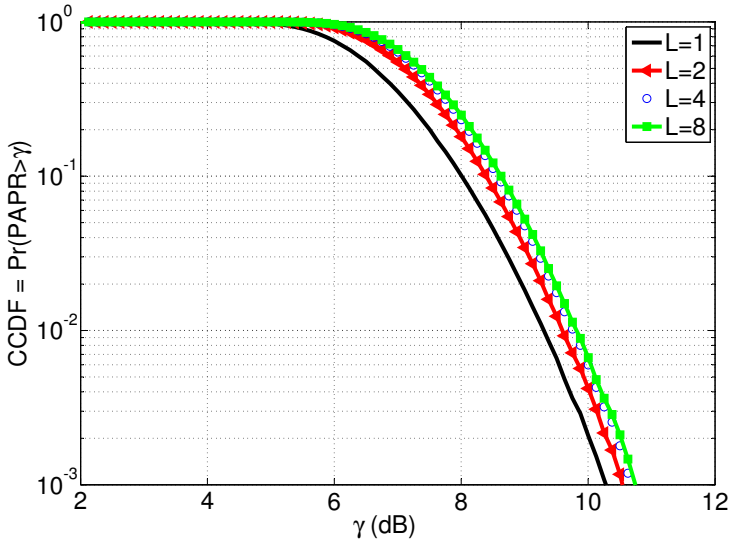

Figure 6: Fonction de répartition du PAPR d'un signal OFDM à N=64 porteuses pour différentes valeurs de facteurs de suréchantillonnage

2.2 Etat de l'art du PAPR d'un signal continu

Pour un facteur de suréchantillonnage élevé $L \gg 1$, une expression obtenue par simulation du PAPR a été donnée [12] :

$$Pr\Big[\text{PAPR}\{\mathbf{x}\} > \gamma\Big]_{L\gg 1} \approx 1 - (1 - e^{-\gamma})^{\alpha N}, \tag{8}$$

où $\alpha \approx 2.8$. Par analogie avec ce qui précède, on déduit qu'une approximation de la moyenne du PAPR d'un signal OFDM continu est donné par :

$$m_{L\gg 1} \approx lnN + \zeta + ln\alpha = lnN + 1.6 \tag{9}$$

Dans la même idée, [13] et [14] ont proposé une expression de la fonction de répartition complémentaire du PAPR pour des fortes valeurs de L :

$$Pr\Big[\text{PAPR}\{\mathbf{x}\} > \gamma\Big]_{L\gg 1} \approx N\sqrt{\frac{\pi}{3}\gamma}e^{-\gamma}. \tag{10}$$

La Fig.7 illustre parfaitement la précision apportée par l'Equ.10 pour décrire le PAPR d'un signal continu. Elle se substitue donc à l'Equ.8, cette dernière étant obtenue par simulation.

L'expression donnée par l'Equ.10 étant la plus proche du comportement du PAPR d'un signal OFDM continu, l'idée est alors d'en déduire les expressions des deux premiers moments (moyenne et variance). Ceci fait l'objet de la partie suivante.

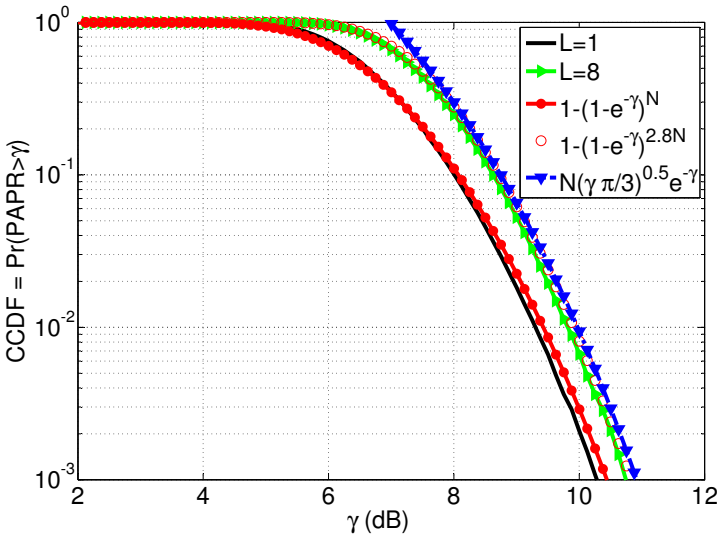

Figure 7: Comparaison des fonctions de répartition du PAPR pour des signaux OFDM à N=64 porteuses

2.3 Contribution sur le premier et le deuxième moment du PAPR d'un signal continu

2.3.1 Expression de la moyenne

La moyenne m d'une variable aléatoire est obtenue à partir de sa densité de probabilité $f(.)$, elle même déduite de la fonction de répartition $F(.)$:

$$m = \int_{-\infty}^{+\infty} \gamma f(\gamma) d\gamma, \tag{11}$$

avec

$$f(\gamma) = d(F(\gamma))/d\gamma. \tag{12}$$

En utilisant l'Equ.10, on déduit que (pour N grand)

$$F(\gamma) = 1 - N\sqrt{\frac{\pi}{3}\gamma}e^{-\gamma} \approx e^{-\sqrt{\frac{\pi}{3}}N\sqrt{\gamma}e^{-\gamma}}. \tag{13}$$

Par le biais de l'Equ.11 et après résolution d'une équation différentielle dont le détail se trouve dans le document, on aboutit à une expression de la moyenne, donnée par :

$$m_{L\gg 1} \approx \mu(lnN + ln\frac{\theta}{\sqrt{e}}). \tag{14}$$

Les variables μ et θ sont alors obtenues selon une régression linéaire et l'on aboutit alors à des valeurs respectives de 1.07 et 5.12. Au final,

$$m_{L\gg 1} \approx 1.07ln(\frac{5.12}{\sqrt{e}}N). \tag{15}$$

2.3.2 Expression de la variance

Une étude sur la précision de la valeur de la variance pour des signaux OFDM continus (à facteurs de suréchantillonnage élevés) montre que la valeur obtenue pour le cas $L = 1$ ($\sigma^2 = \frac{\pi^2}{6}$) est une bonne approximation.

2.3.3 Synthèse des travaux menés sur le PAPR d'un signal OFDM continu

Toute l'étude menée jusqu'ici a pour objectif d'aboutir à une fonction de répartition théorique de PAPR pour des signaux OFDM continus. Cela se justifie par le fait que les signaux multistandards traités dans la suite du document sont continus car décrits en radio fréquence. Sachant que le passage bande de base - radio fréquence augmente le PAPR de 3 dB, on en déduit aisément la fonction de répartition d'un signal OFDM continu et radio fréquence (RF). Cette fonction de répartition est :

$$Pr\Big[\text{PAPR}\{\mathbf{x}\} > \gamma\Big]_{L\gg 1,RF} \approx 1 - (1 - e^{-\frac{\gamma}{2}})^{\tau N^{\mu}}, \tag{16}$$

où $\tau = (\frac{5.12}{\sqrt{e}})^{1.07} e^{-\zeta}$ et $\mu = 1.07$.

3 Analyse du PAPR dans le contexte de la radio logicielle

3.1 Le signal multistandard dans le contexte de la radio logicielle

La radio logicielle est une technologie qui permet de traiter en numérique un ensemble de standards en échantillonnant une large bande en radio fréquence (ou en fréquence intermédiaire dans sa version restreinte). La conception d'un équipement multistandard capable de démoduler n'importe quel type de signal est donc entièrement liée à cette approche. Commençons toutefois par définir un signal multistandard. Soit $x(t)$ un signal composé de S standards $S_i(t)$ $(i = 1, ..., S)$. $x(t)$ est alors donné par :

$$x(t) = \sum_{i=1}^{S} S_i(t). \tag{17}$$

Le signal $x(t)$ sera qualifié de composite. Chaque signal $S_i(t)$ est associé à un standard composé de P_i porteuses. Un signal $S_i(t)$ s'exprime alors par :

$$S_i(t) = \sum_{p=1}^{P_i} r_{i,p}(t) e^{2i\pi f_{i,p} t}. \tag{18}$$

Ici $r_{i,p}(t)$ représente la réponse complexe utile du signal après filtrage et modulation sur la porteuse p dans le standard i. Dans ce cas, $r_{i,p}(t) = fem_i(t) * m_{i,p}(c(t))$, où $m_{i,p}(c(t))$ et $fem_i(t)$ représentent respectivement les fonctions de transfert de la modulation et du filtre de mise en forme, pour la porteuse p et le standard i. On en déduit alors que

$$x(t) = \sum_{i=1}^{S} \sum_{p=1}^{P_i} (fem_i(t) * m_{i,p}(c(t)) e^{2i\pi f_{i,p} t}. \tag{19}$$

L'Equ.19 définit ainsi l'expression générale d'un signal multistandard appelé encore signal radio logicielle.

3.2 Equivalence analytique entre un signal multistandard et un signal OFDM

Conformément à l'Equ.18, si l'espace entre les porteuses $f_{i,p}$ est constant ($= \triangle p$) pour tous les standards considérés, le signal radio logicielle s'écrit :

$$x(t) = \sum_{i=1}^{S} \sum_{p=1}^{P_i} r_{i,p}(t) e^{2i\pi((p-1)\triangle p)t}, \tag{20}$$

Cette condition d'espace interporteuse constant n'est généralement pas vérifiée, les standards adoptant des spécifications très différentes. La seul cas où cela est vrai est lorsque l'on considère un standard unique. Dans ce cas, il y a équivalence entre le signal radio logicielle et OFDM.

3.3 Equivalence gaussienne entre les signaux OFDM et radio logicielle

Il a été vu aux chapitres précédents que le PAPR se décrivait grâce à la fonction de répartition, le PAPR étant vu comme une variable aléatoire. Une hypothèse forte en OFDM réside dans le fait que tous les échantillons du signal modulé suivent un loi normale centrée et de variance donnée. Ceci est dû au théorème de la limite centrale en supposant que les symboles c_k de l'Equ.1 sont indépendants et suivent la même loi. En extrapolant cette hypothèse à un signal radio logicielle et toujours en vertu du théorème de la limite centrale, les échantillons du signal $x(t)$ de l'Equ.20 suivent tous une loi normale. La fonction de répartition du PAPR d'un signal radio logicielle est alors identique à celle d'un signal OFDM. Cette équivalence va être illustrée pour des signaux radio logicielle mono puis multistandard dans la section suivante.

3.3.1 Validation de l'hypothèse gaussienne pour un signal radio logicielle de type modulation GMSK

La modulation GMSK a été normalisée pour le GSM dont chaque porteuse suit dans un plan I/Q un cercle de façon à ce que son PAPR soit exactement 0 dB en bande de base et 3 dB en radio fréquence. Cependant, en considérant un multiplex de porteuses GMSK, le comportement du signal résultant tend vers une loi gaussienne comme le montre la fonction de répartition de la Fig.8 pour 64 et 128 porteuses GMSK.

3.3.2 Analyse du PAPR d'un signal radio logicielle composé de trois modulations

Le signal radio logicielle considéré ici est composé d'un signal OFDM, d'un multiplex de porteuses modulées en GMSK et d'un multiplex de porteuses modulées en QPSK. Cela pourrait s'apparenter à un signal tri-standards de type WLAN (à base d'OFDM), GSM (à base de GMSK) et UMTS (à base de QPSK). Ici seules les formes d'onde des signaux de la couche physique sont considérées. Chaque modulation contient 64 porteuses. Les PAPR des modulations considérés suivent tous la même fonction de répartition, confirmant l'équivalence gaussienne. Ensuite, en prenant en compte le PAPR du signal global radio logicielle, le PAPR reste inchangé. En conclusion tout échantillon d'un multiplex

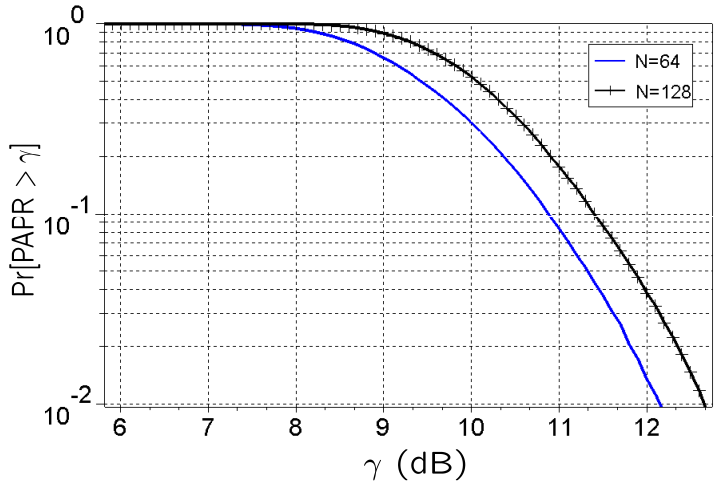

Figure 8: Fonction de répartition du PAPR en radio fréquence d'un multiplex de 64 et 128 porteuses GMSK

de porteuses suit une loi gaussienne, indépendamment des modulations propres à chaque standard et aux valeurs des porteuses. D'un point de vue du PAPR, les signaux OFDM et radio logicielle sont complètement équivalents. On en déduit entre autres que les méthodes utilisées jusqu'alors pour réduire le PAPR des signaux OFDM pourront être appliquées aux signaux radio logicielle.

3.4 Vision fréquentielle du PAPR

Cette partie aborde la vision fréquentielle du PAPR. En effet, il est indispensable de disposer d'un outil permettant d'estimer le PAPR d'un signal à partir de ses composantes fréquentielles, les signaux radio logicielle étant en effet généralement décrits dans le domaine fréquentiel.

A partir d'une représentation temporelle du signal d'origine, un tableau est rempli. Les N_S lignes de ce tableau sont des versions fréquentielles des portions de taille N du signal d'origine. Cela est illustré sur la Fig.10.

Grâce à cette vision du signal, il est alors possible de montrer que le PAPR temporel $PAPR_{temp}(S(n))$ du signal d'origine $S(n)$ peut être majoré par un terme dépendant des PAPR "$PAPR_{f_k}$" calculés par colonne, c'est à dire fréquence par fréquence. La relation est la suivante :

$$PAPR_{temp}(S(n)) \leq \frac{1}{\sum_{k=1}^{N} P_m(k)}[(\sum_{k=1}^{N} P_m(k) \times PAPR_{f_k}) + \max_{k\in[0,N-1]}(\max_{j\in[1,N_s]}(\lambda(j,k)))], \tag{21}$$

où les $P_m(k)$ sont les puissances moyennes calculées fréquence par fréquence et $\lambda(j,k)$ est un terme de corrélation donné par

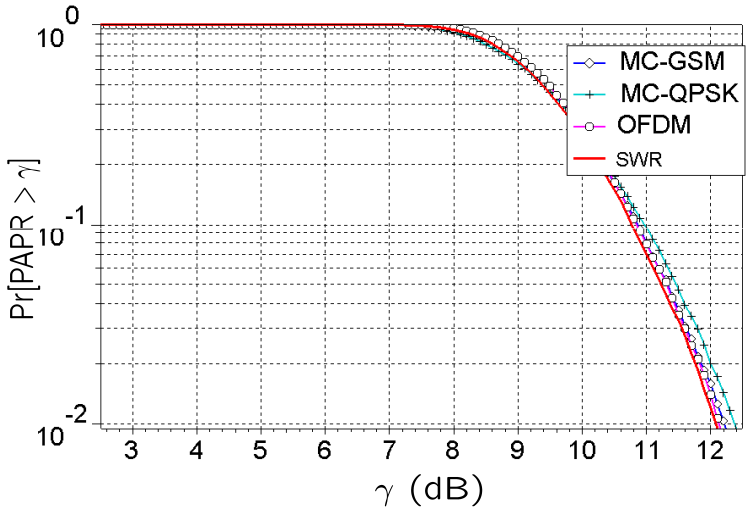

Figure 9: Fonctions de répartition du PAPR en radio fréquence de trois multiplex de porteuses et du signal tri-standard résultant

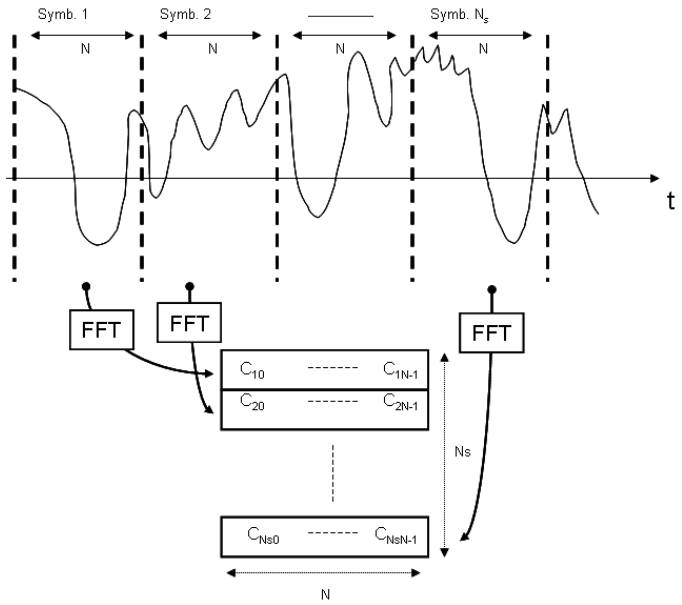

Figure 10: Remplissage de la table temps/fréquence

$$\lambda(j,k) = \sum_{p=1}^{N} C_{j,p} \sum_{p' \neq p} \overline{C_{j,p'}} e^{2i\pi \frac{k(p-p')}{N}}, j \in [1, N_S], k \in [0, N-1].$$

Les simulations ont ensuite montré (Fig.11) que les visions fréquentielles et temporelles du PAPR étaient très proches. Ces simulations ont été menées sur un signal radio logicielle composé de deux standards de type WLAN : un standard WiFi à 64 porteuses et un standard WiMax à 256 porteuses. La taille du signal temporel simulé est de 4096 points,

permettant alors de remplir un tableau de taille 4 × 1024. Le majorant de l'Equ.21 (composé uniquement de termes fréquentiels) permet donc d'approcher de façon précise le PAPR temporel.

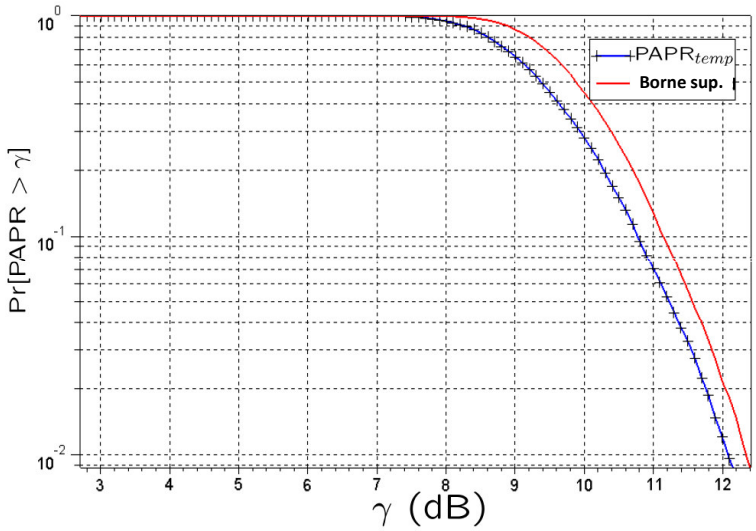

Figure 11: Illustration de l'Equ.21 sur un signal radio logicielle

Ces développements seront repris à la fin du document afin d'estimer analytiquement l'augmentation de PAPR lors d'un accès opportuniste au spectre dans le contexte de la radio intelligente.

4 Réduction du PAPR dans un contexte radio logicielle

4.1 Méthode de la Tone Reservation

Sélectionner une méthode de réduction de PAPR nécessite la prise en compte de facteurs déterminants pour la qualité de la transmission. Il faut donc dans un premier temps privilégier la non dégradation du taux d'erreur binaire, ce qui élimine un certain nombre de méthodes. Ensuite, il est préférable que le récepteur ne soit pas modifié si une méthode de réduction de PAPR est appliquée à l'émetteur. C'est la notion de compatibilité descendante. Enfin il faut veiller à ce que la méthode de réduction du PAPR ne dégrade pas l'efficacité spectrale par le biais par exemple d'une transmission d'une information extrinsèque permettant au récepteur de recouvrer l'information utile. D'autres paramètres doivent aussi intervenir comme la limitation de la puissance moyenne, de la complexité de l'algorithme, ... La classe de méthode sélectionnée dans cette thèse est celle de l'ajout de signal. Cette idée a été présentée dans la partie 1.2.3. Les avantages de l'approche sont les suivants :

- la réduction de PAPR peut être très élevée
- le taux d'erreur n'est pas dégradé si les informations de correction sont ajoutées sur des fréquences non utilisées des standards

- le récepteur n'est pas modifié si les informations de données sont dissociées des porteuses de correction, ces dernières étant de toutes façons ignorées du récepteur
- l'efficacité spectrale n'est pas modifié car aucune information de l'émetteur au récepteur n'est transmise

Cette approche possède malgré cela des inconvénients :

- l'algorithme optimal fournissant les porteuses de correction est complexe. Il conviendra donc de le simplifier
- la puissance moyenne après réduction du PAPR augmente par définition de la méthode. Il conviendra de la limiter

Le travail de référence concernant l'ajout de signal est celui de Tellado [9]. Il est connu sous le nom de Tone Reservation. Il s'agit ainsi de réserver des porteuses dédiées uniquement à la réduction du PAPR. Cette approche a été initialement appliquée à l'OFDM et a été retenue tout récemment pour la future norme de télévision numérique terrestre (DVB-T2) où des porteuses spécifiques pour la réduction du PAPR ont été allouées dans la bande utile. La justification de l'application de cette méthode à un signal radio logicielle est que les porteuses de correction seront ajoutées en dehors des standards, c'est à dire dans les bandes libres du spectre.

D'une façon générale, comme présenté sur la Fig. 12, le signal initial fréquentiel $\mathbf{X}$ est ajouté à un signal de correction $\mathbf{C}$ de façon à ce que le signal temporel $x + c$ ait un PAPR plus faible que x. La recherche des valeurs du vecteur $\mathbf{C}$ constitue la partie la plus délicate de la méthode. La solution optimale présentée par Tellado nécessite la résolution d'un algorithme d'optimisation convexe complexe à mettre en oeuvre et en temps de calcul. Cet algorithme est connu sous le nom de SOCP (Second Order Cone Programming).

4.2 L'algorithme SOCP

Minimiser le PAPR revient à minimiser le maximum de la puissance instantanée, ce qui revient à chercher le vecteur $\mathbf{C}$ vérifiant

$$\min_{C} \max |IFFT(\mathbf{X} + \mathbf{C})|. \tag{22}$$

La résolution de ce type de problème peut se faire à l'aide d'un algorithme d'optimisation convexe de type SOCP [15]. Il est alors équivalent de formuler l'Equ.22 selon :

$$\min_{\mathbf{C}} \max_{0 \leq k \leq NL-1} |x_k + \mathbf{q}_{k,L}^{row} \mathbf{C}|, \tag{23}$$

où $\mathbf{q}_{k,L}^{row}$ est la $k^{ème}$ ligne de la matrice de Fourier $\mathbf{Q}_L$ de taille NL et où les x_k sont les échantillons du signal temporel x. L est le facteur d'échantillonnage. La formulation est alors équivalente à [16]

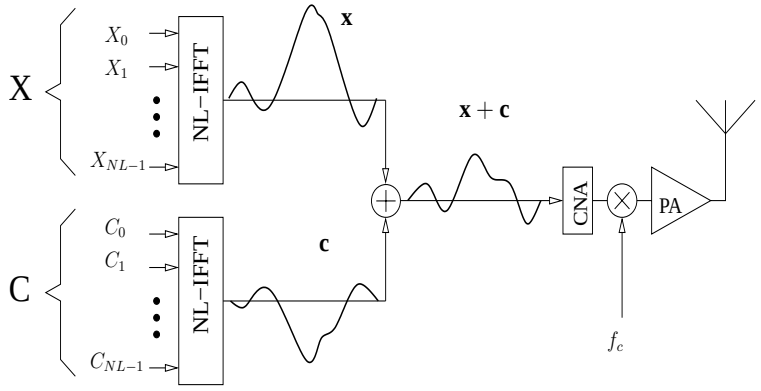

Figure 12: Principe de la méthode de Tone Reservation

$$\begin{gathered} \min \ \beta \\ \text{sachant que} \\ \left| x_k + \mathbf{q}_{k,L}^{row} \mathbf{C} \right| \leq \beta, 0 \leq k \leq NL-1. \end{gathered} \tag{24}$$

La Fig.13 illuste la réduction du PAPR pour un signal OFDM d'origine de $N = 64$ porteuses dont 6 sont réservées pour réduire le PAPR. En appliquant un algorithme SOCP, on constate que la réduction du PAPR est très importante, de l'ordre de 6 dB. Cependant ce résultat a été obtenu sans contrainte sur l'augmentation de la puissance moyenne et sans contrainte sur le masque d'émission du signal (associé à un standard). La prise en compte de ces deux contraintes va limiter la réduction du PAPR.

4.3 Contraintes à prendre en compte dans l'algorithme SOCP

4.3.1 Contrainte sur la puissance moyenne

Par principe de la méthode d'ajout de signal, le signal $x+c$ possède une puissance moyenne plus élevée que le signal x. Ceci est un inconvénient. On exprime l'augmentation de puissance ΔE par [9] :

$$\Delta E = 10 \log_{10} \frac{E\{|\mathbf{x}+\mathbf{c}|^2\}}{E\{|\mathbf{x}|^2\}}. \tag{25}$$

L'objectif est de garder ΔE sous un seuil γ tel que :

$$E\left\{|\mathbf{x}+\mathbf{c}|^2\right\} \leq \gamma E\left\{|\mathbf{x}|^2\right\}. \tag{26}$$

Ainsi la formulation de l'algorithme SOCP devient :

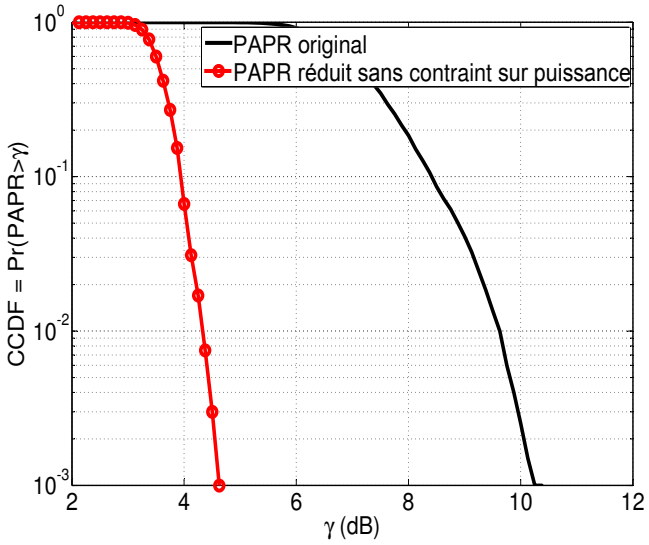

Figure 13: Réduction du PAPR en utilisant la méthode de la Tone Reservation sans contrainte sur les porteuses. ($N = 64$)

$$\begin{gathered} \text{minimize } \beta \\ \text{subject to} \\ \left| x_k + \mathbf{q}_{k,L}^{row}\mathbf{C} \right| \leq \beta, 0 \leq k \leq NL-1 \\ E\left\{ |\mathbf{x}+\mathbf{c}|^2 \right\} \leq \gamma E\left\{ |\mathbf{x}|^2 \right\}. \end{gathered} \tag{27}$$

En tenant compte de cette contrainte, la Fig.14 illustre la réduction de PAPR pour un signal OFDM à N=64 porteuses. On constate que plus la contrainte sur la puissance moyenne se relâche et plus l'augmentation du PAPR est importante et vice versa.

4.3.2 Contrainte sur le masque d'émission

Dès lors que des porteuses sont ajoutées dans un spectre, il est nécessaire qu'elles respectent le masque d'émission du standard. En effet, ces porteuses de correction peuvent être ajoutées dans les bandes de garde dans le cas d'un signal OFDM (c'est à dire en dehors de la bande utile). Ceci ne peut se faire qu'à l'unique condition que les porteuses ajoutées restent sous le masque. Cette condition se traduit alors par :

$$|c_k| \leq \delta_k, k \in R, \tag{28}$$

où R est l'ensemble des indices des porteuses réservées.

4.4 Application de la Tone Reservation à un signal radio logicielle

Le document complet présente l'étude des signaux mono bande OFDM, multi bande OFDM et enfin radio logicielle. Dans ce résumé, seul ce dernier cas est présenté à l'aide

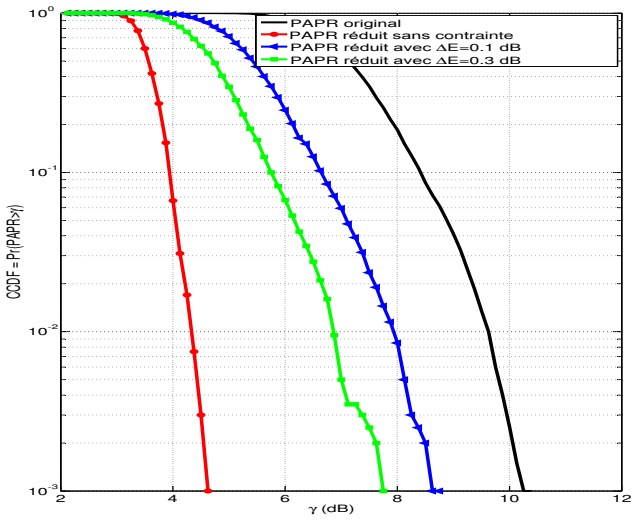

Figure 14: Réduction du PAPR en utilisant la méthode de la Tone Reservation avec contrainte sur les porteuses. ($N = 64$)

de deux types de signaux : un signal bi standard théorique (cas 1) et un multiplex de porteuses GSM (cas 2).

4.4.1 Cas 1 : signal radio logicielle théorique

Pour le besoin de la simulation deux standards théoriques sont simulés. Le premier standard contient $N_1 = 64$ porteuses parmi lesquelles 12 sont non utilisées. Le second standard contient $N_2 = 256$ porteuses dont 56 sont non utilisées. L'espaces interporteuse est constant à l'intérieur de chaque standard et vaut $\delta_1 = 0.31MHz$ pour le premier standard et $\delta_1 = 0.078MHz$ pour le second. Une différence de puissance de ΔP a été considérée entre les deux standards. La bande passante de chacun de ces standards est de 20 MHz. La réduction du PAPR dépend du nombre de porteuses de correction. Ainsi dans un premier temps, seules les porteuses non utilisées des standards ont été utilisées en intégrant la contrainte du respect du masque de transmission. La Fig. 15 illustre le positionnement des porteuses.

Le Tab.1 donne la proportion de porteuses de corrections utilisées à la fois dans les standards mais aussi entre.

Pourcentage de porteuses de correction dans le standard A :	18.75%
Pourcentage de porteuses de correction dans le standard B:	21.87%
Pourcentage de porteuses de correction entre les deux standards :	15.63%
Modulation:	4-QAM

Table 1: Nombre de porteuses de correction utilisé

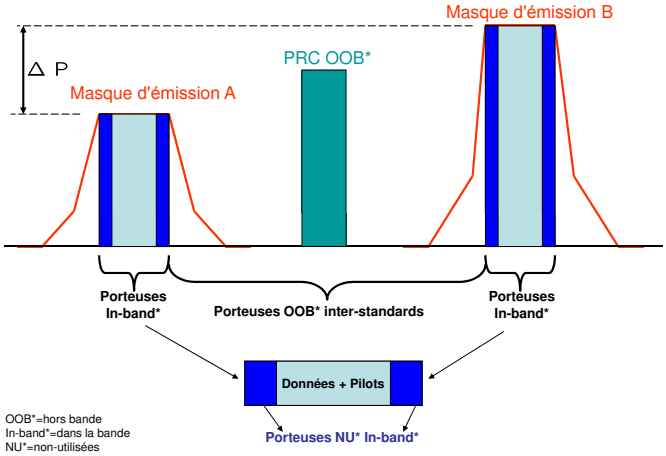

Figure 15: Positionnement des porteuses de correction

Dans un premier temps, seules les porteuses non utilisées des standards ont été optimisées pour réduire le PAPR. Les résultats sont illustrés sur la Fig.16. Un algorithme de type SOCP est utilisée pour optimiser la valeur des porteuses. Ensuite, pour augmenter la réduction du PAPR, des porteuses de correction situées entre les deux standards ont été ajoutées. Cela suppose que la bande entre les deux standards est libre. Des contraintes sur les puissances moyennes ont été imposées dans l'algorithme d'optimisation : 0.2 dB pour les porteuses dans les bandes des standards et 0.8 dB pour celle situées entre les deux standards.
La Fig.16 permet de constater que plus le nombre de porteuses de correction utilisé est élevé et plus le PAPR est réduit. Les résultats présentés font cependant l'hypothèse que les puissances moyennes relatives sont limitées à 0.2 dB pour les porteuses dans la bande des standards et 0.8 dB pour celles situées en dehors des standards. Ces limitations de puissance ont des conséquences sur les performances en terme de réduction de PAPR : on peut aisément supposer que les porteuses de correction situées entre les standards (c'est à dire dans des bandes libres) auront des contraintes moins fortes que celles situées dans les standards eux-mêmes.

La Fig.17 met en valeur les différences obtenues dans la réduction du PAPR lorsque seules les porteuses de correction entre les standards sont utilisées et lorsqu'elles sont soumises à des contraintes différentes sur la puissance moyenne relative. On constate que seules ces porteuses de correction hors bande n'arrivent pas à réduire le PAPR autant que celles situées dans les bandes des standards (en comparaison avec la Fig.16). Cela s'explique par le fait que plus des porteuses de correction sont espacées du signal dont le PAPR est à réduire et plus cette réduction nécessitera de puissance additionnelle pour baisser le PAPR. La proximité des porteuses de correction avec le signal est donc un critère important à prendre en compte. Une étude poussée sur l'influence de la distance des porteuses de correction ainsi que la largeur de bande du signal correctif est donné dans le document.

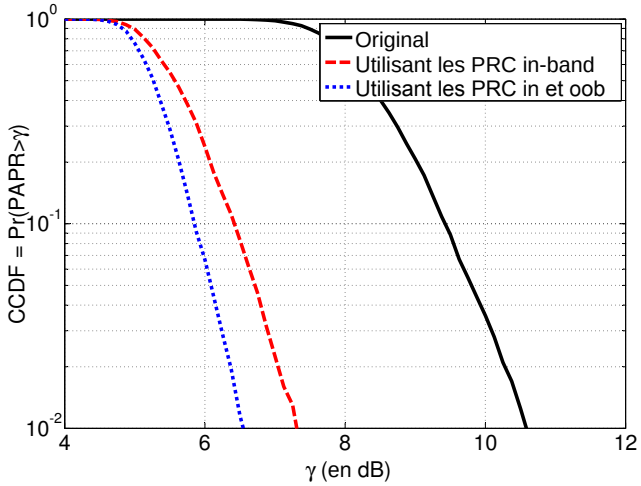

Figure 16: Influence des porteuses de correction dans la bande des standards et entre les standards (respectivement limitées en puissance relatives à 0.2 dB et 0.8 dB).

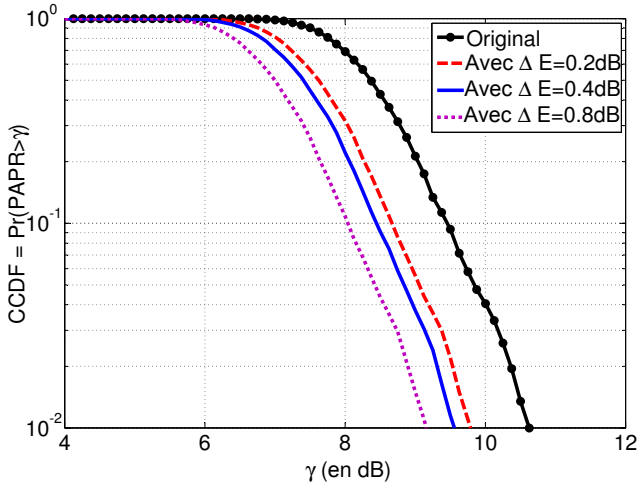

Figure 17: Effet de la limitation de la puissance des porteuses hors bande

4.4.2 Cas 2 : signal radio logicielle GSM

Le cas du GSM est étudié ici. En effet plusieurs porteuses GSM sont en pratique amplifiées ensemble par secteur (4 en général) véhiculant ainsi un fort PAPR. En effet, même si une porteuse GSM a un PAPR de 3 dB en radio fréquence (0 dB en bande de base), le PAPR d'un multiplex de 4 porteuses GSM est de l'ordre de 9 dB (en radio fréquence). L'idée est alors de profiter de la planification de fréquences pour utiliser les bandes GSM "libres" pour une station de base donnée, pour réduire le PAPR, sachant que les informations ajoutées devront respecter le rapport $C/I = -13dB$ imposé par la norme GSM.

Les simulations ont été effectuées selon les conditions suivantes : 4 porteuses GSM ont été considérées (espacées de 800 kHz chacune) et les porteuses de corrections ont été introduites entre les porteuses GSM selon la Fig. 18.

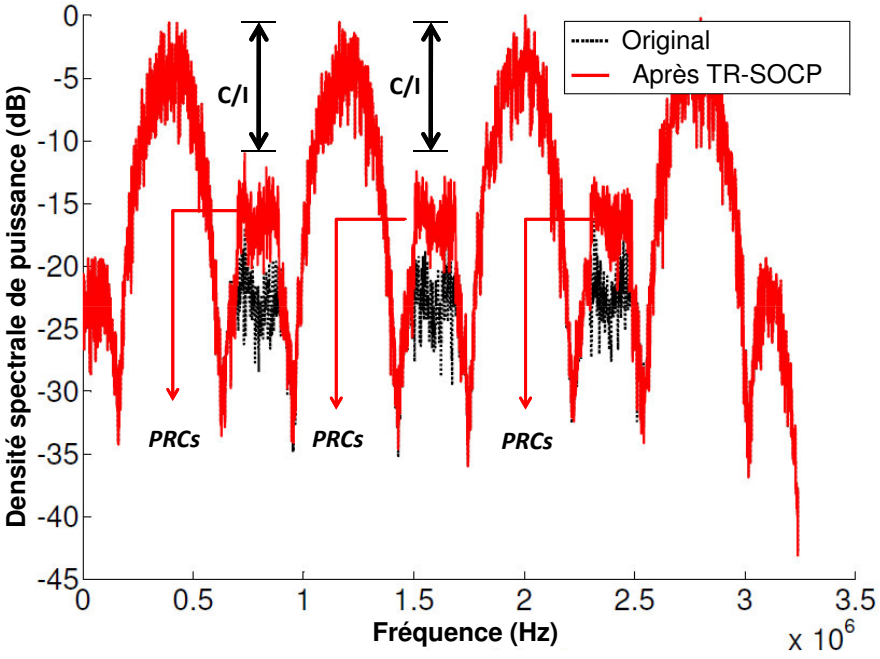

Figure 18: Spectre GSM: avant et après TR-SOCP

Les résultats montrent alors des diminutions moyennes du PAPR de l'ordre de 1.2 dB pour 3 signaux de correction ajoutés (voir Fig. 19). Ces résultats sont très prometteurs car en augmentant encore le nombre de signaux de correction, il est alors possible de fortement baisser le PAPR des signaux GSM et donc de diminuer la forte consommation des stations de base.

5 Variantes de résolution de la méthode "Tone Reservation" pour un signal radio logicielle

Jusqu'à présent, toutes les simulations de réduction de PAPR ont été menées avec l'algorithme SOCP. Nous allons aborder dans cette partie le compromis complexité/performance, mo-

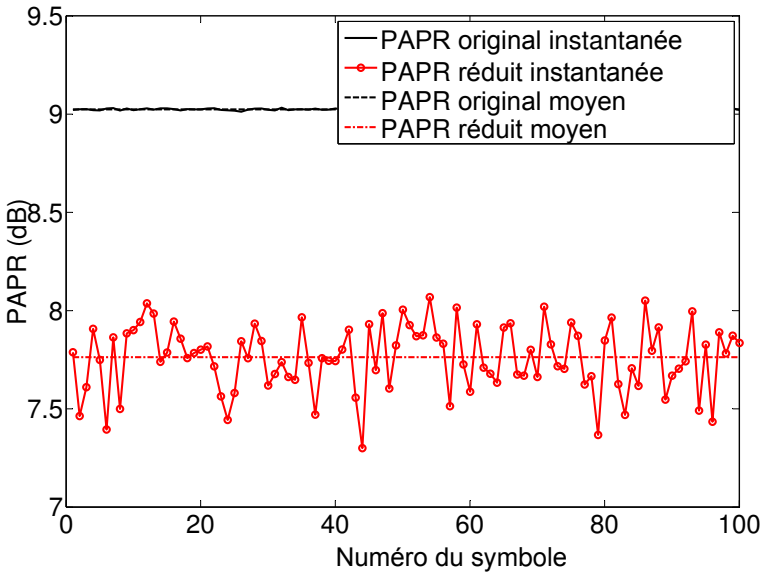

Figure 19: PAPR GSM: avant et après TR-SOCP

tivé par la forte complexité de l'approche SOCP. Deux autres solutions ont alors été utilisées : une basée sur le gradient [17] et une autre sur une approche géométrique [10]. Ces deux méthodes vont fournir des gains de PAPR plus faibles mais avec des complexités plus raisonnables.

5.1 La méthode du gradient

L'approche du gradient utilisée est inspirée de celle développée dans [17].

Le principe général de la méthode du gradient est alors le suivant : Soient A un seuil donné, R l'ensemble des porteuses de correction et μ un paramètre de convergence. Pour $n = 0, 1, \ldots NL-1$, et pour $y_n^{(l)} = x_n + c_n^{(l)}$ le signal au PAPR réduit après la $l^{ème}$ itération, le signal $y_n^{(l)}$ après seuillage s'écrit :

$$\hat{y}_n^{(l)} = \begin{cases} y_n^{(l)} & \text{si} \quad \left|y_n^{(l)}\right| \leq A \\ Ae^{j \arg\left\{y_n^{(l)}\right\}} & \text{si} \quad \left|y_n^{(l)}\right| > A \end{cases} \tag{29}$$

On pose alors :

$$\Delta_n^{(l)} = y_n^{(l)} - \hat{y}_n^{(l)},$$

et la mise à jour des composantes fréquentielles du signal de correction ($c_n^{(l)} = \sum_{p \in K} C_p^{(l)} e^{-2j\pi p \frac{n}{NL}}$) s'effectue selon

$$C_p^{(l+1)} = C_p^{(l)} - \mu \sum_{n=0}^{NL-1} \Delta_n^{(l)} e^{2j\pi p \frac{n}{NL}}. \tag{30}$$

Après itérations, le signal c présente un PAPR réduit.

5.2 Présentation de la méthode géométrique

La méthode temporelle géométrique a été proposée dans [10]. L'objectif est de générer un signal de correction c hors de la bande utile du signal d'origine x de façon à ce que le PAPR du signal $x + c$ soit réduit. Ce signal est ensuite filtré après amplification par un filtre analogique. L'originalité de cette approche réside dans une résolution géométrique simple, d'où son nom. En se donnant un seuil A et des échantillons temporels x_n du signal OFDM, on déduit dans un premier temps les échantillons a_n tels que :

$$a_n = \begin{cases} 0 & , \quad |x_n| \leq A \\ \left(\frac{A}{|x_n|} - 1\right) x_n e^{j\theta_n} & , \quad |x_n| > A \end{cases} \tag{31}$$

Ici $\theta_n \triangleq 2\pi\Delta f \frac{n}{NL} T_s, 0 \leq n \leq NL-1$. Le paramètre $\Delta f \triangleq f_r - f_c$ est la différence entre la fréquence centrale f_r du signal OFDM et f_c du signal ajouté hors bande. Après obtention des échantillons a_n, le signal associé est ensuite filtré (via des opérations de FFT/IFFT) de façon à ne conserver que de l'information sur les porteuses de corrections (ici en dehors de la bande utile). Ce signal temporel $\tilde{a}_n$ est alors pondéré par un coefficient β dont la valeur optimisée est donnée par :

$$\beta^{(opt)} = -\frac{\sum_{n \in S} x_n \tilde{a}_n^*}{\sum_{n \in S} |\tilde{a}_n|^2}, \tag{32}$$

où $(.)^*$ représente l'opération de conjugaison. S est l'ensemble des indices n tels que $|y_n| = |x_n + \beta\tilde{a}_n| > A$. Finalement, le signal transmis y_n à PAPR réduit s'écrit :

$$y_n = x_n + c_n = x_n + \beta^{(opt)} \tilde{a}_n. \tag{33}$$

La Fig.20 illustre le principe de la méthode géométrique.

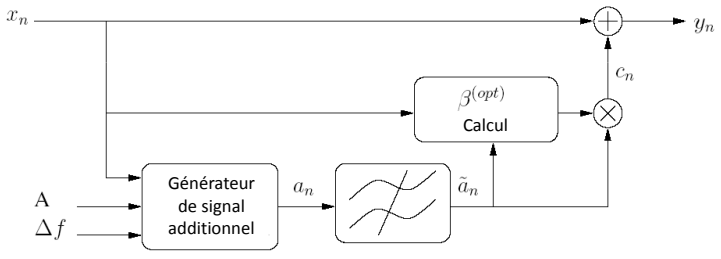

Figure 20: Principe de la méthode géométrique

5.3 Etude du compromis performance/complexité de la méthode Tone Reservation

5.3.1 Présentation du signal radio logicielle utilisé et des conditions de simulation

Le signal radio logicielle utilisé est constitué de deux standards A et B basés sur des formes d'onde type OFDM (voir Fig. 15). Seules les porteuses non utilisées des deux standards sont utilisées pour réduire le PAPR. Une différence de puissance ΔP de 25 dB est supposée entre les deux standards.

Paramètres du système		Paramètres des algorithmes	
δf_1:	0.3125 MHz	μ (Gradient):	5.0
δf_2:	0.0781 MHz	$\Delta f T_s$(Geometric):	1/8
Mapping:	4-QAM	P (Gradient) :	4.0
Inter-standard band:	40 MHz	ΔE(dB):	0.14

Table 2: Paramètres de simulation

Les trois approches (SOCP, gradient et géométrique) sont appliquées pour réduire le PAPR du signal considéré. Les paramètres utilisés sont résumés au Tab.2). Les contraintes de puissance moyenne relative sont identiques pour les trois algorithmes.

5.3.2 Analyse de la réduction du PAPR

Comme cela était prévisible, l'approche utilisant l'algorithme SOCP offre les meilleurs gains en termes de réduction de PAPR (un peu plus de 3 dB) tandis que la méthode géométrique donne les gains les plus faibles (de l'ordre de 1 dB). La méthode du gradient se situent entre les deux.

5.3.3 Analyse de la complexité

La complexité est estimée en comparant le nombre total de multiplications. La méthode SOCP est alors la plus complexe (de l'ordre de 275 fois plus que la méthode géométrique et 14 fois plus que la méthode du gradient). Ceci est illustré au Tab. 3

La méthode du gradient semble donc offrir le meilleur compromis complexité/performance. Le document final montre enfin que le taux d'erreur n'est pas affecté (car les porteuses réservées sont non utilisées) et que les masques des standards sont respectés.

5.4 Réduction de la complexité de l'algorithme SOCP par l'algorithme de FFT tronquée

Nous venons de voir que les meilleurs performances en terme de réduction de PAPR sont obtenues avec l'algorithme SOCP. Etant cependant très complexe, il semble nécessaire de le simplifier. En effet, la réduction du PAPR nécessite d'estimer des composantes fréquentielles C afin que le PAPR du signal temporel $x+c$ soit réduit. Le calcul du PAPR étant fait dans le domaine temporel, un nombre très important d'aller-retour domaine

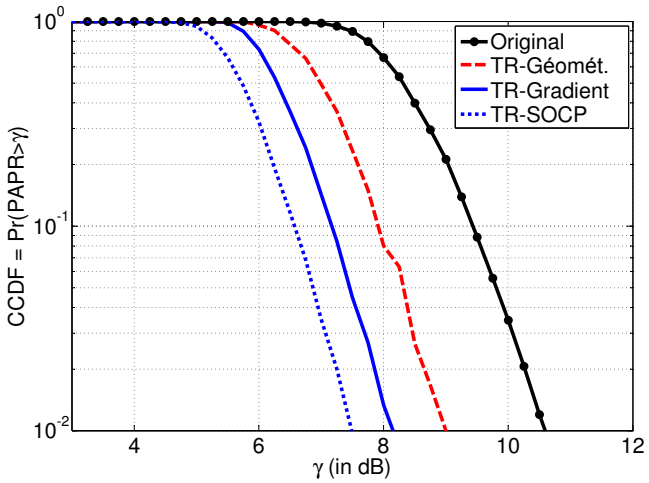

Figure 21: Réduction du PAPR pour les trois approches utilisées pour une même augmentation de puissance relative $\Delta = 0.14dB$

Selon la méthode geometrique	Selon la méthode du Gradient	TR-SOCP
Relations générales de complexité		
$O(NL\log_2 NL)$	$O(NLRP)$	$O(NLR^2)$
Valeurs numériques associées		
$O(3\times 2^{14})$	$O(58\times 2^{14})$	$O(830\times 2^{14})$

NL: IFFT size=1024 × 4=4096; R: =56; P: Itérations=4

Table 3: Comparatif des valeurs numériques de complexité

fréquentiel/domaine temporel sont alors nécessaires, expliquant la complexité importante de l'algorithme. La Fig.22 résume les différentes étapes du processus d'optimisation. Ceci n'est pas uniquement caractéristique de l'algorithme SOCP mais de tous les algorithmes estimant les composantes fréquentielles du signal temporel de correction.

L'objectif de cette partie est alors d'appliquer un algorithme simplifiant le calcul du maximum d'un signal fourni par une transformée de Fourier inverse. Schématiquement, ce maximum n'est pas évalué à partir de tous des échantillons de sortie mais à partir d'une quantité plus faible, sélectionnée selon des critères d'énergie [17].

Le détail de cet algorithme sort du cadre de ce résumé. Le lecteur trouvera les éléments nécessaires dans le document. Cependant l'idée générale est la suivante : chaque étape de l'algorithme de transformée de Fourier rapide discrète inverse fournit un vecteur de taille paire. L'idée de l'algorithme est de ne garder que la moitié de ce vecteur selon le critère du maximum de l'énergie. L'autre moitié n'est plus utilisée. Le calcul de la transformée est alors effectué uniquement sur la moitié conservée et l'on obtient à nouveau un vecteur de taille paire duquel on ne garde que la moitié et ainsi de suite. La fin de l'algorithme fournit le maximum de la transformée avec malgré tout une certaine incertitude due à la possibilité d'éliminer un demi vecteur contenant le maximum. La Fig. 23 montre qu'à chaque étape de la transformée rapide de Fourier, on obtient un vecteur de taille paire.

Les résultats de cet algorithme sont illustrés Fig.24. Ces simulations ont été menées sur un signal OFDM. La courbe référencée "PAPR Réduit" est liée au calcul du maximum avec un algorithme de transformée de Fourier non tronqué (réel). La courbe "PAPR Trunc" fait référence à l'algorithme tronqué. La remarque que l'on peut faire est que les performances ne sont pas aussi bonnes que pour la transformée de Fourier due à l'incertitude mentionnée plus haut. L'utilisation de la transformée tronquée ne peut donc être utilisée comme telle. Une amélioration a été proposée dans ce travail consistant à utiliser conjointement les deux algorithmes (classique et tronqué). Les améliorations sont sensibles, au prix d'une légère diminution du PAPR. Les résultats se trouvent sur la Fig.25.

Aussi la complexité peut-être réduite en utilisant la définition fréquentielle du PAPR qui n'est pas étudié dans ce thèse.

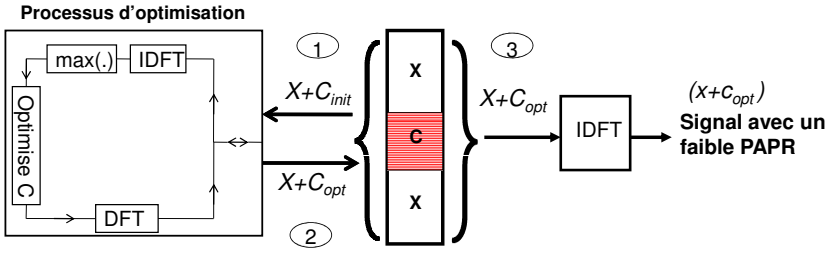

Figure 22: Détail des étapes de l'algorithme de la Tone Reservation

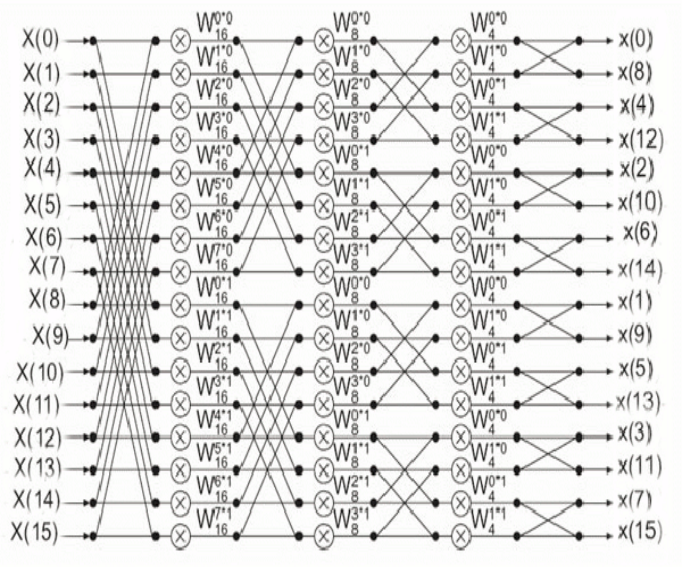

Figure 23: Détail de la FFT sur 16 points à base de radix 2

6 Le PAPR : un capteur de la radio intelligente pour l'accès opportuniste au spectre

6.1 L'accès opportuniste au spectre

La radio intelligente constitue l'évolution naturelle de la radio logicielle à laquelle on associe des capteurs et des organes d'analyse et de prise de décision. Les moyens sensoriels peuvent être en lien direct avec la radio (propagation...) ou le système de communication (consommation de puissance...) mais aussi avec l'environnement sociétal (localisation...) ou le comportement de l'utilisateur (réunion...). La radio intelligente vise donc à ajuster les fonctionnalités du système de communication au contexte d'utilisation sous toutes ses formes. Un des capteurs très largement étudié aujourd'hui est le capteur spectre grâce auquel un terminal intelligent pourra identifier les bandes libres dans son environnement proche (c'est à dire des bandes ne contenant pas de signaux de télécommunications). Ceci est aujourd'hui largement motivé par l'utilisation sous optimale du spectre (voir Fig.26) trop cloisonné et régi par une gestion centralisée [18]. Dans un contexte de radio intelligente, l'utilisateur pourra alors éventuellement accéder à ces bandes libres de façon opportuniste pour établir sa communication. On parle alors d'un utilisateur secondaire qui accède au spectre déjà utilisé par des utilisateurs primaires.
L'accès au spectre n'est pas sans conséquence. En effet, en s'allouant une bande libre, l'utilisateur secondaire risque entre autres d'augmenter le Peak to Average Power Ratio (PAPR) global du signal radio logicielle des utilisateurs primaires. C'est ce paramètre qu'il faut limiter pour ne pas dégrader les performances et en particulier les distorsions introduites par l'amplificateur de puissance. L'objectif est alors de donner une approche fréquentielle du PAPR afin de quantifier les dégradations apportées lors de l'accès au spectre.

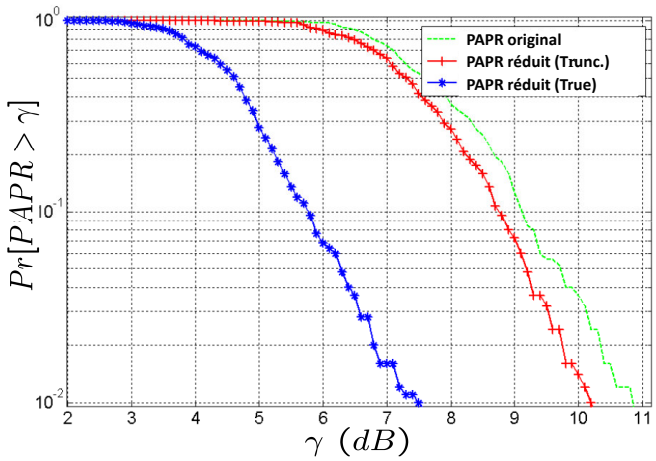

Figure 24: Réduction du PAPR en utilisant deux algorithmes de FFT : classique et tronquée

6.2 Le PAPR : un capteur à prendre en compte pour la radio intelligente

Dans un contexte d'accès opportuniste au spectre d'un signal primaire par un utilisateur secondaire, les caractéristiques de la partie analogique de l'émetteur ne doivent pas être modifiées. Cette partie analogique comprend des filtres, des mélangeurs et des amplificateurs de puissance. Ces derniers focalisent l'attention de cette thèse. En effet, ajouter un signal dans une bande libre se traduit au niveau temporel par une modification des propriétés du signal après accès opportuniste. Ces modifications temporelles viennent alors changer le PAPR initial, ce qui peut avoir des conséquences néfastes dans l'opération d'amplification (saturation, apparition d'intermodulation, ...). Ceci est illustré sur la Fig.27 : après insertion dans le spectre, il peut y avoir saturation du signal à amplifier, amenant deux solutions : un recul (impliquant une baisse du rendement de l'amplificateur) ou une réduction du PAPR (augmentation du rendement). Le PAPR est donc un capteur à prendre en compte au même titre que les autres dans la décision d'accès au spectre. Cependant un outil est indispensable pour connaître l'effet de l'accès au spectre sur le PAPR : une vision fréquentielle du PAPR. Cette approche a été présentée à la fin de la partie 3. En les utilisant, les développements suivants ont alors pour objectif de quantifier analytiquement l'augmentation de PAPR due à l'accès opportuniste dans le spectre.

6.3 Influence de l'accès au spectre d'un signal radio logicielle sur le PAPR

Dans le contexte de la radio intelligente, l'accès au spectre se fait de façon opportuniste en fonction des bandes libres disponibles dans l'environnement proche d'un émetteur. De cette façon, en ajoutant un signal opportuniste secondaire dans les bandes libres d'un signal primaire, le PAPR initial va être modifié et il est alors primordial d'en estimer les

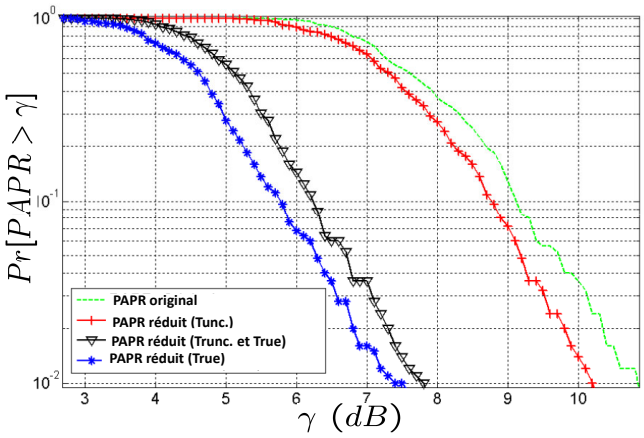

Figure 25: Réduction du PAPR en utilisant une solution conjointe d' algorithmes de FFT : classique et tronquée.

variations. La raison en est la suivante : les points de fonctionnement des amplificateurs de puissance dépendent directement des PAPR des signaux à amplifier. Une augmentation du PAPR entraînerait donc une modification des conditions d'amplification et donc une dégradation des performances. Il est donc important de connaître les variations du PAPR dès lors qu'un signal accède au spectre. La vision fréquentielle du PAPR nous a permis d'apporter une réponse à cette question.

Le PAPR avant insertion du signal est noté $PAPR_p$ (pour utilisateur primaire). Nous avons alors démontré à partir de l'Equ. 21 que le PAPR après insertion du signal de l'utilisateur secondaire est majoré par la somme de deux termes : un terme $PAPR_s$ lié au signal de l'utilisateur secondaire et un terme $PAPR_m$ de corrélation entre les signaux primaires et secondaires. Il est alors possible de maîtriser le PAPR final en fonction des données de l'utilisateur secondaire. Le $PAPR_{temp}$ après insertion est alors majoré par les termes suivants :

$$PAPR_{temp}(S(n)) \leq PAPR_p + \delta_s + \delta_m, \tag{34}$$

avec

$$PAPR_p \approx \frac{\max_{k\in K}(\max_{j\in J}(|\sum_{p\in P} C_{j,p} e^{i2\pi kp/N}|^2))}{\sum_{k=1}^{N} P_m(k)}, \tag{35}$$

$$\delta_s \approx \frac{\sum_{s\in S} P_m(s)}{\sum_{p\in P} P_m(p)} PAPR_s \tag{36}$$

où

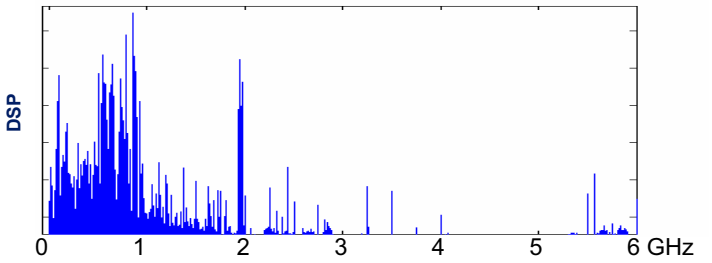

Fréq (GHz)	0~1	1~2	2~3	3~4	4~5	5~6
Utilisation(%)	54.4	35.1	7.6	0.25	0.128	4.6

Figure 26: Illustration de la sous utilisation du spectre

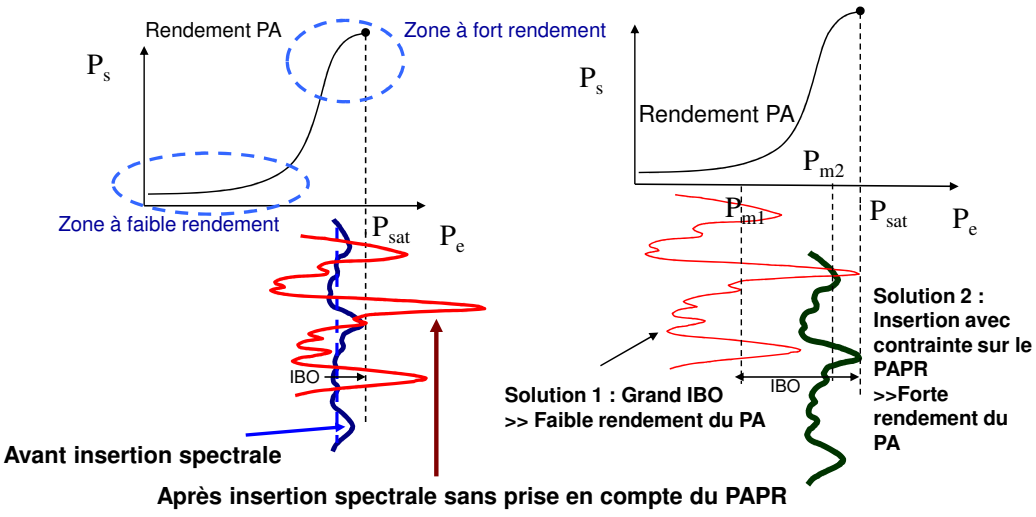

Figure 27: Effet de l'accès au spectre sur le PAPR des signaux à amplifier

$$PAPR_s = \frac{\max_{k\in K}(\max_{j\in J}(|\sum_{s\in S} C_{j,s}e^{i2\pi ks/N}|^2))}{\sum_{k=1}^{N} P_m(k)}. \quad (37)$$

Enfin

$$\delta_m \approx \frac{1}{\sum_{k=1}^{N} P_m(k)}[\max_{k\in K}(\max_{j\in J}(2|\sum_{p\in P} C_{j,p}e^{i2\pi kp/N}|.|\sum_{s\in S} C_{j,s}e^{i2\pi ks/N}|))]. \quad (38)$$

P et S représentent respectivement les ensembles de définition des utilisateurs primaires et secondaires et P_m sont les puissances calculées fréquence par fréquence. $PAPR_p$ et $PAPR_s$ sont respectivement les PAPR des utilisateurs primaires et secondaires.

Cette influence de l'accès au spectre est illustrée sur la Fig.28 où l'augmentation du PAPR suite à l'accès au spectre est clairement mise en évidence. Ces simulations ont été menées sur un signal radio logicielle présenté dans la partie 4.4.1.

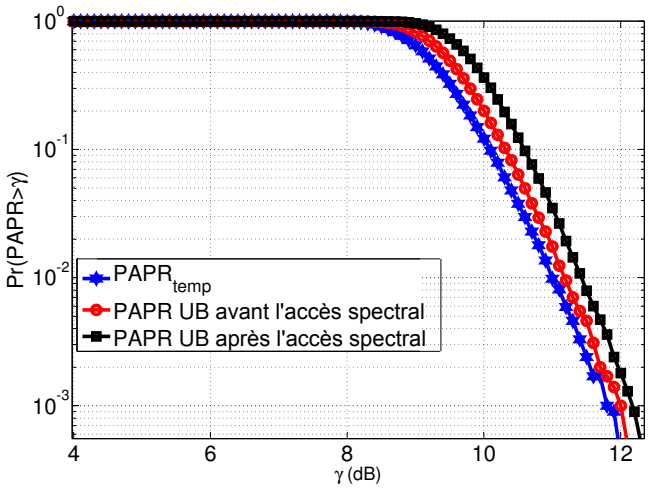

Figure 28: Comparaison des PAPR temporels et fréquentiels

6.4 Schéma conjoint d'accès au spectre

Dans la continuité de ce qui a été présenté ci-dessus, il est alors opportun d'envisager un accès au spectre de façon opportuniste en réservant conjointement des porteuses utiles et des porteuses de correction pour abaisser le PAPR global. En effet, les études précédentes ont montré que l'accès au spectre augmentait le PAPR. Une solution serait donc d'adjoindre à l'utilisateur secondaire des porteuses de correction, directement contigües aux données utiles. Ceci est illustré sur la Fig. 29. Les résultats de la Fig. 30 montrent alors qu'en utilisant 10% de la bande libre pour les porteuses de correction et 90% pour l'information utile, il est possible de gagner près de 1 dB de PAPR. Ces simulations ont été menées sur un signal radio logicielle présenté dans la partie 4.4.1.

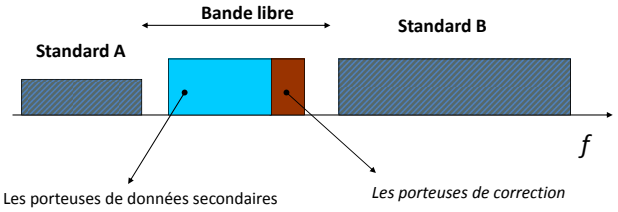

Figure 29: Schéma conjoint d'accès au spectre.

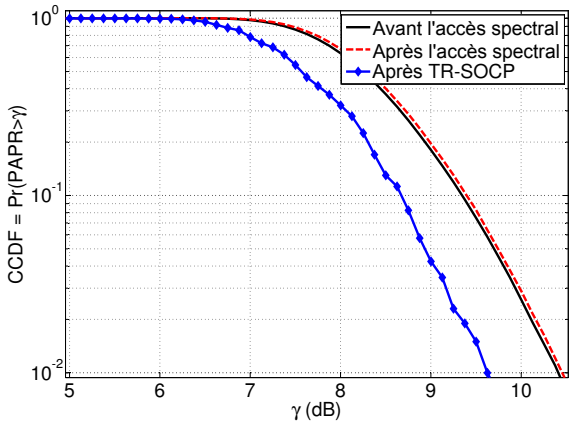

Figure 30: Réduction du PAPR avec accès aur spectre conjoint.

Conclusions et perspectives

Ce travail a permis de mettre en évidence les contraintes liées à l'amplification de puissance d'un signal multistandard dans le contexte de la radio logicielle. Les contributions de cette thèse sont les suivantes :

- expression de la moyenne du PAPR d'un signal continu
- mise en évidence du PAPR d'un signal multistandard et équivalence avec l'OFDM
- proposition de méthodes de réduction du PAPR basées sur la principe de la Tone Reservation
- étude du compromis complexité/performance
- conséquence de l'accès au spectre sur le PAPR dans le contexte de la radio intelligente

La notion de bande libre est de toute importance pour réduire le PAPR d'un signal multistandard. En effet, ces bandes pourront servir non seulement pour transmettre un signal secondaire mais aussi des signaux de réduction de PAPR. La complexité d'un tel traitement reste cependant prohibitive et nécessite des études plus poussées afin de trouver des bons compromis performance/complexité.

General Introduction

For all sorts of telecommunication systems, in order to properly transmit the information, the signal has to be amplified to cope with the channel impairments and attenuations. Hence Power Amplifier (PA) is a vital element in a telecommunication system transmission chain. However, PA is still hard to design because of the key factors related to its performance which include the emitted mask power, battery consumption (linked to power amplifier efficiency), the channel propagation attenuation (linked to power amplifier gain), and the carrier-to-inter modulation ratio requirements (linked to power amplifier linearity). The design problem of PA is exacerbated due to the conflicting parameters of linearity and efficiency: the efficiency is the maximum near the saturation point, the point where non-linear effects are most severe.

In parallel to the PA non-linearity problem, the ever-increasing demands of high data rate transmission, bandwidth improvement, and the greater spectral efficiency have resulted in the birth of several telecommunication standards aiming at the achievement of the above mentioned goals. These standards use almost all the existing physical media capable of broad band data transmission to meet the challenges of highest data rates possible with reliable transmission under any channel conditions. These include both wired (Digital Subscriber Line (DSL), cable etc.) and wireless media. Also the emergence of several standards has lead to the migration of modulation schemes from single carrier to multi carrier. This multi carrier transmission provides considerable immunity to multi path fading and channel impairments. Unfortunately this trend of multi carrier transmission has increased the signal power fluctuations by a great extent, a feature generally characterized by the parameter Peak-to-Average Power Ratio (PAPR). Consequently the efficient power amplification of multi carrier signals in the absence of any special processing induces severe impairments, the well known non-linear distortions. Hence turns up the problem of efficient power amplification of large envelope signals.

In addition to the existing communication standards which 'haphazardly' sprung up to fulfill the ever growing communication demands, there arose the problem of inter compatibility of these standards. Thus the need of a multi standard, multi mode, multi modulation, reconfigurable architecture was felt badly and a system called Software Radio (SWR) [2] was proposed to meet this challenge. It is a system which follows the idea of 'any where, any time' by dynamically configuring its transmission parameters according to channel conditions and resource availability.

Thinking of a SWR base station (BS) which is supposed to transmit a very large band signal comprising of different standards and differently modulated signals, the transmitted signal power variations are supposed to be quite large and in terms SWR signal inherits large PAPR values. Thus the problem of efficient amplification of SWR signals comes into view.

After the introduction of SWR, another term called Cognitive Radio [3] was introduced. This was the natural subsequence of SWR technology. In fact one might argue that Cognitive Radio is basically SWR having some 'brains'. Cognitive Radio, using a set of sensors, senses its environment and under certain constraints establishes the communication. Opportunistic Radio (OR) is a special case of CR which is about finding the unused bands and transmitting over them, the so called idea of dynamic spectrum access. With the dynamic spectrum access, signal dynamics are further increased and when the signal with large dynamics is transmitted through PA, it is bound to generate non linear distortions.

We can say that the problem of PA non linearity which came under spotlight due to multi carrier modulations, has gained further importance in the context of SWR and Cognitive Radio systems.

In fact, PA has been considered as a very important transmitter component since long. So as the problem of PA non linear distortion is not new and has been extensively studied in past for different communication systems. For example,

- For satellite transmission, Traveling Wave Tube (TWT) amplifier is used and its non linear problems are discussed during 80's and 90's [19, 20].
- For multi carriers systems the problem is studied extensively during 90's and 2000's [21].
- Recently, for SWR system a European project, TRUST, highlights this issue [22].
- Also, for Multiple-Input Multiple-Output (MIMO) systems the problem of PA non linearity is discussed [23, 24].

Our goal in this thesis is to study and analyze the PAPR distribution of SWR and Cognitive Radio signals. And then finally contribute to the research in solving the PA non linear distortions problem. In fact, there are two ways proposed in literature to solve this issue,

- Reduce the power fluctuations of the signal by acting on the signal itself using analog/digital processing.
- Linearize the PA using digital processing (pre-distortion, post-distortion).

We shall follow the first option i-e PAPR reduction to tackle the PA non linear distortions issue in SWR and Cognitive Radio context. The whole thesis revolves around this idea presented in six chapters.

The very first chapter **Chapter 1** (Software Radio based Cognitive Radio & Peak to Average Power Ratio) presents all the ingredients used throughout the thesis and defines the problem position. **Chapter 2** (PAPR Analysis of Continuous OFDM Signals) analyzes the PAPR distribution of continuous OFDM signals while **Chapter 3** (PAPR analysis of a SWR signal) does the same for SWR signals. After analyzing the SWR signal we head towards the PAPR reduction of this signal in **Chapter 4** (PAPR reduction of SWR signals) using a specific PAPR reduction method. In **Chapter 5** (Comparison of Tone Reservation based PAPR Reduction Methods for SWR Signals) different PAPR reduction methods are compared in terms of performance and complexity. Finally in **Chapter 6** (PAPR metric based spectrum access in Cognitive Radio context) PAPR problem in the context of Cognitive Radio is discussed.

Now each chapter is briefly delineated here.

Chapter 1 defines and briefly discusses the terms to be used in the thesis. It describes the causes, reasoning and the solutions of the problem to be discussed throughout the document. At first the concept of multi carrier modulation is presented and then that of multi standard system (SWR) which accomplishes the any where, any time radio concept. Finally the concept of Cognitive Radio (CR) is discussed which is nothing but SWR embedded with 'intelligence'. All these systems transmit large power fluctuation signals. The fluctuations are quantified by the term Peak to Average Power Ratio (PAPR). Signals with large PAPR cause problem at the non linear transmitter components like PA. Therefore before dealing the problem of high PAPR, the characteristics of PA are presented. These characteristics uncover that in order to transmit the signal with high PA efficiency, it is necessary to reduce its PAPR. State of the art methods aimed at the PAPR reduction of Orthogonal Frequency Division Multiplexing (OFDM) signals are presented then.

Chapter 2 is dedicated to OFDM, its basic concepts and its PAPR distribution. After presenting the existing rich nomenclature on signal fluctuation quantification, some state of the art OFDM PAPR distribution functions are recalled. Generally Complementary Cumulative Distribution Function (CCDF) is used to measure PAPR. In literature there exist CCDF expressions for OFDM PAPR based on discrete time OFDM signal as well as a couple of expressions for continuous OFDM signals. One of these two distribution functions for continuous OFDM signals is simulation based. We have shown the correctness of this function by analytically proving that the first statistical order of the simulation based and theory based functions are the same. And finally we have formulated a new CCDF expression for continuous OFDM signals [25] which shall be used in the rest of the document. Especially when we talk of SWR signals, the analysis must be performed in Radio Frequency (RF) which in turns means continuous signal analysis and a newly developed PAPR distribution function may help estimate the PAPR behavior of SWR signals to be seen in Chapter 3.

Moving on from OFDM PAPR analysis, **Chapter 3** presents the SWR signal PAPR analysis. As SWR is a multi standard, multi modulation reconfigurable system thus it might inherit high PAPR. We have proved this hypothesis by simulating a SWR signal consisting of multi modulation schemes [26]. Some analogies between OFDM signal and SWR signal are presented. Also, diverting the attention from the traditional PAPR temporal view, a new frequency domain view of PAPR is presented which is more appropriate in the context of SWR signal [27]. In fact the temporal SWR signal is transformed to frequency domain with the help of Discrete Fourier Transform (DFT) and PAPR is calculated on each of the frequency present in the SWR signal. This frequency PAPR view of SWR signals helps in the application of some OFDM PAPR reduction methods to SWR signals to be discussed in Chapter 4.

Next stop, SWR signal PAPR reduction which is presented in **Chapter 4**. As described in previous chapter that frequency domain PAPR view of SWR signal helps the adaptation of OFDM PAPR reduction methods for SWR signals and one of these methods called Tone Reservation (TR) is selected here. TR is selected due to its numerous advantages like downward compatibility, no bit error rate (BER) degradation, no side information (SI) transmission, no data rate loss etc. TR is about reserving some tones which are not specifically used to reduce the data signal peak. Different formulations to obtain the optimized reserved tones are discussed in this chapter and finally Second

Order Cone Programming (SOCP) is selected to obtain the optimized tones. Then the constrained optimization of these tones is presented which not only helps in limiting the additional mean power but also makes it possible to respect different standard spectral mask constraints. After presenting the concept of SWR transceiver, we have performed the SWR PAPR reduction task in small steps, starting from the discussion of reserved tones' parameter influence on mono-band OFDM PAPR reduction performance. Then Multi-band OFDM (MB-OFDM) PAPR reduction is performed and the computational complexity aspect in the PAPR reduction of multi band signals is discussed [28]. Then a bi standard hypothetical SWR signal's PAPR is reduced and the discussion about the influence of reserved carriers' position, power and bandwidth is presented [29]. Also, a more practical scenario of a mono standard SWR signal is presented in the form of a GSM base station (BS) transmitter which amplifies a multi GSM channel signal. This signal has high PAPR which is reduced by allocating the unused GSM carriers in that BS for creating peak reducing signal using TR. The power level on these carriers is limited to respect GSM spectrum mask and carrier-to-interference (C/I) values specified for GSM system.

TR-SOCP is not the only TR implementation scheme and thus it is compared with some other TR implementation schemes like TR-Gradient method and TR-Geometric method in **Chapter 5**. The details of TR-Gradient and TR-Geometric methods are presented and then all the three methods are implemented for Wireless Local Area Network (WLAN) standard first [30] and for a SWR signal afterwards. This chapter compares the performance of these TR methods in terms of PAPR reduction capabilities and computational complexities while justifying that BER remains unvaried upon the application of these methods. Also it is proved that no out of band interference is generated upon the application of these PAPR reduction methods. It is seen that there exist a performance vs complexity trade-off. Performance comparison of these methods is performed for a multi channel GSM standard as well. Finally Truncated Inverse Discrete Fourier Transform (IDFT) algorithm is presented aiming at the reduction of computational complexity of these methods [31].

Last chapter **Chapter 6** deals with the analysis of PAPR in Cognitive Radio context. As discussed earlier that Cognitive Radio signals are in effect SWR signals. The spectrum sensors sense the available bandwidth and transmit under certain constraints like the Quality of Service (QoS) of the primary (licensed) users should not be affected on spectrum access. A new constraint is introduced in this chapter which is PAPR constraint. Spectrum should not be accessed such that it increases the PAPR of Cognitive Radio signal otherwise distortions would occur on the PA stage. Initially the effect on PAPR is observed when the spectrum is accessed dynamically keeping the primary data constant in order to see the variations in PAPR just because of secondary data variations. And then a more practical scenario is discussed where not only secondary data but also the primary data varies in time and the effects on PAPR are observed. Sticking to the frequency domain PAPR view presented in Chapter 3, an upper bound on the variations in PAPR due to dynamic spectrum access is presented [32]. Finally spectrum access is used in a two fold manner by assigning a major share of free spectrum to the secondary data while a small proportion of free spectrum is used to reduce PAPR. Thus the double purpose use of free bandwidth not only makes sure that secondary user benefits from spectrum access but also the spectrum access is performed without increase in PAPR.

Finally general conclusions are drawn along with the presentation of certain perspectives.

Chapter 1

Software Radio based Cognitive Radio & Peak to Average Power Ratio

Contents

1.1 Introduction

This chapter presents the over all picture of the thesis report and can be considered as a detailed introduction. It was considered necessary to outline the problem statement, its reasons and the solutions before going into the profound details. Starting with the multi carrier modulation, Orthogonal Frequency Division Multiplexing (OFDM) details, we discuss the pros and cons of OFDM.

The focus was then turned to an other multi carrier scheme called Software Radio (SWR) which accomplishes the any where, any time radio concept. SWR is basically a multiplex of different standard signals which makes its signal a multi carrier signal. And finally the concept of Cognitive Radio (CR) is discussed which is nothing but SWR embedded with 'intelligence'. It's about sensing the environment and changing the radio parameters accordingly. One of the sensors is spectrum access sensor which is about sensing the free spectrum and the transmission of information over this spectrum.

It turns out that multi carrier signals like OFDM suffer from high power fluctuations quantified by the term Peak to Average Power Ratio (PAPR). Signals with high PAPR when passed through non linear transmitter components like mixer, power amplifier etc. generate distortions. Therefore, it is essential to understand the characteristics of power amplifier which are described after defining PAPR. It is of utmost importance to decrease PAPR in order to increase power amplifier efficiency. There exist several OFDM PAPR reduction methods in literature. All these methods come with some advantages and disadvantages. Few compromise on data rate, some on Bit Error Rate (BER) while others on receiver modifications. The focus in this thesis is to select a method which can reduce PAPR without modifying the existing standard configuration with minimal side disadvantage and then apply it on SWR and CR signals. A method called Tone Reservation (TR) was selected based on its properties that fulfill our requirements and shall be used to reduce SWR (CR) signal PAPR.

1.2 OFDM - A multi carrier modulation

OFDM is a multi carrier modulation scheme. Before going into the details of OFDM, a brief history of the research works on OFDM is presented.

1.2.1 History of OFDM

The idea of multi carrier transmission is quite old, introduced in the mid-sixties at first. In 1966, Chang showed that multi carrier modulation can solve the multi path problem without reducing data rate [33]. This is generally considered the first official publication on multi carrier modulation. Since then OFDM has made a non-ceasing progress as depicted in Table. 1.1 [34].

Year	Milestone
1966	First OFDM scheme proposed by Chang [33] for dispersive fading channels.
1967	Saltzberg [35] studied a multi-carrier system employing Orthogonal QAM (O-QAM) of the carriers.
1970	U.S. patent on OFDM issued [36].
1971	Weinstein and Ebert [1] applied DFT to OFDM modems.
1980	Hirosaki designed a subchannel-based equalizer for an orthogonally multiplexed QAM system [37].
	Keasler et al. [38] described an OFDM modem for telephone networks.
1985	Cimini [39] investigated the feasibility of OFDM in mobile communications.
1987	Alard and Lasalle [40] employed OFDM for digital broadcasting.
1991	ANSI ADSL standard [41].
1994	ANSI HDSL standard [42].
1995	ETSI DAB standard [43]: the first OFDM-based standard for digital broadcasting systems.
1996	ETSI WLAN standard [44].
1997	ETSI DVB-T standard [45].
1998	ANSI VDSL and ETSI VDSL standards [46, 47].
	ETSI BRAN standard [48].
1999	IEEE 802.11a WLAN standard [49].
2002	IEEE 802.11g WLAN standard [50].
2004	ETSI DVB-H standard [51].
	IEEE 802.16 WMAN standard [52].
	Candidate for IEEE 802.11n standard for next generation WLAN [53].
	Candidate for IEEE 802.15.3a standard for WPAN (using MB-OFDM) [54].
2005	Candidate for 4G standards in China, Japan and South Korea (CJK) [55].
2008	ETSI DVB-T2 standard [56].

Table 1.1: OFDM Milestones

1.2.2 OFDM modulation principle

In a conventional serial transmission, the data symbols are transmitted sequentially such that the frequency spectrum of each data symbol occupies the entire available bandwidth. While in parallel data system many data symbols are transmitted simultaneously such that the spectrum of an individual data element normally occupies only a small part of the whole available bandwidth. OFDM is special case of parallel transmission where the available bandwidth is shared among the orthogonal carriers with some portion of each carrier overlaps with the adjacent carriers .

In the OFDM scheme of Fig. 1.1 the serial data stream is passed through a serial-to-parallel converter which splits the data into a number of parallel channels. The data in each channel is applied to a modulator, such that for N channels there are N modulators whose carrier frequencies are f_0, f_1, ..., f_{N-1}. The frequency gap between adjacent channels is Δf and the overall bandwidth is B. Thus the bandwidth occupied by N carriers is $N\Delta f$. In the conventional serial transmission, the traffic data is applied directly to the modulator, transmitting at a carrier frequency positioned at the center of the transmission band and the modulated signal occupies the entire bandwidth B. By contrast, during an N-symbol period of the conventional system, each of the N OFDM sub channel modulators carries only one symbol, each of which has an N time longer duration.

The major advantage of OFDM is that because the symbol period has been increased, the channel's delay spread becomes significantly shorter fraction of a symbol period than in the serial system, making the system less sensitive to channel induced dispersion than the serial system. Another drawback of OFDM systems when transmitted through parallel analog modulators, is their complexity, because of the need of N analog modulators, receiver filters and demodulators. This is particularly relevant since, in order to achieve high resilience against fades in the channel, the block size N must be reasonably large, requiring a large amount of sub channel modems.

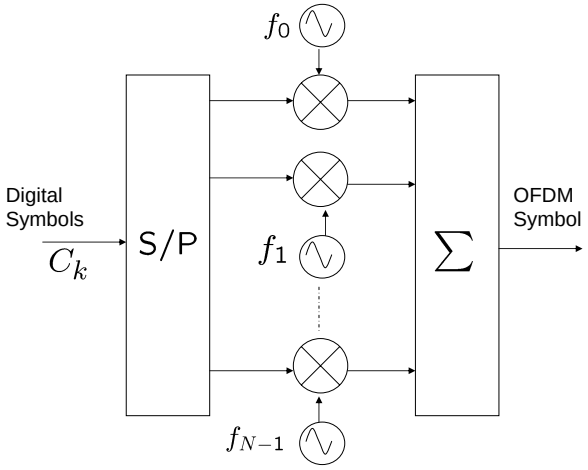

Figure 1.1: Block diagram of OFDM modulator

In Fig. 1.1 the symbols C_k ($C_k = a_k + jb_k$) are the complex numbers defined according to the constellation of the mapping scheme like Quadrature Phase Shift Keying (QPSK), Quadrature Amplitude Modulation (QAM) etc.

The sequence of N digital symbols $\{C_0, C_1, ..., C_{N-1}\}$ constitute the input to generate an OFDM symbol. The k^{th} symbol C_k is carried by frequency f_k thus the resulting signal becomes: $C_k e^{2j\pi f_k t}$ and the overall output signal can be written as,

$$s(t) = \sum_{k=0}^{N-1} C_k e^{2j\pi f_k t}, \quad t \in [0, T], \tag{1.1}$$

where T is the OFDM symbol duration and $s(t) = s_I(t) + js_Q(t)$ is the complex OFDM symbol envelope.

The carrier frequencies become orthogonal as the spacing between any two consecutive frequencies is $\frac{1}{T}$. This orthogonality can be mathematically justified by considering the scaler product in the vector space defined by the base function of the complex exponentials $e^{2j\pi f_k t}$, $0 \leq k \leq N-1$. In fact, each carrier modulating a symbol during a rectangular time window of duration T, is equivalent to a sinc function ($\sin x/x$) in frequency domain, which is zero at all the multiple of $\frac{1}{T}$ (Fig. 1.2). Following,

$$f_k = f_0 + \frac{k}{T}, \qquad k = 0, 1, ..., N-1, \tag{1.2}$$

are the orthogonal frequencies. Here f_0 represents the first carrier frequency.

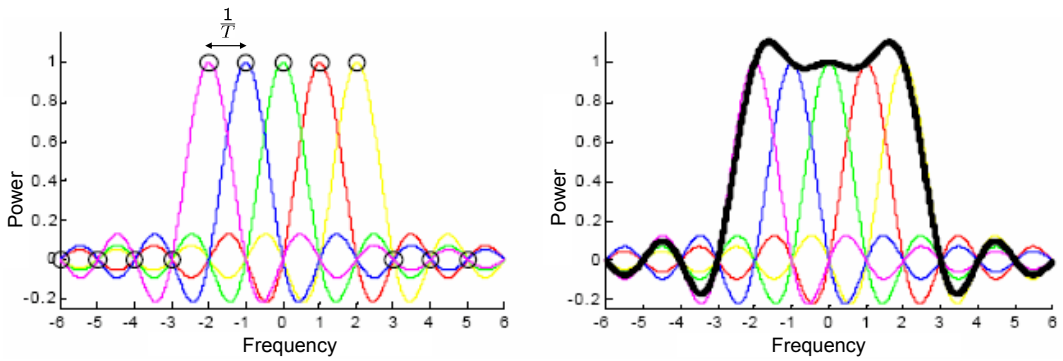

Figure 1.2: OFDM symbol spectrum vision (a) individual carriers (b) the whole symbol

When sampling is performed at the rate of f_k, the signal is detected properly as the power from only one signal is detected while the rest have zero values at the sampling point. Thus inter carrier interference is null and the spectrum is utilized in an optimal manner.

1.2.3 OFDM employing FFT

The complexity issue is resolved if the sub channel modulators/demodulators are implemented using the computationally efficient pair of Inverse Fast Fourier Transform (IFFT) and Fast Fourier Transform (FFT) [1].

According to Eq. (1.1), using Eq. (1.2), $s(t)$ could be written as,

$$s(t) = \sum_{k=0}^{N-1} C_k e^{2j\pi \frac{kt}{T}}, \quad t \in [0, T]. \tag{1.3}$$

with $f_0 = 0$. One can recall the formula of Discrete Fourier Transform (inverse) transformation.

$$x(n) = \sum_{k=0}^{N-1} X_k e^{2j\pi kn/N}, \quad 0 \leq n \leq N-1. \tag{1.4}$$

where X is the frequency domain information vector of size N carried over N orthogonal carriers to make a temporal signal x. The duration of symbol x is T. Making the analogy, one can transmit N mapped symbols C_ks by using Inverse Discrete Fourier Transform (IDFT).

Thus the discrete OFDM symbol can be obtained by sampling the signal at Nyquist sampling frequency. Thus the base band discrete OFDM signal $s(n)$ can be written as,

$$s(n) = \sum_{k=0}^{N-1} C_k e^{2j\pi \frac{kn}{N}}, \quad 0 \leq n \leq N-1. \tag{1.5}$$

The parameter N of OFDM systems is always a power of two ($N = 2^n$ with n being an integer) so as to employ the more computationally efficient Inverse Fast Fourier Transform (IFFT) algorithm as shown in Fig. 1.3 :

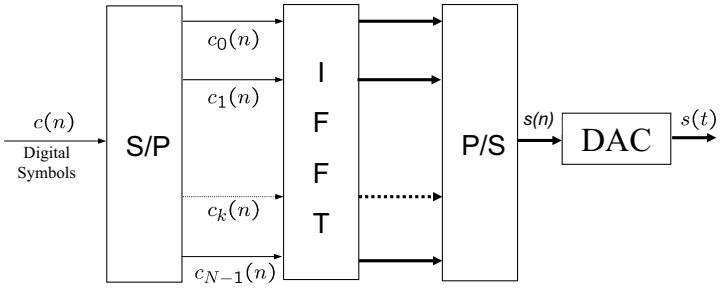

Figure 1.3: Digital OFDM modulator

1.3 Software Radio system

After describing a multi carrier system we head towards a multi standard system which is called Software Radio (SWR). The ideal SWR system will adapt itself to the transmission scenario by gathering information about all of the signals that are present in the air interface and using a single front-end receiver it shall operate on any modulation, channel bandwidth, or carrier frequency [57].

1.3.1 A brief history of Software Radio system

In 1992 Joseph Mitola was the first person to introduce the term "Software Defined Radio", who published the first paper on the topic [2]. And then one of the first public SDR initiatives was a U.S. military project named SpeakEasy [58]. The primary goal of the SpeakEasy project was to use programmable processing to emulate more than 10 existing military radios, operating in frequency bands between 2 and 2000 MHz. Further, another design goal was to be able to easily incorporate new coding and modulation standards in the future, so that military communications can keep pace with advances in coding and modulation techniques.

In year 2000 then, Mitola defined the ultimate goals of SDR by saying that SDR is a radio that employs model based reasoning to achieve a specified level of competence in radio-related domains [3]. It is the point where devices themselves detect the user needs and available resources without human intervention and allocate the appropriate resources to fulfill those demands. This is the basic ideology of the Cognitive Radio systems to be discussed later in this chapter.

1.3.2 Sectors interested in SWR development

1.3.2.1 Industrial sector

This sector has got the most interest in SWR development because of the economical reasons. As the reconfigurability of the terminals comes with the software so the hardware of the new devices shall be easy and rapid to fabricate. Eventually it will decrease the terminal cost. Anyways, some industrialists have shown their concern on the sale of their terminals as they fear it will decrease because of the reconfigurability of the old terminals.

1.3.2.2 Service providers

Service providers are going to benefit the most from SWR technology. The deployment of a cellular network costs a lot and it hinders the technology development. With the SWR it would be very easy to test and apply the new services. Also the investment and maintenance cost of the service providers shall be reduced greatly. In other words it helps in the deployment of new services, network and services convergence and dynamic spectrum access.

1.3.2.3 Users

Users or consumers will also benefit from SWR systems as they would be able to talk any time, any where under any conditions. Also with the operators' competition to provide more and more services, user will benefit from low costs and better quality. Moreover, same devices would be reconfigured for new services and the expenditures of buying new terminals for new services will be avoided.

1.3.3 Software Radio and Software Defined Radio

The discussion in this section is taken from [59].

1.3.3.1 SWR

The ideal concept of SWR is that it is an architectures totally based on software and in terms all the processing is performed on the digital signal. This 'all digital' architecture concept allows the (de) modulation of one or more channels without filtering and down conversion of the analog signal. The general architecture of SWR is shown in Fig. 1.4. As it could be seen that the conversions are performed straight after the antenna and all the signal processing is done in digital domain making the architecture totally reprogram able.

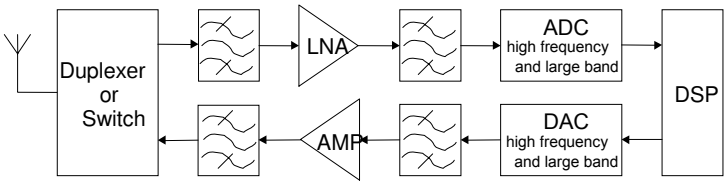

Figure 1.4: Ideal SWR block diagram.

1.3.3.2 SDR

As the realization of SWR is not possible right now and in the near future so sub optimal architecture was proposed called Software Defined Radio (SDR).

The technology has not progressed so far that all the processing can be done on digital signal so a redefined goal of moving the digital part as close as possible to antenna was set. Doing this would mean that after the antenna there is analog processing, followed by analog to digital conversions and then the digital processing which would be reconfigurable as shown in Fig. 1.5. In this figure AFE stands for 'Analog Front End' for all the analog processing and DFE is for 'Digital Front End' for digital processing. Also ADC stands for 'Analog to Digital Converter'.

Figure 1.5: Practical SWR architecture.

Currently the three functions supposed to be performed by DFE are,

1. IQ Transposition: Convert the real digital signal at the output of ADC into base band complex signal.
2. Sampling frequency conversion: To convert the digitized band to symbol or chip frequency.

3. Channel selection: Selection of useful bands from the the whole system band.

All the three functions are shown in Fig. 1.6.

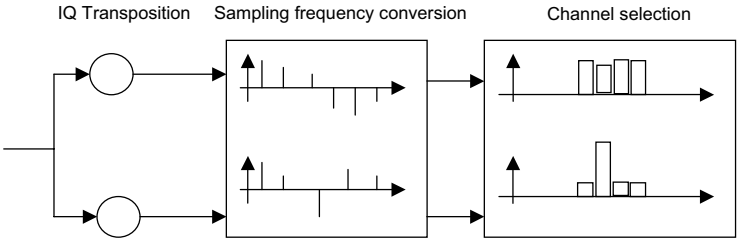

Figure 1.6: DFE functions.

1.3.4 SWR architecture

This section provides an overall picture of all the possible structures of SWR. The figure shown (Fig. 1.7) is taken from AS 37 Software Radio project [60] and it provides all the different possibilities that could lead to a SWR or SDR architecture. As it could be seen that depending upon the functionalities performed at Analog Front End (IF conversion, sampling, IQ conversion), there are different variants of SWR/SDR architecture varying from 'Mono SDR IF & upsample IQ' to 'Monochannel SWR' in a SWR terminal context and from 'SDR IF & upsample IQ' to 'Ideal SWR' in a SWR Base Station (BS) context.

1.3.5 Implementation constraints of SWR

It seems as if the implementation of SWR technology will take at least a decade to be implemented in a complete sense as there are some constraints which are outlined below,

- Analog to Digital Conversion: Analog to digital conversion of a wide band is still not possible as at the SWR base station, especially, the signal transmitted is of different standards and different bands. Hence, the converters with not only a very high sampling frequency would be needed but also they would need to take into account the variations in symbol frequency from one standard to the other standard. In fact, the sampling frequency for the large band SWR signal might have nothing to do with the symbol frequency of any standard present in the SWR signal.
- Terminal consumption: As the signal with large dynamics should be backed off to avoid non linearities, more battery consumption is supposed to take place. So either the amplifiers should be linearized or the methods should be discovered to reduce signal dynamics. Also due to the high computational complexity of the multi-standard system, the terminal consumption is bound to increase with all the processing need to to be done to provide high data rate multimedia services.
- Reconfigurable architecture: The architecture which is totally reconfigurable under all conditions for a large band is still not perceived.

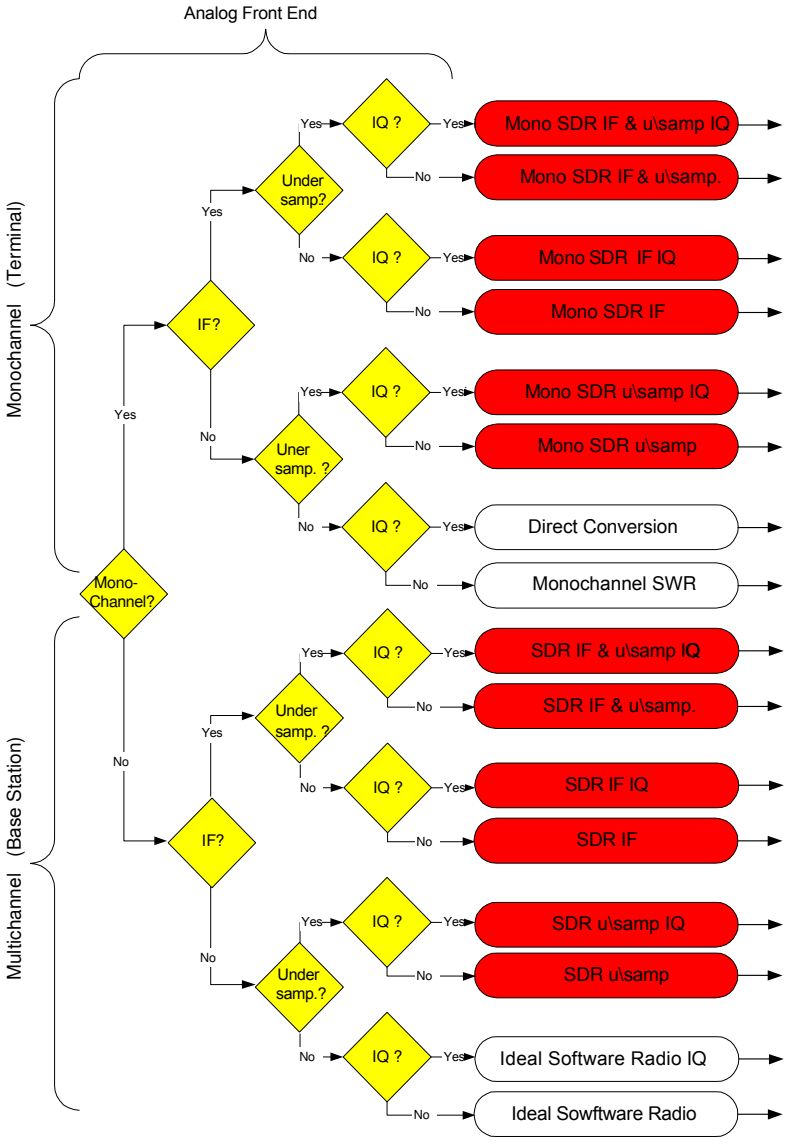

Figure 1.7: All the possibilities of a SWR/SDR receiver.

- Non-linear amplification: As the SWR signal is a multiplex of single and multi carrier signals, it is supposed to have large dynamics (to be discussed in details in the following sections). Today's amplifiers are unable to amplify without non linearities the signal with very large dynamics and occupying a very large band. In this thesis the problem of non-linear amplification is of specific interest.

Based on SWR technology, the concept of Cognitive Radio evolved which superficially means the embedding of 'intelligence' to SWR system. This concept is detailed in next section.

1.4 Cognitive Radio system

Due to rapid developments in the telecommunication field many high data rate services have surfaced up. Several protocols, terminals and standards are developed to satisfy the increasing high data rate demands. Ever so scarce radio spectrum is even more congested with these standards and thus optimized spectrum utilization has become a vital research issue. CR with SWR technology at its heart promises the solution to this mingling standard scenario with intelligent spectrum access for all sorts of signals. Few basic definitions for CR are presented here to elaborate the term.

1.4.1 CR definition

The term "Cognitive Radio" was first coined by Mitola in 1999 [3]. But before presenting his definition of CR we would like to go a little back in history and appreciate the vision of Shannon who vaguely introduced the idea way back in 1948 [61]. In fact three landmark papers written by Shannon at Bell Labs [61, 62, 63] can be considered as historical work regarding reconfigurable techniques. Like a piece of introduction from [63] is presented here,

"This paper is concerned with the problem of constructing a computing routine or a "program" for a modern general purpose computer which will enable it to play chess. Although perhaps of no practical importance, the question is of theoretical interest, and it is hoped that a satisfactory solution of this problem will act as a wedge in attacking other problems of a similar nature and of greater significance. Some possibilities in this direction are:-

1. Machines for designing filters, equalizers, etc.
2. Machines for designing relay and switching circuits.
3. Machines which will handle routing of telephone calls based on the individual circumstances rather than by fixed patterns.
4. Machines capable of translating from one language to another.
5. Machines for making strategic decisions in simplified military operations.
6. Machines capable of orchestrating melody.
7. Machines capable of logical deduction."

As it could be seen that work by Shannon well and truly gave the vision for reconfigurable architecture termed as 'machines' bearing 'mind'. Thinking of a 'computer' which could intelligently move the pieces of chess while playing against 'man'(or against itself for that matter) according to the moves made by its opponent player or dynamic routing of the telephonic calls according to the limitations of circuit resources were the few examples to pave the vision to embed 'intelligence' in 'machines' which could reconfigure themselves according to their environments and requirements. And then late 1970's saw the partial implementation of Shannon's ideology in both the U.S. and Europe. But the term "Cognitive Radio" had to wait till late 90's to be defined by Mitola.

1.4.1.1 Mitola's Definition

Mitola gave the following definition of CR [3],

"A radio or system that senses, and is aware of, its operational environment and can dynamically and autonomously adjust its radio operating parameters accordingly."

According to Mitola, CR is an SWR that is aware of its environment and its capabilities, alters its physical layer behavior and is capable of following complex adaptation strategies. It learns from the previous experiences and deals with the situation not planned at the initial design stages.

1.4.1.2 FCC Definition

According to Federal Communication Commission (FCC) [64],

"A radio frequency transmitter/receiver that is designed to intelligently detect whether a particular segment of the radio spectrum is currently in use, and to jump into (and out of, as necessary) the temporarily-unused spectrum dynamically, without interfering with the transmissions of other authorized users."

This FCC definition is given in the context of spectrum allocation and utilization. In a release on 30th December 2003 [65], FCC made sure that CR technology is considered as the future of telecommunication by saying,

"We recognize the importance of new cognitive radio technologies, which are likely to become more prevalent over the next few years and which hold tremendous promise in helping to facilitate more effective and efficient access to spectrum."

"We seek to ensure that our rules and policies do not inadvertently hinder development and deployment of such technologies, but instead enable a full realization of their potential benefits."

1.4.2 CR Architecture

As could be seen from the CR definitions that SWR is core technology of CR. As shown in Fig. 1.8 that CR is about flexible and reconfigurable architecture like SWR. It supports broad range of frequencies, air interfaces and application software. Also it changes its initial configuration to satisfy user requirements.

Thus with the help of sensors, free spectrum is sensed and because of the reconfigurable features of SWR, that spectrum is utilized to serve the secondary users. The spectrum access scenario is explained in next section.

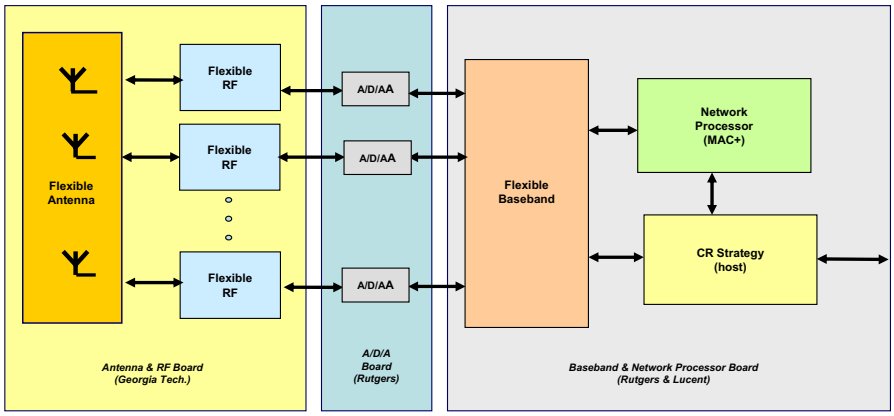

Figure 1.8: SWR based CR block diagram.

1.4.3 Spectrum access in CR

As discussed earlier that SWR technology based CR refers to self-aided and self-established reconfigurable communications where decisions of reconfiguration are taken with the help of a set of sensors. One of these sensors is the spectrum sensor which using an opportunistic approach senses any available bandwidth and thus assists in establishing communication on suitable frequencies.

1.4.3.1 Under utilization of radio spectrum

The following Fig. 1.9 shows the under utilization of spectrum [18]. It should be kept in mind that these measurements were taken in a specific environment and during specific times and can not be generalized. The steps were taken by FCC to better make use of this spectrum.

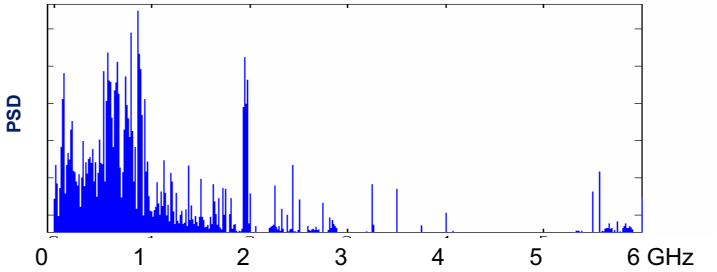

Freq (GHz)	0~1	1~2	2~3	3~4	4~5	5~6
Utilization(%)	54.4	35.1	7.6	0.25	0.128	4.6

Figure 1.9: Under utilization of the radio spectrum.

FCC established a task force SPTF (Spectrum Policy Task Force) in June 2002 to provide road map for spectrum management [66]. It was an initiative to promote new technologies and encourage efficient spectrum use. It provided the guiding series of rule makings, unlicensed use of licensed spectrum targeting the efficient spectrum sharing without interference.

In the SPTF 2003 report it is said that more services and users can be accommodated through the "time dimension" and that the markets determine the best use. In fact 88% of spectrum is quiet on average [67] and there is a great need to "recover" the wasted spectrum resources. And thus there are a lot of ways discussed in literature to "recover" the spectrum [68].

Contrary, in another study [69], it is said that these measurements are misleading and CR has not as bright future as majority thinks.

1.4.3.2 Dynamic Spectrum allocation in CR context

From the above discussion it could be concluded that the inefficient use of spectrum resources is the cause of scarcity of spectrum. Most of the spectrum goes in the dust bin without being utilized. Through CR technology, one of the tasks is to dynamically access and use the non utilized spectrum. This dynamic spectrum access and allocation will make sure that the spectrum is used in an efficient way. Fig 1.10 gives a rough idea how the spectrum can be accessed on free time and frequency slots.

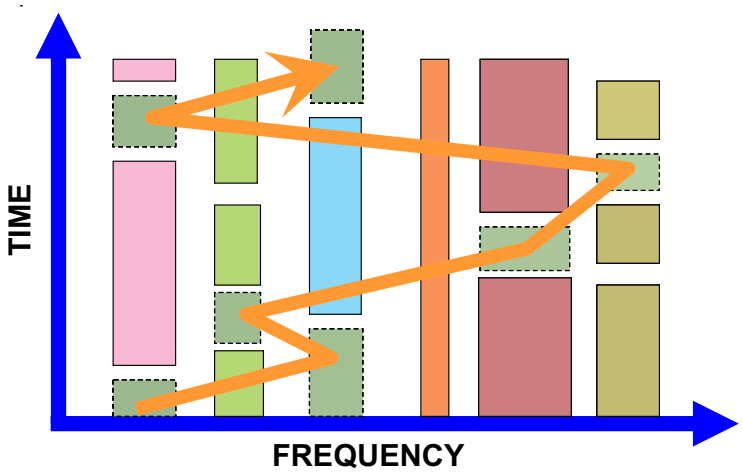

Figure 1.10: Dynamic Spectrum allocation through CR.

1.4.3.3 The inconveniences of spectrum access

In the spectrum access scenario, a terminal should be able to access any available bandwidth in order to fulfill its data needs. Anyhow, this spectrum access in a CR context makes sense only if the bandwidths proposed by spectrum sensor do not imply any modification to the terminal's Analog Front End (AFE). AFE consists of elements like filters, antennas, power amplifiers etc. The design and performance of these AFE components

depend upon temporal and spectral properties of the signal, for example, antennas are designed for a specific frequency range or amplifier design is input amplitude dependent etc.

Also spectral characteristics affect temporal signal properties like signal bandwidth and constellation size relation for a specific data rate demand. Moreover, spectrum access can result in out of band distortions. This results in decrease of Adjacent Channel Power Ratio (ACPR) which degrades system performance as bit error rate increases.

Concluding, spectrum access can affect terminal's AFE design and also temporal signal characteristics. As CR should not modify AFE design thus spectrum should be accessed as to keep signal's temporal and spectral properties within AFE design limits. One of the AFE's elements, Power Amplifier (PA), is of particular interest in this thesis. This element is particularly sensitive to high fluctuating signals due to its well known non linear characteristics which shall be discussed shortly.

1.5 Signal Power fluctuations & Power Amplifier non linear distortions

After describing the details of a multi carrier and multi standard signals, a very basic property of these signals is discussed. This property is about power fluctuations of the signal after modulation. To better elaborate the phenomenon, single carrier power fluctuations are discussed first followed by multi carrier fluctuations study. Consequences of power fluctuations of a signal on its transmission are detailed after wards.

In single carrier communication like the transmission of a QPSK modulated carrier, the data is transmitted over a single carrier frequency. Thus the power fluctuations of this signal depend upon the constellation scheme and shaping filter characteristics. For example in case of amplitude modulations like QAM, more power fluctuations should be observed compared to phase modulations like QPSK as maximum power is more than mean power of the symbols in case of amplitude modulation contrary to phase modulations where maximum and mean power of the symbols are same. Also the characteristics of the shaping filter affect the signal envelope, as in case of Root Raised Cosine (RRC) filter, the envelope varies with the change in filter's roll-off factor. Fig. 1.11 shows the power fluctuations of QPSK modulated single carrier signal with roll-off factor of 0.22.

In general, the power fluctuations of a single carrier signal are not very large. It means that the signal amplitude does not vary a lot around absolute mean amplitude value of the signal.

1.5.1 Power fluctuations in multi carrier signal context

In case of multi carrier communication like OFDM, a large number of sub carriers are added simultaneously to make a multi carrier signal (Eq. 1.5).

According to the central limit theorem, when a large number of identically independent and identically distributed (i.i.d) random variables are added simultaneously, their distribution becomes Gaussian which means that there is a big gap between mean and maximum values. As OFDM signal can be treated like a summation of many i.i.d random variables, its distribution tends to be Gaussian following the central limit theorem which results in high power fluctuations as shown in Fig. 1.12.

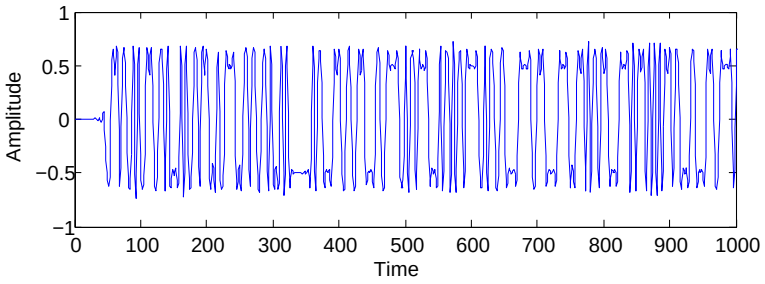

Figure 1.11: Amplitude fluctuations in single carrier signals

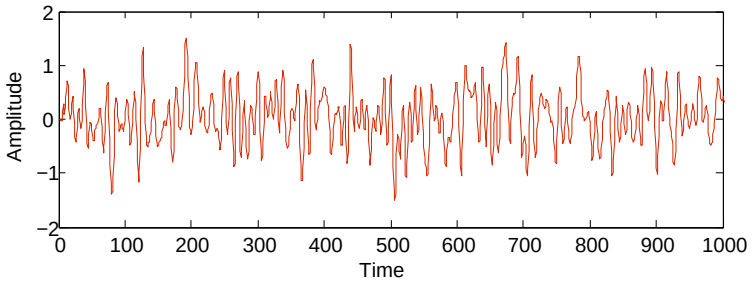

Figure 1.12: Amplitude fluctuations in multi carrier signals

1.5.2 Consequences of high power fluctuations

When a signal with high power fluctuations is passed through a non linear device like converter, power amplifier etc. it is distorted. This non linear process results in in-band and out-of-band distortions creating interference and bit error rate (BER) degradation. The scenario could be better understood if the non linear characteristics of power amplifier are discussed.

1.5.3 Transmitter non linear components

The transmitter consists of different non linear components like digital to analog converter, mixer and power amplifier. The main concern out of these non linear components is about high power amplifier (HPA). High power amplification is required to transmit an RF signal and to counter the channel fading affects [70] and this is done with the help of HPA. When a signal with high power fluctuations is passed through HPA, it gets distorted if the precautionary measurements are not taken. These precautionary measurements include HPA operation in its linear region such that the peaks of the signal to be amplified never enter into non linear amplifier zone. This way of HPA operation leads to a high battery consumption penalty. Therefore, the other measurement could be the processing of the signal to be amplified before the power amplification which means the reduction of the peak values of the signal. This would allow the HPA operation in a high efficiency zone, reducing the battery consumption in turns.

1.5.4 High Power Amplification

High power amplification is required to transmit an RF signal and to counter the channel fading affects [70]. Mainly there are two types of Power Amplifiers (PA) [71, 72]:

- Travelling Wave Tube Amplifier (TWTA) is mostly used in satellite communication system [73].
- Solid State Power Amplifier (SSPA) is widely used in terrestrial radio communications e-g mobile communications [74].

1.5.4.1 PA Efficiency

As shown in the Fig. 1.13, there are different power localizations and accordingly they are titled. The relation between these power values is given by (1.6):

$$P_{in} + P_{dc} = P_{out} + P_{diss}. \tag{1.6}$$

Thus input power P_{in} and battery power P_{dc} are converted to output power P_{out} and power dissipated P_{diss}.

Generally there are two definitions of efficiency in literature [75]:

- Power efficiency: It is the ratio of output power to dc power. This is an important parameter as it indicates the PA consumption. It is given as,

$$\eta = \frac{P_{out}}{P_{dc}}. \tag{1.7}$$

- Power-added efficiency : It takes input power into account and also the PA consumption P_{dc}.

$$\eta_{added} = \frac{P_{out} - P_{in}}{P_{dc}}. \tag{1.8}$$

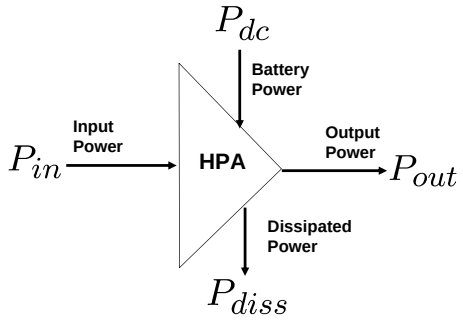

Figure 1.13: Power localization in a Power Amplifier

A typical efficiency curve is shown in Fig. 1.14 with the description of mentioned zones given below.

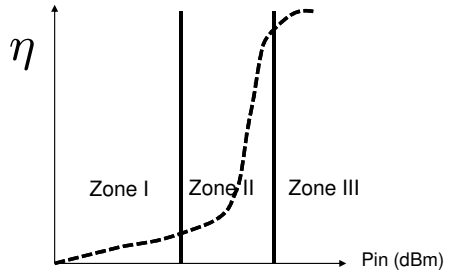

Figure 1.14: A typical PA efficiency curve

1.5.4.2 PA Amplitude and Phase non-linearities

Input-Output relationship, also called transfer characteristic, is of much importance. Part (a) of the Fig. 1.15 relates the output power to input power, called Amplitude/Amplitude or even the AM/AM compression. The part (b) of this figure presents the PA gain as a function of input power while part (c) describes the variation in phase with input power. One can divide the PA characteristics in three zones:

I. **Linear Zone (Zone-I)** : In this region the amplifier works like a linear device and P_{out} is proportional to P_{in} according to the relation called PA gain. And the distortions generated in this region are almost null.

II. **Compression Zone (Zone-II)** : Here, output power is no longer proportional to input power. Signal distortions start appearing and an increase in distortions is observed as it goes deep in the Compression Zone. Gain is also no longer linear as less output power is increased on increasing more input power. A very important point is situated in this zone called 1 dB compression point [70] which is the point at which there is a gap of 1 dB ($P_{in,1dB}$) between ideal gain curve and practical gain curve.

III. **Saturation Zone (Zone-III)** : From a certain point onwards, the output power becomes almost constant and the gain decreases linearly. The output power in this region titled as $P_{out,sat}$ is an important PA characteristic as the non-linearities become more and more evident.

The curve expressing the offset between output and input is characterized as Amplitude/Phase, or AM/PM conversion (Part (c) of the Fig. 1.15). It varies with the PA fabrication technique and it operating conditions [76]. For class A amplifiers, for example, the AM/PM curve remains constant in the linear region, variations start to appear arount 1 dB gain compression point P_{1dB} and can be very large near the saturation zone.

To avoid the non-linearities in the saturation zone, normally the operation point of the power amplifier is backed-off to the linear zone. This shift is normally measured with respect to 1 dB compression point or saturation power [77]. Thus the terms Input Back Off (IBO) and Output Back Off (OBO) are defined to quantify the dimensioning of the amplifier.

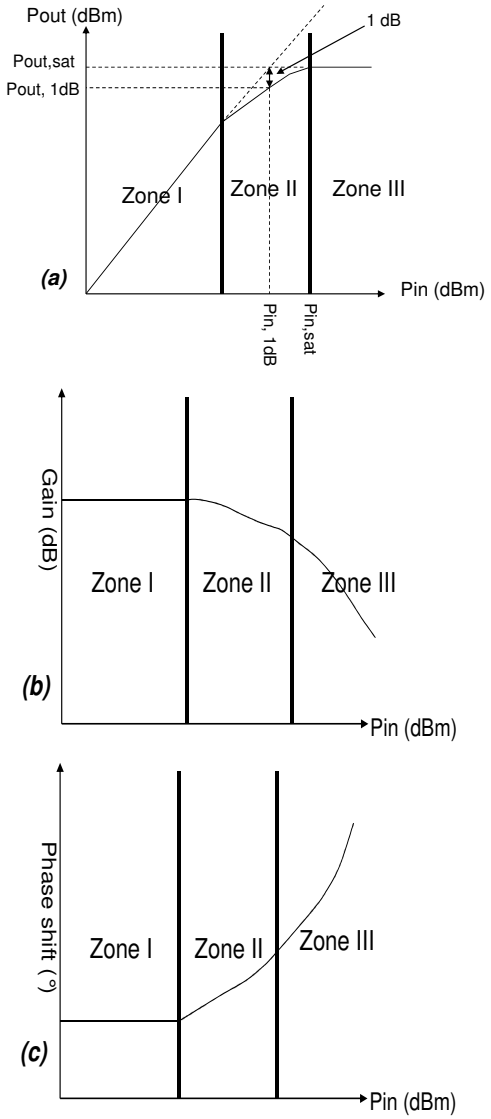

Figure 1.15: Class A SSPA characteristics (a) output-input power relationship, (b) gain vs input power, (c) phase shift vs input power.

Let $P_{out,1dB}$ be the output power at 1 dB compression and $P_{in,1dB}$ be the corresponding input power. The term IBO generally expressed in dB, is the ratio between input power at 1 dB compression (or the saturation power brought back at the input) [78, 79] and mean input power P_{in} of the signal.

$$IBO = \frac{P_{in,1dB}}{P_{in}} \quad or \quad IBO(dB) = P_{in,1dB}(dBm) - P_{in}(dBm). \tag{1.9}$$

or,

$$IBO = \frac{P_{in,sat}}{P_{in}} \quad or \quad IBO(dB) = P_{in,sat}(dBm) - P_{in}(dBm). \tag{1.10}$$

In the same way OBO could be defined which is the ratio of output power at 1 dB compression (or saturation power) to the mean output power P_{out} of the signal.

$$OBO = \frac{P_{out,1dB}}{P_{out}} \quad or \quad OBO(dB) = P_{out,1dB}(dBm) - P_{out}(dBm). \tag{1.11}$$

or even [79],

$$OBO = \frac{P_{out,sat}}{P_{out}} \quad or \quad OBO(dB) = P_{out,sat}(dBm) - P_{out}(dBm). \tag{1.12}$$

More the back off, lesser the distortions. This solution is not feasible, especially for low efficiency amplifiers. This trade off phenomenon is depicted in Fig. 1.16 by showing both the transfer characteristics and efficiency curve for a typical PA. As it could be seen that PA efficiency is quite low when P_{in} is small and approaches maximum around the borders of 'Zone II' and 'Zone III' with the increase in P_{in}. Thus PA efficiency is high near the saturation region and smaller in the linear region so on backing off as the operating point is moved to the linear region, PA efficiency is decreased. Therefore the amplifier must be linearized so that the operating point stays in the high efficiency zone without going into the saturation region. But for a non linear PA with the objective of staying in the high efficiency zone, the power fluctuations of the signal to be amplified should be minimized. These power fluctuations are normally described by the term Peak to Average Power Ratio (PAPR) which would be discussed next.

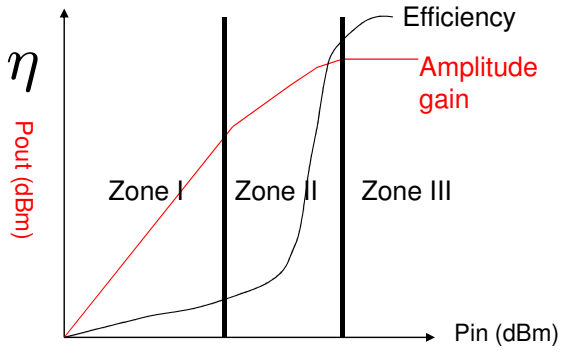

Figure 1.16: Transfer characteristics and efficiency curves of a typical PA

1.5.5 Peak to Average Power Ratio

As discussed above that HPA is a non-linear device and to operate it in the high efficiency zone, the power fluctuations of the signal should be minimized otherwise non linear distortions would occur. These power fluctuations are described by various terms in literature but most common of all is PAPR (Peak to Average Power Ratio). It is defined as the ratio between maximum instantaneous power and mean instantaneous power. Normally PAPR value determines the signal fluctuations but as this value is a random variable in itself. This is because of the PAPR variation from signal to signal. Thus it is always recommended to perform statistical analysis of PAPR and consequently representing it in terms of its distribution function. The details about the existing nomenclature describing power fluctuations is given in the next chapter with the statistical analysis of PAPR for OFDM signals.

1.6 PAPR reduction techniques for OFDM signals

The importance of high PAPR can easily be verified by the number of methods developed to reduce it. There are numerous PAPR reduction techniques presented in literature. These methods include Clipping [80], Clipping and filtering [6, 81], Selective Mapping (SLM)[82, 83], Interleaving [84, 85, 86], Tone Injection [9], Active Constellation Extension (ACE) [87], Partial Transmit Sequence (PTS) [7], Coding [88], and Tone Reservation (TR) [9] etc. And then there are papers which are about the classification of these methods [5, 21, 89, 90]. A brief description of the few of these methods shall be discussed in Appendix A to give an idea about the research orientation in this domain and the compromises with which these methods work to reduce PAPR. Here in this section, only one of these methods shall be discussed which is 'Tone Reservation' with its variant called 'Controlled Tone Reservation', as this is the method used throughout the thesis to reduce OFDM, SWR and CR signal PAPR.

1.6.1 Tone Reservation

Tone Reservation (TR) is an efficient method to reduce PAPR [9]. This method is based on adding an information data-block-dependent time domain signal to the original multi carrier signal to reduce its peaks. The objective is to find a time domain signal c which when added to time domain multi carrier information signal x, decreases the peaks in the information signal. This goal is achieved with the help of vector C with the same size as data block X. The vectors X and C are orthogonal to each other, i-e X has zeros where C is non-zero and has values on zero valued C indexes as shown in Fig. 1.17. These non zero values are called Peak Reducing Carriers (PRCs) or corrected carriers and the method is occasionally referred to as PRC because of this fact [17]. Mathematically speaking,

$$\hat{\mathbf{x}} = IFFT(X_k + C_k); \quad 0 \leq k \leq N-1. \tag{1.13}$$

Again emphasizing on the fact that vectors X and C are orthogonal to each other and thus there is no interference created on adding the PRC vector, C.

PRC values are obtained by optimization which is computationally quite complex in nature and methods have been developed to reduce this complexity. Also the increase in mean power due to added carriers is observed.

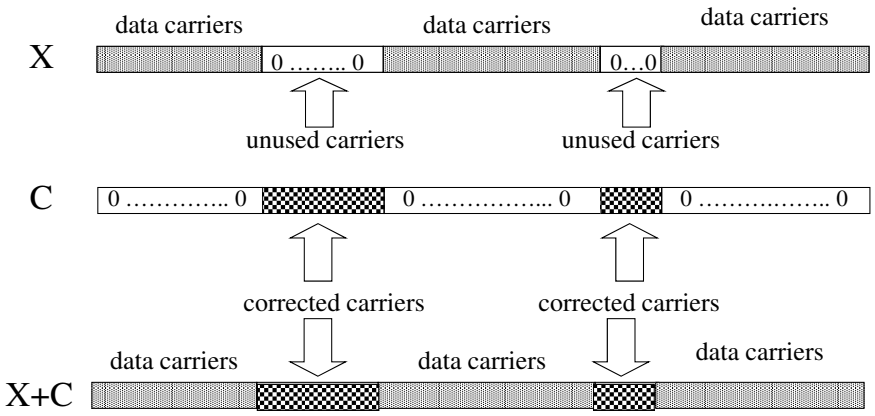

Figure 1.17: Block diagram of Tone Reservation process.

1.6.2 Controlled Tone Reservation

Zabre et al. [16] found an alternative method of using TR with the same methodology in order to nullify the data rate hit factor. The idea was to use the non utilized tones of a standard as PRC. As we know that there are some carriers in the standards which are not used for information transmission and these carriers can be used to transmit optimized tones which reduce the PAPR of the information signal. This use of null carriers would mean that the data rate is not affected by transmitting PRC. Like in the case of Wireless Local Area Network (Wi LAN) IEEE 802.11a standard, there are 12 tones out of 64 which are unused and can be employed to reduce PAPR of the OFDM modulated standard.

Similarly [9] presents a modified version of TR with constraints on mean power increase. Thus the issue of mean power increase can also be tackled with constrained optimization of the added tones. Also, in order to respect the defined spectral masks constraints of the standards, it is of utmost importance to keep the power of each added tone inside the mask limits as not to create inter channel interference.

1.7 Thesis Objectives

In literature, OFDM signals, the non-linearity issues related to power amplifier characteristics due to high PAPR and the the propositions to avoid non-linearity by reducing PAPR are discussed in detail. Our objective in this thesis is to extend that study to another multi-carrier (multi standard) system, Software Radio, and its evolved form, Cognitive Radio. We shall see how the power amplifier non-linear behavior could effect their transmission features. The solutions shall be proposed to avoid power amplifier non-linear distortions int the context of SWR and CR systems.

1.8 Conclusion

In this chapter it was tried to provide all the basic ingredients required to better understand the rest of the manuscript. We started with multi-carrier signals (OFDM) and after describing the basic principles of OFDM we found that with the evolution of technology, the multi-carrier signals were not restricted to OFDM only, rather multiplex of standard signals were being discussed under the umbrella of SWR technology. Further the implantation of 'brain' in SWR had lead to a new term called Cognitive Radio. Along with the numerous advantages that these technologies brought in the field of communications, many implementation problems arose as well. One of these problems was due to the high signal fluctuations (PAPR) property which multi carrier signals inherited. These high signal fluctuations rendered to system performance degradation when the non-linear transmitter component (HPA) was operated in high efficiency region. To avoid power penalty at HPA without performance degradation, the signal fluctuations should had been reduced. Several methods aiming at the objective of OFDM PAPR reduction had been proposed in literature. Now the aim would be to use one of these methods to reduce the power fluctuations of SWR and CR signals.

Chapter 2

PAPR Analysis of Continuous OFDM Signals

Contents

2.1 Introduction

In this chapter, the principal concepts related to Orthogonal Frequency Division Multiplexing (OFDM) modulation are presented. In fact many modern day high speed communication systems like Asymmetric Digital Subscriber Line (ADSL), Digital Audio Broadcasting (DAB), Digital Video Broadcasting (DVB), Wireless Local Area Network (WLAN) etc. use OFDM at Physical (PHY) layer because of its many features including immunity to multi-path fading effects and the simplified receiver structure etc. Unfortunately, the multi carrier nature of OFDM gives birth to high power fluctuations. Any high power fluctuating

signal when passed through a non linear device like High Power Amplifier (HPA), results in in-band and out-of-band distortions. Note that the transmission side of OFDM communications system shall be discussed here as the non linearities are produced because of the transmitter non linear components like HPA, converter etc. There exist a wide nomenclature to express power fluctuations like Peak to Average Power Ratio (PAPR), Crest Factor (CF), Power Ratio (PR). All these terms are defined and the most common of these terms in literature, PAPR, is selected as the term to be used through out the document. Complementary Cumulative Distribution Function (CCDF) is normally used to measure PAPR. CCDF expressions are given in literature for discrete OFDM signals and also a couple of examples for the distribution function of continuous OFDM signals exist. One of these two distribution functions for continuous OFDM signals is simulation based without any theoretical justification. It is analytically proved that the first statistical order of the simulation based and theory based functions are the same. Also a new CCDF expression is given for continuous OFDM signals.

2.2 Peak to Average Power Ratio

As discussed in the previous section that PA is a non-linear device and to operate it in the high efficiency zone, the power fluctuations of the signal should be minimized otherwise non linear distortions occur. These power fluctuations are described by various terms in literature but most common of all is PAPR (Peak to Average Power Ratio). It is defined as the ratio between maximum instantaneous power and mean instantaneous power. The term is alternatively used under several different titles like PEP (Peak Envelope Power) or CF (Crest Factor). Then there is another term PR (Power Ratio) which unifies all the mentioned terms under one notion. In this section all these different terms shall be defined in detail.

2.2.1 Definition of PAPR

For a complex base band signal, $s(t) = s_I(t) + s_Q(t)$, PAPR would be defined as,

$$\text{PAPR}\{s(t)\} = \frac{\max\limits_{t} |s(t)|^2}{\lim\limits_{T\to\infty} \frac{1}{T}\int_0^T |s(t)|^2}. \tag{2.1}$$

When the same signal $s(t)$ is transposed over Radio Frequency (RF) signal with $f_0 = \frac{\omega_0}{2\pi}$ being the carrier frequency the PAPR would be defined as,

$$\text{PAPR}\{s(t)\} = \frac{\max\limits_{t} |Re(s(t)e^{j\omega_0 t})|^2}{\lim\limits_{T\to\infty} \frac{1}{T}\int_0^T |Re(s(t)e^{j\omega_0 t})|^2 dt}. \tag{2.2}$$

The relation between base band signal PAPR, $PAPR_{BB}$, and RF signal PAPR, $PAPR_{RF}$, is given by [91],

$$\text{PAPR}_{RF}\ dB \approx \text{PAPR}_{BB}\ dB + 3\ dB. \tag{2.3}$$

As it could be seen that PAPR exhibits the variations in the peak of the signal with respect to its mean power and consequently its dynamic range.

2.2.2 Definition of Crest Factor

Crest Factor (CF) is the square root of PAPR [92] whether in base band or RF :

$$\mathrm{CF} = \sqrt{\mathrm{PAPR}}. \tag{2.4}$$

2.2.3 Definition of Peak Envelope Power

Peak Envelop Power (PEP) is used to express the maximum power of the signal envelope [93]. Thus it uses only the numerator of the term PAPR,

$$\mathrm{PEP} = \max_t |s(t)|^2. \tag{2.5}$$

2.2.4 Power Ratio (PR)

As described above that there exist many different notions to reflect power fluctuations, Palicot and Louët [94] introduced a general term called Power Ratio (PR) to cover all these terms under one notion. The definition of PR is given according to the conditions of the signal. The index c (for continuous) and d (for discrete) shall represent continuous and discrete signal respectively while i (for infinite) and f (for finite) shall indicate the infinite and finite time of integration of the signal for the calculation of PR (Fig. 2.1).

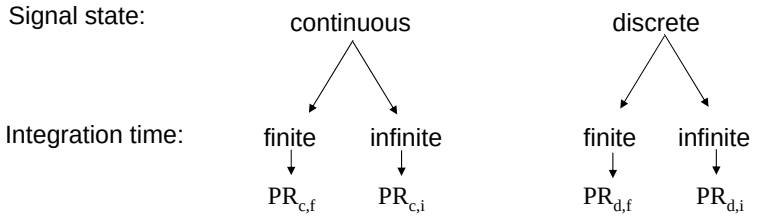

Figure 2.1: The different representations of PR.

Note that in the following developments the signal shall be considered ergodic meaning that statistical expectation can be calculated with the temporal mean.

2.2.4.1 PR definition for continuous signal

For a continuous signal $s(t)$ with infinite time of integration, the PR can be defined as,

$$\mathrm{PR}_{c,i}\{s(t)\} = \frac{\max\limits_t |s(t)|^2}{\lim\limits_{T\to\infty} \frac{1}{T}\int_0^T |s(t)|^2 dt}. \tag{2.6}$$

As the time of integration is normally finite, thus a new definition $\mathrm{PR}_{c,f}$ for time of integration T is given by,

$$\mathrm{PR}_{c,f}(T)\{s(t)\} = \frac{\max\limits_{t\in[0,T]} |s(t)|^2}{\frac{1}{T}\int_T |s(t)|^2 dt}. \tag{2.7}$$

2.2.4.2 PR definition for discrete signal

For a discrete signal with an infinite number of samples, the PR definition becomes,

$$\mathrm{PR}_{d,i}\{\mathbf{s}\} = \frac{\max\limits_{k} |s(k)|^2}{\lim\limits_{N_s\to\infty} \frac{1}{N_s}\sum_{k=0}^{N_s-1} |s(k)|^2}. \tag{2.8}$$

Also for a discrete signal with N_s number of samples of the signal $\mathbf{s} = [s(0), ..., s(N_s - 1)]$, the PR definition of a finite sampled signal is as follows,

$$\mathrm{PR}_{d,f}(N_s)\{\mathbf{s}\} = \frac{\max\limits_{k\in[0,N_s-1]} |s(k)|^2}{\frac{1}{N_s}\sum_{k=0}^{N_s-1} |s(k)|^2}. \tag{2.9}$$

Although introduction of the term PR was a refreshing effort to unify the multi notion nomenclature under one umbrella but it could not get the acknowledgment it deserved and the term PAPR remained dominant to describe the signal fluctuations. Thus we shall continue with the term PAPR throughout the document where this term would be equivalent to $PR_{d,f}(N_s)\{\mathbf{s}\}$ by default unless otherwise stated. It means that PAPR shall be calculated over N_s discrete samples of the signal which constitute one OFDM or SWR symbol.

2.2.5 Definition of Effective Peak Factor and Complementary Cumulative Distribution Function

As PAPR is a random variable as it is calculated for random signals, it should be measured by it distribution function. Thus a limit or an approximation should be defined as in [95] which defines Effective Peak Factor (EPF) as,

$$Pr(\mathrm{PAPR} \geq \mathrm{EPF}) = \epsilon, \tag{2.10}$$

where ϵ approaches zero.

EPF is a threshold for which the probability that PAPR is greater than this threshold is negligible. The calculation of ϵ allows to upperbound PAPR. This distribution function of PAPR is more commonly known as the term Complementary Cumulative Distribution Function (CCDF) and is given by the expression,

$$CCDF(PAPR_0) = Pr[\mathrm{PAPR} \geq PAPR_0]. \tag{2.11}$$

2.3 Analysis of PAPR in multi carrier modulations

As discussed earlier that multi carrier modulations like OFDM exhibit large dynamic range because of the strong power fluctuations. And these power fluctuations are quantified by PAPR. In this section deterministic as well as statistical analysis of PAPR shall be discussed.

2.3.1 Deterministic PAPR study

In the case of OFDM, recalling that PAPR of a signal $x(t)$ is given by the relationship,

$$\text{PAPR}(x(t)) = \frac{\max\limits_{t\in[0,T]} |x(t)|^2}{\frac{1}{T}\int_0^T |x(t)|^2 dt}, \tag{2.12}$$

where $x(t)$ represents the base band OFDM signal with N sub carriers given by,

$$x(t) = x_I(t) + jx_Q(t) = \sum_{k=0}^{N-1} C_k e^{2j\pi\frac{k}{T}t}. \tag{2.13}$$

C_k is the complex symbol of the k^{th} sub carrier and T is the OFDM symbol time.

For the discrete time symbol $x_n; 0 \leq n \leq N-1$, PAPR would be defined as,

$$\text{PAPR}(\mathbf{x}) = \frac{\max\limits_{0\leq n\leq N-1} |x_n|^2}{E\{|x_n|^2\}}, \tag{2.14}$$

where $E\{.\}$ is the expectation operation. The instantaneous power of OFDM signal is given by,

$$\begin{aligned} |x_n^2| &= \sum_{k=0}^{N-1}\sum_{k'=0}^{N-1} C_k C_{k'}^* e^{2j\pi n(k-k')/N} \\ &= \sum_{k=0}^{N-1} |C_k|^2 + \sum_{k=0}^{N-1}\sum_{k'\neq k} C_k C_{k'}^* e^{2j\pi n(k-k')/N} \end{aligned} \tag{2.15}$$

The relation between time and frequency domain mean power is,

$$E\{|x_n|^2\} = NE\{|C_n|^2\} \tag{2.16}$$

Now the maximum power of OFDM symbol would be given by,

$$\begin{aligned} \max_{0\leq n\leq N-1} |x_n|^2 &= \max_{0\leq n\leq N-1} \{\sum_{k=0}^{N-1} |C_k|^2 + \sum_{k=0}^{N-1}\sum_{k'\neq k} C_k C_{k'}^* e^{2j\pi n(k-k')/N}\} \\ &\leq N \max_k |C_k|^2 + \max_{k,k'} \{\sum_{k=0}^{N-1}\sum_{k'\neq k} C_k C_{k'}^* e^{2j\pi n(k-k')/N}\} \\ &\leq N \max_k |C_k|^2 + \sum_{k=0}^{N-1}\sum_{k'\neq k} \max_k |C_k|^2 \\ &\leq N \max_k |C_k|^2 + N(N-1) \max_k |C_k|^2 \\ &\leq N^2 \max_k |C_k|^2 \end{aligned} \tag{2.17}$$

Thus Eq. (2.14) would become,

$$PAPR(\mathbf{x}) \leq N \frac{\max\limits_{0 \leq k \leq N-1} |C_k|^2}{E\{|C_k|^2\}}. \tag{2.18}$$

The above inequality turns to equality only if the value of all C_k's is maximal. In that case the PAPR would be maximum denoted by $PAPR_{max}$,

$$PAPR_{max} = N \frac{\max\limits_{0 \leq k \leq N-1} |C_k|^2}{E\{|C_k|^2\}}. \tag{2.19}$$

Treating the case of phase modulation schemes where maximum and mean symbol power is the same, the above equation would become,

$$PAPR_{max,PSK} = N. \tag{2.20}$$

When the modulated symbols are that of a M-ary QAM modulation, $\max_k |C_k|^2 = 2(\sqrt{M}-1)^2$ and $E\{|C_k|^2\} = \frac{2}{3}(\sqrt{M}-1)$. Thus $PAPR_{max}$ would be given by [96],

$$PAPR_{max,M-QAM} = 3N \frac{\sqrt{M}-1}{\sqrt{M}+1}, \tag{2.21}$$

where M is the number of modulation states.

The probability that PAPR reaches its maximum value is $\frac{1}{M^{N-2}}$ [14]. To better give the idea of this figure, consider the case of IEEE 802.11a standard, where $m = 4$ (QPSK modulation) and $N = 64$. The probability to reach the maximum value of this upper bound is 4^{-62}. With the symbol period $T = 3.2\mu sec$ in IEEE 802.11a case, the theoretically maximum PAPR shall be observed statistically only once in 2×10^{18} million years!

As this is a very big upper bound and never reached in practical scenarios, thus statistical methods are used to better define the PAPR distribution function.

2.3.2 Statistical properties of OFDM signal

An OFDM signal is a linear combination of N i.i.d variables, with different amplitudes. Thus OFDM symbol is a random variable with some large peak values compared to the mean of the symbol according to the central limit theorem. Consequently, PAPR of the OFDM symbol is also a random variable and thus can not used as a sole parameter to compare the PAPR of different systems. Therefore distribution function of PAPR is introduces which gives the probability of PAPR exceeding a certain threshold.

The real and imaginary parts of OFDM signal follow gaussian distribution with zero mean and $\frac{1}{2}E(|C|^2)$ variance for a very large value of N [14, 97, 98] as shown in Fig. 2.2. Here C represents the mapped information data. Also the absolute value of a gaussian random variable follows Rayleigh distribution as shown in Fig. 2.3.

There exist many PAPR distribution function formulations, obtained either experimentally or analytically. Considering the samples mutually independent and uncorrelated, Van Nee [97] shows that the CCDF of PAPR for a base band OFDM signal $\mathbf{x} = [x_0, ..., x_{N-1}]$ can be given by the relation (2.22) :

$$Pr\Big[\mathrm{PAPR_d}\{\mathbf{x}\} > \gamma\Big] \approx 1 - (1 - e^{-\gamma})^N. \tag{2.22}$$

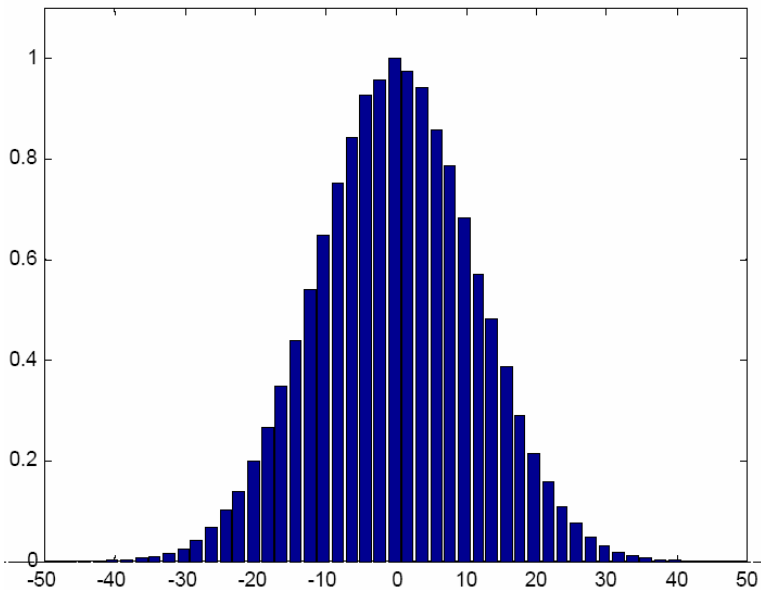

Figure 2.2: Histogram of the real part of an OFDM signal, $N = 128$.

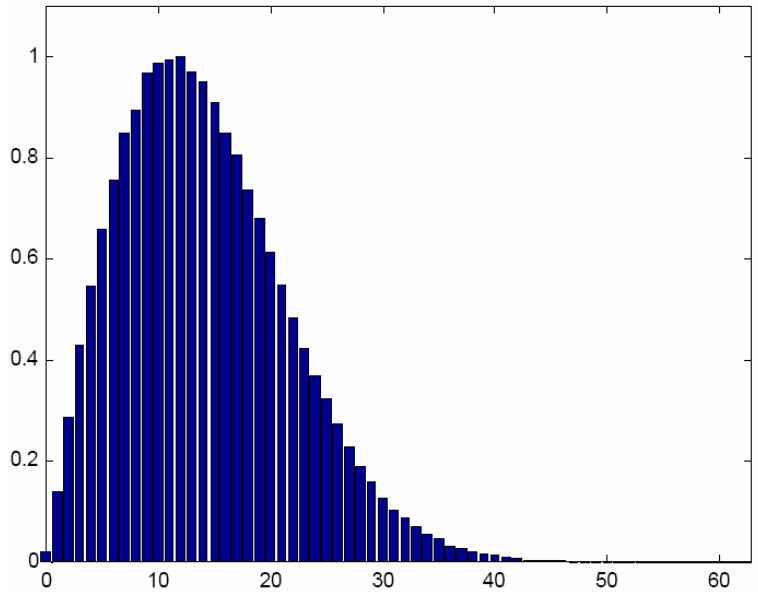

Figure 2.3: Histogram of the OFDM signal amplitude, $N = 128$.

The relation (2.22) is only valid for an oversampling factor $L = 1$ and therefore PAPR is subscripted by d to illustrate the fact that PAPR is calculated over Nyquist rate discrete samples of the signal. PAPR calculated in this manner may not depict exactly the signal fluctuations as there is the probability of missing the peaks at this sampling rate. Therefore

PAPR is calculated for an oversampled version of the signal to better estimate the signal variations by taking more signal sample values.

Thus the oversampled version of Eq. 2.13 becomes,

$$x(n/L) = x_I(n/L) + jx_Q(n/L) = \sum_{k=0}^{NL-1} c_k e^{2j\pi \frac{kn}{NL} t}, \tag{2.23}$$

where $0 \leq n \leq NL-1$ with L being the oversampling factor used to better approximate the analog PAPR.

In Fig. 2.4, the effect of oversampling factor on the PAPR distribution is demonstrated. QPSK modulated OFDM symbols are simulated for $N = 64$. It could be seen that as the oversampling factor L increases, the PAPR values also increase. An oversampling factor of 4 is generally taken as to simulate a continuous OFDM signal [99].

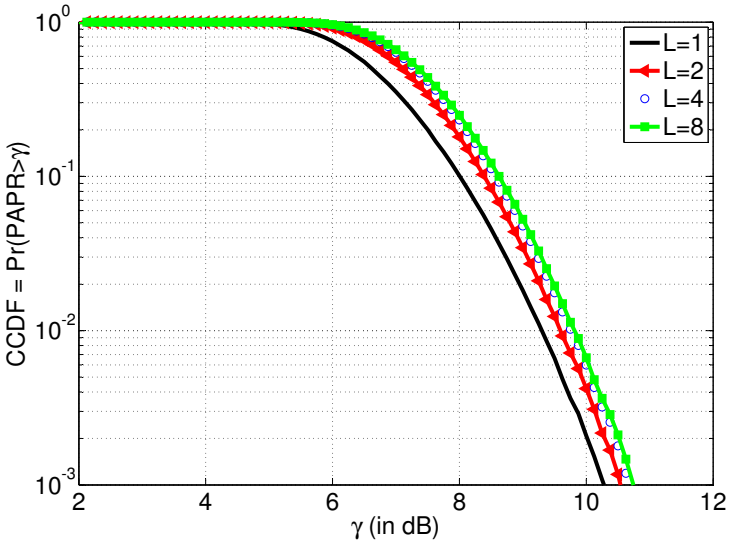

Figure 2.4: CCDF of PAPR for $L \in \{1, 2, 4, 8\}$ ($N = 64$, QPSK constellation) for a base band OFDM signal

For an oversampled signal, the PAPR is given by the relation,

$$\text{PAPR}\{\mathbf{x}\} = \frac{\max\limits_{n\in[0,NL]} |x(n)|^2}{\frac{1}{NL}|\sum_{n=0}^{NL-1} x(n)|^2}. \tag{2.24}$$

For an oversampling factor $L > 4$, [12] gave an approximation of the CCDF of PAPR by the following relation,

$$Pr\Big[\text{PAPR}_c\{\mathbf{x}\} > \gamma\Big] \approx 1 - (1 - e^{-\gamma})^{\tau_1 N}, \tag{2.25}$$

where $\tau_1 \approx 2.8$ is a constant obtained by simulations. Here PAPR is subscripted by c to show that PAPR is calculated over approximately continuous signal.

In [13] and [14], an analytical CCDF upper bound has been proposed for high over-sampling factor values, simulating nearly the continuous signals,

$$Pr\Big[\mathrm{PAPR_c}\{\mathbf{x}\} > \gamma\Big] \approx N\sqrt{\frac{\pi}{3}\gamma}e^{-\gamma}. \tag{2.26}$$

This relationship is simplified using a limiting form of exponential function and modified Cumulative Distribution Function (CDF) is given as [14],

$$F_c(\gamma) = Pr(PAPR_c(x) \leq \gamma) \approx e^{-\sqrt{\frac{\pi}{3}}N\sqrt{\gamma}e^{-\gamma}}. \tag{2.27}$$

In Fig. 2.5, different PAPR distribution functions presented in literature are shown along with discrete OFDM PAPR distribution ($L = 1$) and continuous OFDM PAPR distribution ($L = 8$) for a 64 point QPSK modulated OFDM signal. It can be noted that Eq. (2.22) approximates the discrete signal PAPR while Eq. (2.25) and Eq. (2.26) approximate the continuous OFDM signal PAPR.

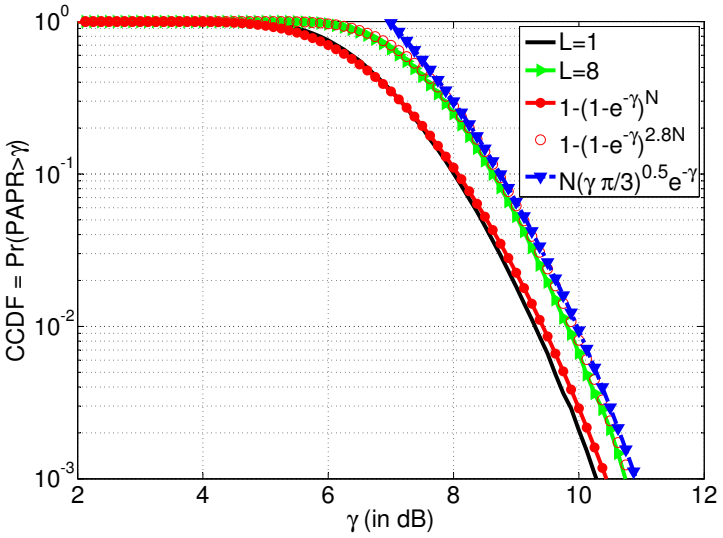

Figure 2.5: CCDF of PAPR for $L \in \{1, 8\}$ ($N = 64$, QPSK constellation) and some theoretical approximations for a base band OFDM signal

One very interesting thing to note about PAPR distribution function is that it is independent of the mapping scheme of the OFDM symbols provided that the number of sub carriers is large. In Fig. 2.6 this fact is demonstrated by showing the PAPR CCDF for QPSK, 16-QAM, 64-QAM and 256-QAM modulated OFDM symbols. It is clear that all the differently mapped symbols show almost the same PAPR behavior. The reason being that as the number of sub-carriers increase, the process becomes Gaussian following the central limit theorem and hides the PAPR dependence on mapped data.

But the PAPR distribution is not independent of the number of sub-carriers. In fact as the number of sub-carriers increases, so does the PAPR and we see the CCDF curve shifting towards right as shown in Fig. 2.7. This is due to the fact that the summation of more number of variables results in more peaks and thus larger PAPR values.

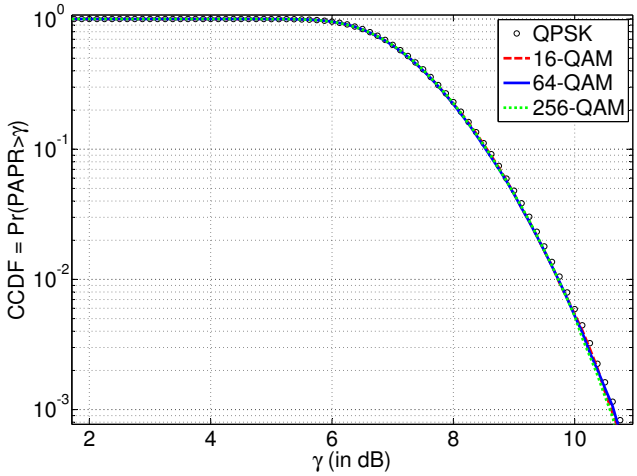

Figure 2.6: CCDF of PAPR for $L = 4$, $N = 64$ with different modulation schemes for a base band OFDM signal

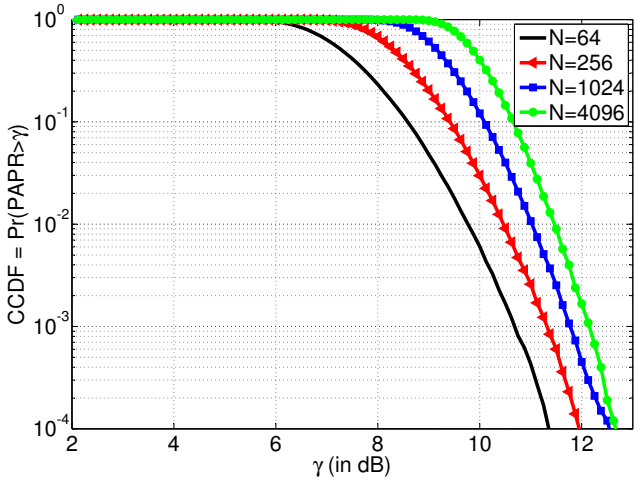

Figure 2.7: CCDF of PAPR for $L = 4$, QPSK constellation with different number of sub-carriers of a base band OFDM signal

2.4 Proposed PAPR statistical analysis for continuous OFDM signal

Distribution function for continuous OFDM signals is already presented in literature as given by Eq. 2.25 and Eq. 2.27. But one of these distributions is simulation based (Eq. 2.25) while the other is based on analytical developments. Also inspite of the fact that CCDF are very important to describe the statistical distribution of PAPR, the first and second statistical orders are also important. Thus first order statistical for both the distributions mentioned above is presented for continuous OFDM signals and it is verified that the mean values obtained with both simulation based and theoretical analysis based distribution are the same. It validates the correctness of the simulation based distribution. Also it is shown that the second statistical order remains almost unvaried when discrete OFDM signal is oversampled to be a continuous signal. Also a new CCDF of PAPR is given for base band continuous signal and it matches the already developed formulations [25].

2.4.1 PAPR statistical orders

From the previous discussion, it can be derived that the probability density function related to CCDF given in Eq. 2.22 can be written as,

$$f_d(\gamma) = Ne^{-\gamma}(1 - e^{-\gamma})^{N-1}. \tag{2.28}$$

Then, after some mathematical developments, it can be shown [11] that the first associated statistical order m_d for large N values can be written as,

$$m_d = \int_{-\infty}^{+\infty} \gamma f_d(\gamma) d\gamma \approx \ln N + \zeta, \tag{2.29}$$

where ζ is the Euler constant ($\zeta \approx 0.577$).

In the same way, the second statistical order σ_d^2 for large N values [11] is given by,

$$\sigma_d^2 = \int_{-\infty}^{+\infty} \gamma^2 f_d(\gamma) d\gamma \approx \frac{\pi^2}{6}. \tag{2.30}$$

The mean approximations provided by (2.29) are very close to simulation results as shown in Table 2.1.

However, Eq. (2.30) does not satisfactorily matches the simulation results as shown in Table 2.2. These simulations are performed for QPSK modulated 10^5 base band OFDM symbols with an oversampling factor $L = 1$ and different values of OFDM subcarriers N. As we are interested in continuous signal analysis ($L \geq 4$) therefore we shall compare the mean and variance values in that context. Tables 2.3 and 2.4 recount results for OFDM signal with an oversampling factor $L = 4$ to better estimate the analog PAPR.

One conclusion can be drawn from Tables 2.1 to 2.4 that Eq.(2.29) is no longer valid for an oversampling factor greater than one. Next section will discuss the derivation of a new mean PAPR expression for continuous base-band OFDM signals.

Table 2.1: Mean values comparison between simulations (m_s) and (2.29) for $L = 1$

N	m_s	$Eq.(2.29)$
64	4.8	4.73
128	5.47	5.42
256	6.15	6.12
512	6.83	6.81
1024	7.52	7.5
2048	8.2	8.2
4096	8.9	8.89

Table 2.2: Variance values comparison between simulations (σ_s^2) and (2.30) for $L = 1$

N	σ_s^2	$Eq.(2.30)$
64	1.36	1.64
128	1.46	1.64
256	1.52	1.64
512	1.57	1.64
1024	1.6	1.64
2048	1.63	1.64
4096	1.6	1.64

Table 2.3: Mean values comparison between simulations (m_s) and (2.29) for $L = 4$

N	m_s	$Eq.(2.29)$
64	5.58	4.73
128	6.31	5.42
256	7.03	6.12
512	7.75	6.81
1024	8.47	7.5
2048	9.18	8.2
4096	9.91	8.89

Table 2.4: Variance values comparison between simulations (σ_s^2) and (2.30) for $L = 4$

N	σ_s^2	$Eq.(2.30)$
64	1.52	1.64
128	1.62	1.64
256	1.69	1.64
512	1.72	1.64
1024	1.74	1.64
2048	1.71	1.64
4096	1.76	1.64

2.4.2 Mean PAPR Expression

2.4.2.1 Theoretical Developments

By definition, first statistical order is related to density function $f_c(\gamma) = d(F_c(\gamma))/d\gamma$ by,

$$m_c(N) = \int_{-\infty}^{+\infty} \gamma f_c(\gamma) d\gamma. \tag{2.31}$$

Starting from Eq.(2.27), the probability density function f_c associated to $F_c = 1 - CCDF$ verifies

$$\gamma f_c(\gamma) = -\frac{N}{2}\sqrt{\frac{\pi}{3}}(1-2\gamma)\sqrt{\gamma}e^{-\gamma}e^{-[\sqrt{\frac{\pi}{3}}N\sqrt{\gamma}e^{-\gamma}]}. \tag{2.32}$$

The first statistical order m_c vs N is then equal to the sum of two terms A and B, where

$$A = -\frac{N}{2}\sqrt{\frac{\pi}{3}}\int_0^{+\infty} \sqrt{\gamma}e^{-\gamma}e^{-[\sqrt{\frac{\pi}{3}}N\sqrt{\gamma}e^{-\gamma}]}d\gamma, \tag{2.33}$$

and

$$B = N\sqrt{\frac{\pi}{3}}\int_0^{+\infty} \gamma\sqrt{\gamma}e^{-\gamma}e^{-[\sqrt{\frac{\pi}{3}}N\sqrt{\gamma}e^{-\gamma}]}d\gamma. \tag{2.34}$$

Let us investigate the first term A. A simple integration by parts yields,

$$m_c(N) = \int_0^{+\infty} (1 - e^{-[\sqrt{\frac{\pi}{3}}N\sqrt{\gamma}e^{-\gamma}]})d\gamma, \tag{2.35}$$

and

$$\frac{dm_c(N)}{dN} = \sqrt{\frac{\pi}{3}}\int_0^{+\infty} \sqrt{\gamma}e^{-\gamma}e^{-[\sqrt{\frac{\pi}{3}}N\sqrt{\gamma}e^{-\gamma}]}d\gamma. \tag{2.36}$$

A is then exactly equal to,

$$A = -\frac{N}{2}\frac{dm_c(N)}{dN}. \tag{2.37}$$

On the other hand, exact calculation of B happens to be really difficult. Plot of factor B shows that it can be approximated by something like $\mu \ln(\alpha N)$; meaning

$$B \approx \mu \ln(\alpha N). \tag{2.38}$$

Here natural logarithmic function is used for approximation as this function can equate factor B using minimum number of coefficients. Finally, m_c is the solution of the following differential equation,

$$m_c(N) + \frac{N}{2}\frac{dm_c(N)}{dN} \approx \mu \ln(\alpha N), \tag{2.39}$$

from which we get

$$m_c(N) \approx \mu(\ln N + \frac{1}{N^2} + \beta), \quad \beta = \ln \frac{\alpha}{\sqrt{e}}. \tag{2.40}$$

As this $m_c(N)$ is obtained *analytically*, thus will be labeled as $m_{c,a}(N)$ to distinguish from *simulation* based formulations.
As N is quite large in practical OFDM transmissions, thus $\mu(1/N^2)$ can be neglected without loss of generality and Eq.(2.40) can be rewritten as

$$m_{c,a}(N) \approx \mu(\ln N + \beta), \quad \beta = \ln \frac{\alpha}{\sqrt{e}}. \tag{2.41}$$

As mentioned earlier that in [12], the authors have proposed an empirical relationship of the PAPR cumulative distribution function for continuous signals. This approximation is,

$$F_{c,s}(\gamma) \approx (1 - e^{-\gamma})^{\tau_1 N}, \tag{2.42}$$

where $\tau_1 \approx 2.8$ is obtained with simulations without theoretical justifications. Thus $F_{c,s}(\gamma)$ is a *simulation* based distribution function for *continuous* signals. Starting from this relation and analogy with Eq.(2.29), the mean PAPR value is about,

$$m_{c,s}(N) \approx \ln N + \zeta + \ln \tau_1 \approx \ln N + 1.60. \tag{2.43}$$

As mentioned before that Eq.(2.34) is almost unsolvable using basic mathematics. Thus the task of getting the approximate solution of the mentioned equation using minimum number of coefficients was achieved using 'curve fitting' technique. Initially this equation was plotted for different values of N to get the idea of its solution's form. Thus Eq.(2.34) plot revealed that it follows natural logarithmic curve shape. Thus $y = c_1 \ln(c_2 N)$ was thought to be the solution. To get the values of the coefficients, 'Non-linear Least Square' method was used to fit a nonlinear model to data. A nonlinear model is defined as an equation that is nonlinear in the coefficients, or a combination of linear and nonlinear in the coefficients. It is a type of 'Least Square' method in which the coefficient values are obtained by minimizing the sum of the square of the difference between data value and fitted response value. If y_i and $\hat{y}_i$ are i^{th} data value and fitted value after using estimated coefficients respectively, then target is to minimize $S = \sum_{i=1}^{N}(y_i - \hat{y}_i)^2$ for N point data fitting. The process of finding optimized coefficients is iterative in nature. It starts with initial estimated values of the coefficients and corresponding value of S is calculated.

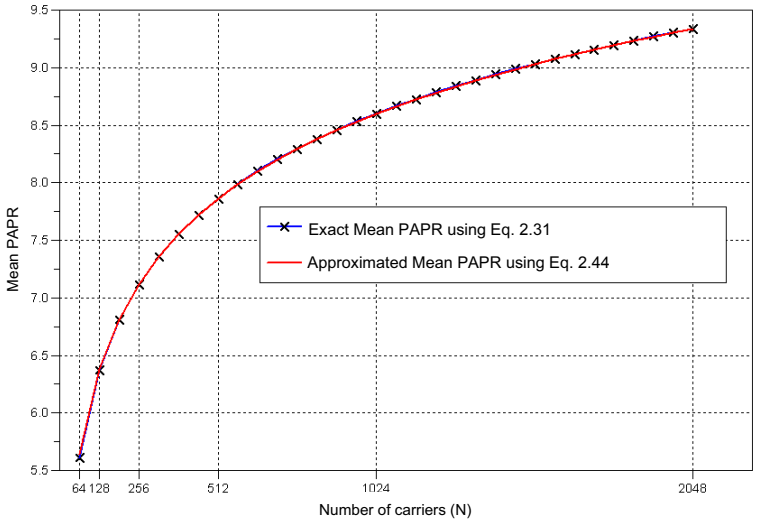

Figure 2.8: Comparison between Exact and Approximate Analytical Mean PAPR Values

Based on certain fitting algorithm, coefficient values are adjusted to minimize S. These algorithms include Trust-region, Levenberg-Marquardt, Gauss-Newton etc. Trust-region algorithm [100] is used here because of its improved and efficient performance to solve non-linear problems than others. The optimized results were obtained for 500 iterations of the algorithm. So, after implying 'Non-linear Least Square' method, values of the coefficients μ and α in Eq.(2.38) were found to be 1.07 and 5.12 respectively. Thus mean PAPR would be,

$$m_{c,a}(N) \approx \mu(\ln N + \ln \frac{\alpha}{\sqrt{e}}) = 1.07 \ln(\frac{5.12}{\sqrt{e}} N). \tag{2.44}$$

One can easily see that mean PAPR for discrete signals (Eq.(2.29)) is less than mean PAPR for continuous signals (Eq.(2.44)) as probability of seizing the signal peak is more in the later case.

Fig.2.8 presents the comparison between the exact solution of Eq.(2.31) and its fitted solution (Eq.(2.44)) versus different N values. It seems that fitted solution almost matches the exact solution.

Also in Fig. 2.9 mean PAPR values for different values of N, obtained by simulations (m_s), using Eq.(2.43) ($m_{c,s}(N)$) and Eq. (2.44) ($m_{c,a}(N)$) are compared. Here mean PAPR using simulations stands for mean PAPR value over 10^5 OFDM symbols taken from Table. 2.3. The results show that $m_{c,a}(N)$ and $m_{c,s}(N)$ are similar thus theoretically providing the truthfulness of Eq.(2.42). Also $m_{c,s}(N)$ seems to be a better fit than $m_{c,a}(N)$ to simulation results m_s.

2.4.3 A Novel PAPR Distribution Function

As it is said earlier that the continuous OFDM signal PAPR CCDF presented in [12] given by Eq. (2.25) is obtained by simulations using hit-and-trial method. While the distribution function for continuous OFDM signal PAPR distribution given by Eq. (2.27)

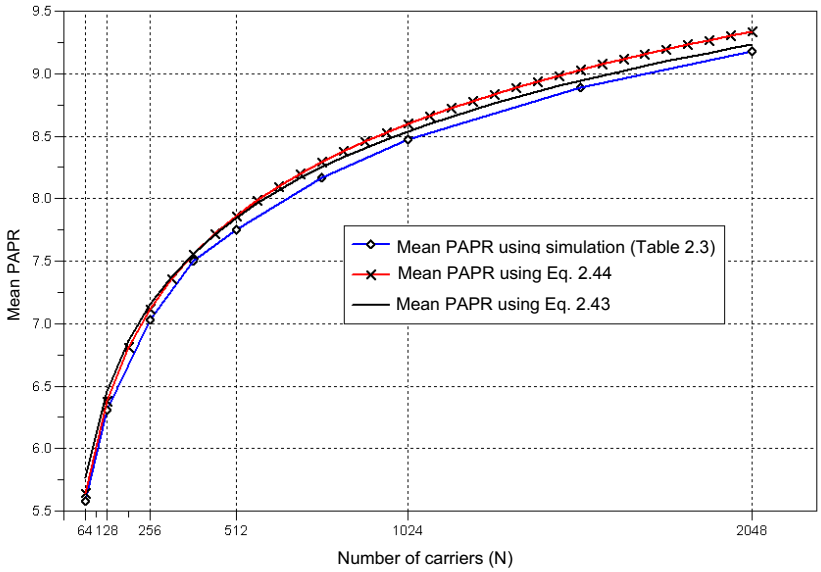

Figure 2.9: Comparison between Mean PAPR values for different N.

is presented with theoretical justifications [14]. Both these functions are quite useful in the estimation of PAPR behavior of continuous OFDM signals.

Our aim was to analytically link the simulation based results with theoretical results and thus provide a 'kind of' theoretical justification of the simulation based results. We started with the theoretical distribution function (Eq.(2.27)) and derived its mean. Then we verified that the mean of the simulation based function and theoretical function for continuous OFDM signals is almost the same. Based on the mean value obtained through theoretical distribution function we shall derive a new distribution function for continuous signals and shall compare with the simulation based distribution function.

Thus based on the mean value obtained in Eq. (2.44) which is in fact the mean PAPR for continuous OFDM signals obtained *analytically*, the PAPR cumulative distribution function for *continuous* signal can also be approximated under the form,

$$F_{c,a}(\gamma) \approx (1 - e^{-\gamma})^{\tau_2 N^{\mu}}, \quad \tau_2 = (\frac{\alpha}{\sqrt{e}})^{\mu} e^{-\zeta}. \tag{2.45}$$

Contrary to [12] and Eq.(2.42), an analytical form of the PAPR cumulative function for continuous signals has been proposed with theoretical justifications. Although it is just another PAPR distribution function for continuous signals, it helps bridging the gap between simulation and theory based results by proving the similarities between them.

Especially, knowing the fact the SWR signal PAPR analysis must be performed in the RF domain which in turns means a continuous signal PAPR analysis, this result may help in approximating the SWR signal PAPR behavior.

Now solving Eq.(2.45) using 'Non-linear Least Square' method,

$$F_{c,a}(\gamma) \approx (1 - e^{-\gamma})^{\tau_2 N^{\mu}} = (1 - e^{-\gamma})^{\tau_2 N^{1.07}}. \tag{2.46}$$

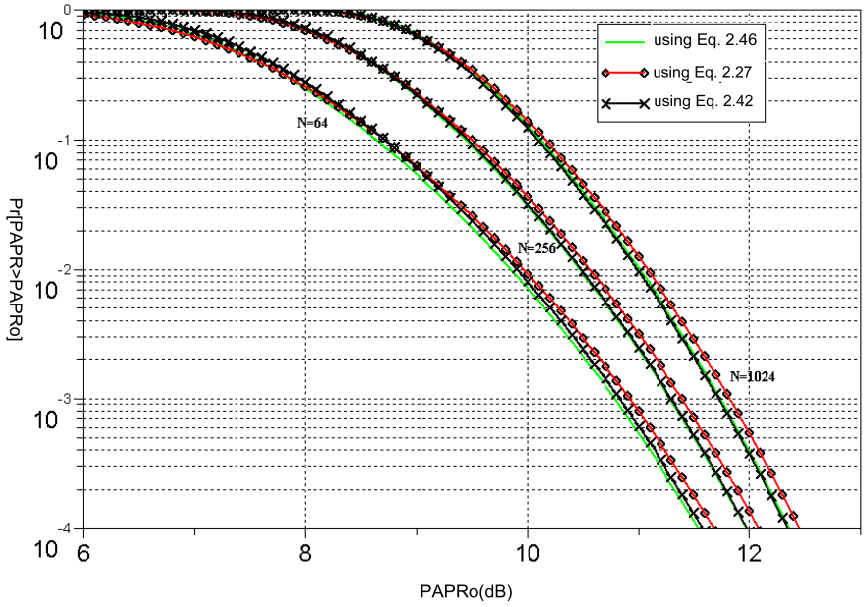

Figure 2.10: CCDF Comparison for different N values.

where $\tau_2 = (\frac{5.12}{\sqrt{e}})^{1.07} e^{-\zeta}$. Fig. 2.10 compares PAPR Complementary Cumulative Distribution Function ($CCDF = 1 - CDF$) for continuous signals. The curves are plotted using Eq.(2.27), Eq.(2.42) and Eq.(2.46) for $N = 64$, 256 and 1024. Again similarity in distribution functions states the trueness of simulation based formula.

2.5 Conclusion

Multi-carrier signals like OFDM have high power fluctuations and these fluctuations are generally quantified by the term PAPR. There are also some other terms like PEP, CF and PR to demonstrate the same multi-carrier signal feature. All these terms were discussed in this chapter. PAPR when calculated over a Nyquist rate sampled signal does not demonstrate the exact power fluctuations of the signal thus the signal should be oversampled to better approximate analog PAPR. Also PAPR being a random variable is measured by its CCDF as the deterministic PAPR study does not lead to realistic PAPR measurements. Thus appeared the need of a CCDF expression which could better approximate the PAPR behavior of continuous OFDM signals. In this chapter a new CCDF of PAPR was developed for a continuous OFDM signal which matched the already developed two formulations in literature. One of these two CCDF expressions was theoretically obtained while the other was a simulation based expression. We had analytically proved that the first statistical orders of these two distribution functions were almost same. Thus we tried to analytically justify the simulation based results. After discussing the PAPR distribution for OFDM we now head towards an other multi carrier transmission scheme which is Software Radio (SWR) to be discussed in the next chapter and shall see the PAPR distribution for SWR signals. Keeping in mind that PAPR analysis of SWR signals must be

performed over continuous SWR signals, the PAPR distribution obtained in this chapter for continuous OFDM signals may also prove helpful for SWR signals.

Chapter 3

PAPR analysis of a SWR signal

Contents

3.1 Introduction

In the previous chapter PAPR analysis of continuous OFDM signals was presented and it was concluded that multi carrier signals exhibit high PAPR and this PAPR is better estimated when the signal is oversampled to behave as a continuous signal. In this chapter PAPR analysis of an other multi carrier system, Software Radio (SWR), is presented. With

the growth of high data-rate applications demanding better Quality of Service (QoS) than ever, many systems and technologies have been developed recently. The ever so scarce frequency spectrum is crowded with the multi system scenario. It has evoked the need of a reconfigurable architecture which can satisfy 'any where, any time' radio requirement. This lead to the development of SWR technology which is about reconfigurability of a terminal to better adapt according to its environment like channel conditions, air interface etc. Thus SWR is about a multi standard terminal which can operate on a large spectrum band. One of the inconvenience in SWR implementation is the non-linear devices like PA, mixers etc. As SWR signal is a multi standard signal thus it might inherit high power fluctuation i-e high PAPR. This hypothesis is proved by simulating a SWR signal consisting of multi modulation schemes. Also some analogies are presented between OFDM signal and SWR signal as they both are multi carrier signals. Finally a new frequency vision of PAPR metric is presented associates signal's spectral information with PAPR.

3.2 SWR system model

As discussed earlier that SWR is a multiplex of multi standard signal. Fig. 3.1 explains multi-standard and multi-carrier concept where different standards GSM, WLAN, DVB-T, WiMAX and UMTS are shown. Some of these standards like GSM and UMTS transmit a multiplex of single carrier signal while the rest transmit a multi-carrier signal. Also it should be noted that each standard has its own symbol frequency different from the other standards. The Fig. 3.1 presents a very general view for SWR system at base station. Below we shall discuss some practical cases in mono-standard and multi-standard SWR context.

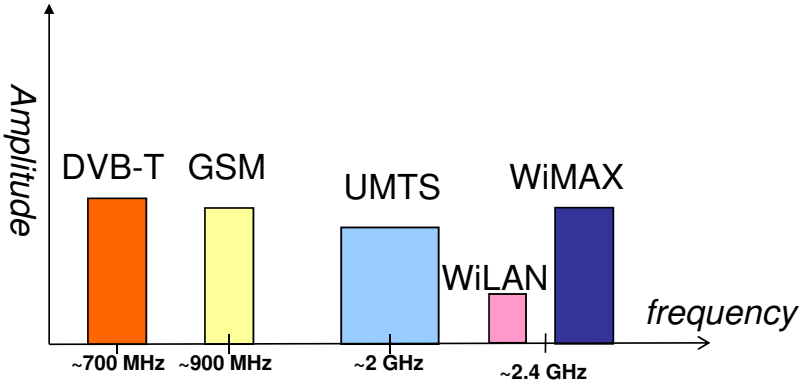

Figure 3.1: SWR System: A multi-standard system where each standard contains multi-carrier signal

3.2.1 Mono-standard SWR system model

In this section we shall treat a special case of mono-standard SWR system. It concerns DVB-T standard. It is used for broadcast transmission of digital terrestrial television. OFDM with IFFT size 2-K (2K-mode) or 8-K (8K-mode) is used to generate the multi-

carrier signal. There are actually 1705 or 6817 data carriers that are approximately 4 kHz or 1 kHz apart. DVB-T transmission is mainly on UHF 8 MHz channels and the channels are separated by integer multiple of 8 MHz respectively to avoid inter-channel interference. Thus a multi-channel DVB-T standard becomes a mono-standard SWR system as shown in Fig. 3.2.

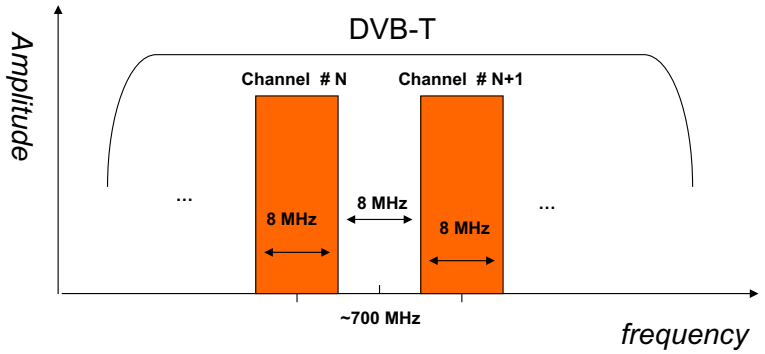

Figure 3.2: A multi-channel DVB-T can be considered as a mono-standard SWR system.

3.2.2 Multi-standard SWR system model

In case of a multi-standard SWR system, there are two scenarios. First, where the transmission power gap between standards is very large as in the case of WLAN and WiMAX. WiMAX base station transmission power is approximately +43 dBm (20 W) while that of a WLAN Access Point (AP) is approximately +18 dBm (60 mW). This power gap is denoted by ΔP in Fig. 3.3 (a). There is an inconvenience associated with power amplification of this signal which shall be shortly discussed. In Fig. 3.3 (b) we consider a case where multi-standard SWR system consists of standards with approximately the same transmission power. The approximate transmission power of GSM and UMTS base stations is around $20 - 40$ W.

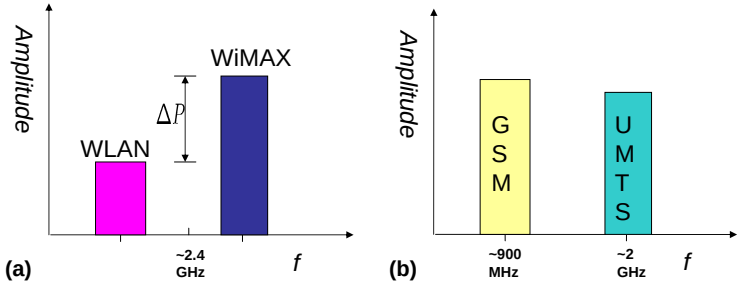

Figure 3.3: A bi-standard SWR system (a) WLAN & WiMAX with large transmission power gap. (b)GSM & UMTS with negligible transmission power gap.

3.2.3 Brief discussion about power amplification of SWR signal

An ideal SWR system would amplify a very large band consisting of several standards. In practical scenario there are standards with smaller transmission power compared to others as we have just discussed the case of WLAN and WiMAX whose transmission powers are separated by 25 dB. While the input to the amplifier does not vary a lot from standard to standard, amplification of different standard signals by a single power amplifier with a constant gain would violate the transmission power constraints of standards. This aspect of power amplification should be kept in mind while designing the future SWR systems. As HPA design is not the objective of this thesis we shall not discuss this issue in detail. However, a very intuitive approach could be the attenuation of the low transmission power standard by a certain scaling factor before the power amplification. In this way, when the attenuated signal is amplified by an amplifier with large gain, the output would respect the power mask as the signal was already appropriately scaled down. This concept is explained in Fig. 3.4 where WLAN signal is attenuated by a factor m as to make the output of HPA respect the difference between transmission powers of WLAN and WiMAX standards.

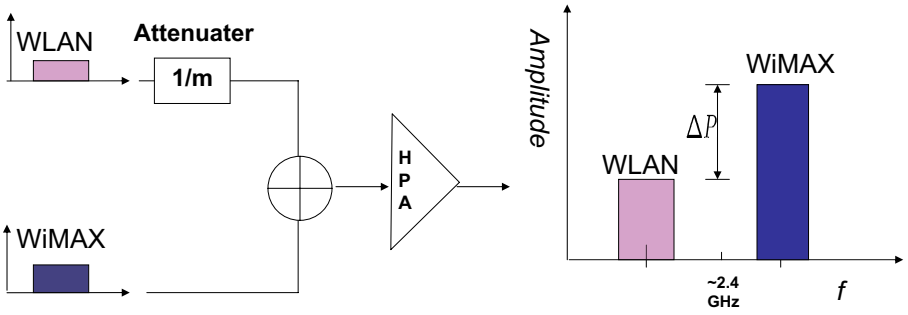

Figure 3.4: Amplification of multi-standard SWR signal.

3.3 Some SWR modulation schemes

In this section some modulation techniques will be discussed which are used in a SWR system containing some major standards like GSM, UMTS, Satellite Digital Video Broadcasting (DVB-S), Terrestrial Digital Video Broadcasting (DVB-T), Digital Audio Broadcasting (DAB) and WLAN.

3.3.1 OFDM

Recalling from Chapter 1 that OFDM is a modulation technique used in many standards like DVB-T, DAB, WLAN etc. In these standards IFFT (Inverse Fast Fourier Transform) is applied to mapped symbols in order to get a multi-carrier signal. These carriers are orthogonal and with constant inter carrier spacing $\Delta f = 1/T$ where T is OFDM symbol duration. A discrete time OFDM symbol $x(n)$ can mathematically be written as

$$x(n) = \sum_{k=0}^{N-1} C_k e^{2\pi jnk/N}, \tag{3.1}$$

where C_k is mapped data for $n = 0, 1, 2, ..., N-1$ and N is IFFT size. Fig. 3.5 shows a simple OFDM transmitter.

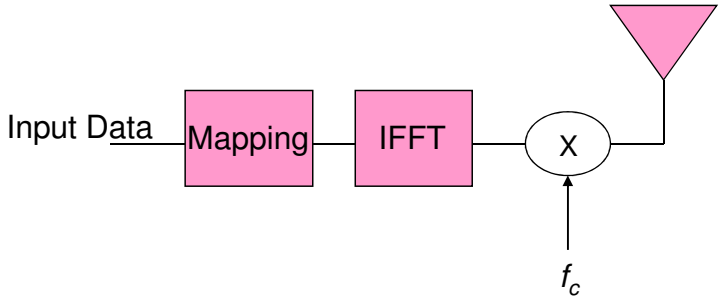

Figure 3.5: A simple OFDM transmitter.

In WLAN IEEE 802.11a/g and WiMAX IEEE 802.16a standards OFDM is used as modulation scheme with IFFT size of 64 and 256 respectively with $\Delta f = 0.3125\ MHz$ for WLAN IEEE 802.11a/g and $\Delta f = 0.078125\ MHz$ for WiMAX IEEE 802.16a. However the bandwidth occupied by the symbols of both standards is the same which is 20 MHz.

3.3.2 GMSK

Gaussian Minimum Shift Keying (GMSK) is the modulation scheme used in GSM, DECT and EDGE. Input signal is passed through Gaussian filter with time impulse response

$$g(t) = \sqrt{2\pi/\ln 2} B_{3dB} e^{-(2/\ln 2)(\pi B_{3dB} t)^2} \tag{3.2}$$

where B_{3dB} is $3dB$ bandwidth of the filter. In GSM, $BT = 0.3$ where T is bit duration while $BT = 0.5$ for DECT. Filtered data is then passed through Frequency Shift Keying (FSK) based MSK transmitter. Basic block diagram of a GMSK modulator is given in Fig. 3.6.

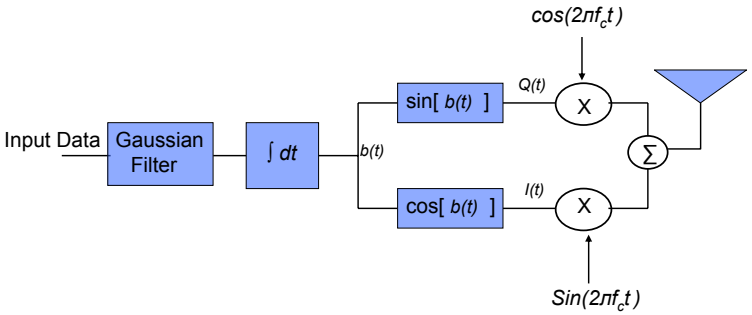

Figure 3.6: A simple block diagram of GMSK modulator

In GSM standard, at Base Station (BS) a large number of GMSK modulated signals are transmitted on different carrier frequencies as shown in Fig. 3.7. It generates a

'frequency division multiplex of single carrier signals' (multi-carrier signal) which affects PAPR distribution. This effect will be discussed in next section.

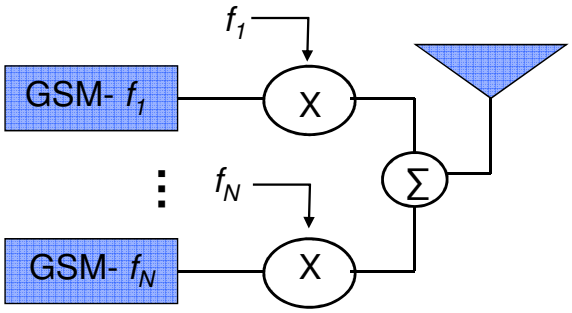

Figure 3.7: An N-carrier frequency division multiplexed GSM signal generation

3.3.3 QPSK

Quadrature Phase Shift Keying (QPSK) is a phase shift keying in which data is divided into two phases, quadrature to each other. This modulation is used in UMTS, DVB-S. In UMTS, Root Raised Cosine (RRC) filter is used as shaping filter with roll-off factor $\alpha = 0.22$ while in DVB-S $\alpha = 0.30$. Here is RRC time impulse response,

$$h(t) = 4\alpha \frac{\cos((1+\alpha)\pi t/T) + \frac{\sin((1-\alpha)\pi t/T)}{(4\alpha t/T)}}{\pi\sqrt{T}(1-(4\alpha t/T)^2)} \tag{3.3}$$

Fig. 3.8 shows single carrier and multi-carrier transmission of QPSK modulated data.

In Fig. 3.9 some of the communications standards including digital cordless telephone (DECT), wireless data (WLAN, WiMAX, WiBRO) and digital communication (UMTS, GSM, EDGE) standards are presented with some of their prominent features.

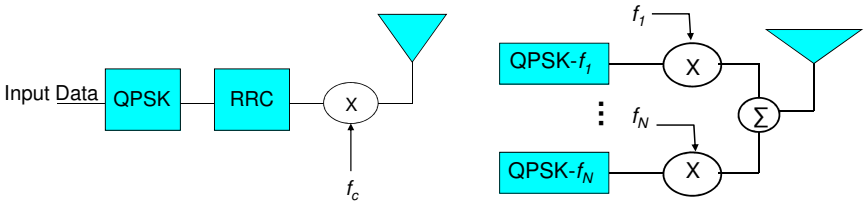

(a) A QPSK modulator (b) MC-QPSK transmission

Figure 3.8: Single carrier and MC-QPSK modulator

Standard	DECT	WiLAN 802.11b	WiLAN 802.11g	WiMAX 802.16a	WiBRO	WCDMA/UMTS	GSM	EDGE	DVB-T
Mobile frequency range (GHz)	1.88-1.90	2.41-2.462 (N. America) 2.412-2.472 (Europe)	2.41-2.462 (N. America) 2.412-2.472 (Europe)	2-11	2.3-2.4	Rx:0.869-0.894 Tx:0.824-0.849 Rx:1.930-1.990 Tx:1.850-1.910	Rx:0.925-0.960 Tx:0.880-0.915 Rx:1.805-1.880 Tx:1.710-1.785	Rx:0.925-0.960 Tx:0.880-0.915 Rx:1.805-1.880 Tx:1.710-1.785	0.3-3 (UHF)
Multiple Access method	TDMA/ FDMA	CSMA/CA	CSMA/ CA	TDMA/ OFDMA	OFDMA	CDMA/ FDMA	TDMA/FDMA	TDMA/ FDMA	FDMA
Duplex method	TDD	TDD	TDD	TDD/ FDD	TDD	FDD	FDD	FDD	--- (simplex)
Channel spacing	1.728 MHz	FHSS: 1 MHz DSSS: 25 MHz	20 MHz	20/25 MHz (USA) 28 MHz (Europe)	9 MHz	5 MHz	200 KHz	200 KHz	8 MHz (UHF), 7 MHz (VHF)
Modulation	GMSK (0.5)	DBPSK, DQPSK, CCK	OFDM, 64-QAM, 16-QAM, QPSK, BPSK	BPSK, QPSK, 4/16/64/2 56-QAM	4/16/64-QAM	QPSK, OQPSK	GMSK (0.3)	GMSK(0.3) 8-PSK	OFDM QPSK, 16/64 QAM
Peak data rate	1.152 Mbps	11 Mbps	54 Mbps	70 Mbps	18.432 Mbps	1.2288 Mbps	14.4 kbps	384 kbps	5-32 Mbps

Figure 3.9: Some communication standard with salient features.

3.4 SWR signal and ODFM signal analogies

As already explained, SWR can be defined as a system able of modulating and demodulating any kind of signal, anywhere, on any network [101]. Consequently any SWR signal $x(t)$ is a composite signal given by,

$$x(t) = \sum_{i=1}^{S} S_i(t), \tag{3.4}$$

where S is the number of standards contained in the composite SWR signal and S_i represents i^{th} standard. Each signal $S_i(t)$ associated to a given standard of P_i carriers can be expressed as,

$$S_i(t) = \sum_{p=1}^{P_i} r_{i,p}(t) e^{2j\pi f_{i,p} t},$$

where $r_{i,p}(t)$ represents the modulated and filtered signal associated to carrier p of the standard i. In this case, $r_{i,p}(t) = fem_i(t) * m_{i,p}(c(t))$, where $m_{i,p}(c(t))$ represents the modulation relative to the carrier p and standard i and $fem_i(t)$ is the shaping filter function of standard i. Using the two aforementioned equations, a multi-standard signal can be written as,

$$x(t) = \sum_{i=1}^{S} \sum_{p=1}^{P_i} (fem_i(t) * m_{i,p}(c(t)) e^{2j\pi f_{i,p} t}. \tag{3.5}$$

After formulating SWR signal, we shall present the analogies between OFDM and SWR signals. Here, SWR signal is a multi-carrier modulated signal where QPSK, GMSK and OFDM are the techniques used for modulation. All multi carrier signals show high PAPR as in the case of OFDM, Multi-Carrier Direct-Sequence Code Division Multiple Access (MC-DS-CDMA) [102] and Multi-Carrier GMSK [103]. In [104] it is shown that SWR and OFDM have the same behavior regarding the ratio between the symbol duration and the sampling duration. From their frequency representation, they also show the same analytical behavior for a mono standard SWR signal. This is the first level of analogy. The second level of analogy is the Gaussian equivalence which shows that PAPR distribution of any standard is similar to that of OFDM because of the multiplicity of carriers, under the non overlapping assumption. Extending this result, it has been shown that a multi-modulation signal reveals a Gaussian process and thus shows PAPR characteristics similar to those of OFDM. This result is of major importance because it provides the possibility to apply OFDM PAPR mitigation methods to SWR signals.

3.4.1 Analytical equivalence

In this section we shall analyze the conditions in which these two types of signals are equivalent. The direct consequence of this eventual equivalence would be the applicability of OFDM PAPR definition to SWR.

If the carrier inter spacing is constant for all standards, SWR signal will become a multi carrier signal, given by

$$x(t) = \sum_{i=1}^{S} \sum_{p=1}^{P_i} r_{i,p}(t) e^{2j\pi((p-1)\triangle p)t}, \tag{3.6}$$

where $\triangle p$ is the carrier inter spacing which is supposed to be constant for all standards. Generally speaking, this condition cannot be verified because the distance between carriers is different from one standard to the other [105]. Also the channel bandwidths of different standards are different which vary from 25 kHz for Personal Digital Cellular (PDC) to 20 MHz for WiMAX.

We suppose now a mono standard SWR signal. By definition then

$$S_i(t) = \sum_{p=1}^{P_i} r_{i,p}(t) e^{2j\pi f_{i,p} t}, i \in [1, S], \tag{3.7}$$

which is equivalent to

$$S_i(t) = \sum_{p=1}^{P_i} r_{i,p}(t) e^{2j\pi((p-1)\triangle p)t}, i \in [1, S]. \tag{3.8}$$

From an analytical point of view, Eq.3.8 is formulated in the same way as equation Eq.3.1 models an OFDM signal.

In all other cases, we cannot create any relation between SWR and OFDM signal and an OFDM signal remains a particular case of a SWR signal.

3.4.2 Gaussian equivalence

OFDM PAPR distribution has been discussed a lot in literature as mentioned in Chapter 1. [14] deals with PAPR distribution for OFDM signals and gives some Complementary Cumulative Distribution Function (CCDF) upper bounds. Also as discussed in previous chapter that we have given a new CCDF expression for OFDM signals with large over-sampling factors (continuous signals). Following Eq. 2.46,

$$Pr[PAPR \geq \gamma] \approx 1 - (1 - e^{-\gamma})^{\tau_2 N^{\mu}} = 1 - (1 - e^{-\gamma})^{\tau_2 N^{1.07}}. \tag{3.9}$$

where $\tau_2 = (\frac{5.12}{\sqrt{e}})^{1.07} e^{-\zeta}$. Soon we shall prove that OFDM PAPR CCDF is similar to PAPR CCDF for mono standard and multi standard SWR signals.

3.5 PAPR analysis of SWR signal

In this section PAPR analysis of SWR signal shall be performed. As SWR signal is a composite signal made by the addition of many i.i.d random variables, it should follow central limit theorem and exhibit Gaussian distribution. First PAPR analysis of a single standard SWR signal shall be done followed by multi standard SWR signal analysis. But before that central limit theorem is presented.

- Central Limit Theorem: Let $X_1, X_2, X_3, ...$ be a sequence of random variables which are defined on the same probability space, share the same probability distribution and are independent. Assume that both the expected value μ and the standard

deviation σ exist and are finite. Then the expected value of sum $S_n = X_1 + ... + X_n$ is $n\mu$ and its standard error is $\sigma n^{1/2}$ and the distribution of S_n approaches the normal distribution $N(n\mu, \sigma^2 n)$ as n approaches infinity.

3.5.1 PAPR analysis for a Mono Standard SWR signal

Gaussian equivalence between OFDM and mono standard SWR has been demonstrated first under the assumption of a large number of carriers by analyzing PAPR. This mono standard SWR signal follows complex Gaussian law. Simulations are performed for Multi Carrier GMSK (MC-GMSK), MC-QPSK and OFDM signals treating each modulation scheme at a time.

3.5.1.1 MC-GMSK PAPR analysis

GSM underlying modulation techniques is GMSK. GMSK is based on MSK which is itself a form of phase shift keying. The constellation diagram of GMSK modulated symbols is presented in Fig. 3.10 where the modulated symbols can take on any value on the circle. It means that the maximum and mean power values are the same. Thus $PAPR_{BB}$ of a single carrier GSM is 0 dB and $PAPR_{RF}$ is 3 dB as PAPR increases by 3 dB on RF transformation [94]. Here $PAPR_{BB}$ and $PAPR_{RF}$ are the base band and RF signal's PAPR respectively.

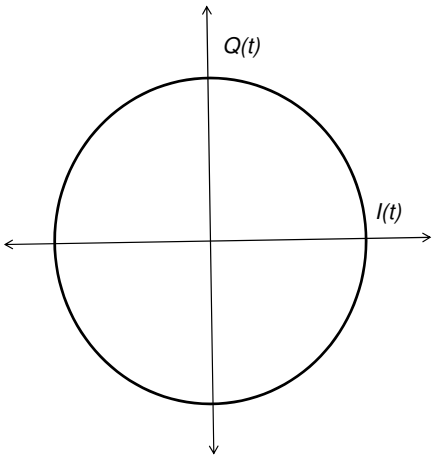

Figure 3.10: Constellation diagram of GMSK modulation.

But in practical environment, single carrier GSM signal is not transmitted. In fact, GSM signal transmitted from BS is a multiplex of single carrier GSM signals over different frequencies. Thus it is recommended to analyze GSM PAPR in multi-carrier situation. First of all we shall derive an upper bound for the maximum PAPR value and then shall discuss the distribution function.

- **Maximum MC-GMSK PAPR:** It is realized that maximum PAPR is attained when all the carriers are modulated with same input data. On doubling the number

of carriers, in this case, PAPR is increased by around 3 dB. This is because maximum of each carrier occurs at the same time, which doubles the signal peak. Consequently the maximum signal power becomes four times while average power becomes double. Thus PAPR becomes twice (3 dB increment). Maximum PAPR of MC-GMSK can be formulated as,

$$PAPR_{BB,MC-GSM,max} = 10log_{10}(N) \tag{3.10}$$

$$PAPR_{RF,MC-GSM,max} = 10log_{10}(N) + 3\ dB \tag{3.11}$$

where N is the number of GSM carriers. This is a non-practical scenario as it is almost impossible to get same input for all carriers, so after defining PAPR upper bound, instantaneous PAPR will be considered.

- **Instantaneous MC-GMSK PAPR:** As MC-GMSK signal is multi-carrier composite signal so according to central limit theorem it should be normally distributed as the number of carriers become large. Fig. 3.11 shows $PAPR_{RF}$ distribution of GMSK modulated symbols containing 64 and 128 carriers. Bandwidth-time product $BT = 0.3$ is used here.

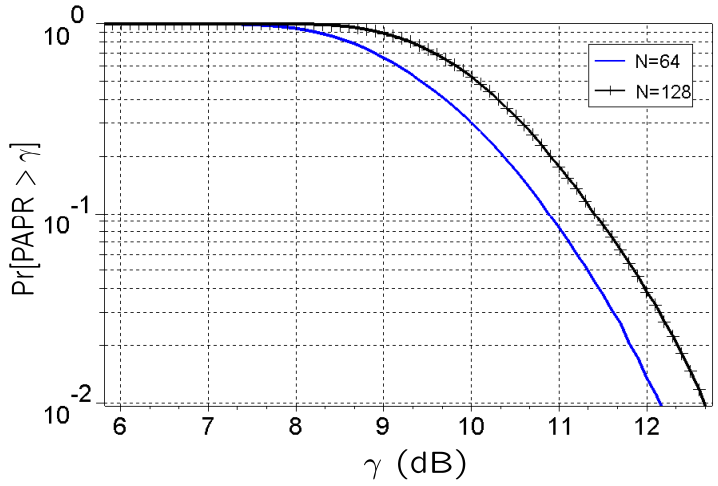

Figure 3.11: $PAPR_{RF}$ analysis of MC-GMSK with N=64,128

3.5.1.2 MC-QPSK PAPR analysis

QPSK is a phase modulation. In phase modulation schemes only the phase of the constellation point varies while the amplitude remains the same as shown in Fig. 3.12. So it is obvious that the maximum and mean values of the signal are same that means their ratio is equal to 1.

Thus $PAPR_{BB}$ and $PAPR_{RF}$ for a single carrier is 0 dB and 3 dB respectively at Nyquist rate, in the absence of a shaping filter. But after implying RRC filter, PAPR is influenced. This filter effect depends on many factors like filter length, roll-off factor etc. Now maximum and instantaneous PAPR in MC-QPSK case will be analyzed taking into account the filter effects.

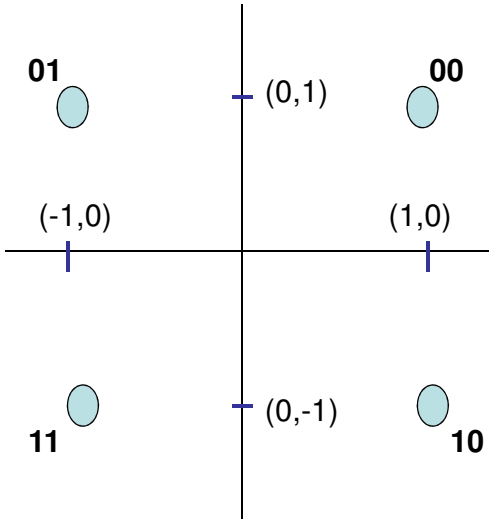

Figure 3.12: QPSK constellation diagram.

- **Maximum MC-QPSK PAPR:** Single carrier QPSK PAPR in the absence of filter, at Nyquist rate, is 0 dB and 3 dB in base-band and RF respectively. Therefore the expressions for maximum MC-QPSK PAPR are identical as Eq. (3.10) and Eq. (3.11).

  But in the presence of the filter, base band single carrier QPSK PAPR varies from around 7 dB to around 3.5 dB as roll-off factor changes from 0.01 to 1 as shown in Fig. 3.13. Also an analytical study is done on the RRC filter effect on PAPR in [106] and PAPR upper bounds are given for different roll-off factor values.

  Thus PAPR of a single carrier QPSK modulated RRC filtered signal is not a fix value as it depends upon the roll-off factor value. Also in MC-QPSK scenario on doubling the number of carriers, PAPR increases by 3 dB if the input data on all the QPSK carriers is same. Thus maximum PAPR of MC-QPSK can be formulated as:

$$PAPR_{BB,MC-QPSK,max} = 10log_{10}(N) + PAPR_{SC,BB} \tag{3.12}$$

$$PAPR_{RF,MC-QPSK,max} = 10log_{10}(N) + PAPR_{SC,RF} \tag{3.13}$$

  where N is the number of QPSK carriers and $PAPR_{SC,BB}$ and $PAPR_{SC,RF}$ are the PAPR values of single carrier QPSK in BB and RF conditions respectively. $PAPR_{SC,BB}$ and $PAPR_{SC,RF}$ values depend upon the value of roll-off factor of the filter. For the same roll-off factor $PAPR_{SC,RF}$ is 3 dB more than $PAPR_{SC,BB}$ due to the RF transposition.

- **Instantaneous MC-QPSK PAPR:** To analyze a practical scenario with random input data at the inputs of all the QPSK modulators , simulations are performed for of 10^4 MC-QPSK symbols containing 64 and 128 carriers with oversampling factor

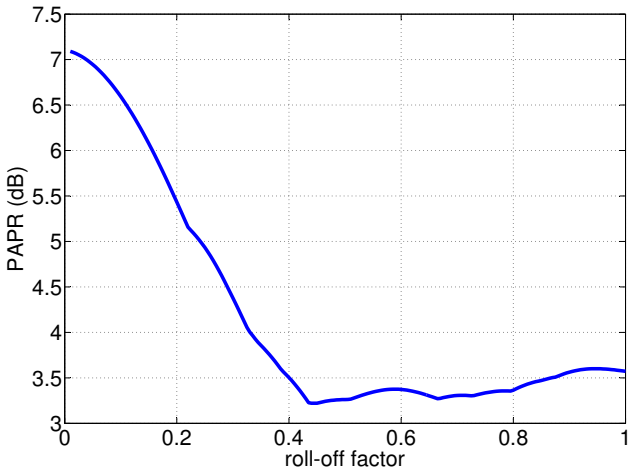

Figure 3.13: Influence of filter roll-off factor on QPSK PAPR.

of 4 in RF conditions. As the signal is sum of large number of i.i.d carriers thus it follows central limit theorem. Accordingly its PAPR distribution is alike MC-GMSK PAPR distribution as depicted in Fig. 3.14.

3.5.2 PARP analysis of a Multi Standard SWR signal

PAPR analysis of a multi standard SWR signal containing OFDM, MC-GMSK and MC-QPSK signals, is considered. General specifications used for each standard are same i.e. $N = 64$ carriers/sub carriers and 10^4 symbols. This analysis is done in RF conditions. First one can see in Fig. 3.15 that the probability density function of the real part of SWR signal shows Gaussian distribution following central limit theorem. Then PAPR CCDF of SWR signal is presented in Fig. 3.16. First, it can be shown that all standards have almost similar PAPR CCDF, confirming Gaussian equivalence. Secondly, from a statistical point of view, as SWR signal is generated by the combination of these standards, PAPR CCDF of a SWR signal also demonstrates Gaussian distribution. In conclusion, any multiplex of carriers or standards, exhibits Gaussian distribution, independent of the modulation techniques and the carrier frequencies. From a PAPR point of view, SWR and OFDM show similar behaviors. Recently PAPR evaluations in a multi-mode SDR transmitter as well as receiver are studied in [107].

3.6 Frequency Domain Interpretation of PAPR Metric

After describing the analogies between OFDM and SWR signal, we propose a new PAPR definition based on frequency components' information of a signal. This frequency based PAPR definition is more compatible SWR context where different standards occupy different frequency bands. We shall start with classical time domain PAPR definition and end up at a frequency PAPR definition after some mathematical developments.

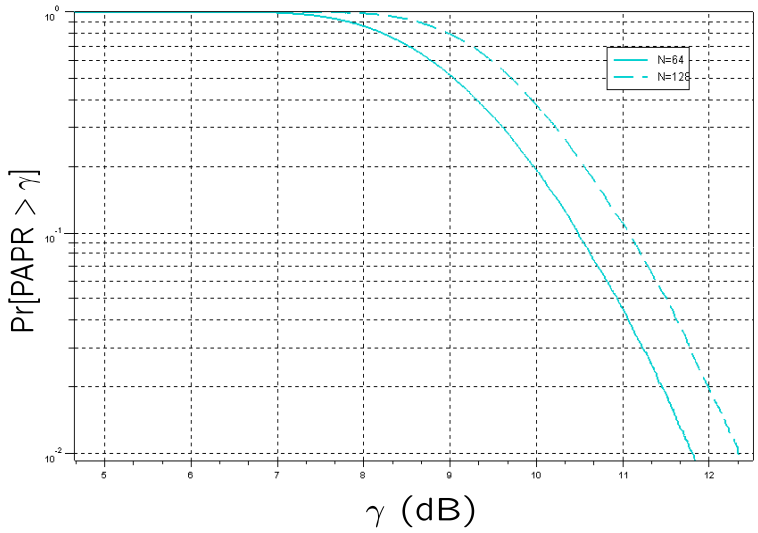

Figure 3.14: $PAPR_{RF}$ analysis of MC-QPSK with N=64,128

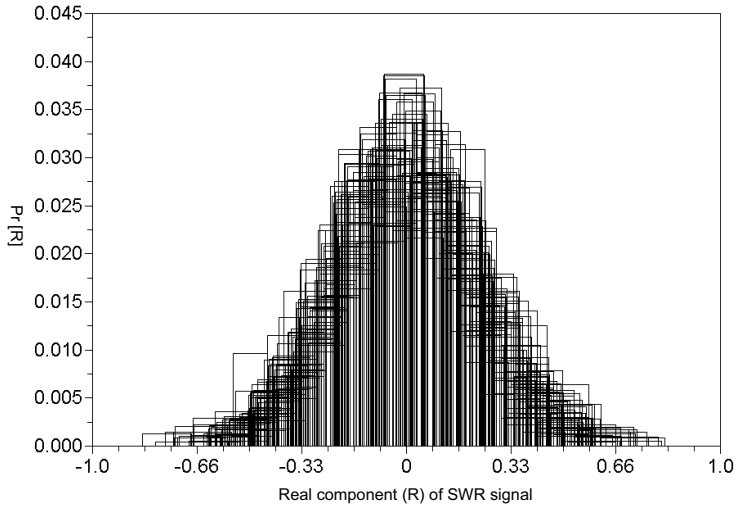

Figure 3.15: Probability density function of real part of SWR signal

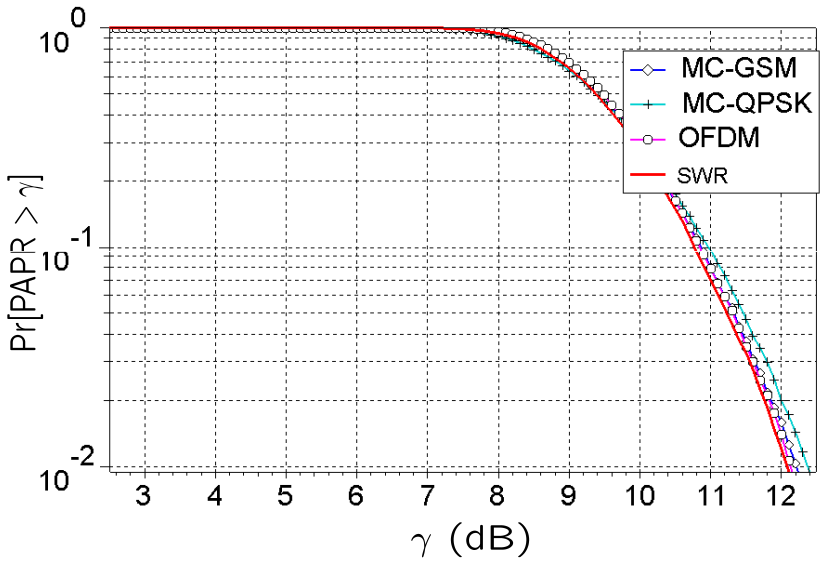

Figure 3.16: PAPR distribution of a SWR signal with MC-GMSK, MC-QPSK and OFDM modulation in RF.

3.6.1 PAPR Definition in OFDM Context

According to [94] theoretical PAPR ($PAPR_{th}$) of a given temporal signal $S(t)$ defined over $[0, T]$ is the ratio between the maximum value of the instantaneous power and its expectation value given by

$$PAPR_{th}(S(t)) = \lim_{T\to\infty} \frac{\max\limits_{t\in[0,T]} |S(t)|^2}{E[|S(t)|^2]}. \tag{3.14}$$

Practical cases involve the use of sampled signals under the ergodic assumption, turning the expectation calculation to a classical sum. Subsequently $PAPR_{th}$ is viewed as an upper bound which is attained by simulating oversampled signals. Then, the resulting PAPR $PAPR_N(s(k))$ of a sampled signal of components $s(k)$ calculated on N samples is given by

$$PAPR_N(s(k)) = \frac{\max\limits_{k\in[0,N-1]} |s(k)|^2}{\frac{1}{N}\sum_{k=0}^{N-1} |s(k)|^2}. \tag{3.15}$$

If this metric is computed on an infinite number of samples, we obtained a very good approximation of theoretical PAPR upper bound. In an OFDM context, this well known result gives the maximum power ratio value versus number of subcarriers N. This upper bound is

$$PAPR_{th} = 10log_{10}(N). \tag{3.16}$$

This result will be used when we proceed to compute PAPR for a large number of OFDM symbols. We start with a very intuitive approach: larger the number of symbols to

compute PAPR, closer the results to the theoretical upper bound. To do so, we consider here a large number (N_s) of OFDM symbols. The resulting complex baseband signal becomes

$$S(n) = \sum_{j=1}^{N_s} S_j(n), n = 0, ..., N_S N - 1, \tag{3.17}$$

where each OFDM symbol of N points is defined by

$$S_j(n) = \sum_{k=0}^{N-1} C_{j,k} e^{2j\pi \frac{kn}{N}}, n \in [(j-1)N, jN-1], j \in [1, N_S]. \tag{3.18}$$

Let us define $I = [0, N_S N - 1]$, $J = [1, N_S]$ and $K = [0, N - 1]$. By taking into account that the signals $S_j(n)$ are defined over separate intervals

$$\max_{n \in I} |S(n)|^2 = \max_{n \in I}(\max_{j \in J}(|S_j(n)|^2)). \tag{3.19}$$

On the other hand, after some maths and under ergodic assumption, it can easily be shown that

$$E[|S(n)|^2] = \frac{1}{N_s} \sum_{j=1}^{N_S} E[|S_j(n)|^2]. \tag{3.20}$$

Finally, according to the theoretical PAPR definition, we get

$$PAPR_{N_s}(S(n)) = \frac{\max_{n \in I}(\max_{j \in J}(|S_j(n)|^2))}{\frac{1}{N_s} \sum_{j=1}^{N_s} E[|S_j(n)|^2]}, \tag{3.21}$$

which is PAPR of an OFDM signal calculated over N_S symbols. Eq.3.21 can also be expressed in terms of information symbols $C_{j,k}$'s. Actually, as

$$\max_{n \in I} |S_j(n)|^2 \leq N^2 \max_{k \in K} |C_{j,k}|^2, \tag{3.22}$$

and

$$\sum_{j=1}^{N_S} E[|S_j(t)|^2] = N \sum_{j=1}^{N_S} E[|C_{j,k}|^2], \tag{3.23}$$

we also have

$$PAPR_{N_s}(S(n)) \leq N \frac{\max_{j \in J}(\max_{k \in K}(|C_{j,k}|^2))}{\frac{1}{N_s} \sum_{j=1}^{N_s} E[|C_{j,k}|^2]}. \tag{3.24}$$

This way of PAPR computation is illustrated in Fig.3.17. It clearly shows the necessity of calculating PAPR of OFDM signals over a large number of symbols (here $N_S = 10^5$). This leads to a novel PAPR vision, i.e. carrier per carrier which is explained in the next subsection.

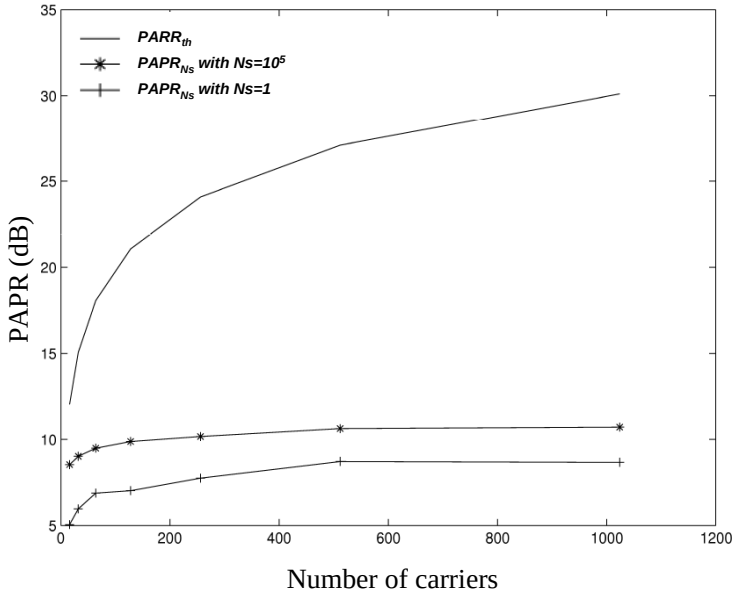

Figure 3.17: PAPR calculation for N_S OFDM symbols.

3.6.2 Carrier per Carrier Vision of OFDM PAPR

Starting from the previous multi symbol OFDM vision, the proposed principle is to fill an N_S by N table whose each row refers to frequency components of an individual OFDM symbol of length N. Fig.3.18 represents the division of OFDM input data into N_s by N table. As depicted in Fig.3.19, each row in table 'C' refers to frequency components $X_i(n)[i \in [J]]$ present in temporal OFDM symbol $S_i(n)$ and each column is associated to a signal $\nu_k(n)$. In this case, a column k is associated to a carrier f_k and the idea is to calculate PAPR column wise and to show that it is similar to PAPR calculated row wise. Fig. 3.19 illustrates this way of calculation where each $\nu(.)$ function is given by

$$\nu_k(j) = \sum_{m=0}^{N_S-1} C_{m,k} e^{2j\pi \frac{jm}{N_s}}, k \in K, j \in J. \tag{3.25}$$

This clearly shows that PAPR of $X(n)(= \sum_{i=1}^{N_s} X_i(n), n = 0, ..., N_S N - 1)$ can either be calculated with $\nu_k(n)$ or with $X_j(n)$ functions. As

$$\max_{n \in I} |X(n)|^2 = \max_{n \in I}(\max_{k \in K}(|\nu_k(n)|^2)), \tag{3.26}$$

and with the help of Parsaval theorem, this directly leads to an other PAPR definition of $S(n)$

$$PAPR_{N_s}(S(n)) \leq N \frac{\max_{k \in K}(\max_{j \in J}(|C_{j,k}|^2))}{\frac{1}{N_s}\sum_{j=1}^{N_s} E[|C_{j,k}|^2]} = N \frac{\max_{k \in K}(|\nu_k(n)|^2)}{\frac{1}{N_s}\sum_{j=1}^{N_s} E[|C_{j,k}|^2]}. \tag{3.27}$$

Then, it is possible to get PAPR of a signal calculated over a large number of signals with the help of intermediate signals as $\nu_k(n)$.

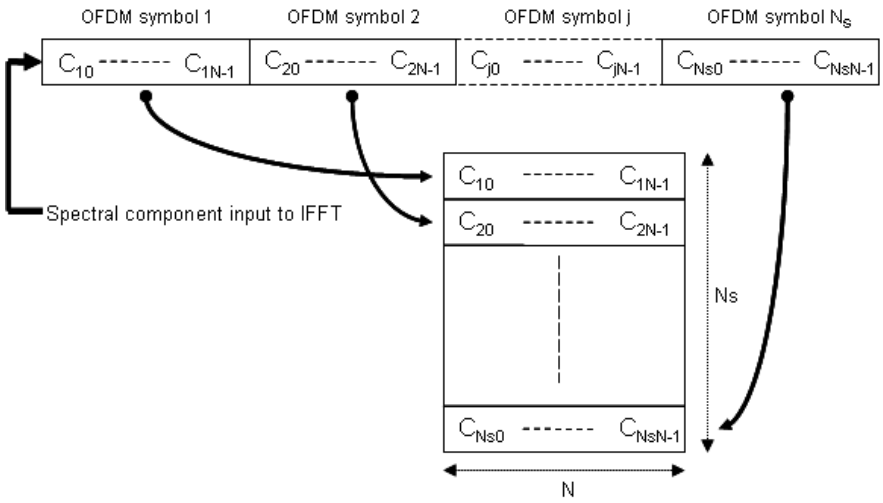

Figure 3.18: Frequency symbol wise vision of an OFDM signal.

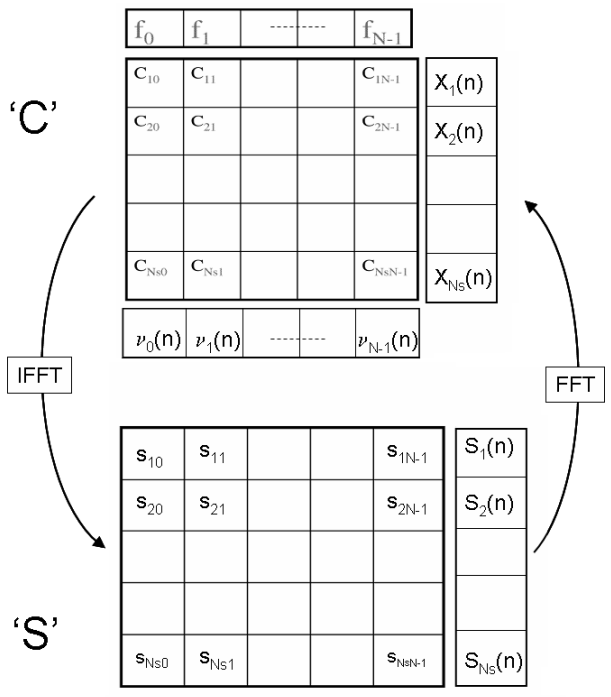

Figure 3.19: Time and frequency vision of an OFDM signal.

This new vision paves the way to a carrier wise analysis of PAPR whose objective is to find a relation between $PAPR_{N_S}$ and individual power ratios $PAPR_{f_k}$ calculated on each carrier f_k given by

$$PAPR_{f_k} = \frac{\max\limits_{j\in J} |C_{j,k}|^2}{\frac{1}{N_S}\sum_{j=1}^{N_S} |C_{j,k}|^2} = \frac{\max\limits_{j\in J} |C_{j,k}|^2}{P_m(k)}, \tag{3.28}$$

where $P_m(k)$ refers to mean power calculated on carrier f_k.

By using temporal expression of the OFDM symbols, it can be easily shown that

$$PAPR_{N_s}(S(n)) = \frac{\max\limits_{k\in K}(\max\limits_{j\in J}(|s_{j,k}|^2))}{\frac{1}{N_s}\sum_{j=1}^{N_s} E[|s_{j,k}|^2]}, \tag{3.29}$$

where the $N_S N$ $(s_{j,k})_{j,k\in J\times K}$ components are obtained by computing N_s N-length IFFTs on each row of 'C' to fill bottom table 'S' in Fig. 3.19. Now we get

$$|s_{j,k}|^2 = \sum_{p=1}^{N} |C_{j,p}|^2 + \lambda(j,k), j \in J, k \in K. \tag{3.30}$$

with

$$\lambda(j,k) = \sum_{p=1}^{N} C_{j,p} \sum_{p'\neq p} \overline{C_{j,p'}} e^{2j\pi\frac{k(p-p')}{N}}, j \in J, k \in K.$$

As

$$\max_{j\in J} |C_{j,k}|^2 = P_m(k) \times PAPR_{f_k}, \tag{3.31}$$

and the final result is

$$PAPR_{N_s}(S(n)) \leq \frac{(\sum_{k=1}^{N} P_m(k) \times PAPR_{f_k}) + \max\limits_{k\in K}(\max\limits_{j\in J}(\lambda(j,k)))}{\sum_{k=1}^{N} P_m(k)}. \tag{3.32}$$

In this equation, $PAPR_{N_s}$ is upper bounded by addition of the weighted average of all $PAPR_{f_k}$ metrics and a constant depending on the frequential component correlation. From now on $PAPR_{N_s}$ will be termed as $PAPR_{temp}$ to underline temporal PAPR.

Fig.3.20 confirms this result in an OFDM context. Simulations are performed for 16-QAM mapped OFDM symbols. In fact, it is clear by computing both sides of Eq.3.32 that $PAPR_{temp}$ can be approximated by a combination of individual PAPRs calculated over all the signal carriers.

This carrier per carrier PAPR calculation vision leads to another PAPR calculation manner in which temporal signal is first sliced in N_s symbols of N samples each. These symbols fill the N_s rows of table 'S'. Then, each row is processed with N point FFT to get the spectral components of the signal and thus table 'C' is filled in Fig.3.19. Then, PAPR is computed as explained above. This process of slicing the temporal signal is illustrated

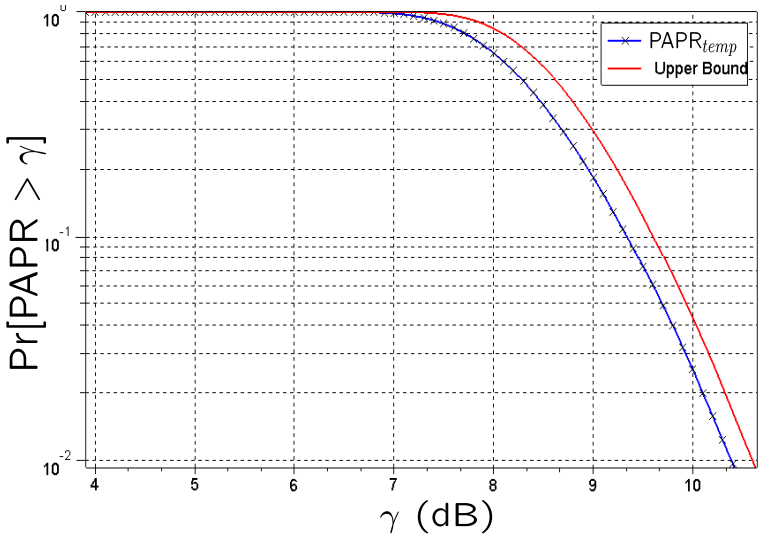

Figure 3.20: Frequency PAPR calculation for 64 carrier base band 16-QAM-OFDM signal.

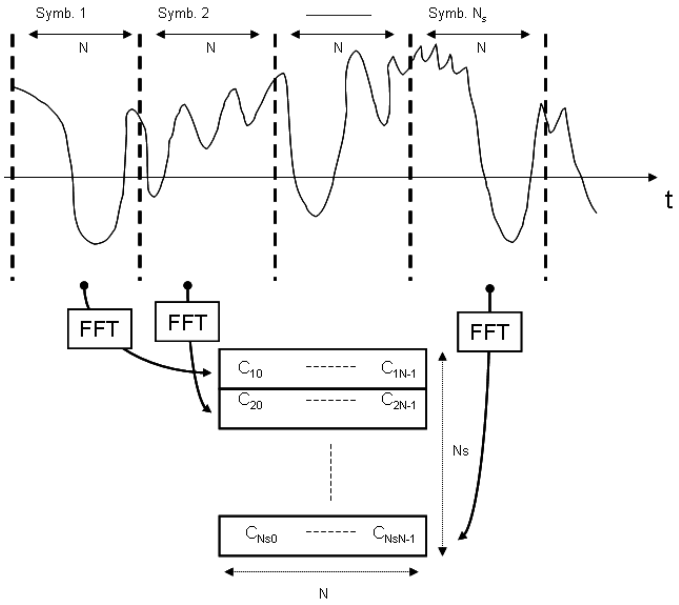

Figure 3.21: Temporal signal slicing for PAPR upper bound calculation.

in Fig.3.21.

This result clearly shows the link between temporal and frequential PAPR calculations. Last section will extend this result to SWR signals.

3.6.3 Carrier per Carrier Vision of SWR PAPR

According to the previous sections, we know that there is a strong equivalence between SWR signal and OFDM signal. Therefore the frequency domain interpretation given above for an OFDM signal should also be true for SWR signal. In fact, as shown in the Fig.3.21, it is always possible from a temporal signal $S(t)$ to derive its frequency domain counterpart through FFT operation. Then the obtained FFT blocks can easily be put in a table as the OFDM table in Fig.3.19. It is straightforward to apply Eq.3.32 to this new situation. We shall first see this theory for mono standard SWR signal before simulating it for multi standard SWR signal.

3.6.3.1 Mono standard SWR Case

The justification of the upper bound can be provided with the help of any multi carrier signal other than OFDM. Here, a multi-carrier GMSK signal is considered. Simulations were performed for a multiplex of 64 carrier GMSK signal. Fig.(3.22) exhibits that frequency PAPR definition upper bounds temporal PAPR values. FFT was applied to get the spectrum values of the multi-carrier signal and placed in the table of 4 rows.

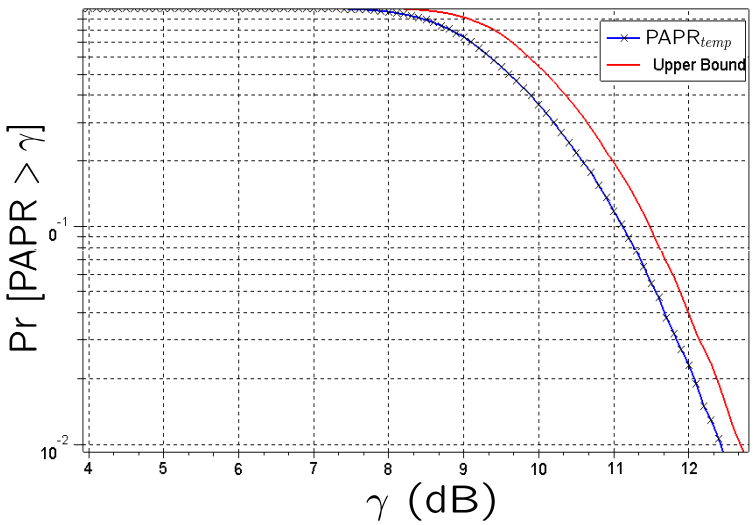

Figure 3.22: Frequency PAPR calculation for 64 carrier GMSK.

3.6.3.2 Multi standard SWR Case

A composite signal of multi carrier modulation schemes of three standards (GSM, UMTS and WLAN) was simulated with each of the standard containing 64 carriers. This SWR

signal was mapped to the mentioned table format where each row of the table 'S' representing time domain SWR symbols. 10^4 SWR signals were simulated. The table was transformed to frequency domain using FFT to fill 'C'. Fig.3.23 demonstrates the application of Eq.3.32 to SWR signal.

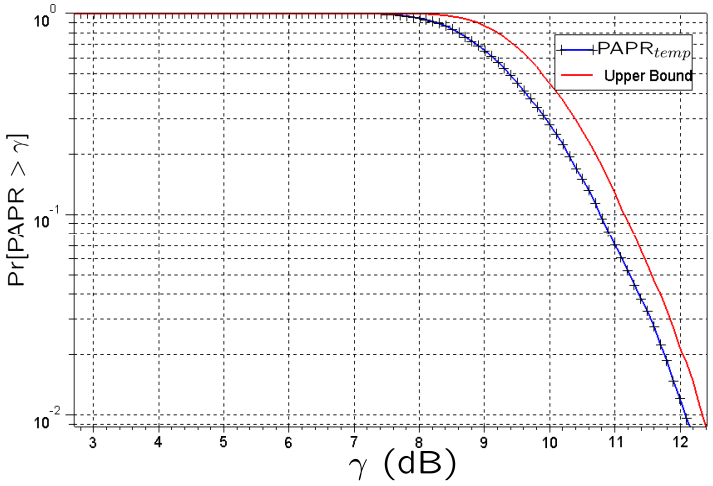

Figure 3.23: Frequency PAPR calculation for SWR signal.

3.6.4 Discussions

There are a couple of factors which affect upper bound values and in this section we shall discuss them.

3.6.4.1 FFT Size Effect

Dimension of the table is an important issue in the calculation of upper bound. When the symbols are mapped such that the row size (FFT size in turns) in the table is small, the difference between upper bound and $PAPR_{temp}$ is large. As we go on increasing the row size, upper bound approaches $PAPR_{temp}$ until it matches $PAPR_{temp}$ when number of rows become one i-e FFT is taken over the whole data. Fig.3.24 explains this fact where SWR signal is simulated. SWR symbols of size 256 are mapped to the tables of row size (FFT size) 32, 128 and 256. It is obvious that $PAPR_{temp}$ remains same as FFT size changes but as the row size goes on increasing upper bound approaches $PAPR_{temp}$. Let us clarify that the cross over of the curves is just an artifact of simulation.

3.6.4.2 Modulation Type Effect

OFDM symbols are mapped before the application of IFFT. Any modulation technique can be used to map input bits like QPSK, QAM etc. In calculation of PAPR using carrier per carrier PAPR vision, if the modulation techniques is PSK (Phase Shift Keying) then $PAPR_{temp}$ and upper bound have the same values but in case of any other modulation technique $PAPR_{temp}$ is upper bounded by right hand side (RHS) of Eq.3.32. This fact is illustrated in Fig.3.20 and Fig.3.25 where $PAPR_{temp}$ is upper bounded by RHS of Eq.3.32

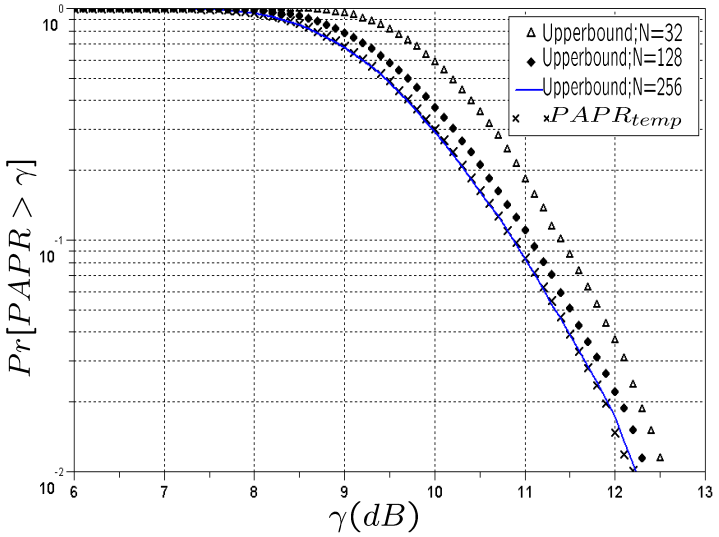

Figure 3.24: FFT Size Effect on Frequency PAPR calculation for SWR signal.

for non PSK modulation (QAM) and is exactly equal to upper bound for PSK modulation (QPSK) respectively.

3.6.4.3 Reasons

The reason lies in the variation of factor, $\sum_{k=1}^{N} P_m(k) \times PAPR_{f_k}$, with N in Eq.3.32. Keeping in mind Eq.3.31 it is clear that this factor is the sum of maximum values on all carriers. For a fixed signal length, when N is small, number of rows N_s of the table become large. Thus increases the possibility of getting maximum or comparatively large values of the constellation on all frequencies which in turns increases $\sum_{k=1}^{N} P_m(k) \times PAPR_{f_k}$ and thus the upper bound. When N is made equal to signal length both sides of Eq.3.32 become exactly equal following classical definition of FFT. Thus there is a trade-off between FFT size N and tightness of the upper bound to $PAPR_{temp}$. Smaller the FFT size, farther the upper bound from $PAPR_{temp}$ and vice versa.

Similarly for PSK modulations as maximum and mean of the constellation are equal so $\sum_{k=1}^{N} P_m(k) \times PAPR_{f_k}$ does not vary with N and thus the upper bound remains equal to $PAPR_{temp}$.

3.7 Conclusion

In this chapter SWR system and signal was discussed. Then SWR signal was presented and it was shown that SWR signal is a multi standard, multi carrier signal with carriers on different frequencies and modulated with different modulation schemes. Analytical and Gaussian equivalence was proved between OFDM and SWR signals. Then the PAPR analysis was performed for mono standard and multi standard SWR signals. OFDM, GMSK and QPSK modulation based multi-carrier signals were considered here. The PAPR distribution of multiplexed single carrier signals like MC-GMSK and MC-QPSK was found

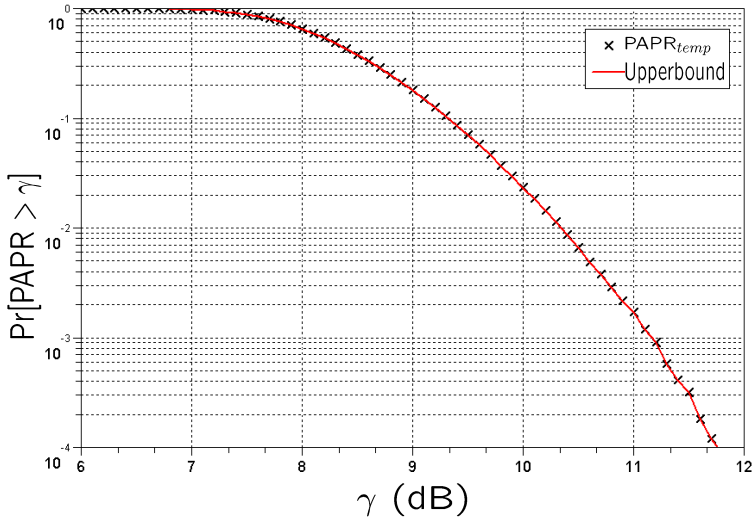

Figure 3.25: Frequency PAPR calculation for 64 carrier base band QPSK-OFDM signal.

to be identical to classical multi carrier OFDM PAPR distribution. A SWR signal was then generated by the combination of the signals which were modulated by the mentioned modulation techniques. Its PAPR analysis revealed that it also demonstrates Gaussian distribution following central limit theorem. In short, any multi-carrier signal with a large number of carriers, exhibited Gaussian distribution, independent of the modulation techniques and the frequencies of the carriers. Further, frequency domain interpretation of PAPR was presented which is in more harmony with the frequency view of SWR systems. It was demonstrated that an upper bound on PAPR can be obtained with the help of only frequency components of a signal. Thus when a time domain SWR signal is transformed to its frequency domain and the information on each carrier can lead to the PAPR calculations. This frequency view along with OFDM-SWR analogies further helps in the implementation of some OFDM PAPR reduction techniques on SWR systems like Tone Reservation discussed in Chapter 1. In Tone Reservation, certain tones are reserved for OFDM PAPR reduction. Same will be the case in SWR where added tones might be placed in between or inside the standards to reduce PAPR of the whole SWR signal while respecting each standard's spectrum mask constraints. This issue shall be detailed in coming chapter.

Chapter 4

PAPR Reduction of SWR Signals

Contents

4.1 Introduction

As already discussed that SWR signals suffer from high PAPR. Thus to avoid PA non-linear distortions, the PAPR of SWR signal should be reduced. This chapter deals with the PAPR reduction of theoretical SWR signals. After briefly discussing the already developed PAPR reduction methods for OFDM systems, one of them is selected for SWR systems known as Tone Reservation. As discussed in Chapter 1 that Tone Reservation is a method where a subset of carriers is not used to transmit information, rather it is used to transmit a corrective signal which reduces the PAPR of information signal. Tone Reservation method is discussed in detail here. Different formulations to obtain the optimized reserved carriers are discussed. The addition of correcting signal to information signal results in mean power increase. Different aspects of this mean power increase are underlined by adding constraints in the optimization function. These constraints include the constraints on the overall mean power of the correcting signal and constraints on each reserved carrier's power. These constraints not only help in controlling the additional mean power but also make the reduced PAPR signal respect spectral power mask constraints, if there are any.

SWR signal's PAPR reduction analysis is not a straight forward task keeping in mind the SWR bandwidth which renders to high computational complexity. Also the fact that different standards have different symbol duration, bandwidth, carrier frequency etc. Therefore, SWR PAPR reduction shall not be performed in one step rather different aspects of SWR PAPR reduction using Tone Reservation method shall be discussed in various steps. These steps are highlighted below:

- Starting with a simple OFDM case, the effect of some corrective signal properties which influence the PAPR reduction performance are discussed. It is revealed that corrective signal's bandwidth and power are proportional to PAPR reduction gain while the bandwidth gap between useful and corrective carriers is inversely proportional to the PAPR reduction gain.

- Then Multi-band OFDM (MB-OFDM) PAPR reduction through Tone Reservation is performed. In this case, two OFDM symbols are separated by a certain frequency band and some PAPR reducing carriers are associated to both OFDM symbols. These reserved carriers' properties are selected with the help of previously gained knowledge for simple OFDM case. MB-OFDM PAPR reduction is performed with mean power constraints on corrective signal. The MB-OFDM scenario can be thought of as a DVB-T standard where OFDM modulated various channels are transmitted on different carrier frequencies separated by a specific band.

- Multi-channel GSM case is considered next. A GSM BS transmitter is considered with four GSM channels. The free GSM channels in between these used GSM channels are utilized to transmit special signal which reduces the GSM PAPR. The power

of PAPR reduction signal is kept under C/I values defined in GSM standard in order to avoid inter-channel interference.

- MB-OFDM PAPR reduction method is generalized for PAPR reduction of a multi-standard SWR signal. In fact two OFDM based arbitrary standards with different transmission spectral power mask constraints are considered. There are some unused carriers inside these standards which are used to reduced the PAPR. Then further PAPR is reduced with an improvisation that reserved carriers are positioned in between the standards on free band with some power constraints. The PAPR reduction performance by intra-standard and inter-standard reserved carriers is compared. Also the effect of variation in mean power, bandwidth and position of inter-standard peak reducing carriers on PAPR reduction performance is discussed in this chapter.

4.2 OFDM Peak to Average Power Ratio Reduction Methods: a Brief Discussion

The conventional solution of high PAPR problem is to back-off the operating point of non-linear amplifier. This way the constraints on the signal dynamics are reduced as the probability of signal's peak entering the saturation zone of PA is reduced. But as we know that PA efficiency reduces as we back-off from saturation zone and thus this approach results in a significant power efficiency penalty. The alternative solution is the reduction of PAPR while operating the PA in high efficiency region. And several methods have been designed to reduce the PAPR of the OFDM signal [4, 5].

The simplest approach is to clip the OFDM signal but clipping itself is a nonlinear process and causes in-band and out-of-band distortions that results in performance degradation [6]. Some other techniques use coding, in which a data sequence is embedded in a larger sequence and only a subset of all the possible sequences are used to exclude patterns with high PAPR [88]. Also some multiple signal representation techniques have been proposed which include Partial Transmit Sequence (PTS) technique [7], Selective Mapping Technique (SLM) [8], and interleaving technique [84]. These techniques require side information to be transmitted to recover the original data from the received signal. Another kind of method called Tone Reservation [9] uses the reserved tones to generate the reducing signal. Wang [108] proposes a method with low complexity also based on the concept of Tones Reservation. Unfortunately, this method uses a trial-and-error approach without a deep theoretical justification. Recently, a method using convex optimization subject to constraints on the allowed constellation error to reduce PAPR has been presented [109]. Contrary to Tones Reservation methods, it reduces PAPR by adding a corrective signal to all data carriers that degrade the BER. Also [16] proposed the improvements of the methods proposed in [9] and [108] by modeling them as a Second Order Cone Program (SOCP). In [110] SOCP is used to reduce PAPR of MIMO systems.

We have selected Tone Reservation to reduce SWR signal PAPR. It is selected due to numerous reasons. Firstly, Tone Reservation is about optimization of specific carriers (frequency domain vision) which better suites the SWR vision as SWR is composed of different standards on different frequencies and it provides a better view to insert reserved carriers on proper frequencies. Secondly, the objective is not to modify the already developed standards. When the reserved carriers are positioned on the unused carriers of any

standard, the receiver modifications are not necessary as the contents of unused carriers are ignored. The need to transmit side information is also avoided. No BER degradation occurs as the reserved carriers are orthogonal to data carriers. No data rate loss is another positive of this method due to the reason that reserved carriers are carried on unused carriers of the standards. The main disadvantage of this method is the increase in mean power due to corrective signal addition which can be constrained according to PA characteristics. Also the spectrum mask constraints should be taken care of while using the unused carriers of the standards. These carriers are kept unused intentionally so as to avoid inter channel interference, thus the use of unused carriers as peak reducing carriers should not increase inter channel interference. Further, the high computational complexity to calculate corrective tones can not be ignored.

4.3 Tone Reservation based PAPR reduction

Tone Reservation (TR) is a subclass of Adding Signal method class [5] for PAPR reduction. Adding Signal methods decrease the PAPR by adding signal on any frequency whether in- or out- of the standard band, over used or unused carriers. The signal after PAPR reduction can or can not suffer from BER degradation like clipping [6] is an adding signal method where the modified (clipped) signal loses information and results in BER degradation while on the other hand TR methods do not result in BER degradation. Below, TR technique is detailed along with a scheme that implements this concept.

4.3.1 Tone Reservation Methodology

As discussed earlier that all the existing PAPR reduction methods come at some cost. In case of some methods the price is BER degradation as in Clipping, Tone Injection etc. While some methods suffer receiver modifications like coding methods. On the other hand some methods need SI transmission to recover the data like PTS, SLM methods. The focus in this thesis is on a method that does not change the standard specifications and the receiver design. Also no data-rate loss and no BER degradation occurs on PAPR reduction.

TR technique is about reserving specific tones for PAPR reduction such that the PAPR after adding these tones is reduced compared to initial PAPR. These reserved tones are called 'peak reducing carriers' (PRC) in literature and alternatively the TR method is called PRC [17]. Onwards, the reserved tones shall be designated by *PRC*. As shown in the Fig. 4.1, '**C**', *PRC*, which are orthogonal to the data tones '**X**', when added to data tones result in a signal with reduced peak. Because of the orthogonality, *PRC* do not create in-band interference i-e no BER degradation. There is no need of transmitting SI as *PRC* are transmitted on unused carriers in our case and the receiver already knows the position of unused carriers defined by the standard specifications. Also no receiver modifications are required as nothing is modified at the transmitter except the addition of a signal which is filtered out automatically as the receiver ignores the *PRC* contents. One of the disadvantages of TR is the increase in mean power of the transmitted signal because of corrective signal addition. Secondly, the computational complexity of the optimization algorithm to calculate the optimized corrective tones which reduce original signal's PAPR. Also the use of unused tones of a standard should be performed very carefully so as not to create inter channel interference and to respect the spectrum mask.

Here, we would also like to describe that *PRC*s can also be artificially created by performing oversampling (with the help of zero-padding in frequency domain). These carriers are called 'Ghost carriers' due to their physical non-existence [111].

There are certain methods to optimize the corrective tones. As discussed earlier SOCP optimization is one of them which will be detailed shortly.

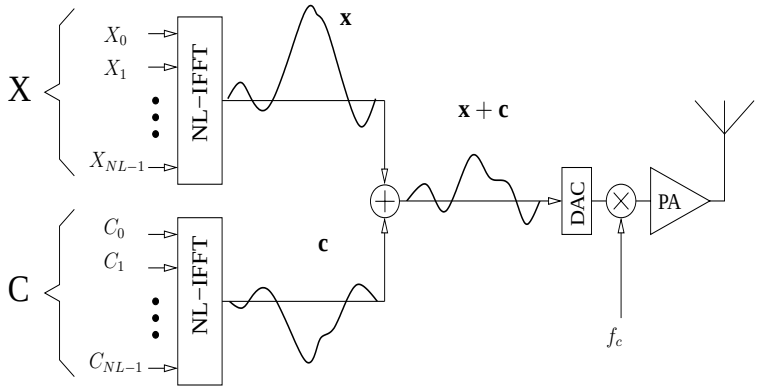

Figure 4.1: TR methodology based PAPR reduction.

Just a little clarification, 'PRC' written in normal and italic shapes represent PRC methodology and peak reducing *carriers* respectively.

4.3.2 Tellado Formulation of Tone Reservation

By construction Tellado [9] forces the data vector **X** and *PRC* vector **C** to be orthogonal. That means,

$$X_k + C_k = \begin{cases} C_k, & \text{if} \quad k \in \Omega \\ \\ X_k, & \text{if} \quad k \in \Omega^c \end{cases}, \tag{4.1}$$

where $\Omega = \{i_0, i_1, ..., i_{R-1}\}$ denotes the set of indexes of the tones reserved for PAPR reduction and Ω^c being its compliment.

The search optimal values of **C**, Tellado uses Linear Programming (LP) to simplify the problem with the assumption that the OFDM information symbol and added signal should be in base band and real. This approach though reduces the complexity but makes TR a restrictive method.

In this approach, the additive signal **c**, with the hermitian hypothesis ($C_k = C^*_{N-k}$ to get real baseband OFDM signal), can be written as,

$$\mathbf{c} = \sum_{k=0}^{R/2-1} \Re[C_{i_k}]cos(\frac{2\pi n i_k}{NL}) - \Im[C_{i_k}]sin(\frac{2\pi n i_k}{NL}) = \check{Q}_L \check{C} \tag{4.2}$$

where $\check{\mathbf{C}}^T = [C_{i_0}^{re}\ C_{i_0}^{im}\ ...\ C_{i_{R/2-1}}^{re}\ C_{i_{R/2-1}}^{im}]$ with $C_{i_k}^{re} = \Re(C_{i_k})$ and $C_{i_k}^{im} = \Im(C_{i_k})$ and $\check{\mathbf{Q}}_L$ is a $NL \times R$ matrix.

In this simplified case, the PAPR minimization problem can be formulated under LP as:

$$\min\ \beta, \qquad \text{subject to: } \begin{bmatrix} \check{\mathbf{Q}}_L & -\mathbf{1}_{NL} \\ -\check{\mathbf{Q}}_L & -\mathbf{1}_{NL} \end{bmatrix} \begin{bmatrix} \check{\mathbf{C}} \\ -\beta \end{bmatrix} \leq \begin{bmatrix} -\mathbf{x}_L \\ \mathbf{x}_L \end{bmatrix} \tag{4.3}$$

where $\mathbf{1}_{NL}$ is a column vector with NL ones.

4.3.3 SOCP Formulation of Tone Reservation

The problem of peak power control can be formulated as a convex optimization problem as follows,

$$\min_{C} \max |IFFT(\mathbf{X} + \mathbf{C})| \tag{4.4}$$

The *PRC* value $\mathbf{C}$ is determined with the help of $\mathbf{X}$ before IFFT on orthogonal frequencies as shown in Fig. 4.1. The problem of minimization in Eq. (4.4) can be expressed in the Semi Definite Program (SDP), SOCP, Quadratically Constrained Quadratic Programming (QCQP) form. The QCQP formulation for PAPR minimization is used by Tellado [9] that finally formulates it in Linear Programming form. But the processed signal should be real which makes it a restrictive method. However, it is much easier to formulate the problem of minimization of the maximum norm in SOCP form than SDP or QCQP form [15]. SOCP is a convex optimization problem class that minimizes a linear function over the intersection of an affine set and the product of second-order (quadratic) cones [15].

The problem of PAPR minimization formulated in Eq. (4.4) involves a minimization of maximum of norms. However it is known that this class of problem can be expressed in the form of a SOCP [15],

$$\begin{gathered} \text{minimize}\ \ F^T Y \\ \text{subject to} \\ \|A_m Y + H_m\| \leq E_m^T Y + g_m \end{gathered} \tag{4.5}$$

where $Y \in \Re^n$ is the optimization variable and $F \in \Re^n$, $A_m \in \Re^{(n_m-1)\times n}$, $H_m \in \Re^{(n_m-1)}$, $E_m \in \Re^n$ and $g_m \in \Re$ are the problem parameters with $m = 0, 1, ..., NL-1$. The norm appearing in the constraints is the standard Euclidean norm, i.e., $||U|| = (U^T U)^{1/2}$.

The objective function of the problem in Eq. (4.4) can be reformulated in time domain elements as [16],

$$\min_{\mathbf{C}} \max_{0 \leq k \leq NL-1} |x_k + \mathbf{q}_{k,L}^{row} \mathbf{C}|, \tag{4.6}$$

where $\mathbf{q}_{k,L}^{row}$ is the k-th row of $\mathbf{Q}_L$ and $\mathbf{Q}_L$ is the IFFT matrix of size NL. The above convex problem is equivalent to,

$$\begin{gathered} \text{minimize}\ \ \beta \\ \text{subject to} \\ \left| x_k + \mathbf{q}_{k,L}^{row} \mathbf{C} \right| \leq \beta, 0 \leq k \leq NL-1 \end{gathered} \tag{4.7}$$

Due to SOCP characterization, this convex optimization problem can be restructured as a SOCP with the following variables values in Eq. (4.5),

- $A_m = \begin{pmatrix} Z_{i_0}(m) & \dots & Z_{i_{R-1}}(m) & 0 \end{pmatrix} \in \Re^{2\times(2R+1)}$
  where $Z_{i_r}(m) = \begin{pmatrix} cos\varphi_{i_r}(m) & -sin\varphi_{i_r}(m) \\ sin\varphi_{i_r}(m) & cos\varphi_{i_r}(m) \end{pmatrix}$ with $\varphi_{i_r}(m) = 2\pi i_r \frac{m}{NL}$.
- $H_m = \begin{pmatrix} \Re e(x_m) \\ \Im m(x_m) \end{pmatrix} \in \Re^{2\times 1}$
- $E_m^T = \begin{pmatrix} 0 & \dots & 0 & 1 \end{pmatrix} \in \Re^{2R+1}$
- $F^T = \begin{pmatrix} 0 & \dots & 0 & 1 \end{pmatrix} \in \Re^{2R+1}$
- $g_m = 0 \in \Re$
- $Y^T = \begin{pmatrix} C_{i_0}^{re} & C_{i_0}^{im} & \dots & C_{i_{R-1}}^{re} & C_{i_{R-1}}^{im} & t \end{pmatrix} \in \Re^{2R+1}$ with $C_{i_k}^{re} = \Re e(C_{i_k})$ and $C_{i_k}^{im} = \Im m(C_{i_k})$

In Fig. 4.2 OFDM signal PAPR is reduced using TR-SOCP method. For a 64 carrier OFDM symbol which is oversampled by a factor 4, 6 carriers are reserved to reduce its PAPR. As it could be seen that PAPR is decreased by a considerable amount but Fig. 4.3 shows that out-of-band radiations are increased as well which might result in system interference. This is due to the fact that reserved carriers carry more power than data carriers and their power should be limited in order to limit the out-of-band radiations.

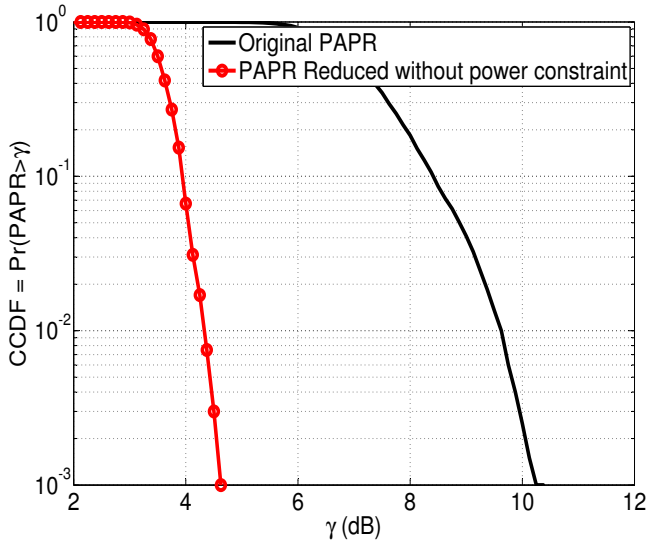

Figure 4.2: OFDM PAPR reduction using TR-SOCP method without any constraints on carriers. ($N = 64$)

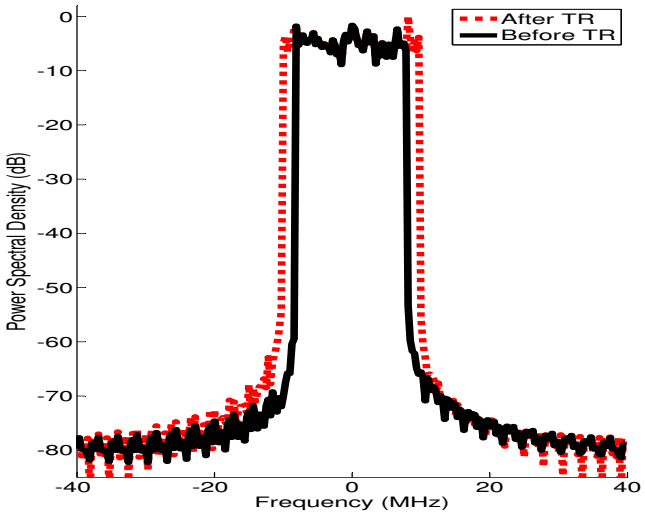

Figure 4.3: Power spectrum density before and after PAPR reduction without constraints on carriers. ($N = 64$)

4.3.4 Constrained SOCP modeling of Tone Reservation method

4.3.4.1 Mean power constraint

Ideally the aim should be to reduce the peak of the combined signal $(\mathbf{x}+\mathbf{c})$ while keeping the mean power constant. Mathematically it follows as,

$$E\{|\mathbf{x}+\mathbf{c}|^2\} \approx E\{|\mathbf{x}|^2\}. \tag{4.8}$$

However signal addition results in the mean transmitted power increase. The relative increase in mean power ΔE is defined as [9],

$$\Delta E = 10\log_{10}\frac{E\{|\mathbf{x}+\mathbf{c}|^2\}}{E\{|\mathbf{x}|^2\}}. \tag{4.9}$$

The aim should be to keep this ΔE as small as possible to meet power amplifier constraints. Thus it must be upper bounded as [16],

$$\Delta E \leq \gamma dB, \tag{4.10}$$

which follows,

$$E\left\{|\mathbf{x}+\mathbf{c}|^2\right\} \leq \lambda E\left\{|\mathbf{x}|^2\right\}, \tag{4.11}$$

where $\lambda = 10^{\gamma/10}$ is a constant related to power amplifier characteristics.

Thus the final objective function with constraints becomes,

$$\begin{gathered} \text{minimize} \quad \beta \\ \text{subject to} \\ \left|x_k + \mathbf{q}_{k,L}^{row}\mathbf{C}\right| \leq \beta, 0 \leq k \leq NL-1 \\ E\left\{|\mathbf{x}+\mathbf{c}|^2\right\} \leq \lambda E\left\{|\mathbf{x}|^2\right\}. \end{gathered} \tag{4.12}$$

In Fig. 4.4, a schematic diagram is shown where the mean power of peak reducing carriers is supposed to vary with the variation in the value of ΔE. Constrained TR-SOCP is applied to 64 carrier OFDM signal with different mean power constraints. As shown in Fig. 4.5 that more the constraints on mean power, lesser will be PAPR reduction as PAPR reduction with $\Delta E = 0.1$ dB is less compared to that of $\Delta E = 0.3$ dB. Fig. 4.6 and Fig. 4.7 demonstrate that as the constraints on mean power are increased, the side lobe power is decreased accordingly which could be used to reduce out-of-band interference.

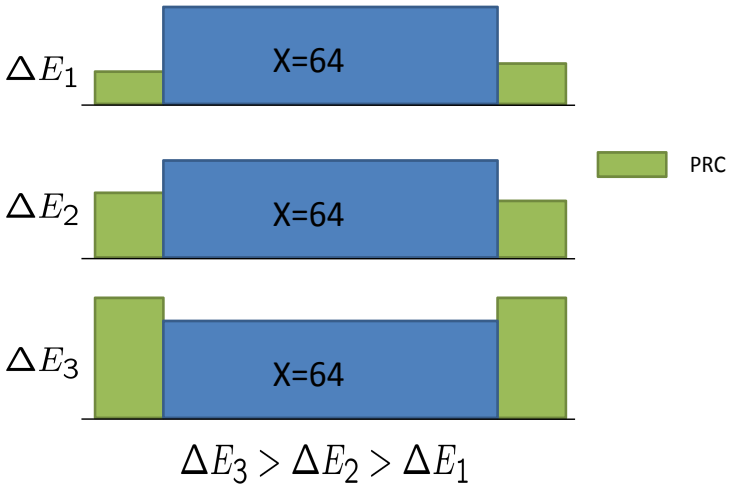

Figure 4.4: Schematic diagram of OFDM PAPR reduction using TR-SOCP method with mean power constraints on carriers.

4.3.4.2 Mask constraint

To make the added carriers respect the mask, there is another constraint added to the above constraint. This constraint is on the absolute value of each peak reducing carriers so as to make it respect the mask limitations. The following line is added in the *subject to* part of the above equation.

$$|C_k| \leq \delta_k, k \in R, \tag{4.13}$$

where R is the index set of all the reserved carriers and δ_k are the instantaneous values of the transmission mask. Thus this constraint makes sure that the reserved carriers do not bypass the mask constraints. This constraint shall be discussed in detail when standards with mask constraints will be analyzed.

4.4 Correction Signal's Parameter Influence on Mono-band OFDM PAPR Reduction

In this section, we shall first analyze the effects of some of the parameters related to correction tones on PAPR reduction in the context of single band OFDM signals. Below these parameter effects are detailed.

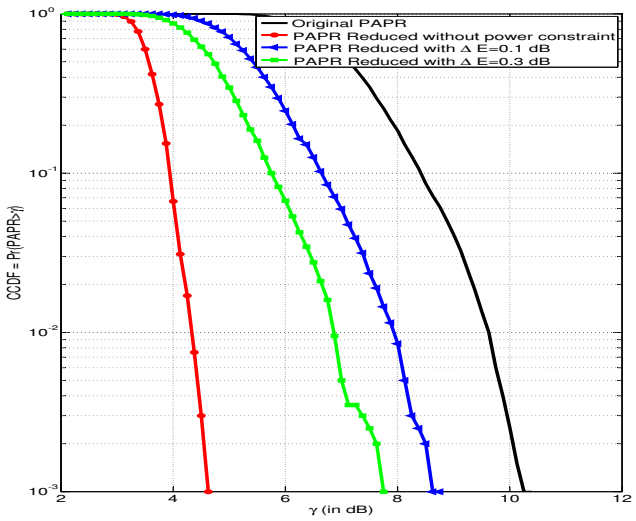

Figure 4.5: OFDM PAPR reduction using TR-SOCP method with mean power constraints on carriers. ($N = 64$)

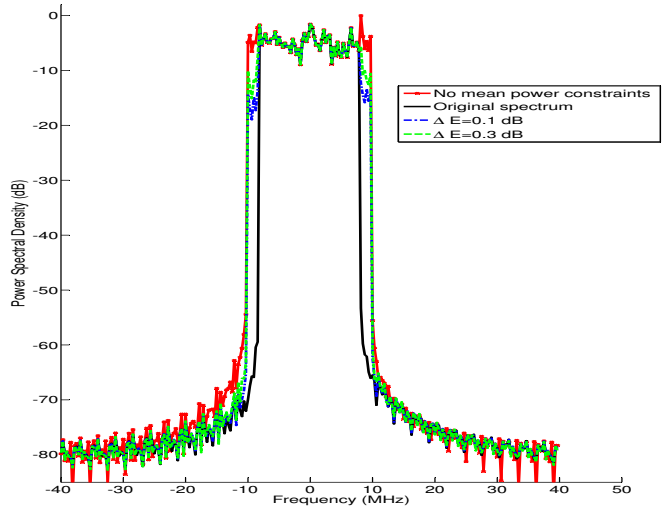

Figure 4.6: Power spectrum density before and after PAPR reduction with mean power constraints on carriers. ($N = 64$)

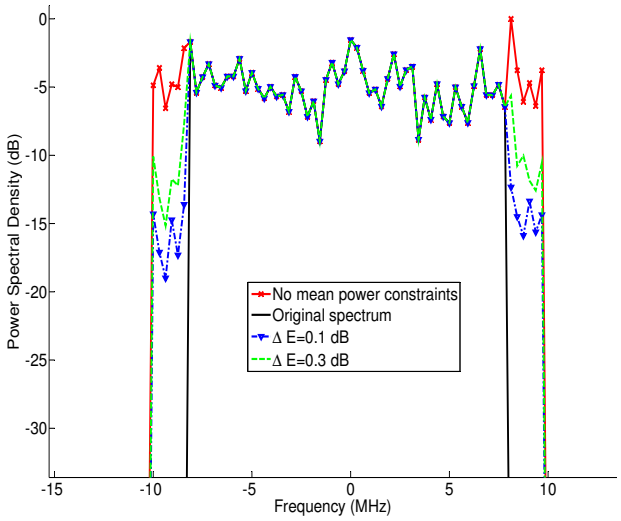

Figure 4.7: Zoomed Power Spectrum Density before and after PAPR reduction with mean power constraints on carriers. ($N = 64$)

4.4.1 *PRC*'s Bandwidth Effect

Bandwidth of the added signal (number of reserved carriers) affects the performance of PAPR reduction scheme. More the bandwidth allocated for added signal more will be the PAPR reduction as more tones can be used to reduce PAPR but at the same time the average power of the added signal increases. Also it is not easy to find free bandwidth to transmit adding tones. In Fig. 4.8 a schematic diagram is shown where 2, 4 and 6 carriers are added adjacent to 64 OFDM data carriers to reduce PAPR. Fig 4.9 testifies the fact that more PAPR is reduced with more *PRC*s. Also Fig. 4.10 and Fig. 4.11 show the power spectral density in this case.

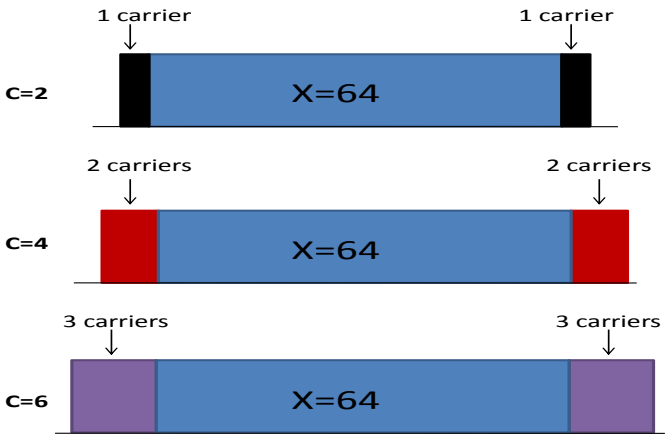

Figure 4.8: Schematic diagram of *PRC*'s BW allocation for PAPR reduction.

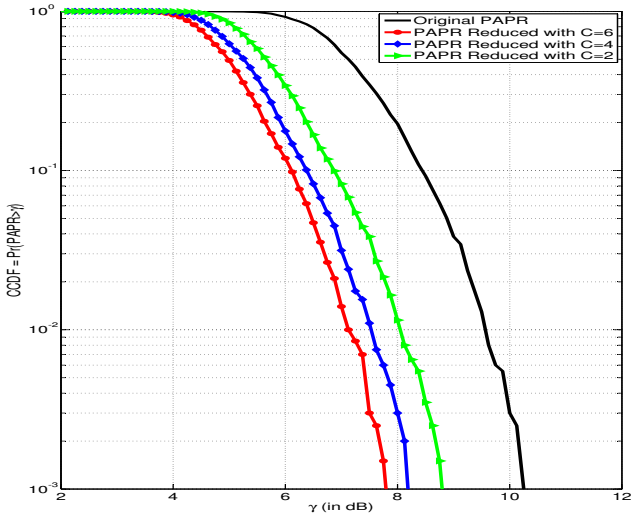

Figure 4.9: PAPR reduction with different BWs allocated for added signal.

4.4.2 *PRC*'s Position Effect

PRC's position affects a lot the PAPR reduction performance. The tones nearer to the useful carriers reduce more PAPR than the farther tones. Let d's be the frequency gaps between useful OFDM carriers and corrective carriers as shown in Fig. 4.12. Fig 4.13 shows that 4 added tones (2 on each side of the OFDM symbol) at $d_1 = 25$ MHz reduce less PAPR than those at $d_2 = 15$ MHz and $d_3 = 0$ MHz. Fig. 4.14 and Fig. 4.15 show the spectral density for the *PRC*s placed at different positions.

4.4.3 *PRC*'s Power Effect

It is not always possible to use the bandwidth closer to the useful band because it might result in interference and violate the spectrum mask. Thus in order to achieve the same performance as with the closer tones, the power of the tones at larger distances must be increased. This fact is represented by a schematic diagram in Fig. 4.16. To have almost the same performance, mean power of the signal at d_2 ($\Delta E = 0.45dB$) must be doubled to $\Delta E = 0.90dB$ if corrective signal is placed at d_1 instead. Fig 4.17 highlights this mean power comparison. Fig. 4.18 and Fig. 4.19 present the power spectral density graphs.

We have seen the influence of different *PRC* parameters like bandwidth, mean power and position, on the PAPR reduction in the context of mono band OFDM. After discussing these parameters' influence, we shall now discuss the case of multi band OFDM and shall see how the computational complexity factor comes into play for multi band signals.

Concluding we can say that the PAPR reduction performance of TR scheme depends upon many parameters and a proper selection of these parameters should be made so as to respect the spectrum mask, avoid BER degradation, avoid mean power increase beyond a certain limit etc. Generally speaking, for instance, large bandwidth reserved for *PRC*'s

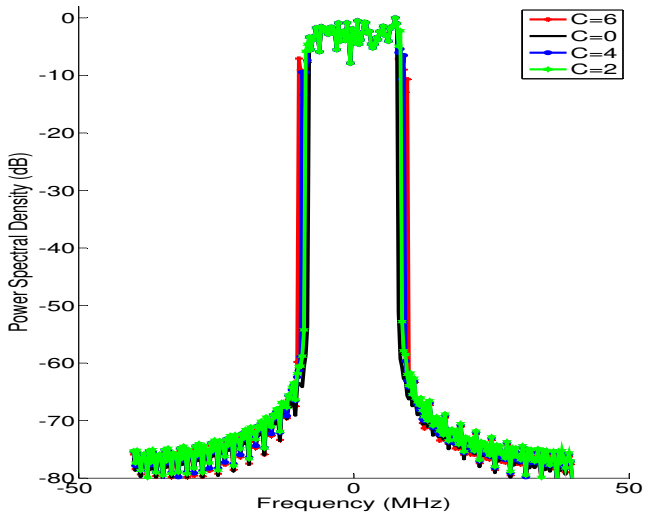

Figure 4.10: Spectrum: PAPR reduction with different BWs allocated for added signal.

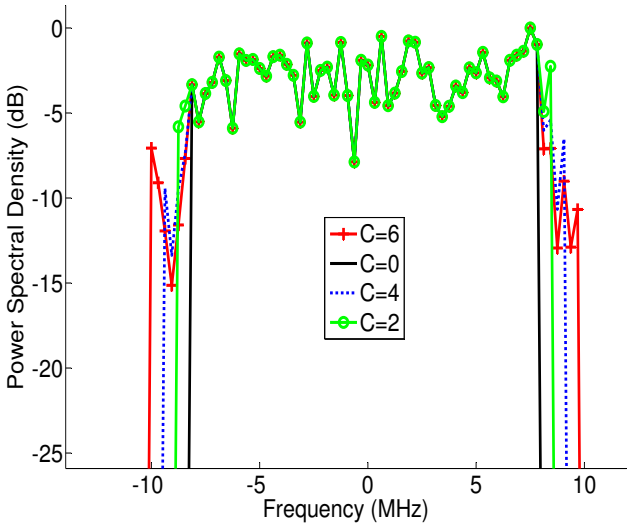

Figure 4.11: Zoomed spectrum: PAPR reduction with different BWs allocated for added signal.

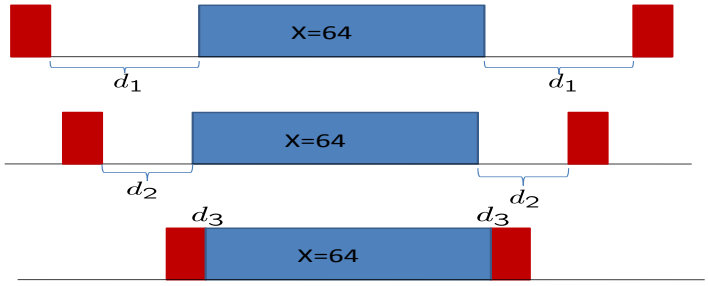

Figure 4.12: Schematic diagram of *PRC*'s positions for PAPR reduction.

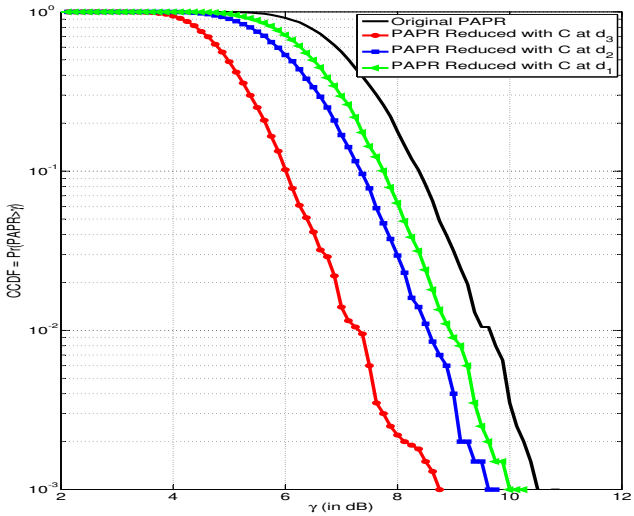

Figure 4.13: PAPR reduction with different frequency gaps between useful and added carriers.

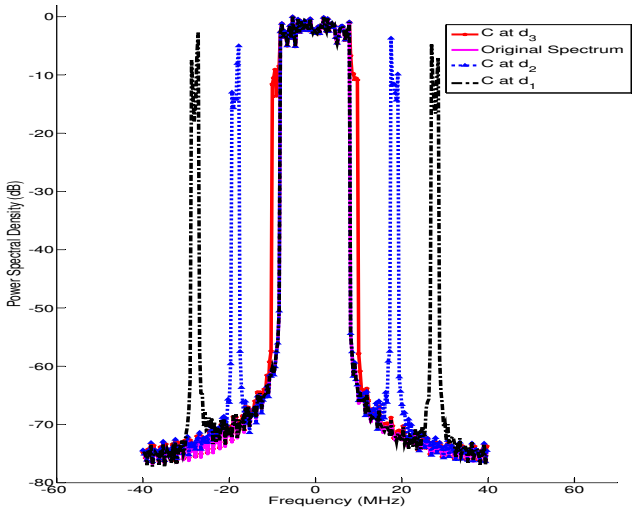

Figure 4.14: Spectrum: PAPR reduction with different frequency gaps between useful and added carriers.

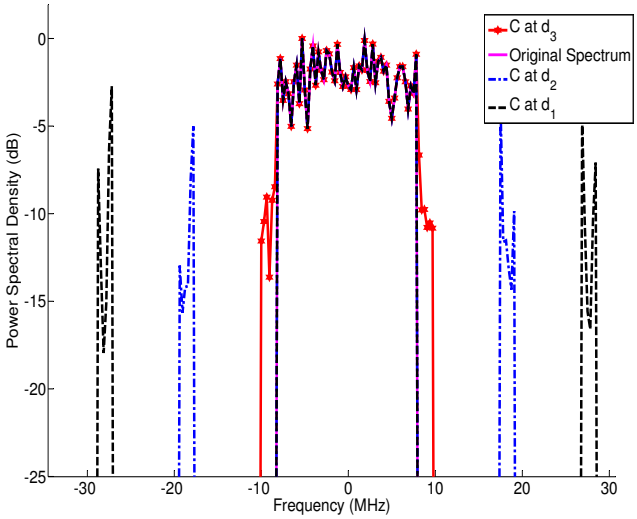

Figure 4.15: Zoomed Spectrum: PAPR reduction with different frequency gaps between useful and added carriers.

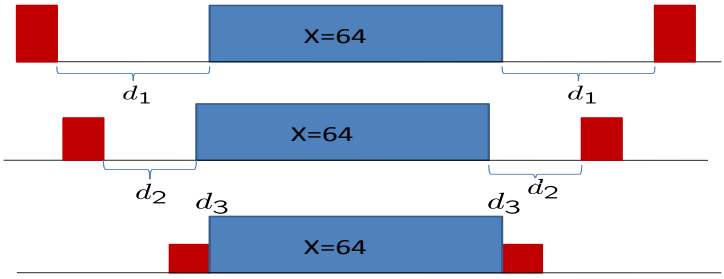

Figure 4.16: Schematic diagram of *PRC*'s positions and power allocation for PAPR reduction.

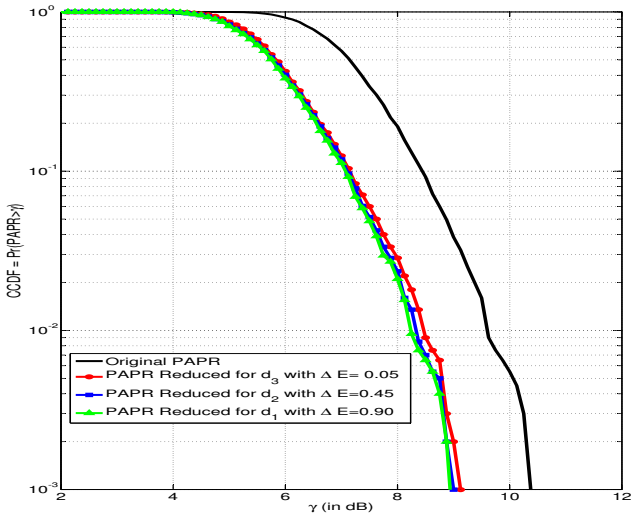

Figure 4.17: PAPR reduction with different mean powers for different positions for added signal to get same performance.

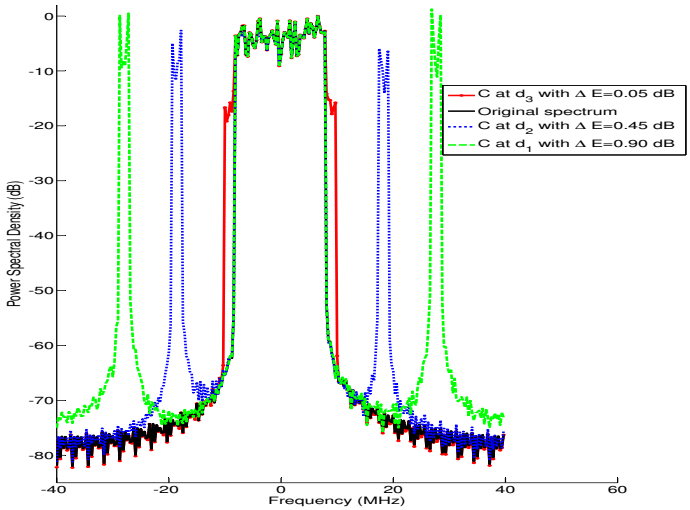

Figure 4.18: Spectrum: PAPR reduction with different mean powers for different positions for added signal to get same performance.

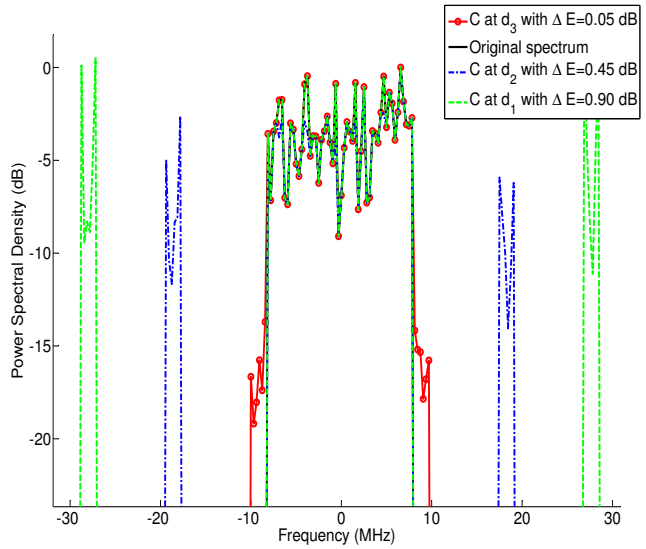

Figure 4.19: Zoomed spectrum: PAPR reduction with different mean powers for different positions for added signal to get same performance.

can reduce large PAPR but it may effect the data-rate if the bandwidth reserved exceeds the unused bandwidth of the standard. Similarly reserved carriers should be placed as near as possible to the data carriers on the frequency axis to benefit from large PAPR reduction gain but there comes the question of spectrum mask and inter channel interference. Talking of the effects of increase in mean power due to addition of reserved carriers, it should not be increased beyond the PA characterized limits. In short, *PRC*'s should be positioned as near as possible to the information carriers (to get large PAPR reduction gain), on the unused carriers of a standard if available (to avoid data-rate loss), with mean power constraints (to respect spectrum mask). Soon we shall discuss the possibility of placing the reserved carriers outside spectrum mask and see their effects on PAPR reduction.

4.5 SWR signal PAPR reduction using TR

Now we shall perform SWR signal PAPR reduction with a method which was originally designed for OFMD systems. But before doing that we shall present the generation process of SWR signal at the transmitter which will give us a better idea on the use of OFDM PAPR reduction methods for SWR signals.

4.5.1 SWR Transmitter

At the transmitter of a SWR system, different standards having different specifications are amplified by a large band PA. Now each standard has its own features like modulation scheme, data rate, inter symbol spacing etc. Fig. 4.20 shows a very simple bi-standard SWR transmitter where each standard is transmitted on its standard carrier frequency.

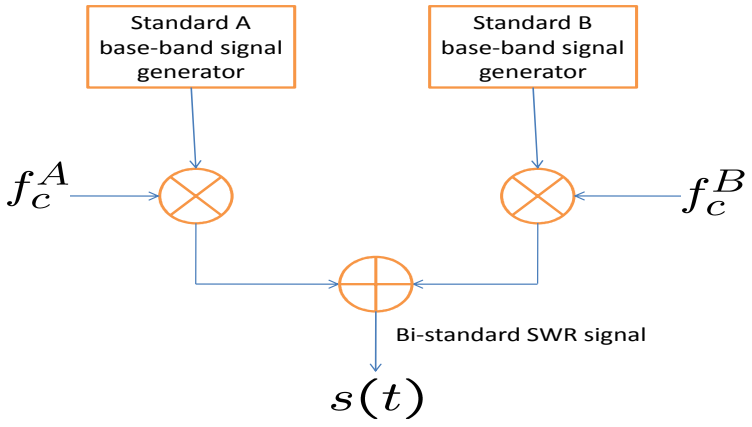

Figure 4.20: A simple bi-standard SWR transmitter.

4.5.2 Frequency Domain vision of SWR signal

As discussed in Chapter 3 that a time domain SWR signal is sliced to 'pieces' of certain length such that the each 'piece' contains all the frequency information when transformed to frequency domain using DFT. Fig. 4.21 shows the decomposition of one SWR symbol

into its frequency domain. SWR symbol spectrum shows the presence of two standards, Standard A and Standard B, generated in Fig. 4.20. Now we have a frequency vision of SWR signal as we have in case of OFDM systems before the application of IDFT. With this analogy in mind we can use Tone Reservation for SWR PAPR reduction as it is about reserving certain tones for reducing the peak of the signal.

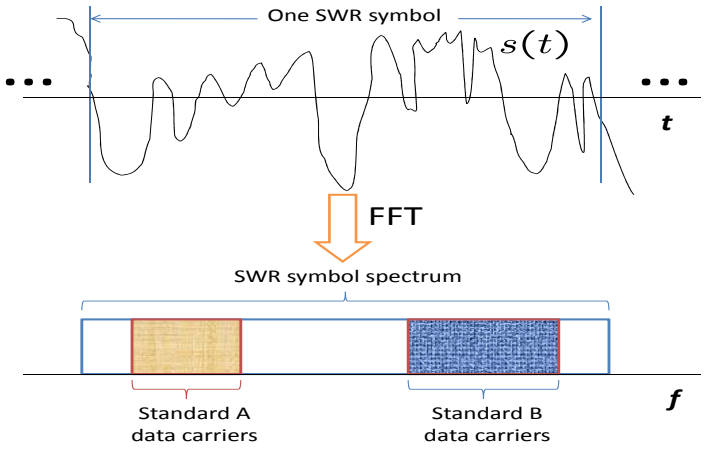

Figure 4.21: Transformation of SWR signal from time to frequency domain.

The possible positions of *PRC*'s are shown in Fig. 4.22. Of course, we may not be able to use all of these carriers because of spectrum mask constraints but the use of any of these carriers will result in a modified signal $s(\tilde{t})$ with reduced PAPR.

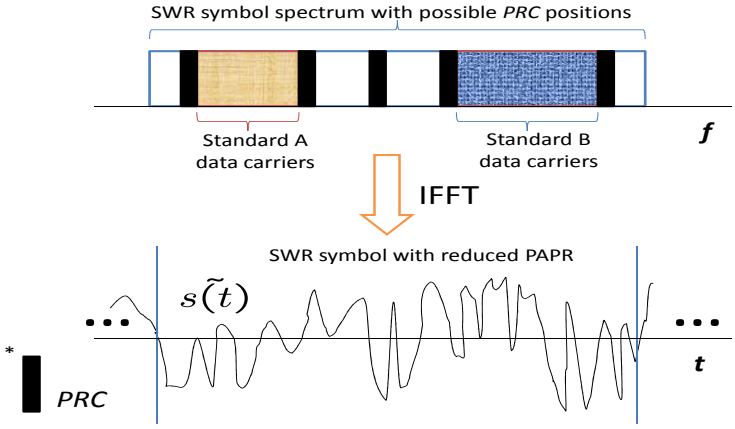

Figure 4.22: PRC insertion on the spectrum axis of the SWR signal.

4.5.3 SWR receiver

As far as reception side is concerned, a SWR receiver should be able to demodulate any of the standards present in the SWR signal following that particular standard's receiver architecture [112]. As could be seen in Fig. 4.23, at the receiver the modified SWR signal

$\tilde{s(t)}$ is decomposed into its standards after channelization. As the PRC are inserted on the unused frequency carriers of the standards under certain constraints therefore BER is not supposed to degrade at the receiver.

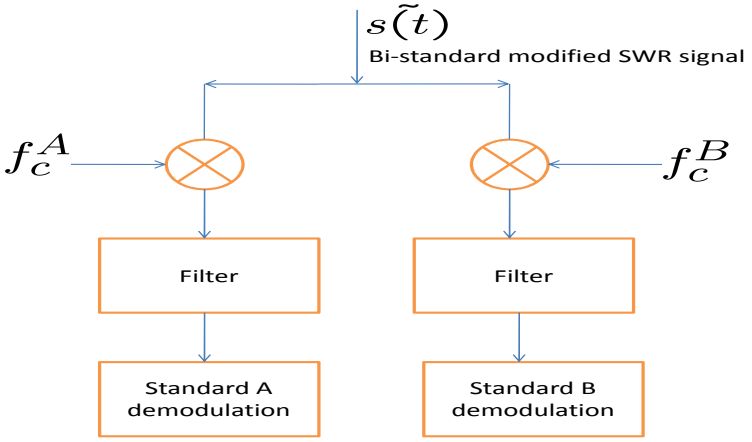

Figure 4.23: A simple bi-standard SWR receiver.

In the following part, the SWR signal shall be generated using the transmission methodology presented above. The transformation to frequency domain, insertion of PRC's shall follow the mentioned pattern and the receiver shall be designed as detailed above.

4.6 Discussion about f^s_{symb} and f_{samp}

There is one very important point about the symbol frequency of a standard present in SWR signal and the sampling frequency of the overall SWR signal. Firstly, the symbol frequency of a standard s, f^s_{symb}, may be different from the symbol frequency of the other standards present in a multi-standard SWR signal. Referring to Fig. 4.24, we show two different standards with different symbol durations, T^A_{symb} and T^B_{symb} for Standard A and B respectively. Different symbol durations mean that for a time window of particular size, there may be several symbols of one standard while the other standard may have only one symbol in that duration. Therefore, it should be kept in mind while slicing the time domain SWR signal that it contains at least one symbol of each standard present in it.

Secondly, considering the large bandwidth of SWR signal, the sampling frequency of this signal may have no relationship with the symbol frequencies of the standards present in the SWR signal. As shown in Fig. 4.25, each standard is carried by its specific carrier frequency and has its own bandwidth. If a lone standard Standard A is transmitted, then its sampling frequency would be $f^A_{samp} \geq 2f^A_{max}$ where f^A_{max} is the maximum frequency present in Standard A. But as SWR contains different standards and transmits a very large band thus sampling frequency of SWR signal would be $f^{SWR}_{samp} \geq 2f^{SWR}_{max}$ which is much higher than f^A_{samp}. This thing is of utmost importance especially after the transformation of the SWR signal into frequency domain. Because the carriers that we might see in the frequency domain for a certain standard may not be the original data carriers as the signal is sampled at a much higher rate than the original symbol rates of the standards.

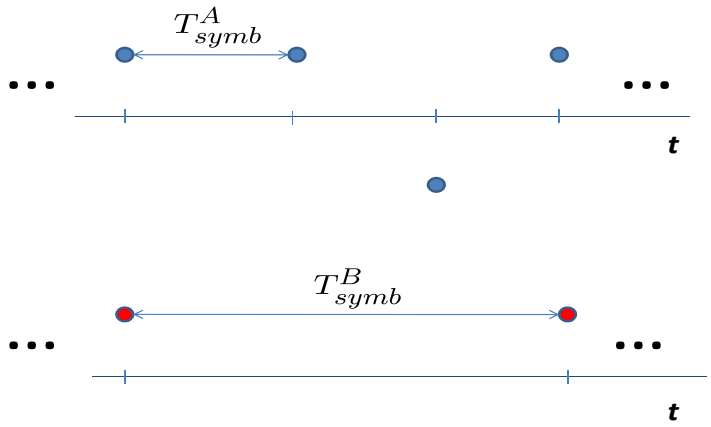

Figure 4.24: Different SWR standards have different symbol duration.

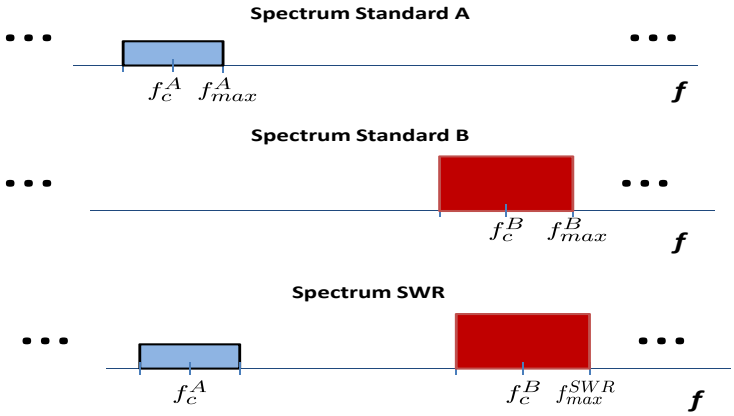

Figure 4.25: SWR signal is sampled at a very high rate due to its large bandwidth.

After presenting the SWR transceiver, the methodology to reduce SWR signal PAPR, now we shall perform the task of SWR PAPR reduction by considering three different SWR signal scenarios.

- **Mono-standard SWR signal comprising of multi OFDM bands:** At first, SWR signal containing a single hypothetical standard shall be considered which transmits multiple OFDM modulated channels spaced by a certain frequency. In practice, this scenario can be thought of a DVB-T standard which transmits multiple OFDM channels of 8 MHz each spaced by 8 MHz in UHF band. In this scenario, the symbol duration of all channels is same. The purpose of this study is to show the performance vs complexity trade-off when PAPR reduction is performed over each channel individually compared to that when PAPR reduction is performed over the whole bandwidth of this mono-standard SWR signal.
- **Mono-standard SWR signal comprising of multi GSM channels:** Next, a multiplex of single carrier standard, GSM, is considered. At GSM BS multiple GSM channels are amplified by a single PA. The multiplexed signal has a high PAPR which is reduced using TR-SOCP where the *PRC*'s are transmitted over the unused GSM carriers in that BS respecting the C/I value of GSM standard.
- **Multi-standard SWR signal comprising of two different standards:** Finally, a multi standard SWR signal comprised of two different hypothetical standards is considered. These standards transmit different power, at different frequencies, contain different number of carriers and different symbol duration. Practically speaking, we can think of a SWR system containing WiMAX and WLAN standards where these standards transmit with an approximate power gap of 25 dB. WiMAX and WLAN use 256 and 64 point IFFT at the transmitter respectively. While symbol duration for WiMAX and WLAN is 12.8 μsec and 3.2 μsec respectively .

4.7 PAPR Reduction for MB-OFDM System using TR-SOCP

Considering a mono-standard SWR system which has multiple OFDM channels. All the channels have equal bandwidth, equal transmission power, symbol duration and number of sub-carriers.

4.7.1 MB-OFDM Signal

Let us denote the OFDM data of length N as a vector $X = [X_0, X_1, ..., X_{N-1}]$ where N is equal to the number of sub-carriers. Each OFDM symbol modulates each of the N subcarriers,$[f_n; n = 0, 1, ..., N-1]$ which are orthogonal to each other. The complex envelop of the transmitted OFDM signal with duration T_S can be expressed as,

$$x(t) = \frac{1}{\sqrt{N}} \sum_{k=0}^{N-1} X_k e^{j2\pi f_k t}, 0 \leq t \leq T_S. \tag{4.14}$$

MB-OFDM is the transmission of these OFDM symbols over different frequency bands. Thus an MB-OFDM symbol can be written as,

$$x(t) = \frac{1}{\sqrt{N}} \sum_{b=1}^{B} \sum_{k=0}^{N-1} X_k^b e^{j2\pi f_{k,b} t}, 0 \leq t \leq T_S. \tag{4.15}$$

Here B is the number of bands over which the OFDM signal is transmitted while $f_{k,b}$ is the frequency of the k^{th} data sample on b^{th} band. This scenario can be treated as DVB-T standard where several channels of equal bandwidth, equal FFT size and same symbol frequency are transmitted. These channels are separated by specific bandwidth defined by DVB-T standard.

As complex time-domain samples of MB-OFDM signals are approximately Gaussian distributed due to the statistical independence of carriers. This results in the generations of some very high peaks.

4.7.2 MB-OFDM PAPR Reduction

After dealing with the parameters affecting the TR-SOCP PAPR reduction method in mono-band OFDM context we head towards the implementation of this scheme for a hypothetical MB-OFDM signal. For simplicity two OFDM symbols are considered which are separated by 40 MHz. Each symbol has 64 sub-carriers. Then 6 tones are added (3 at each side of the OFDM symbol) at d_3 for each of the two OFDM symbols as shown in Fig. 4.26 and Fig. 4.27. Thus a total of 12 *PRC* is used to reduce PAPR . An oversampling factor of 4 is used to better approximate PAPR.

Now PAPR reduction using TR-SOCP is performed in two ways. At first the optimization of the tones was performed over the whole spectrum reducing the PAPR of the overall signal. This means that a signal $s(t)$ was generated first as that in Fig. 4.20. It was then sliced and transformed to frequency domain as in Fig. 4.21. Then **PRC**'s were placed on both sides of each OFDM symbol at d_3 and optimized to reduce the overall signal PAPR.

Secondly, TR-SOCP was performed for individual OFDM symbols separately. It means that TR-SOCP was applied on each symbol separately before the summation of the two signals in Fig. 4.20. Thus $s(t)$ is a signal which the sum of two signals whose PAPR is reduced independently from each other. Although both the signals to be added up have low PAPR but when they are summed up, the PAPR increases due to the sum of multi-carrier signals. Thus the overall PAPR reduction gain in this case is less than that in the former case as depicted in Fig 4.29. The power spectral density is shown in Fig. 4.27 and 4.28.

4.7.3 Performance-Complexity comparison

The computational complexity of TR-SOCP method (to be detailed in next chapter) depends largely on FFT size ($O(NLR^2)$ where NL and R are the FFT size and number of *PRC* respectively). In the first case, where the PAPR of the overall signal is reduced, FFT size is large compared to the case where PAPR is reduced individually. It means that process of reducing the PAPR of the multi-band SWR signal is more complex than reducing the PAPR of single bands and then summing them up to make a SWR signal. But the later comes at the cost of reduction in PAPR gain. For this very simple case of multi-band OFDM system Table. 4.1 summarizes the results for $R = 12$. Also the FFT size, NL is 256 and 1024 for individual and global PAPR reduction respectively.

	Global Optimization	Individual Optimization
PAPR Gain at 10^{-2}	≈ 3 dB	≈ 1.5 dB
Computational Complexity	$O(9 \times 2^{14})$	$O(9 \times 2^{11})$

Table 4.1: Performance vs Complexity comparison for MB-OFDM system using $R = 12$

Thus a gain of about 1.5 dB in PAPR reduction is obtained at the cost of 8 times more computational complexity. Hence appears the complexity vs performance compromise to be taken care of.

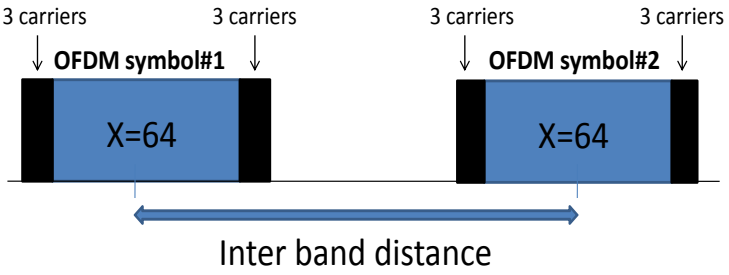

Figure 4.26: Schematic diagram of PAPR reduction in MB-OFDM context.

To see the effects of number of *PRC*'s and in turns the reserved bandwidth, the number of reserved carriers are varied to 8 and 4 and the variations on PAPR reduction performance are noted as shown in Fig. 4.30 and 4.31.

The process of adding optimized tones to reduce PAPR can be generalized for more than two OFDM symbols scenario or more than two channels for that matter. Next we shall consider the case of multi-channel GSM system where the PAPR of 4 GSM channel BS transmitter is reduced using TR-SOCP.

4.8 PAPR reduction of multiple channel GSM standard using TR-SOCP method

In this section a more practical scenario is considered. At first we shall present the background of PAPR issue at GSM base stations with few important GSM specifications and then we shall reduce PAPR with the help of TR-SOCP method.

4.8.1 Some GSM PHY layer specifications

GSM is operated over two frequency bands 900 MHz and 1800 MHz and named after their bands as GSM-900 and GSM-1800 respectively. The term GSM-900 is used for any GSM system which operates in the following band:

- 890 - 915 MHz for mobile station (MS) to BS (uplink)
- 935 - 960 MHz for BS to MS (downlink)

While GSM-1800 is divided into 2 x 75 MHz frequency bands as follows:

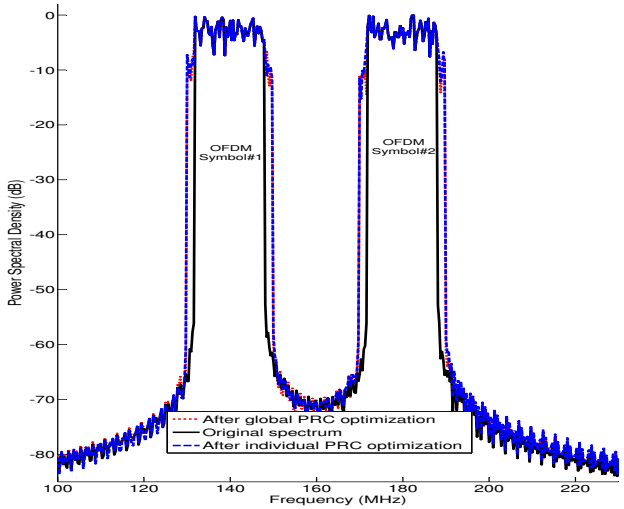

Figure 4.27: MB-OFDM Spectrum.

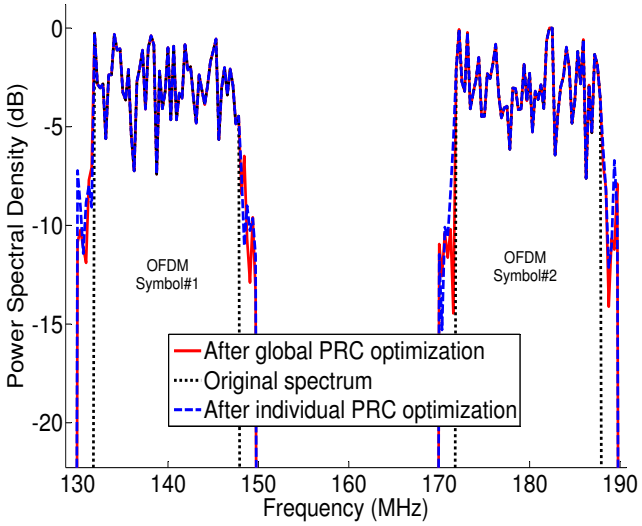

Figure 4.28: MB-OFDM Zoomed Spectrum.

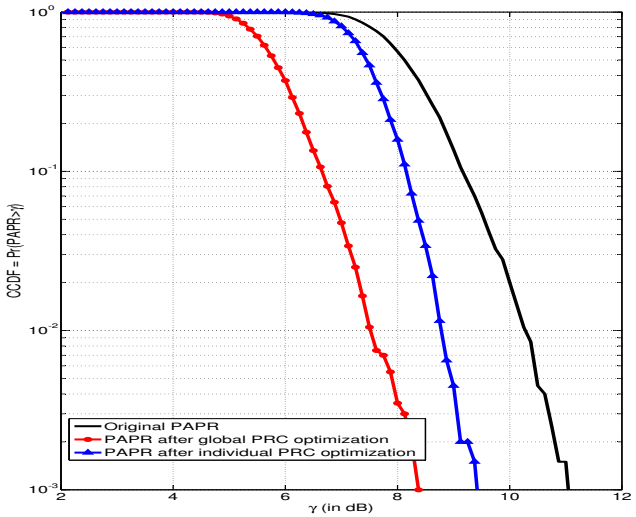

Figure 4.29: MB-OFDM PAPR reduction with PRC=12.

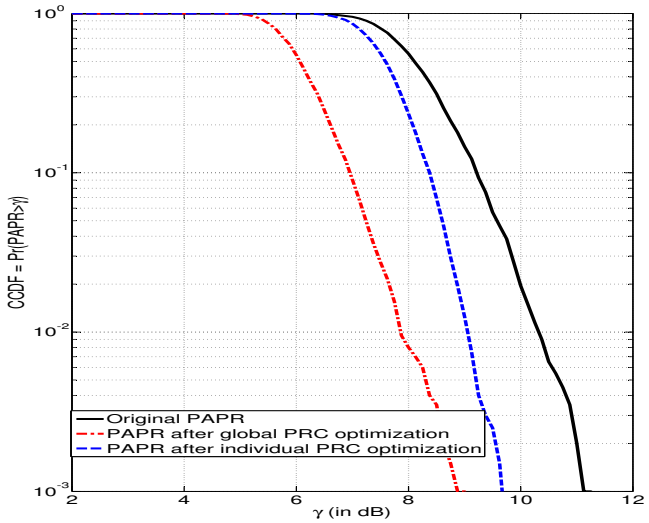

Figure 4.30: MB-OFDM PAPR reduction with 8 PRC.

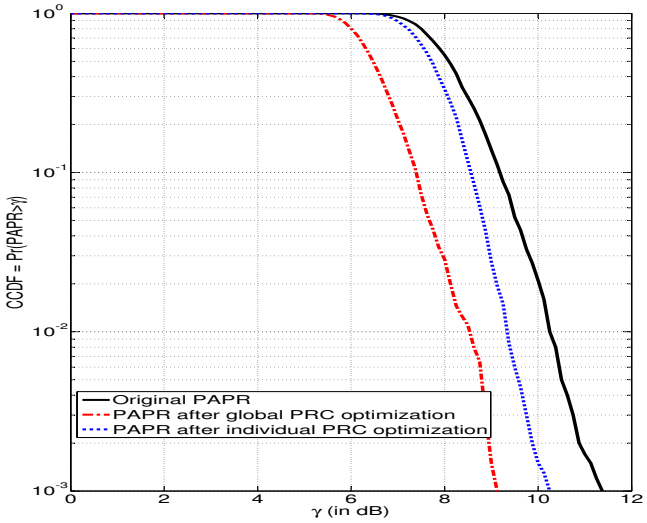

Figure 4.31: MB-OFDM PAPR reduction with 4 PRC.

- 1710 - 1785 MHz for MS to BS (uplink)
- 1805 - 1880 MHz for BS to MS (downlink)

Thus the duplexing technique used in GSM is Frequency Division Duplexing (FDD). Each uplink and downlink band is divided into sub-bands called channels. Each channel occupies a bandwidth of 200 kHZ and it is assigned a carrier frequency. Each channel is numbered by the Absolute Radio Frequency Channel Number (ARFCN). The frequency value of the carrier n in the lower band (uplink band) is called $F_L(n)$ while $F_U(n)$ is the corresponding frequency value in the upper band (downlink band). For GSM-900, these frequencies are given by the following equations:

$$F_L(n) = 890 + 0.2n \; with \;\; 1 < n < 124$$

$$F_U(n) = F_L(n) + 45.$$

Now each channel (carrier) supports 8 time slots. These time slots are used to carry user's data which means that GSM uses Time Division Multiple Access (TDMA) technique. Fig. 4.32 shows the overall division of GSM frames starting from 'hyper frame' which contains 2715648 TDMA frames while each TDMA frame contains 8 time slots of duration 4.615 msec each. One time slot has a 156.25 bit durations and it contains data bits, flags, guard period and trail bits.

4.8.2 GSM frequency distribution

After describing briefly some of the GSM PHY layer parameters, now shall discuss the distribution of the GSM channels over several base stations and see the parameters which influence this distribution.

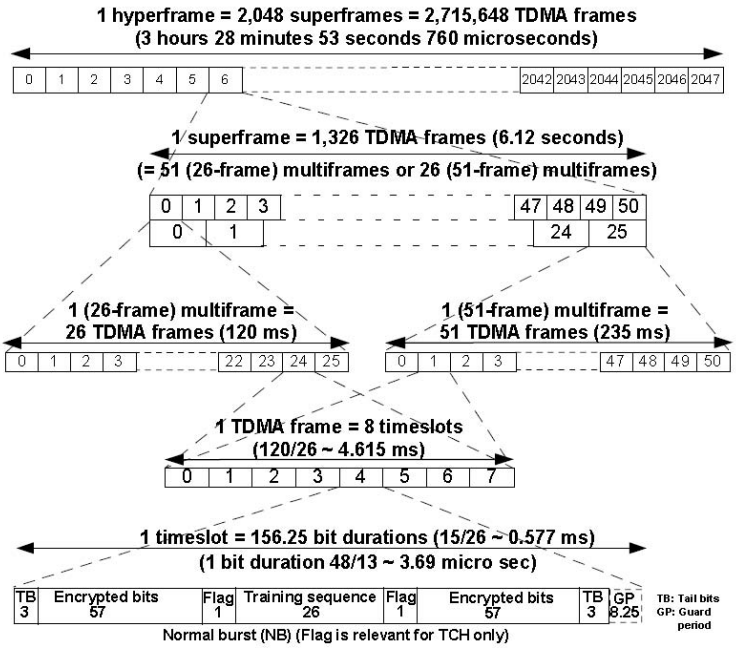

Figure 4.32: GSM Framing structure.

Normally each BS is divided into 3 sectors (for (sub) urban areas) or 2 sectors (for road coverage.) Omni sites are used for rural areas.

Now 'Frequency reuse' is the core concept of the cellular mobile radio systems, given the fact that the number of allowed frequencies is fixed. A frequency can be reused simultaneously in different cells, provided that the cells using the same frequency set are far enough separated so that co-channel interference is kept at an acceptable level most of the time.

The frequency reuse factor is the rate at which the same frequency can be used in a network. It is $1/K$ where K is the number of cells which can not use the same set of frequencies for transmission. In case of N sector antennas on the same base station site, each with different direction, the base station site can serve N different sectors. N is typically 3. A reuse pattern of N/K denotes a further division in frequency among N sector antennas per site.

In practice, as the total number of allocated frequencies is fixed. When K is too large, the number of frequencies assigned to each of K cells becomes too small. The challenge is to find the smallest K value which can still meet the system performance requirements which involves estimation of the co-channel interference, calculation of the minimum frequency reuse distance D to meet the co-channel interference criterion. The practical values for K range up from 3 to 21.

Frequency planning can be done in different ways, it could follow a fixed pattern where the cells are assigned fixed number of channels or it could follow dynamic configuration which means that the number of channels may be varied for a cell depending upon the requirements.

Now there is very important parameter which should be taken care of, is the carrier to interference (C/I) value which is the ratio of carrier power to the interference power. This

is closely associated to another term called Distance to Cell Radius which is given by,

$$D/R = \sqrt{3K}, \tag{4.16}$$

where K is the reuse factor, D is the distance separation between cell centers and R is the cell radius as shown in Fig. 4.33. As K decreases, the D/R ratio becomes smaller and the C/I ratio goes down which means that interference increases. As the number of sector increases, the number of potential interferers decreases. In GSM conventional frequency planning, the 4/12 reuse pattern is typical. Using the inverse 3.5 exponent law, a mean C/I ratio of 13dB would be found at the edge of the cell.

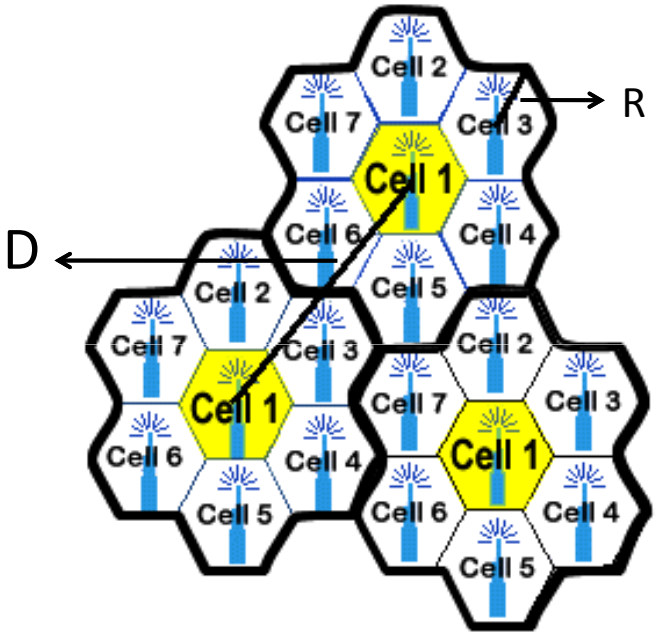

Figure 4.33: Frequency reuse concept in GSM networking.

The number of channels allocated to a cell depends upon the population (user) density in the cell location and in turns, it depends upon the traffic needs. One would need to allocate more channels in a busy area like super market, airport etc. while less number of carriers would be needed for a less crowded area like high ways. On average, a BS may be allocated with 12 GSM channels and for a 3-sector BS, each sector would have 4 GSM channels.

4.8.3 TR-SOCP application to reduce MC-GSM PAPR

After defining the basic features of GSM transmission we head towards multi-channel PAPR reduction. As it is discussed in Chapter 3 that PAPR of a single GSM carrier in base band is 0 dB due to the GMSK modulation. But when multiple GSM channels are transmitted at a GSM base station, the PAPR increases. In our case, we have simulated one sector of a GSM base station transmitter with 4 GSM carriers. Signals were generated at 4 separate GSM transmitters. Their time domain signals were added and then transformed

to frequency domain using FFT. And then on some specific carriers, *PRC*s were added to reduce PAPR. All this process was performed following the details given in Section 4.5.

Generally, a minimum of 400 kHz spacing is provided between two GSM channels at the same transmitter to avoid inter-channel interference. In our simulations we have kept this value to 800 kHz. Theoretically speaking all the GSM channels in between the used GSM channels are free and can be used under C/I constraint. Initially we have used only one free GSM channel at the center of the overall bandwidth to be amplified. This carrier is at 400 kHz from its neighboring channels to avoid any sort of inter-channel interference. The power level is kept under the permissible -13 dB threshold value of C/I.

One thing to be noted here is that as we are not simulating a very large number of carriers (channels), so the PAPR distribution is not Gaussian rather it is behaves more in a deterministic manner. So to compare the PAPR performance before and after the TR-SOCP implementation the instantaneous PAPR values shall be used. Fig. 4.34 shows the instantaneous and mean PAPR values before and after TR-SOCP implementation. Note that instantaneous and mean PAPR values before TR-SOCP implementation are almost the same. Mean PAPR before TR-SOCP (solid-black line) is approximately 9.02 dB while instantaneous PAPR before TR-SOCP (dotted-black line) does not vary a lot about mean PAPR value of 9.02 dB. These two values are so close that on plot they almost seem like a single line. As far as mean and instantaneous PAPR values after TR-SOCP are concerned (plotted in dash-dot red and solid-red marked with circle lines respectively), one can easily see the variations because more PAPR is reduced for certain MC-GSM symbols compared to the others. Mean PAPR after TR-SOCP is about 8.55 dB, thus on average PAPR gain of approximately 0.45 dB is obtained with TR-SOCP application.

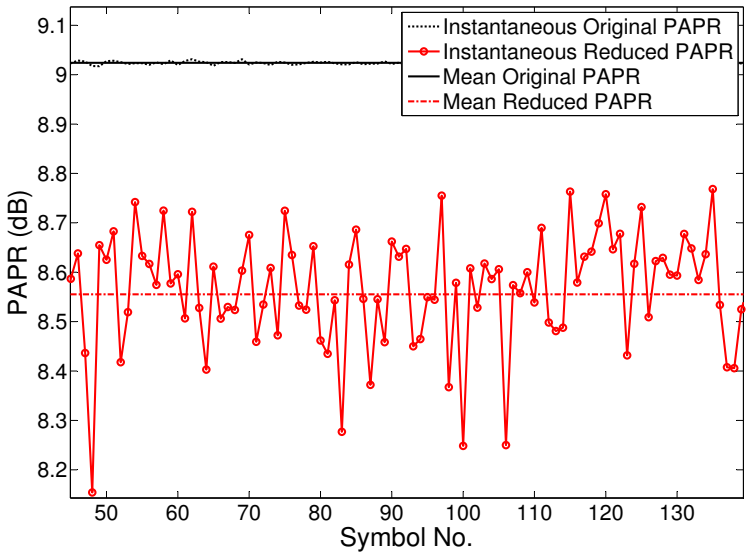

Figure 4.34: PAPR reduction of 4 GSM channels using 1 free GSM channels as *PRC*.

Fig. 4.35 demonstrates the spectrum density. One can see the increase in power at the center of the spectrum due to *PRC* addition. Also note that additional carriers' power respects the C/I value.

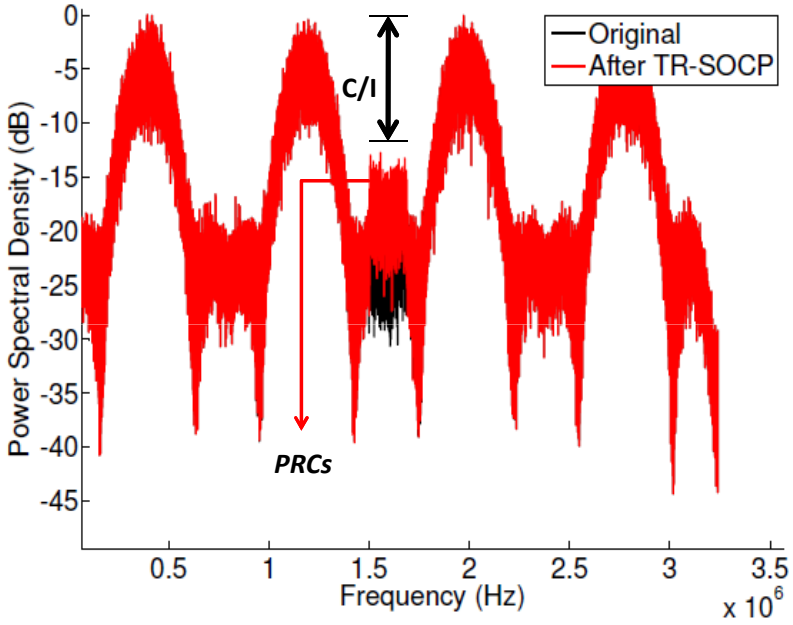

Figure 4.35: Spectrum after TR-SOCP application (1 *PRC*).

In the second step, we used a total of 3 GSM free carriers to further reduce the PAPR. At 400 kHz from each used GSM channel, we inserted peak reducing carriers. Fig. 4.36 demonstrates the instantaneous and mean PAPR values before and after TR-SOCP application. Again as it could be seen in Fig. 4.36 that mean and instantaneous PAPR values before TR-SOCP (represented in black) are almost same (i-e 9.02 dB). The variations in mean and instantaneous PAPR after TR-SOCP (represented in red) can be clearly seen with mean PAPR value of approximately 7.8 dB after TR-SOCP. Thus, on average, a gain of about 1.2 dB was obtained in this case.

Fig. 4.37 shows the spectrum density before and after the insertion of peak reducing carriers and verifies that GSM spectrum mask and C/I value is respected.

4.9 PAPR reduction of a bi-standard SWR signal using TR-SOCP method

As discussed in Chapter 3 that SWR technology has gained importance in the rapidly developing wireless world. Besides many issues related to SWR implementation, high PAPR is an important issue related to PA non-linearities. Also it was proved that SWR PAPR distribution follows central limit theorem. Thus making it possible to apply OFDM PAPR reduction methods on SWR signal.

A SWR base station would transmit a multiplex of standards signal where each standard having its own transmitting power requirements different from the other standards

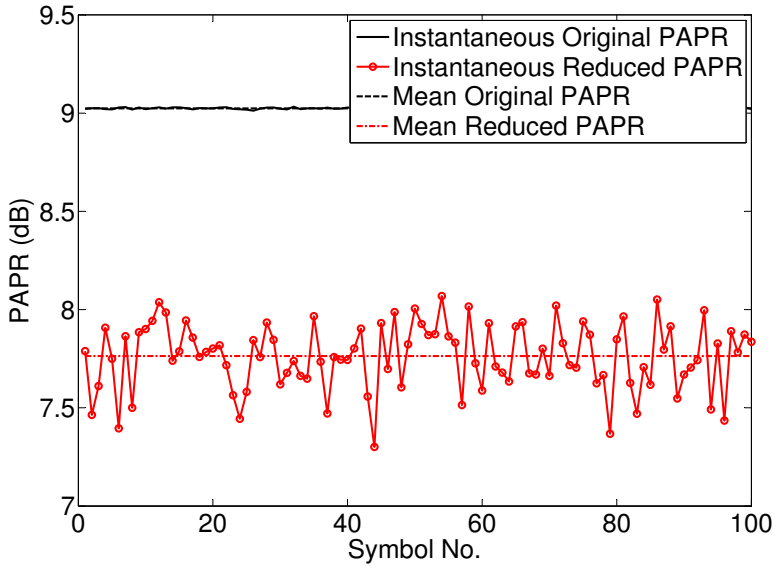

Figure 4.36: PAPR reduction of 4 GSM channels using 3 free GSM channels as *PRC*.

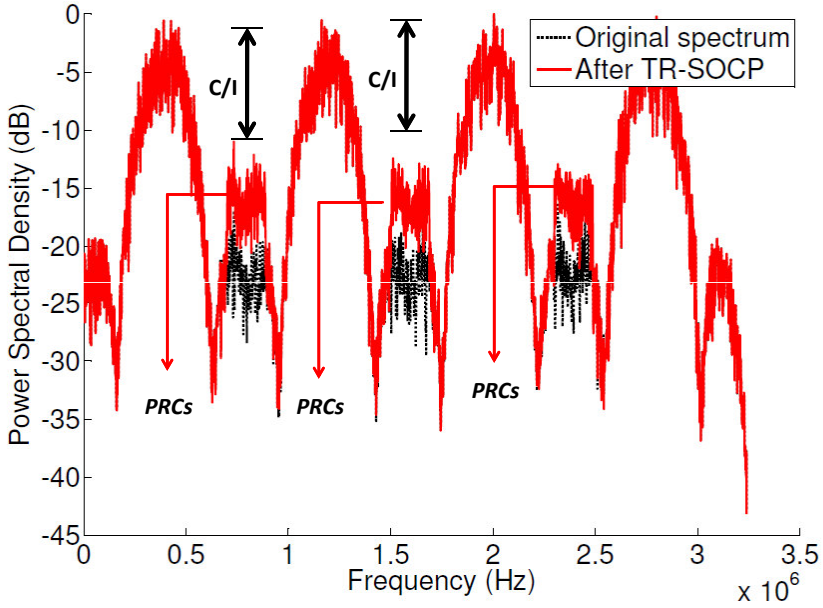

Figure 4.37: Spectrum after TR-SOCP application (3 *PRC*).

present in the SWR signal. An initial study is done for a bi-standard SWR system to see the variations in PAPR reduction gain with the variations in transmit power gap between the standards. Then TR-SOCP method is employed to reduce PAPR of a bi-standard SWR system containing standards with transmit power gap of 25 dB. PAPR is not only reduced by using in-band unused carriers of the standards as peak reducing carriers but also some inter-standard out-of-band (OOB) carriers are also used to reduce PAPR. The PAPR reduction performance by in-band and OOB peak reducing carriers is compared. Also the effect of variation in mean power, bandwidth and positions of OOB peak reducing carriers on PAPR reduction performance is discussed.

4.9.1 Software Radio System Model

As discussed in Chapter 3, that SWR signal can be written as,

$$S_i(t) = \sum_{p=1}^{P_i} r_{i,p}(t) e^{2j\pi f_{i,p} t},$$

where $r_{i,p}(t)$ represents the modulated and filtered signal associated to carrier p of the standard i. In this case, $r_{i,p}(t) = fem_i(t) * m_{i,p}(c(t))$, where $m_{i,p}(c(t))$ represents the modulation relative to the carrier p and standard i and $fem_i(t)$ is the shaping filter function of standard i.

In OFDM modulation based standard IFFT is applied to the mapped symbols in order to get a multi-carrier signal. These carriers are orthogonal and with constant inter carrier spacing $\delta f = 1/T_s$ inside a standard where T_s is symbol duration. Hence a base-band continuous OFDM modulation based standard's signal $S_i(t)$ can be written as,

$$S_i(t) = \frac{1}{\sqrt{N_i}} \sum_{k=0}^{N_i-1} X_k^{(i)} e^{2j\pi kt/T_{s_i}}; 0 \leq t < T_{s_i} \tag{4.17}$$

where $X_k^{(i)}$, N_i and T_{s_i} are the k^{th} mapped data, IFFT size and the symbol duration for i^{th} standard respectively.

Thus OFDM modulation based multi-standard SWR signal in the radio frequency (RF) domain can be written as,

$$x(t) = \sum_{i=1}^{S} \frac{1}{\sqrt{N_i}} \sum_{k=0}^{N_i-1} (X_k^{(i)} e^{2j\pi kt/T_{s_i}}) e^{2j\pi f_{i,p} t}; 0 \leq t < T_{s_i} \tag{4.18}$$

A SWR system containing two hypothetical OFDM based standards is discussed in this chapter whose PAPR shall be decreased using TR-SOCP method. In [113] a clipping and post-compensation method based PAPR reduction of a SDR transmitter is presented. However, the system treated is that of a mono-standard OFDM based SDR transmitter where the standard treated is that of WiMAX.

In our case, the first standard, Standard A, consists of IFFT size $N_A = 64$. Out of these 64 subcarriers, $D_A = 48$ subcarriers are used for data, while $P_A = 4$ subcarriers are used for pilots. The rest $R_A = 12$ subcarriers are unused (null) subcarriers. The inter carrier spacing is $\delta f_A = 0.3125$ MHz. Few MHz away on the radio spectrum axis, lies our second standard, Standard B, comprising of $N_B = 256$ subcarrier OFDM symbols. Out of

these 256 subcarriers, $D_B = 192$ subcarriers are used for data, while $P_B = 8$ subcarriers are used for pilots. The rest $R_B = 56$ subcarriers are unused (null) subcarriers. The inter carrier spacing is $\delta f_B = 0.078125$ MHz. There is a transmission power gap ΔP of 25 dB between the two standards. Initially only R_A and R_B shall be used to reduce PAPR and then a part of bandwidth between these standards shall be used to further reduce PAPR under the assumption that the spectrum between the standards is free and can be used under power mask constraints. Fig. 4.38 describes the SWR system with the positioning of the in-band and out-of-band carriers.

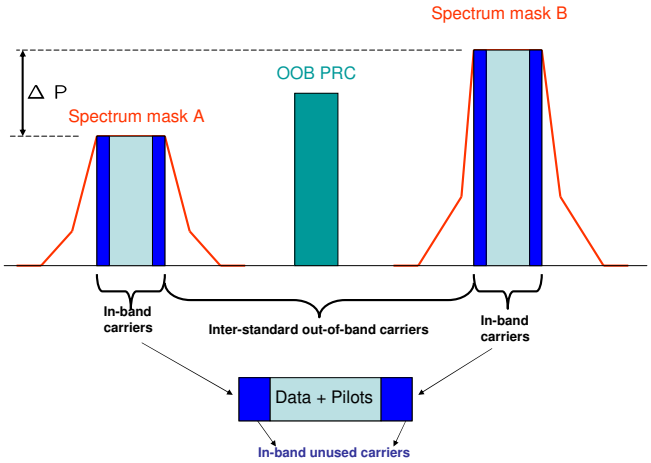

Figure 4.38: SWR system model with in-band and out-of-band carrier positioning.

Referring to the earlier discussion in this chapter about the generation of SWR signal and frequency transformation in Section 4.5, Standard A and Standard B symbols are added to make SWR signal, transformed to frequency domain, respecting the ratio of symbol frequency and sampling frequency corrective tones are added to reduce PAPR.

4.9.2 SWR PAPR reduction performance

The simulations are performed for a theoretical SWR system containing Standard A and Standard B described before. TR-SOCP based PAPR reduction method is applied to this system (system parameters given in Table. 4.2) with the constraints on added mean power. The performance is evaluated in terms of PAPR reduction capability and system interference (BER).

%age of in-band Standard A PRC:	18.75%
%age of in-band Standard B PRC:	21.87%
%age of out-of-band PRC:	15.63%
Mapping scheme:	4-QAM

Table 4.2: Simulation model parameters.

PAPR of SWR signal is reduced initially with the in-band unused carriers and then out-of-band inter-standard carriers are used to further reduce PAPR.

We would like to precise here that by in-band unused carriers we mean the carriers which are left unused in the standard specifications. Now once the SWR signal is brought

to frequency domain after the application of FFT, there appear many virtual carriers (zeros) because of the high sampling rate of the SWR signal than symbol rate of the standards. These virtual carriers could be used for PAPR reduction by carefully assigning them power as to obey spectrum mask constraints. In our case, however, we select only those of the virtual carriers which correspond to the unused standard carriers. The ratio of sampling rate to symbol rate should be used to search out these carriers out of all virtual carriers.

4.9.2.1 PAPR reduction gain and transmit power gap

As discussed before that all the standards in a SWR system may not transmit at the same power level e-g WLAN (IEEE 802.11a/g) would be transmitted with 25 dB less power than WiMAX (IEEE 802.16a). Thus we shall see the effects on PAPR reduction performance with the difference in transmit power levels of the standards. Initially a simple case is considered where the two standards are identical (Standard A taken as case study here) and the variations in power level are discussed. The transmit power level of one of the two identical standards is reduced and it is noted that the effect of reserved carriers positioned in the attenuated standard band starts to vanish as the power gap goes on increasing. Following table summarizes the scenario where Δ Gain is the difference in PAPR reduction performance between $PAPR_{gain2}$ and $PAPR_{gain1}$. Here $PAPR_{gain2}$ and $PAPR_{gain1}$ are the PAPR reduction gains when the reserved carriers of both standards and only one standard are employed to reduce PAPR respectively. Also Δ P is the transmit power difference between two standards. It could be seen that around 30 dB power gap, the value of Δ Gain is almost zero stating that the reduction with only one standard will be sufficient to have the same gain as with the peak reducing carriers of both standards. This would mean the same performance at reduced complexity.

Δ P (dB)	0	10	20	30
Δ Gain (dB)	0.72	0.50	0.20	0.07

Table 4.3: Transmit power gap and PAPR reduction performance.

The reason of the ineffectiveness of peak reducing carriers with attenuated power is obviously the power gap. In fact, even the useful data carriers of the attenuated standard do not add much to the PAPR distribution because of reduced power level. Thus it would be preferable to use only the peak reducing carriers of the standard with the highest transmit power level when the inter standard power gap is large.

In another case where SWR system was comprised of two different standards, Standard A and Standard B. The value of Δ Gain was reduced to 0.18 dB at Δ P of 25 dB which was 1.5 dB at Δ P of 0 dB.

Practically speaking, SWR system comprising of two identical standards with equal transmit power can be analogous to a mono standard SWR system containing DVB-T standard with two identical channels of 8 MHz separated by 8 MHz [114]. On the other hand, the SWR system having two different standards with transmit power difference can be thought of a WLAN and a WiMAX combination where WiMAX signal is 25 dB more powerful than WLAN signal.

In the following simulations, the SWR system containing Standard A and Standard B shall be considered with power level of Standard B being 25 dB more than Standard A.

Also, only the peak reducing carriers of Standard B, R_B, shall be used with some of the out of band carriers.

4.9.2.2 PAPR reduction with in-band and out-of-band *PRC*

As shown in Fig. 4.39 that PAPR of SWR signal is reduced by around 3 dB at clipping rate of 10^{-2} by only employing in-band free carriers of Standards B. PAPR is further reduced by around 0.8 dB on using some of the inter-standard out-of-band carriers as peak reducing carriers. Mean power constraint γ is kept equal to 0.2 dB and 0.8 dB for in-band and out-of-band peak reducing carriers respectively. As it could be seen that out-of-band peak reducing carriers do not reduce PAPR as effectively as in-band carriers because of the positioning of these carriers away from the data carriers.

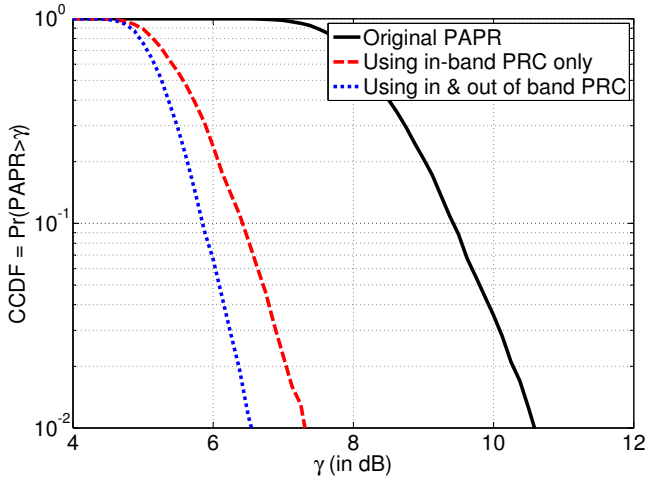

Figure 4.39: PAPR reduction using in band and out-of-band PRC.

Fig. 4.40 shows that the spectrum mask of each standard is respected. Here arbitrarily a mask is assigned to each standard. Also 80 carriers of free inter-standard band are used as out-of-band peak reducing carriers. As the in-band PRC have to follow the defined spectrum masks of the standards so their power can not be increased indefinitely but some of the out-of-band PRC can be transmitted with increased power under a relaxed power constraint and with the assumption that inter-standard band is free and can be used for PAPR reduction purpose.

4.9.3 Out-of-band *PRC*'s parameter influence

4.9.3.1 Out-of-band *PRC*'s mean power effect

As discussed above that out-of-band PRC reduce less PAPR than in-band *PRC* but the constraints on out-of-band *PRC* are lesser than those of in-band. The reason being the standard spectrum mask which should be respected and due to this fact the mean power of in-band can not be increased beyond a certain limit. Contrary, in case of out-of-band *PRC* the constraints on mean power are lesser with the assumption that the inter-standard

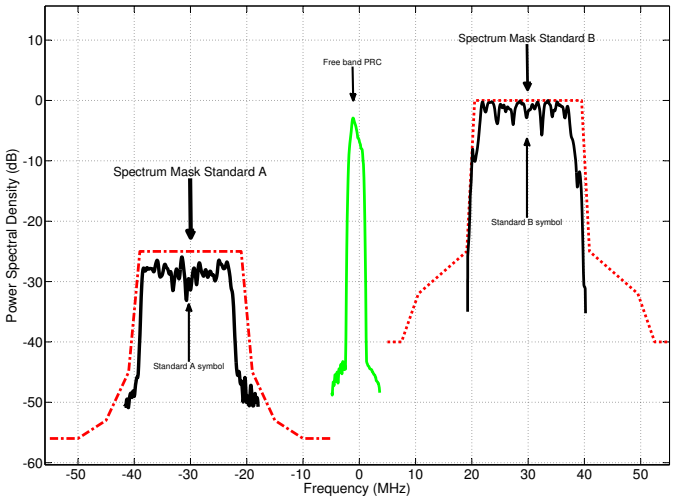

Figure 4.40: Each standard's spectrum mask is respected on PAPR reduction.

spectrum is free to use and there is no mask to be respected. Fig. 4.41 depicts the PAPR reduction with only out-of-band *PRC* application with different mean power constraints. Thus there is the compromise between PAPR reduction performance and increased mean power. Fig. 4.42 presents the spectral view of the mean power variations.

4.9.3.2 Out-of-band PRC's BW effect

Now the bandwidth of the *PRC* are varied to see the effects of number of reserved carriers on PAPR reduction. Only the out-of-band *PRC* are used to reduce PAPR. One can note that the number of *PRC* can vary dynamically according to the non-utilized spectrum states and the reduction in PAPR varies accordingly. More the reserved bandwidth for PAPR reduction, more the PAPR reduction gain and vice versa as shown in Fig. 4.43. Also the variation in bandwidth with the variation in *PRC* number is depicted in Fig. 4.44.

4.9.3.3 Out-of-band *PRC*'s position effect

Finally the position of out-of-band *PRC* is discussed. As mentioned earlier that transmitted power of Standard B is 25 dB more than that of Standard A. We see that as the PAPR reduction carriers approach the Standard B carriers, their effect on PAPR reduction is enhanced and vice versa. The fact that most of the PAPR contribution comes from the higher transmitted power standard (Standard B), makes it understandable that as the distance between the Standard B carriers and *PRCs* reduces, the effect of *PRCs* is pronounced and larger gain in PAPR reduction is observed as shown in Fig. 4.45. Fig. 4.46 demonstrates the spectrum and it could be seen that the positioning of reserved carriers is very important as we might violate the spectrum mask constraints. We can see that bringing the *PRC* near to the useful carriers results in high PAPR reduction but at the

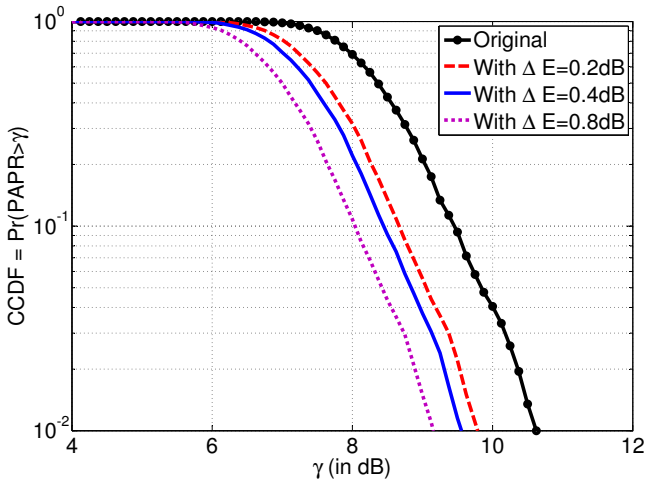

Figure 4.41: Out-of-band PRC's mean power effects on PAPR reduction.

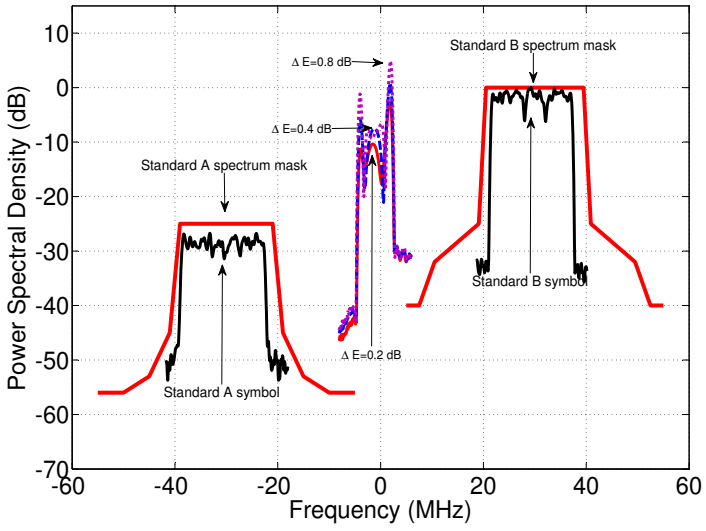

Figure 4.42: Spectrum of out-of-band PRC's mean power effects.

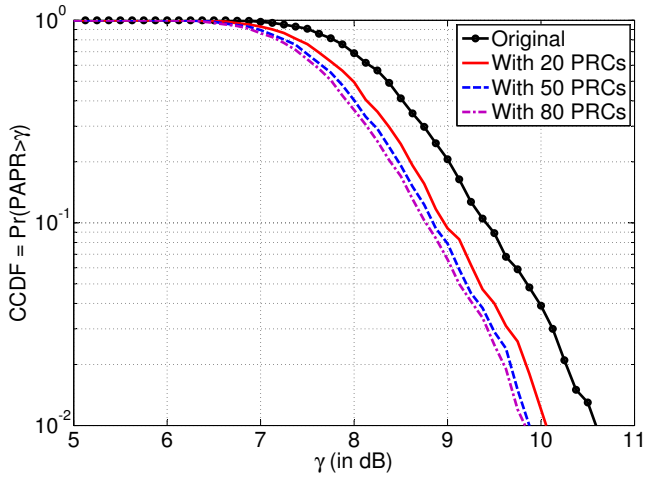

Figure 4.43: Out-of-band PRC's bandwidth effects on PAPR reduction.

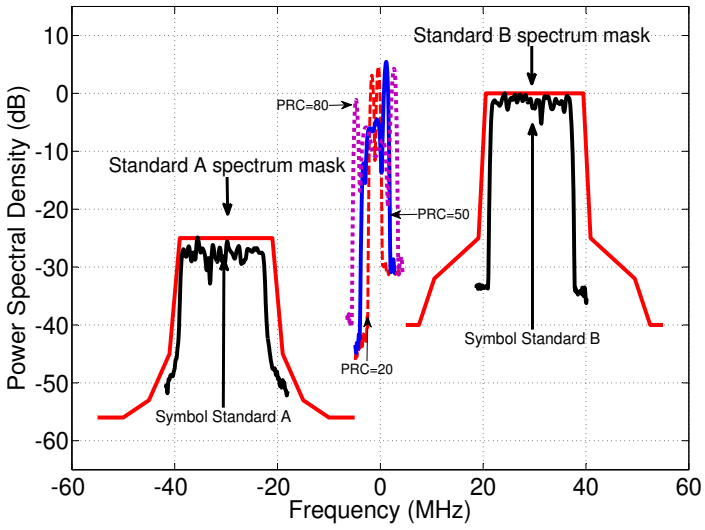

Figure 4.44: Spectrum of out-of-band PRC's bandwidth effects.

same time it results in spectrum mask constraints violations. Therefore, the position of the *PRC* should be selected with great care as not to generate interference.

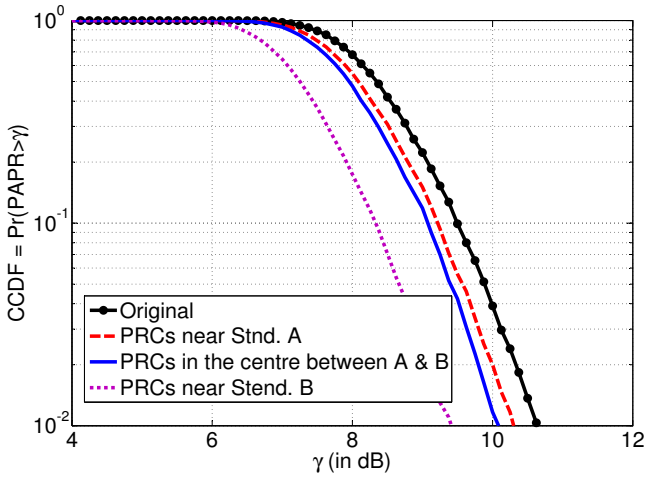

Figure 4.45: Out-of-band PRC's position effects on PAPR reduction.

4.9.4 Bit-Error-Rate Analysis

Referring again to Section 4.5, at the receiver each standard should be demodulated without any modifications in its architecture to keep the method down compatible. Demodulation at the Standard A and Standard B receiver were performed and it was found that in both cases BER matched the conventional BER rate curve as shown in Fig. 4.47 and Fig. 4.48 thus proving the hypothesis that out of useful band tones do not create in-band interference and thus no BER degradation takes place. The inter-standard *PRC*'s are automatically filtered out at the receiver because of their positioning outside spectrum mask.

Concluding we observe that TR method decreases PAPR while respecting spectrum masks of standards and also does not degrade BER. The PAPR reduction performance depends upon many factors like the bandwidth, position and power of *PRC*s. All these factors must be chosen carefully so as not to degrade BER or create inter-channel interference while providing the maximum PAPR reduction gain.

4.10 Conclusions

SWR systems suffer from high PAPR as OFDM based communication systems. Several methods have been devised to reduce OFDM signal PAPR and due to the similar PAPR characteristics of OFDM and SWR signal discussed in Chapter 3, these methods could be applied to reduce SWR signal PAPR. Among these methods, TR based PAPR reduction methods enjoy the unique feature of reducing the PAPR without standard modifications when the peak reducing carriers are transmitted over unused carriers of the standards. Also without degrading BER of the system, the transmitter needs not to transmit any SI. SOCP

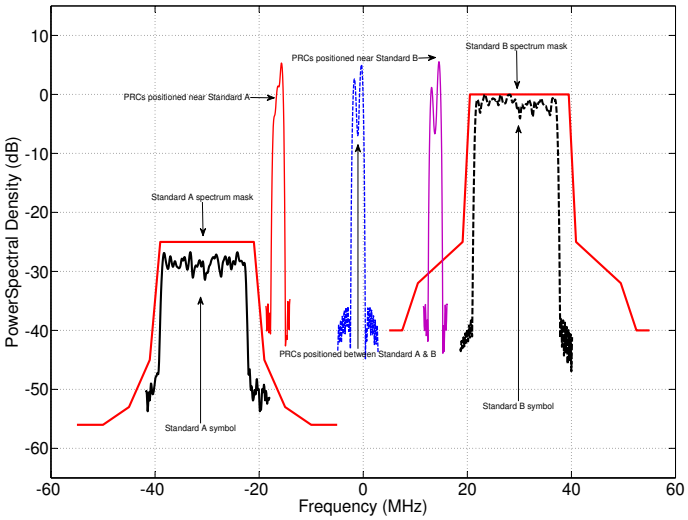

Figure 4.46: Spectrum of out-of-band PRC's position effects.

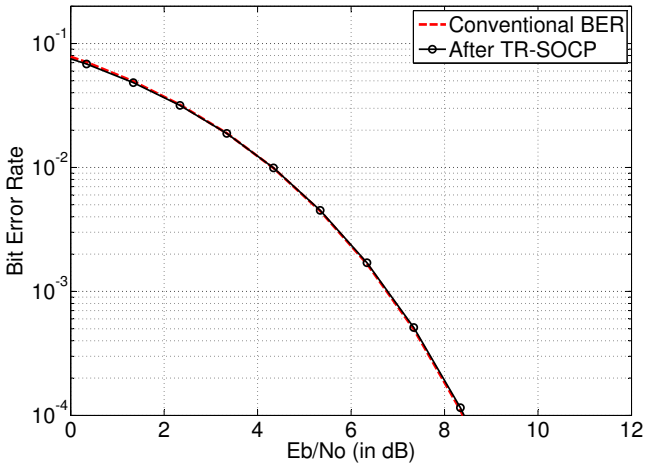

Figure 4.47: BER analysis before and after PAPR reduction for Standard A.

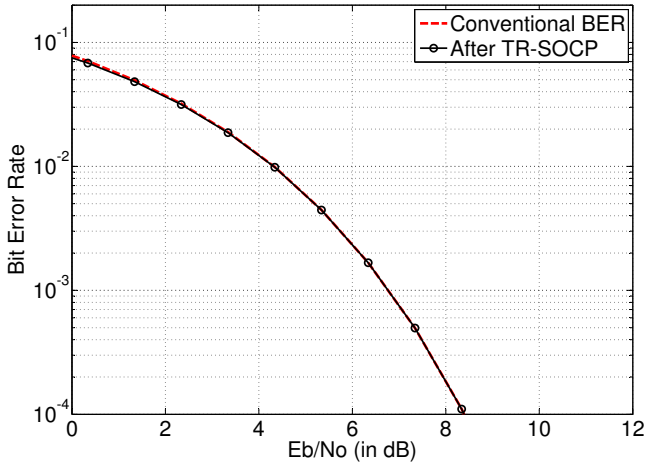

Figure 4.48: BER analysis before and after PAPR reduction for Standard B.

based modeling of the TR methodology was used in this chapter to reduce SWR PAPR. Initially, a very basic SWR transceiver was presented. Also the process of transforming time domain SWR signal into frequency domain was described to make SWR signal used for PAPR reduction using TR-SOCP method. Step by step SWR PAPR reduction was performed starting with multi-band OFDM case and ending up at multi-standard case. Initially, MB-OFDM PAPR was reduced and the complexity-performance trade-off was presented when PAPR was reduced over the global SWR signal or reduced over individual OFDM bands. Then PAPR reduction of a multi-channel GSM standard was performed by employing the channels which were unused at a GSM BS transmitter. The power on these unused channels was made to respect GSM's specified C/I values. Finally, a bi-standard SWR system was considered. Its PAPR was reduced by employing not only the in-band unused carriers of the standards but also some of the inter-standard free carriers to further reduce the PAPR. Also the out-of-band PRC's mean power, bandwidth and position variation effects on PAPR reduction were discussed and it was proved that BER performance was not affected on using TR-SOCP method.

Chapter 5

Comparison of Tone Reservation based PAPR Reduction Methods for SWR Signals

Contents

5.1 Introduction

As discussed earlier that Tone Reservation is one of the many PAPR reduction schemes for multi-carrier signals where peak reducing signal is generated by using reserved carriers to reduce the PAPR. There exist different methods to generate the peak reducing carriers like TR-Geometric method, TR-Gradient method and TR-Second Order Cone Programming (SOCP) based optimization method. We have already presented TR-SOCP method in the previous chapter and in this chapter we look for alternative TR methods and see if there is any compromise to be made between PAPR reduction performance and other parameters like computational complexity. After presenting the details of TR-Gradient and TR-Geometric methods this chapter compares the performance of these TR methods with TR-SOCP method for a Wireless Local Area Network (WLAN) system in terms of PAPR reduction capabilities and computational complexities while justifying that BER remains unvaried upon the application of these methods. Then the same performance parameter comparison of these TR methods is performed for a multi-channel GSM standard and bi-standard SWR system. Apart from multi-channel GSM case, it is found that, TR-SOCP reduces more PAPR than TR-Geometric method but its computational complexity is higher than that of TR-Geometric method. While TR-Gradient method lies in between these two methods regarding performance and complexity criteria, this chapter presents a trade-off between PAPR reduction performance and complexity for three different TR implementation schemes. In multi-channel GSM case, TR-Gradient and TR-Geometric methods do not decrease PAPR due to the position of PRCs away from data carriers. Finally Truncated IFFT algorithm is presented aiming at the reduction of computational complexity of these methods. In fact this algorithm finds the peak of an IFFT with lesser complexity than classical IFFT thus reduces the overall optimization process complexity.

5.2 Tone Reservation based PAPR reduction schemes

One of the TR implementation schemes based on SOCP modeling has been discussed in Chapter 4. There are other methods too for the implementation of TR concept. In [17], Gradient-type method is used instead of SOCP to get the optimized tones. As this method provides a sub-optimal solution thus a loss in PAPR reduction performance is observed. We shall designate this mehtod as TR-Gradient method. Also, [10] obtains the added tones by operating on the time domain signal using Geometric method. This method shall be called as TR-Geometric method.

Below, TR-Gradient and TR-Geometric methods are detailed.

5.2.1 TR-Gradient Method

In Gradient method [17], the PRC are generated directly from the help of frequency domain knowledge of the information signal before IFFT. The difference between TR-SOCP and TR-Gradient methods is the optimization technique as far as implementation is concerned. TR-Gradient method is a gradient-based algorithm for creating the peak canceling signal $\mathbf{C}$ by utilizing the reserved tones.

The optimization problem may be reduced to minimization of A such that,

$$\max_{0 \leq k \leq NL-1} |IFFT(X_k + C_k)| < A. \tag{5.1}$$

This is a QCQP problem and its solution is computationally challenging. In TR-Gradient method, a simple gradient-type algorithm is used to solve the above minimization problem. It is a sub-optimal method but it leads to a tremendous reduction in the complexity.

The algorithm of Gradient method for PAPR reduction proposed in [17] is as,

- Set a threshold A, the PRC set K, an initial peak canceling signal $C_p^{(1)}$, and parameter μ. The set K is the index set of R unused carriers.
- Let for $n = 0, 1, \ldots NL-1$,

$$c_n^{(l)} = \sum_{p \in K} C_p^{(l)} e^{-2j\pi p \frac{n}{NL}}, \tag{5.2}$$

$$\hat{y}_n^{(l)} = \begin{cases} y_n^{(l)} & \text{if } \left|y_n^{(l)}\right| \leq A \\ Ae^{j \arg\left\{y_n^{(l)}\right\}} & \text{if } \left|y_n^{(l)}\right| > A \end{cases}, \tag{5.3}$$

and

$$\Delta_n^{(l)} = y_n^{(l)} - \hat{y}_n^{(l)},$$

where $y_n^{(l)} = x_n + c_n^{(l)}$ is the PAPR reduced signal at l-th iteration.

- Then, for $p \in K$, the update on step $l+1$ of the algorithm is

$$C_p^{(l+1)} = C_p^{(l)} - \mu \sum_{n=0}^{NL-1} \Delta_n^{(l)} e^{2j\pi p \frac{n}{NL}}. \tag{5.4}$$

To further reduce the PAPR, the algorithm should be iterated. After an optimal number of P iterations (determined experimentally), the maximum PAPR reduction gain is achieved.

5.2.2 TR-Geometric Method

TR-Geometric method [10] is a PAPR reduction method where corrective signal is determined by Geometric method. Let us consider the discrete time OFDM symbol sample defined in Eq. (5.5).

$$x_n = \frac{1}{\sqrt{NL}} \sum_{k=0}^{NL-1} X_k e^{2j\pi nk/NL}; n = 0, 1, 2, ..., NL-1 \tag{5.5}$$

According to the principle of the Geometric method for PAPR reduction proposed in [10], the adding signal a_n for PAPR reduction is expressed as

$$a_n = \begin{cases} 0 & , \quad |x_n| \leq A \\ \left(\frac{A}{|x_n|} - 1\right) x_n e^{j\theta_n} & , \quad |x_n| > A \end{cases}, \tag{5.6}$$

where A is the magnitude threshold, θ_n is defined as $\theta_n \triangleq 2\pi\Delta f \frac{n}{NL} T_s, \quad 0 \leq n \leq NL-1$.

The details about the generation of signal a_n can be found in Appendix B (Section B.2). The parameter Δf is defined as $\Delta f \triangleq f_r - f_c$, where f_c and f_r are the carrier frequencies of the OFDM signal and adding signal respectively.

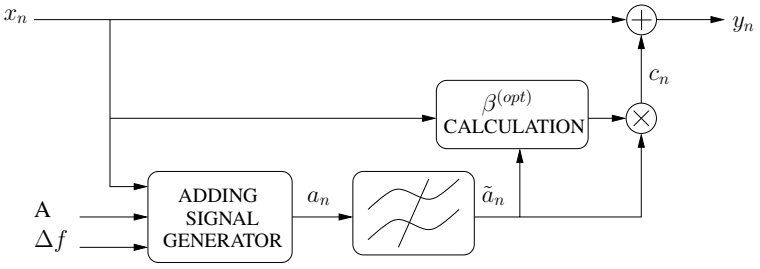

Figure 5.1: Geometric method for PAPR reduction.

To place the corrective tones on the unused carrier positions, the filtered adding signal $\tilde{a}_n$ for PAPR reduction is obtained by passing a_n through a filter based on FFT/IFFT pair whose pass bands are on *PRC*. Thus the digital filter makes sure that the corrective tones are placed on *PRC*. One can see that Geometric method creates the adding signal with the help of time domain information signal $\mathbf{x}$ while maintaining the orthogonality between information signal tones and added tones (*PRC*) by introducing the digital filter. The description about filter based FFT/IFFT are given in Appendix B (Section B.3).

Moreover, in order to outperform the PAPR reduction performance, the peak-canceling signal c_n can be considered as a scaled version of the filtered adding signal i.e., $c_n = \beta\tilde{a}_n$ as shown in Fig.5.1, where β is the scaling factor. To improve the PAPR reduction performance, β should be optimized. Thus the optimization problem becomes,

$$\min_{\beta} \max_{0 \leq n \leq NL-1} |y_n|^2, \tag{5.7}$$

where y_n is the PAPR reduced signal and can be written as $y_n = x_n + \beta\tilde{a}_n$. In [115], it is shown that, a sub-optimal solution of Eq. (5.7) is to minimize the total power of the samples with $|y_n| > A$. Therefore, solving Eq. (5.7) leads to

$$\min_{\beta} \sum_{n \in S_p} |x_n + \beta\tilde{a}_n|^2, \tag{5.8}$$

where, $S_p = \{n : |y_n| > A\}$. The above minimization problem is a linear least-squares problem and the solution is given by

$$\beta^{(opt)} = -\frac{\sum\limits_{n \in S_p} x_n \tilde{a}_n^*}{\sum\limits_{n \in S_p} |\tilde{a}_n|^2}, \tag{5.9}$$

where $(.)^*$ is the mathematical conjugate function. In conclusion, the PAPR reduced signal y_n can be written as,

$$y_n = x_n + c_n = x_n + \beta^{(opt)}\tilde{a}_n. \tag{5.10}$$

5.3 Performance comparison of TR based implementation schemes for WLAN systems

5.3.1 OFDM based WLAN system

As discussed earlier, OFDM is a modulation technique used in many standards like DVB-T, DAB, WLAN, WiMAX etc. In these standards IFFT is applied to the mapped symbols in order to get a multi-carrier signal. Here we shall treat the case of WLAN standard.

In WLAN IEEE 802.11a/g standard [116] IFFT size (N) is 64. Out of these 64 subcarriers, $D = 48$ subcarriers are used for data, while $P = 4$ subcarriers are used for pilots. The rest $R = 12$ subcarriers are unused (null) subcarriers and only these unused subcarriers shall be utilized for PAPR reduction of the WLAN signal. These peak reducing carriers are equally distributed and positioned at the left and right edges of the information carriers. It should be noted that the power of these correction carriers should be limited to make them respect the power spectrum mask specified for IEEE 802.11a/g standard.

All the three aforementioned TR based PAPR reduction methods are applied to this system (system parameters given in Table. 5.1) with same constraints on added mean power. The performance of these methods is compared in terms of PAPR reduction capability, computational complexity and system interference (BER). Also the power spectral density (PSD) presentations are provided to show that peak reducing carriers do not increase the system bandwidth, neither they violate spectrum mask specifications when used under proper mean power constraints.

System Parameters		Method Specific Parameters	
%age of PRC:	18.75%	μ (TR-Gradient):	5
Mapping scheme:	64-QAM	P (TR-Gradient):	4
Oversampling factor:	4	$\Delta f T_s$ (TR-Geometric):	1/8

Table 5.1: Simulation model parameters.

5.3.2 PAPR reduction performance comparison

PAPR reduction performance is compared in two ways, mean PAPR reduction $\Delta PAPR$ is plotted as a function of mean power constraint ΔE and also it is compared in terms of CCDF for a constant $\Delta E = 0.25$ dB. Here $\Delta PAPR$ is the mean PAPR reduced for N_s OFDM symbols i-e $\Delta PAPR = \frac{1}{N_s}\sum_{i=1}^{N_s} \Delta PAPR_i$ where $\Delta PAPR_i$ is the PAPR reduction for the i-th OFDM symbol. All the simulations are performed for a very large value of N_s (e-g $N_s = 10^5$). As it can be seen in Fig. 5.2 that TR-SOCP method outperforms the other two methods (around 2.5 dB and 2.0 dB more $\Delta PAPR$ than TR-Gradient and TR-Geometric methods respectively). Also mean PAPR reduction $\Delta PAPR$ increases as the constraint on mean power is relaxed, i-e ΔE is increased but it should be limited by PA characteristics. Fig. 5.3 verifies the results in Fig. 5.2 and it could be noted that TR-SOCP turns out to be the best PAPR reduction method among the three compared.

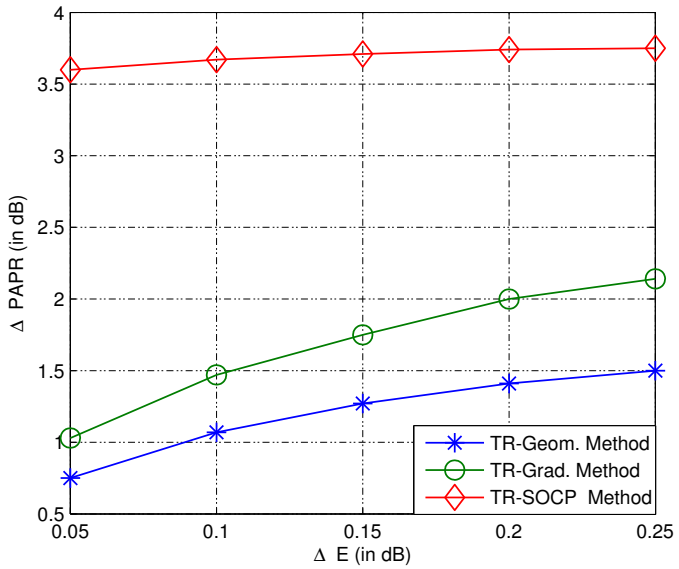

Figure 5.2: Mean PAPR reduction performance as a function of ΔE for the three different implementation schemes for TR methods.

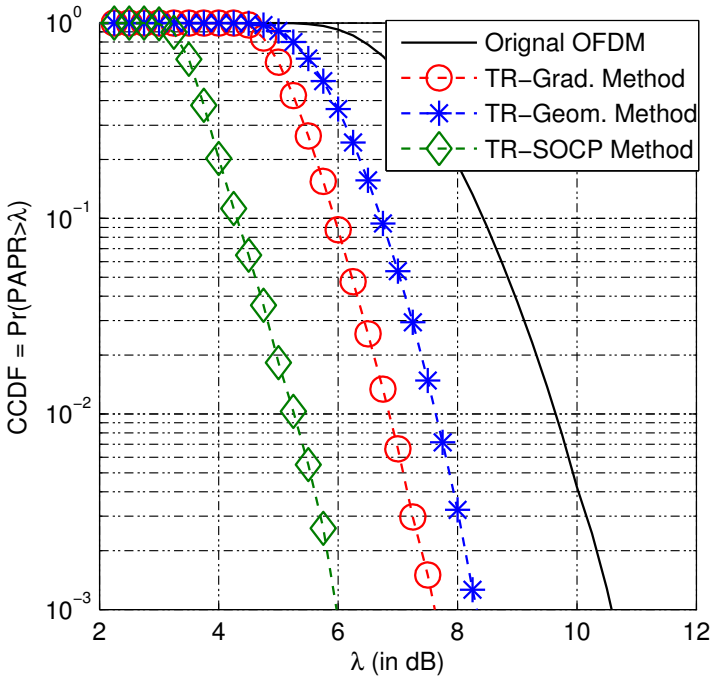

Figure 5.3: CCDF for the three implementation schemes for TR methods for a fix ΔE=0.25 dB.

5.3.3 Complexity Analysis

In this section, we evaluate the complexity performance of the three different implementation schemes for TR methods described in this chapter. Only the runtime complexity in terms of number of operations is considered and the complexity of the initialization stage is omitted since it occurs only once.

5.3.3.1 TR-SOCP Method Complexity Analysis

SOCP optimization problem is solved through Interior Point methods like SeDuMi or SDPT3 [117]. This problem is the minimization of l_∞-norm (Chebyshev approximation: $\|.\|_\infty$) which with some standard tricks is converted to Linear Programming problem. As Convex optimization includes Linear Programs as a special case whose optimal solution could be found by SOCP.

Complexity analysis of Interior Point methods is very complex and needs profound knowledge of optimization domain for rigorous solution. However the approximated complexity of the SDPT3 method used is $O\left(NLR^2\right)$ [118], where R is the number of reserved carriers.

5.3.3.2 TR-Gradient Method Complexity Analysis

Now, let us consider the Gradient algorithm for PAPR reduction. Let us start by evaluating the complexity of the algorithm in the loop.

(i) The complexity of calculating $\hat{y}_n^{(l)}$ expressed in Eq. (5.3) is $O\left(\hat{\eta}^{(l)}NL\right)$, where $\hat{\eta}^{(l)} = \Pr\left\{\left|\hat{y}_n^{(l)}\right| > A\right\}$.

(ii) The complexity of calculating the frequency domain samples of peak-canceling signal $C_p^{(l+1)}$ expressed in Eq. (5.4) and the time-domain samples of peak-canceling signal $c_n^{(l+1)}$ expressed in Eq. (5.2) is $O\left(NLR\right)$.

One can note that the complexity of calculating $\hat{y}_n^{(l)}$ is very low compared to the complexity in Eq. (5.2) and Eq. (5.4). Thus, in the loop, the complexity of the algorithm is approximated as $O\left(NLR\right)$. Therefore, for P iterations, the complexity of the algorithm is evaluated as $O\left(NLRP\right)$.

5.3.3.3 TR-Geometric Method Complexity Analysis

Let us consider the Geometric algorithm for PAPR reduction.

(i) In Eq. (5.6), the complexity of calculating a_n is $O\left(\nu NL\right)$, where $\nu = \Pr\left\{|x_n| > A\right\}$. As $|x_n|$ is a Rayleigh random variable, so $\nu = 1 - e^{-A^2/P_x}$, with $P_x = E\left\{|x_n|^2\right\}$. Let us note that, $\forall A \geq 0, \quad \nu \leq 1$.

(ii) The filtered adding signal $\tilde{a}_n$ is obtained by using a filter based on FFT/IFFT pair. Using the decimation-in-time (DIT) radix-2 FFT algorithm [119], the complexity of calculating $\tilde{a}_n$ is evaluated as $O\left(NL\log_2 NL\right)$.

(iii) The complexity of calculating the optimal scaling factor $\beta^{(opt)}$ given in Eq. (5.9) is $O(\eta NL)$, where $\eta = \Pr\{|y_n| > A\}$.

The complexity of calculating a_n and $\beta^{(opt)}$ is very low compared to the complexity of calculating $\tilde{a}_n$ and can be omitted. Therefore, the complexity of the algorithm is approximated as $O(NL \log_2 NL)$.

Below is the table (Table 5.2) comparing the computational complexities of the three methods for IEEE 802.11a/g standard specifications, clearly suggesting that TR-SOCP is 18 and 3 times more computationally complex than TR-Geometric and TR-Gradient methods respectively while TR-Gradient method is 6 times more complex than TR-Geometric method.

TR-Geometric Method	TR-Gradient Method	TR-SOCP Method
Generalized Complexities Comparison		
$O(NL \log_2 NL)$	$O(NLRP)$	$O(NLR^2)$
IEEE 802.11a/g Specific Complexities Comparison		
$O(2^{11})$	$O(6 \times 2^{11})$	$O(18 \times 2^{11})$

NL: IFFT size=256; R: *PRC* number=12; P: Iterations=4

Table 5.2: Computational complexity comparison of the TR schemes.

5.3.4 In-band & Out-of-band Interference Analysis

It is evident in the Fig. 5.4 that all three methods match the conventional BER rate curve thus proving the hypothesis that out of useful band tones do not create in-band interference and thus no BER degradation takes place. It should be noted that BER calculations are performed for useful carriers only.

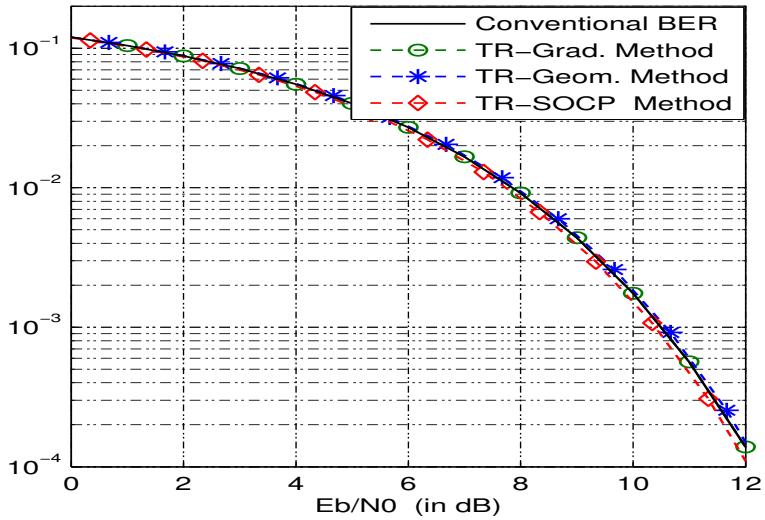

Figure 5.4: BER vs E_b/N_0 for the three implementation schemes of TR methods.

Also, the out-of-band distortions are nullified by employing constraints on additional mean power. This fact is demonstrated in Fig. 5.5 where the signal PSD after correction

carriers addition with $\Delta E = 0.10$ dB is given for all the three methods. It is clear that all the three TR schemes respect the spectrum mask defined for IEEE 802.11g standard.

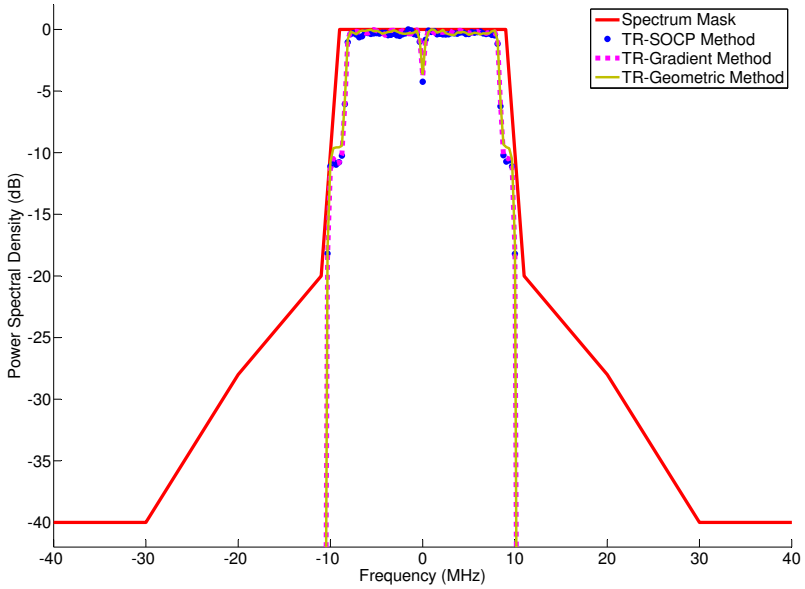

Figure 5.5: PSD of the three implementation schemes of TR methods.

In this section we have compared three different TR implementation schemes for WLAN standard in terms of PAPR reduction gain, complexity and interference. We extend this study to a multi-channel and multi-standard system scenario in the next section.

5.4 Performance comparison of TR based implementation schemes for MC-GSM system

In this section the same multi-channel GSM system shall be considered as that in Chapter 4. The aforementioned PAPR reduction schemes shall be applied to this system and we shall see the influence on PAPR reduction due to these schemes.

5.4.1 PAPR reduction performance comparison

PAPR reduction using TR-SOCP is already discussed in Chapter 4 for a multi-channel GSM standard. Here we shall only discuss PAPR reduction performance using TR-Geometric and TR-Gradient method.

5.4.1.1 Using TR-Geometric method

TR-Geometric method was applied to the mentioned GSM signal at the base station with 4 GSM channels separated by 800 kHz each while at 400 kHz from each channel we added

*PRC*s to generate the corrective signal in order to decrease PAPR. The power of this corrective signal was limited by the C/I value (−13 dB).

Instantaneous and mean PAPR values before and after the application of TR-Geometric method are plotted in Fig. 5.6 with the power spectrum density plots given in Fig. 5.7. It could be seen in Fig. 5.6 that mean and instantaneous PAPR before TR-Geometric method are almost same (represented by black and purple colors) lying around 9.02 dB. Mean and instantaneous PAPR values after TR-Geometric method (represented by red color) show variations with mean PAPR value after TR-Geometric application is about 9.7 dB. At first sight the results might seem astonishing as instead of decrease in PAPR, an increase is observed. Noting that TR-Geometric method is not an optimal PAPR reduction method. When the peak reducing signal is added to the original signal, peak regrowths occur if the frequency gap between useful carriers and peak reducing carriers is beyond a certain threshold [120]. The discussions about peak regrowth and the PAPR reduction variations as a function of frequency gap between useful and corrective carriers in the OFDM context are given in Appendix B (Section B.4).

As in the multi channel GSM context we are using a frequency gap of 400 kHz between useful GSM channel frequency and *PRC*'s frequency therefore in this context it is not beneficial to use TR-Geometric method.

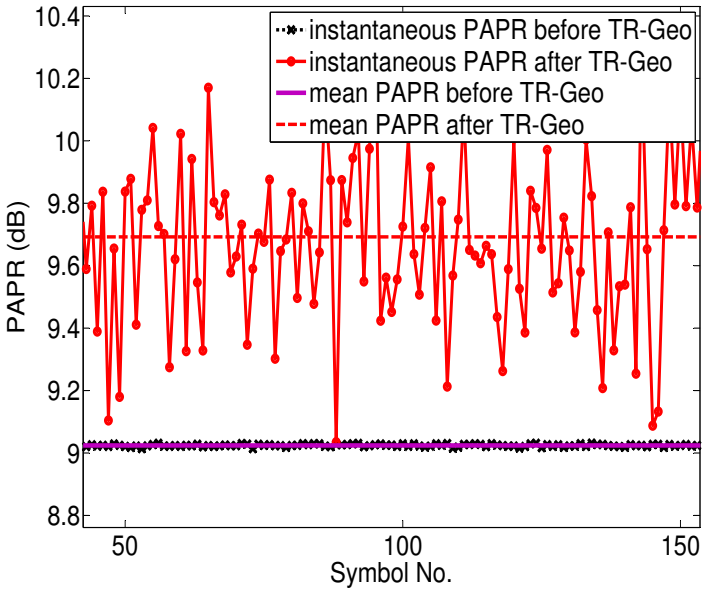

Figure 5.6: PAPR 'reduction' of MC-GSM signal using TR-Geometric method.

5.4.1.2 Using TR-Gradient method

Similarly when TR-Gradient method was applied to MC-GSM signal, the results were not found different from those of TR-Geometric method as shown in Fig. 5.8 (PSD plots given in Fig. 5.9). One can see in Fig. 5.8 that mean and instantaneous PAPR before

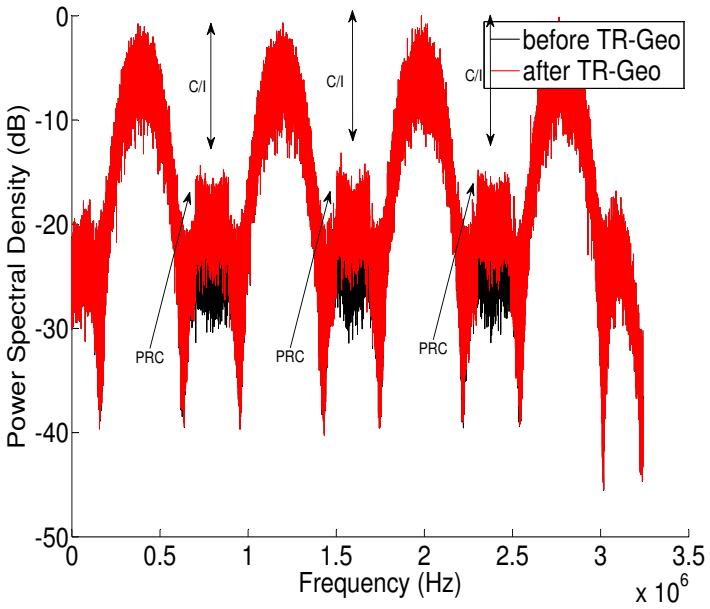

Figure 5.7: Spectrum of MC-GSM signal before and after TR-Geometric method application.

TR-Gradient method are almost same (represented by black and purple colors) and are about 9.02 dB. While mean and instantaneous PAPR values after TR-Gradient method (represented by red color) show variations with mean PAPR value after TR-Gradient is found to be around 9.6 dB. Again the same reason that TR-Gradient is a sub-optimal method and can not always assure best results in all circumstances.

Both TR-Gradient and TR-Geometric methods are basically the evolved form of clipping methods (adding an opposite value at a certain point is equal to subtraction/clipping) with the difference that the additive signal is carried by carriers orthogonal to data carriers in order not to degrade BER. Thus peak regrowths occur when certain parameters (e-g the position of the PRCs) are not kept in mind.

Concluding, we can see that TR-Geometric and TR-Gradient methods do not work for MC-GSM case in the simulation conditions given in our case. And therefore, it was not deemed appropriate to carry out a complexity analysis.

However, if somehow the peak reducing carriers could be placed near to GSM data carriers while respecting the GSM spectrum mask constraints and C/I values, PAPR reduction might be observed.

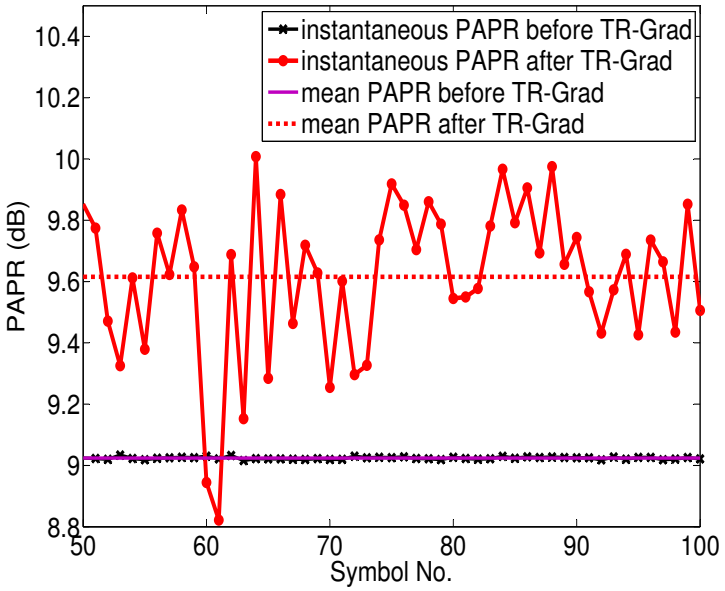

Figure 5.8: PAPR 'reduction' of MC-GSM signal with TR-Gradient method.

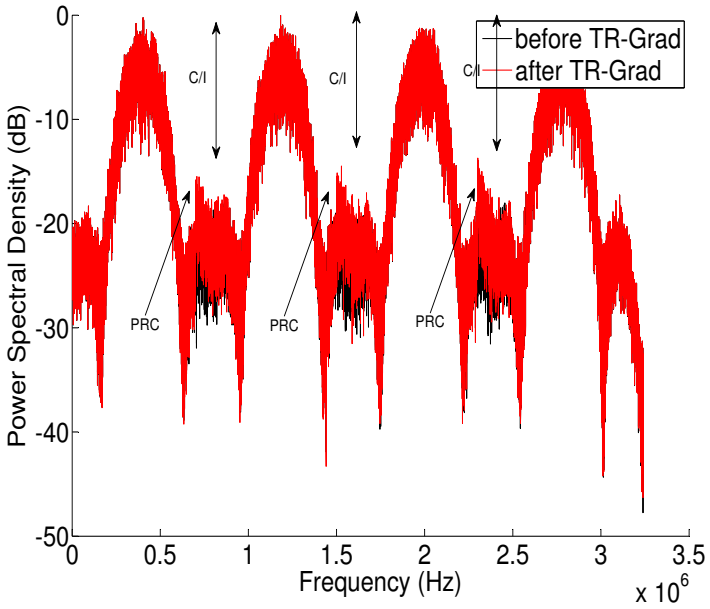

Figure 5.9: Power spectral density of MC-GSM signal before and after the TR-Gradient method.

5.5 Performance comparison of TR based implementation schemes for bi-standard SWR system

5.5.1 Bi-standard SWR system model

Now the method performance is compared for SWR signal. The signal simulated is a multiplex of two OFDM based standards. Standard A and Standard B of the previous chapter make the SWR signal (see Fig. 4.38). The sum of two standards signal is transformed to frequency domain using FFT and based on this spectral vision and keeping in mind the sampling frequency-symbol frequency ratio, corrective tones are added on unused carriers to reduce PAPR. As there is a gap of 25 dB in transmission power of the two standards, and as discussed previously that the PRCs of standard with low transmit power do not reduce much PAPR, therefore only the PRCs of the standard with greater transmission power are used to reduce PAPR at reduced complexity.

All the three TR based PAPR reduction methods are applied to this SWR system (system parameters given in Table. 5.3) with same constraints on added mean power. The performance of these methods is compared in terms of PAPR reduction capability, computational complexity and system interference (both in-band and out-of-band).

SWR System Parameters		Method Specific Parameters	
δf_A:	0.3125 MHz	μ (TR-Gradient):	5.0
δf_B:	0.0781 MHz	$\Delta f T_s$(TR-Geometric):	1/8
Mapping:	4-QAM	P (TR-Gradient) :	4.0
Inter standard band:	40 MHz	ΔE(dB):	0.14

Table 5.3: Simulation model parameters.

5.5.2 PAPR reduction performance comparison

In Fig. 5.10 it could be noted that TR-SOCP turns out to be the best PAPR reduction method among the three compared. The PAPR reduction gain for TR-SOCP is approximately 0.7 dB and 1.5 dB more compared to TR-Gradient and TR-Geometric methods respectively at the clipping rate of 10^{-2}.

5.5.3 Complexity Analysis

Using the same complexity analysis performed for WLAN standard, SWR signal PAPR reduction complexity analysis is performed.

Below is the table comparing the computational complexities of the three methods for SWR signal, clearly suggesting that TR-SOCP is approximately 275 and 14 times more computationally complex than TR-Geometric and TR-Gradient methods respectively while Tr-Gradient method is approximately 19 times more complex than Geometric method.

5.5.4 In-band & Out-of-band interference Analysis

It is evident in the Fig. 5.11 and Fig. 5.12 that all three methods match the conventional BER rate curve for both standards thus proving the hypothesis that out of useful band tones do not create in-band interference and thus no BER degradation takes place.

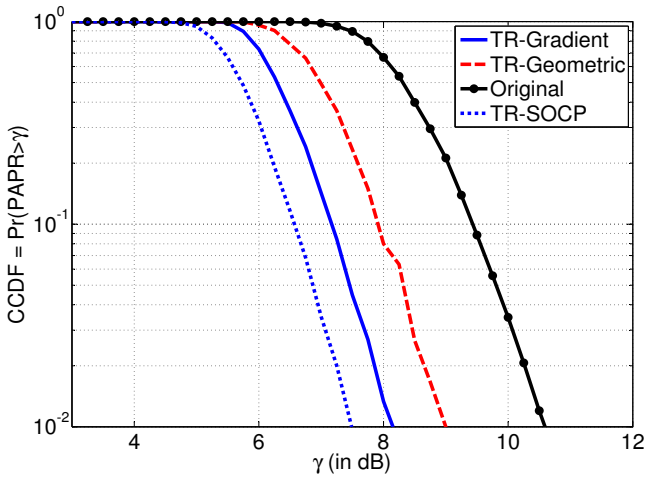

Figure 5.10: CCDF for the three implementation schemes for Tone Reservation methods for a fix ΔE=0.14 dB.

TR-Geometric	TR-Gradient	TR-SOCP
Generalized Complexities Comparison		
$O(NL\log_2 NL)$	$O(NLRP)$	$O(NLR^2)$
SWR Signal Specific Complexities Comparison		
$O(3\times 2^{14})$	$O(58\times 2^{14})$	$O(830\times 2^{14})$

NL: IFFT size=1024 × 4=4096; R: =56; P: Iterations=4

Table 5.4: Computational complexity comparison of the TR schemes.

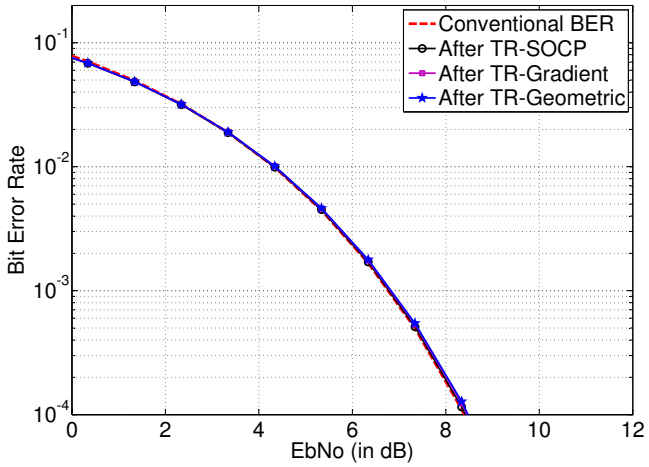

Figure 5.11: BER vs E_b/N_0 for the three implementation schemes of TR methods for Standard A.

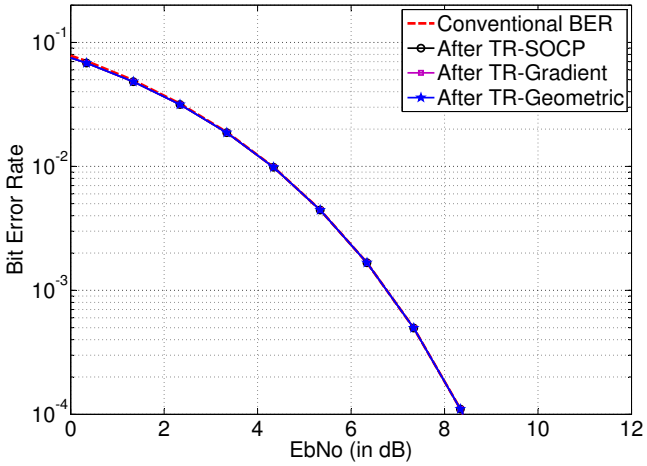

Figure 5.12: BER vs E_b/N_0 for the three implementation schemes of TR methods for Standard B.

Fig. 5.13, 5.14 and 5.15 show the power spectral density of the SWR signal before and after the implementation of these three TR schemes. As it could be seen that the reserved carriers respect the specified power mask for each standard by employing constraints on additional mean power. Thus no out-of-band interference takes place.

Until now we have compared different TR schemes for WLAN and a hypothetical SWR standard. We have seen that the optimization problem to obtain PRC uses FFT function extensively and this contributes a lot to the computational complexity of the methods. In the following section we shall present an algorithm which reduces the TR method complexity by reducing the complexity of maximal IFFT element calculation.

5.6 Tone Reservation's complexity reduction using fast calculation of maximal IDFT element

Till now we understand that TR-SOCP is the most efficient TR method for PAPR reduction but it is the most complex at the same time. In this section we shall reduce the complexity of this method using a special algorithm which calculates only the maximum value of the IDFT output. In fact, in peak power control, fast peak calculation of the signal is of utmost importance. Many PAPR reduction techniques need frequent peak calculations in order to mitigate the PAPR as in TR. In TR the process of adding tones is done in frequency domain while their effect on the peak of the signal is seen in time domain after Inverse Discrete Fourier Transform (IDFT) operation. To get the optimized values of the tones to be added, frequent exchanges between frequency and time domain are performed. This makes TR a computationally expensive technique. If by somehow the complexity of finding the signal's peak is reduced, TR complexity will be considerably reduced. Truncated IDFT algorithm [17] calculates the peak of IDFT output with complexity which is linear in IDFT size N compared to $O(Nlog_2(N))$ complexity when

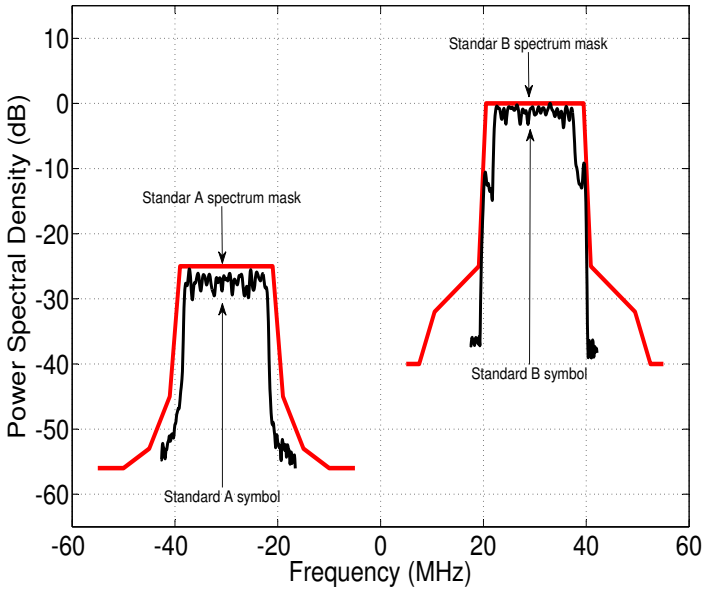

Figure 5.13: Power spectral density of SWR signal after implementation of TR-SOCP.

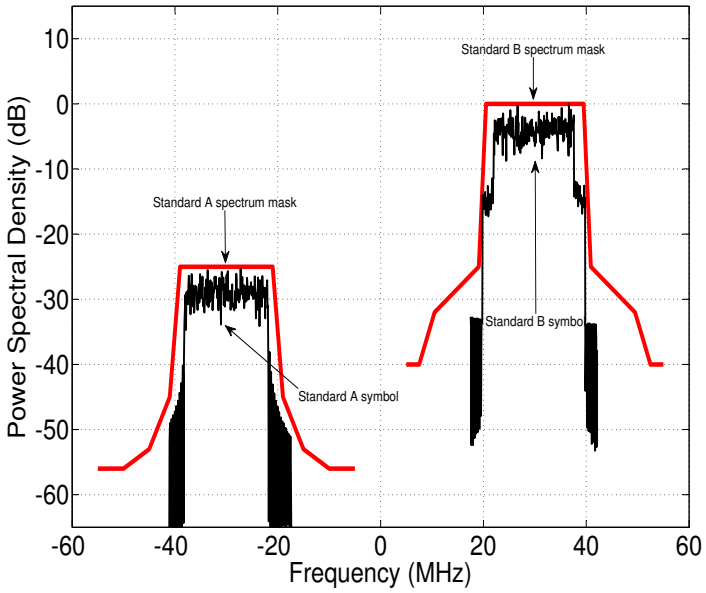

Figure 5.14: Power spectral density of SWR signal after implementation of TR-Gradient.

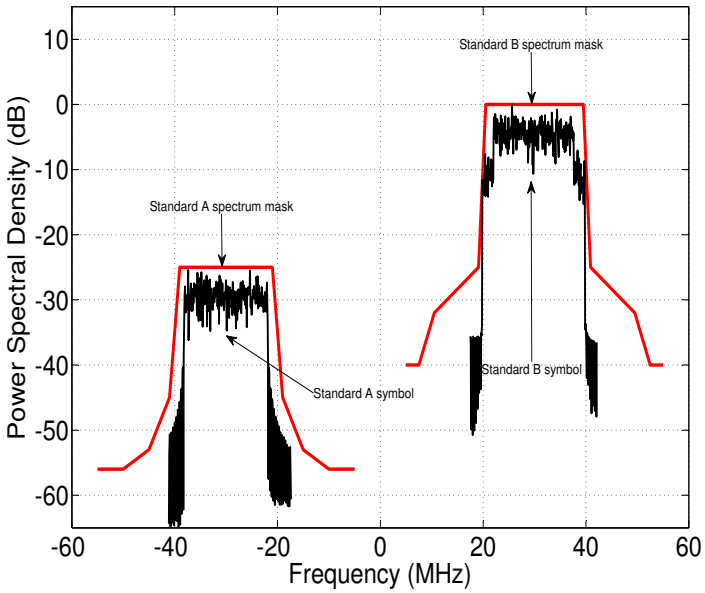

Figure 5.15: Power spectral density of SWR signal after implementation of TR-Geometric.

classical IFFT (Inverse Fast Fourier Transform) [119] is used. In this section this Truncated IDFT algorithm is applied to TR technique to reduce the complexity of this PAPR reduction technique. It is found that there is not much PAPR reduction gain using [17] and thus modifications are made to improve the performance. Almost optimal results are obtained with this variant along with reduced complexity.

We shall first present Truncated IDFT algorithm.

5.6.1 Truncated IDFT Algorithm

As we have seen that TR-SOCP is about minimizing the maximum of the IDFT output. To perform this minimization, the optimization technique needs to calculate tones 'C' which reduce the peak of the temporal signal $(x + c)$. Thus frequent IDFT operations are required to calculate peak of the signal which contributes to the high complexity of TR technique. The process of optimization is outlined in Fig. 5.16 which demonstrates that frequent transforms are required to obtain the optimum values of the added tones which reduce the PAPR of the original signal. Here C_{init} is the initial value of vector 'C' provided to optimization algorithm. During optimization, the value of 'C' is varied according to a certain law and constraints to minimize $max(x + c)$. After certain number of algorithm iterations optimal value of C, C_{opt}, is returned such that $PAPR(x+c_{opt}) < PAPR(x)$. Let N_{itr} be the number of iterations required by optimization technique to generate optimal tones, then the computational complexity of 'Fourier Transform' block for the optimization would be $O(N.N_{itr}.log_2(N))$ which is quite large.

Basic idea of Truncated IDFT algorithm is to estimate the maximal value IDFT element without calculating all the IDFT output values. This would mean that certain

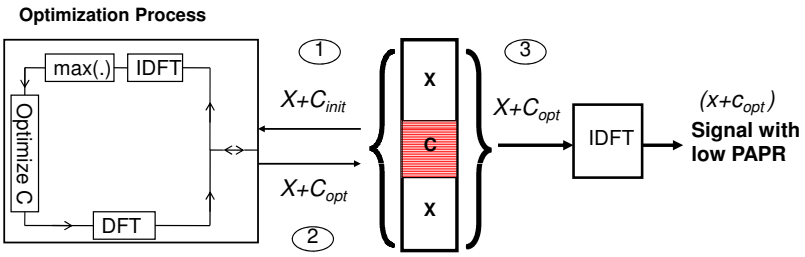

Figure 5.16: Tone Reservation optimization process.

elements' calculations are omitted based on certain criterion and few transformations are done which lead to the maximal element. This can be better explained with a 'decimation in frequency' IFFT butterfly diagram (Fig. 5.17). Here $\mathbf{X}$ and $\mathbf{x}$ are the IDFT input and output vectors respectively and $W_N^{n.k} = e^{2\pi\iota n.k/N}$. In this method transformation is done in $log_2 N$ steps. A bird's eye view can easily detect that results at each intermediate step depend only on some inputs at previous steps and not all. In fact at very first step we have two halves of $N/2$ values each and the second step values are either depending solely upon one half or the other. The idea is to leave the half with less energy and move on with the one with more energy. This way at each step, the half with less energy is truncated and we move on with the half having more energy. At final step we reach the maximum element (with certain probability of error) without going through calculations of rest of the elements.

After having described the basic idea of the algorithm, a general mathematical description of this algorithm is presented below [17].

Let $N = n_1 n_2 ... n_m$ and, $q_k = n_{k+1} n_{k+2} ... n_m$ for $k = 0, 1, ..., m-1$. Clearly $N = q_0$ and let $q_m = 1$. For an input sequence $\mathbf{a} = (a_0, a_1, ..., a_{N-1})$, we are searching for M where

$$\mathbf{M(a)} = \max_{j=0,1,...,N-1} |\sum_{k=0}^{N-1} a_k e^{2\pi\iota jk/N}|.$$

1. For $l = 1$ up to m, perform steps 2-6.
2. Arrange the entries of $\mathbf{a}$ in matrix $G = [g_{k,j}]$, $k = 0, 1, ..., n_l - 1$, $j = 0, 1, ..., q_l - 1$,

$$G = \begin{pmatrix} a_0 & a_1 & ... & a_{q_l-1} \\ a_{q_l} & a_{q_l+1} & ... & a_{2q_l-1} \\ ... & ... & ... & ... \\ a_{(n_l-1)q_l} & a_{(n_l-1)q_l+1} & ... & a_{n_l q_l-1} \end{pmatrix}.$$

3. Implement the IDFT of dimension n_l on the columns of G. The resulting matrix $T = [t_{k,j}]$, $k = 0, 1, ..., n_l - 1$, $j = 0, 1, ..., q_l - 1$, is computed as follows:

$$t_{k,j} = \sum_{r=0}^{n_l-1} g_{r,j} e^{2\pi\iota rk/n_l}. \tag{5.11}$$

4. Compute the vector $\mathbf{p} = (p_0, p_1, ..., p_{n_l-1})$,

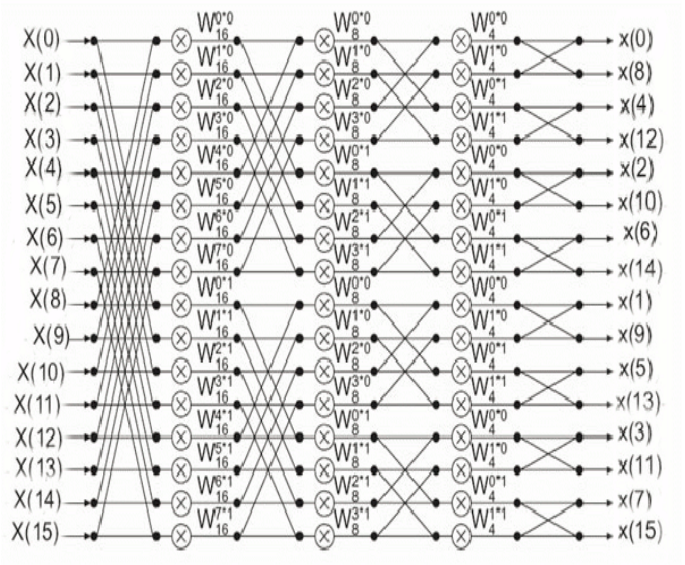

Figure 5.17: Radix-2 decimation in frequency butterfly diagram for 16 point IFFT.

$$p_k = \sum_{j=0}^{q_l-1} t_{k,j} t^*_{k,j}. \tag{5.12}$$

5. Find $b_l \in \{0, 1, ..., n_l - 1\}$, the index of the maximal entry in $\mathbf{p}$. If $l = m$ go to step 7.

6. Compute the new vector $\mathbf{a} = (a_0, a_1, ..., a_{q_l-1})$,

$$a_j = t_{b_l,j} e^{2\pi\iota b_l j/q_l}. \tag{5.13}$$

7. Output $M = p_{b_m}$.

8. Stop.

In a particular case for $N = 2^m$ the complexity is $O(2N)$ whereas normal IFFT complexity is $O(Nlog_2(N))$. Note that it is not always necessary to divide the input data into two halves as shown in Fig. 5.17. Rather it can be divided in any combination following certain constraints and in fact the complexity is even reduced to $O(1.5N)$ when N is written as increasing order of factors. The problem with this algorithm is that it does not always give correct results. Experiments show that it results in maximal IDFT entry most of the times but in some cases it results in any other IDFT value which in most of the cases is either second or third highest value of the IDFT output. The reason of the failure is the criterion of selection or rejection of the branches at each step which is energy in our case. It is quite difficult to formulate the probability of falling to a wrong branch at each butterfly stage as a function of IDFT size and it still remains an open problem. Anyhow one can see that the worst case probability of falling to a wrong branch at first butterfly step would be 1/2. This worst case occurs when IDFT size is infinite which means that the energy in the two halves approaches a constant value. Thus the probability of wrong maximum selection would be 1/2 at first butterfly step.

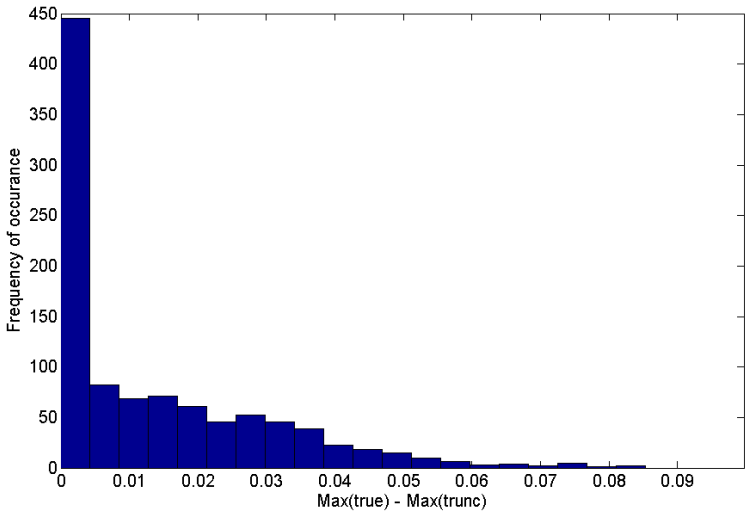

Figure 5.18: Histogram showing that most of the times truncated IDFT algorithm works fine.

5.6.2 Making the algorithm work better

As described above that the algorithm does not always result in the maximal IDFT value. This fact is demonstrated by Fig. 5.18 which clearly verifies that most of the times the difference between the maximum element returned by IDFT algorithm (Max_{true}) and by truncated IDFT algorithm (Max_{trunc}) is zero for a 64 carrier OFDM system. In case of failure, sometimes, the difference of maximal values can be quite large. Note that the difference never gets the negative value as the maximum provided by truncated IDFT algorithm is always equal or less than maximal IDFT value.

In order to get better results, one idea is to carry the top two intermediate results to the next step instead of only one result as discussed previously. Thus the probability of falling to a wrong branch is reduced but at the cost of complexity as we keep two intermediate results at each step and perform the necessary calculations. Fig. 5.19 clearly demonstrates the performance improvement as more peaks are detected accurately. Thus the application of truncated IDFT algorithm for Tone Reservation would show better results than simple truncated IDFT algorithm at the cost of complexity increment.

5.6.3 PAPR reduction with Truncated IDFT

As explained earlier that TR is a classical application of Truncated IDFT algorithm where frequent signal peak calculations make it computationally exhaustive. Truncated IDFT algorithm calculates the peak with a much lesser complexity and thus reduces the computational complexity of the TR technique by large.

The results of truncated IDFT algorithm application on TR method are shown in Fig. 5.20 for mean power constraint $\gamma = 0.4$dB. One curve, 'PAPR Original', is the CCDF for QPSK mapped OFDM signal with 64 point IDFT. These 64 points comprise of 48 data carriers and 16 added tones. The curve 'PAPR Reduced(true)' is obtained after the optimization using classical IDFT operation inside 'Fourier Transform' block in Fig. 5.16. Similarly 'PAPR Reduced(trunc)' is obtained when Truncated IDFT is used inside

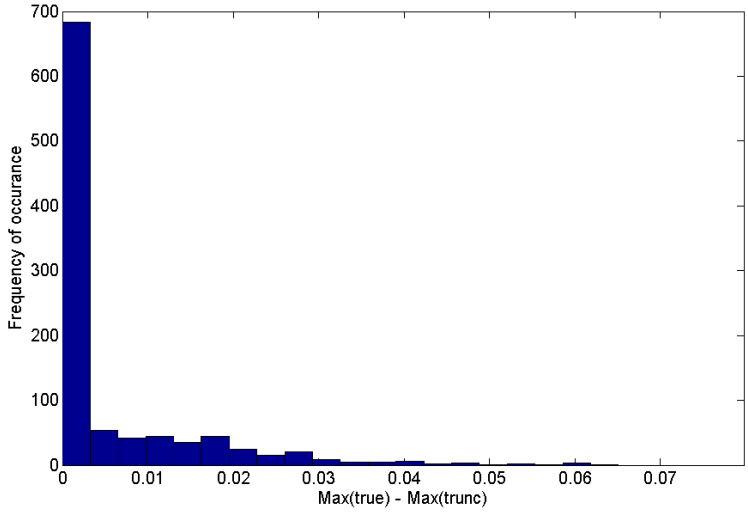

Figure 5.19: Histogram showing that performance is improved by keeping top two results at each intermediate step.

'Fourier Transform' block. In this way the complexity is reduced by $log_2(N)/2 = 3.0$ times but as it could be seen PAPR reduction gain is not much when compared to 'PAPR Reduced(true)'.

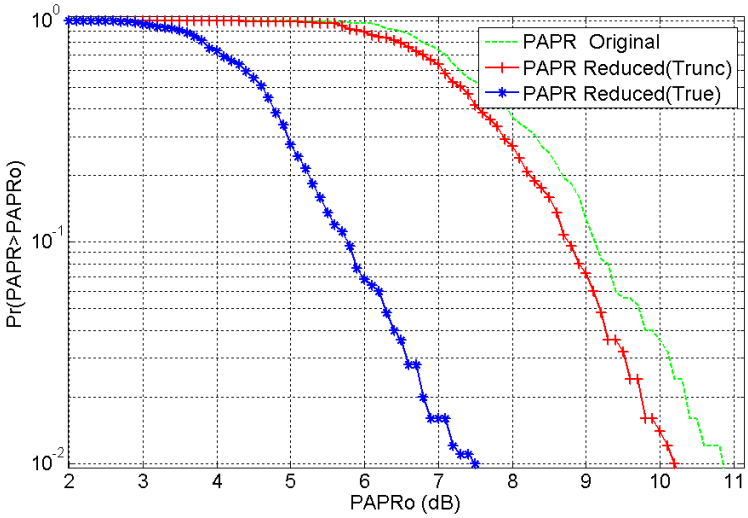

Figure 5.20: PAPR reduction using Tone Reservation with true and Truncated IDFT algorithm.

As shown in Fig. 5.20 that the results with Truncated IDFT algorithm are not much beneficial. The reason is that during the optimization process whenever the optimization technique finds a false maximal value it stores it as the optimal point. The reason of this behavior is that the false value is always less than the true value and the purpose of minimization is better served by false values than the true. Therefore the results are not much satisfactory. The optimization process is modified as to get the improved re-

sults by introducing a compromise between performance and complexity. Optimization is performed with both classical and Truncated IDFT algorithms. At the start of optimization Truncated IDFT is used while at the final stages of optimization classical IDFT is used. Although the use of classical IDFT increases the complexity relatively but the PAPR reduction gain is also increased. Let α be the factor of utilization of Truncated IDFT algorithm and $\beta = 1-\alpha$ be the factor of utilization of classical IDFT inside 'Fourier Transform' block of Fig. 5.16 such that $0 \leq \alpha \leq 1$. Also let g be the ratio of Tone Reservation's 'Fourier Transform' block's complexity using classical IDFT only to that using the combination of Truncated and classical IDFT. Then g would be,

$$g = \frac{N.N_{itr}.log_2(N)}{2\alpha N.N_{itr} + \beta N.N_{itr}.log_2(N)} = \frac{log_2(N)}{2\alpha + (1-\alpha)log_2(N)}$$

The g versus α curve is plotted in Fig. 5.21 using above equation while keeping N constant. It demonstrates that complexity gain varies with factor of utilization of Truncated IDFT. For a specific case of $N = 64$, g varies between 1 and 3. Generalizing the range of g, for $N = 2^m$, it varies between 1 and $m/2$.

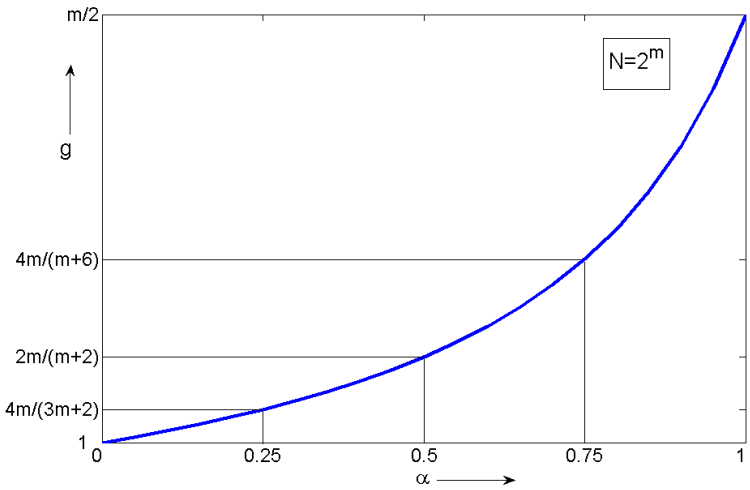

Figure 5.21: Variation of g with α for constant N.

This methodology was used with most of the iterations (75% of N_{itr} in our case, $\alpha = 0.75$) of minimization algorithm are performed with Truncated IDFT algorithm while rest (25% of N_{itr}, $\beta = 0.25$) are performed with classical IDFT function. The performance is degraded by a bit (0.3dB at 10^{-2}) as shown in Fig. 5.22 by the curve 'PAPR Reduced(Trunc & True)' when compared to classical IDFT performance but complexity is reduced to half as detailed below,

$$g = \frac{log_2(64)}{0.75 * 2 + 0.25log_2(64)} = 2.0$$

Thus there exists a compromise between complexity of Tone Reservation algorithm and its performance with the percentage utilization of Truncated IDFT algorithm. As α approaches to 1, the performance curve heads toward 'PAPR Reduced(trunc) curve. Contrary as α approaches to 0, performance of PAPR reduction matches 'PAPR Reduced(true)' curve.

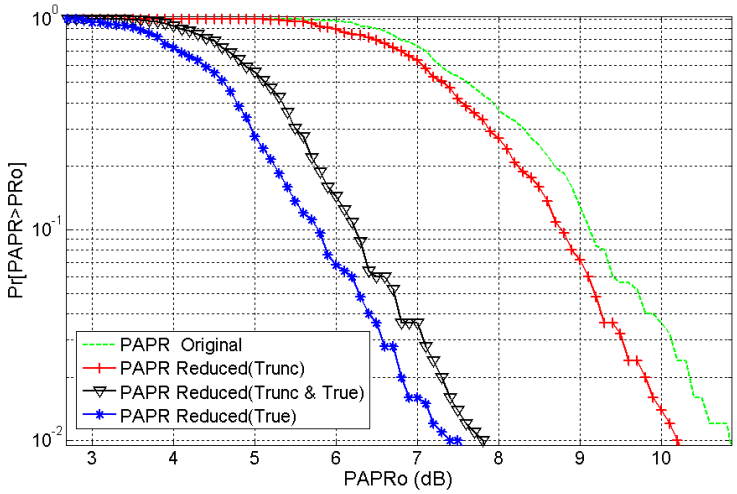

Figure 5.22: PAPR reduction using Tone Reservation with a mix of true and Truncated IDFT algorithm.

One can feel that with the help of frequency domain PAPR interpretation the complexity of PAPR reduction algorithms can also be reduced as it avoids the time domain-frequency domain exchanges to calculate PAPR and adjust PRCs values accordingly. Thus with the frequency domain PAPR vision, PAPR could be calculated and adjusted in the frequency domain and thus would reduce the overall algorithm complexity.

5.7 Conclusion

TR is one of the PAPR reduction techniques for multi carrier signals. There are different schemes to implement this TR methodology like TR-Geometric, TR-Gradient and TR-SOCP methods. These TR schemes were discussed in detail here and compared in terms of PAPR reduction performance and computational complexities for OFDM signal first. Then all the three TR schemes were implemented on bi-standard SWR signal and the results were compared. It was shown that there exists a compromise between complexity and PAPR reduction performance as the most PAPR reduction efficient scheme happened to be the most complex and vice versa i-e TR-SOCP which was highly efficient PAPR reduction technique but highly computationally complex at the same time. TR methods comparison for multi-channel GSM standard showed that sub-optimal methods (TR-Geometric and TR-Gradient) do not decrease PAPR. Finally the complexity of TR methods was reduced. High computational complexity of TR-SOCP is due to its enormous use of IDFT to optimize the added tones. Its complexity was reduced by using Truncated IDFT algorithm whose complexity is linear in N compared to typical $O(N\log_2(N))$ IDFT complexity. Truncated IDFT algorithm was used along with classical IDFT to reduce PAPR with half the complexity of known methodology at the cost of small PAPR reduction performance loss.

Chapter 6

PAPR metric based spectrum access in Cognitive Radio context

Contents

6.1 Introduction

PAPR analysis of SWR signal revealed that it faces the same non linearities problems as an OFDM signal. Also, a SWR system is reconfigurable with the signal processing being performed in the digital domain. When an SWR system is given 'intelligence', it becomes a Cognitive Radio (CR). In fact SWR is an enabling technology for CR systems. Thus CR signals are virtually SWR signals and inherit the high PAPR problem. Now one of the many 'intelligent' features of CR is spectrum sensing and access meaning that it detects the free bandwidth and uses that for communications in an optimized manner. Spectrum access should respect certain rules, for example, the Quality of Service (QoS) of the primary (licensed) users should not be affected on spectrum access. In this chapter we introduce an other parameter (PAPR) which should be kept in mind on free spectrum utilization in order to maintain a good QoS. Also the basic concepts of spectrum access are presented and its consequences on the PAPR of CR signal are discussed. Based on the

frequency vision of PAPR presented in Chapter 3, a new PAPR upper bound is developed to better estimate the variations in PAPR based on the spectral knowledge of secondary (unlicensed) user's data. Finally, a joint spectrum access scheme is presented which along with secondary data transmission, makes use of spectrum access to reduce CR signal PAPR.

6.2 CR signal and its PAPR

CR uses SWR as its implementation technology. In SWR based-systems, PAPR may be quite large due to the fact that the transmitted signal is a sum of a large number of modulated carriers as discussed earlier. Moreover, a reconfigurable transmitter, Software Defined Radio (SDR) base station for instance, should be able to amplify single carrier and multi carrier modulation signals as well as many non-constant envelope modulation signals. Thus CR signals inherit high PAPR and this factor asks for PAPR information based spectrum access decisions. This reason emphasizes the necessity of a frequency domain PAPR approach in a spectrum access scenario.

It could be concluded that the CR signal is like SWR signal,

$$x(t) = \sum_{i=1}^{S} \sum_{p=1}^{P_i} (fem_i(t) * m_{i,p}(c(t)) e^{2i\pi f_{i,p} t}. \tag{6.1}$$

where $m_{i,p}(c(t))$ represents the modulation relative to the carrier p and standard i and $fem_i(t)$ is the shaping filter function of standard i.

When spectrum is accessed by non-licensed (secondary) users, the signal equation changes to,

$$x(t) = \sum_{i=1}^{S} \sum_{p=1}^{P_i} (fem_i(t) * m_{i,p}(c(t)) e^{2i\pi f_{i,p} t} + \sum_{u=1}^{U} (fem(t) * m_u(c(t)) e^{2i\pi f_u t} \tag{6.2}$$

where U are the total number of secondary user carriers.

Being a multi-carrier signal, CR signal might pose the same PA non linearities problems as SWR because of its probability distribution function which follows Gaussian law.

6.3 Spectrum access and PAPR problem

In a CR context spectrum access is about finding the free bandwidth within a standard or in between the standards for communication using an opportunistic approach as shown in Fig. 6.1. There are certain parameters which should be kept in mind during spectrum access for example Quality of Service (QoS), out of band interference etc. Our emphasis in this report is on the influence of spectrum access on PA efficiency.

PA characteristics are already discuss in Chapter 1. PA efficiency curve is shown in Fig. 6.2 following the context of the discussion here. Generally it is preferred to operate PA in the maximum efficiency region near saturation point. But for that signal fluctuations should be kept as small as possible otherwise non-linearities would occur because of PA operation in saturation region. Now spectrum access would definitely modify

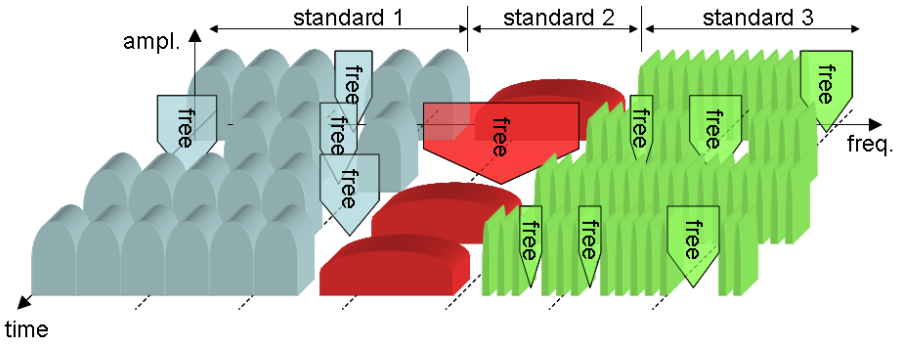

Figure 6.1: Spectrum access in a multi-standard system scenario.

signal properties namely mean power, bandwidth, amplitude etc. As the signal fluctuations are modified on spectrum access, the operating point of PA needs to be modified also so as to avoid non-linearities. Consider that the signal fluctuations increase on spectrum access which is generally the case after signal addition to useful band, one solution can be large Input Back Off (IBO) labeled as 'Solution 1: Large IBO' in Fig. 6.2. This large IBO results in the PA operation in less efficient zone which is obviously not recommended. Also, one needs to add some electronic components for run-time operating point modifications according to signal fluctuations. This hardware implementation not only comes at the cost of more energy consumption but also it is difficult to realize on the transmitter circuitry.

The solution which we propose in here, labeled as 'Solution 2: Insertion with PAPR constraint' in Fig. 6.2, is to insert the added tones respecting the signal fluctuation constraints. If the added signal does not increase signal fluctuations, high efficiency PA operation is easily possible. Thus a frequency view of PAPR is highly essential to see the effect of the added signal on PAPR and to decide whether to insert the signal on some available band or not and if yes then what should be the characteristics of the added signal like amplitude or constellation size, bandwidth and position of the added carriers.

6.4 Benefits of Carrier per Carrier Vision for CR Spectrum Access

Let us now explain the advantages of using carrier per carrier view for PAPR computation over a temporal PAPR calculation approach in a CR spectrum access scenario.

As mentioned previously that spectrum access influences the transmitted signal properties and subsequently its PAPR. PAPR of the signal to be amplified i-e signal between f_{min} and f_{max} in Fig.6.3 might be increased after spectrum access where W is the available free bandwidth and B is the allocated bandwidth during spectrum access. This increase in PAPR can cause signal distortion. Therefore, in order to see the effects on PAPR due to the allocated bandwidth, a classical temporal vision would need constant exchanges between frequency domain (for bandwidth allocation) and time domain (for PAPR computation) in order to select a bandwidth which does not increase PAPR of the signal to be amplified after spectrum access. This implies a tremendous increase in computational complexity. In the proposed carrier per carrier view, only N_s FFTs need to be performed at the start of allocation process to get the SWR signal spectrum. Temporal PAPR is sim-

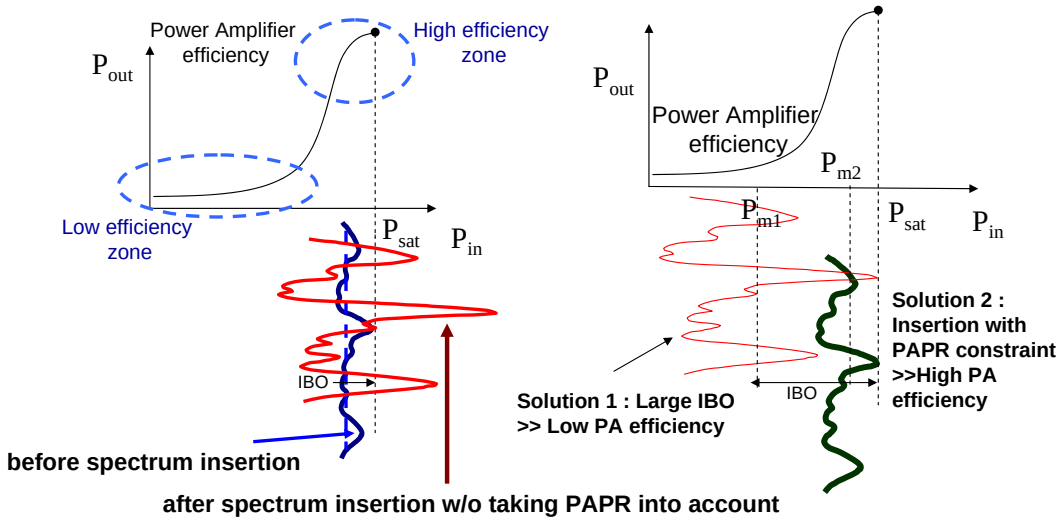

Figure 6.2: Spectrum access effect on PAPR and in turns on PA efficiency.

ply calculated then with the help of these spectral values. Now the effects on PAPR due to any available band allocation can be seen in the frequency domain without going back to time domain for PAPR calculations. Moreover, this spectrum knowledge can be used by other CR sensors like [121] uses power spectral density of the signal for blind standard recognition. As Fig.6.3 explains that this approach facilitates bandwidth allocation with respect to PAPR metric in CR context. A two standard SWR signal is depicted with an available bandwidth W. After slicing of the temporal signal and FFT operation, a table is filled with signal's spectral components. Then a suitable bandwidth B is allocated by the CR system while $PAPR_{temp}$ computations are performed staying in the frequency domain during bandwidth selection procedure. Also a knowledge of each carrier's PAPR can also be obtained by carrier per carrier PAPR vision. Moreover, when properly synchronized, it is very easy to calculate PAPR because in that case it is nothing else but mono-carrier PAPR calculations.

This frequency vision also helps in PAPR mitigation. PAPR reduction by signal adding method [10] and 'Tone Reservation' [9] are about adding/reserving tones in frequency domain to reduce PAPR for OFDM signals. This process is same as bandwidth allocation. Knowing the fact that OFDM and SWR signals show similar characteristics and carrier per carrier vision facilitates bandwidth allocation, OFDM PAPR mitigation methods can easily be applied to SWR signals.

6.5 PAPR variations due to spectrum access

Now we shall see the effects on PAPR due to spectrum access. A bi-standard SWR system containing Standard A and Standard B is considered here. This study will be done in two steps. Firstly, PAPR variations shall be noted when the primary users' data values is kept constant while secondary data is changed with time. Secondly, a more practical scenario shall be considered where both the primary and secondary data are randomly generated.

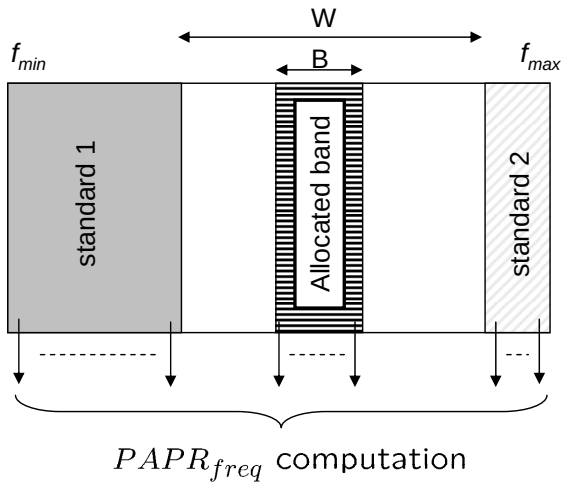

Figure 6.3: Illustration of PAPR computation with a two standards SWR signal and an allocated bandwidth B.

6.5.1 PAPR variations due to spectrum access keeping primary data fixed

The purpose of this case study is just to see whether PAPR is in effect varied on spectrum access by keeping the primary data same and randomly generating the secondary data. Secondary data is composed of 16-QAM modulated OFDM symbols occupying the 'free' bandwidth between Standard A and Standard B. As primary data is fixed and it has a single PAPR value during our experiment time window so we can not see the variation in PAPR by plotting the CCDF.

Therefore, we have plotted instantaneous PAPR values after spectrum access. It could be noted that PAPR before DSA is fixed so its mean and instantaneous value is the same. This PAPR value is varied on spectrum access in a random fashion. At times it decreases but most of the times it increases as shown in Fig. 6.4.

6.5.2 PAPR variations due to spectrum access with variable primary data

After observing that PAPR is actually varied on spectrum access, although in a random fashion, we now study the practical scenario where both primary and secondary data are varied in time. Fig. 6.5 shows the CCDF before and after DSA.

To see the same situation in a different way, we have plotted the instantaneous PAPR values in Fig. 6.6. Again we can see the at times PAPR increases and at times decreases after DSA. PAPR is varied randomly after spectrum access but we can conclude with assurance on two points:

1. Mean PAPR increases after DSA.

2. Instantaneous PAPR increases on several occasions after DSA.

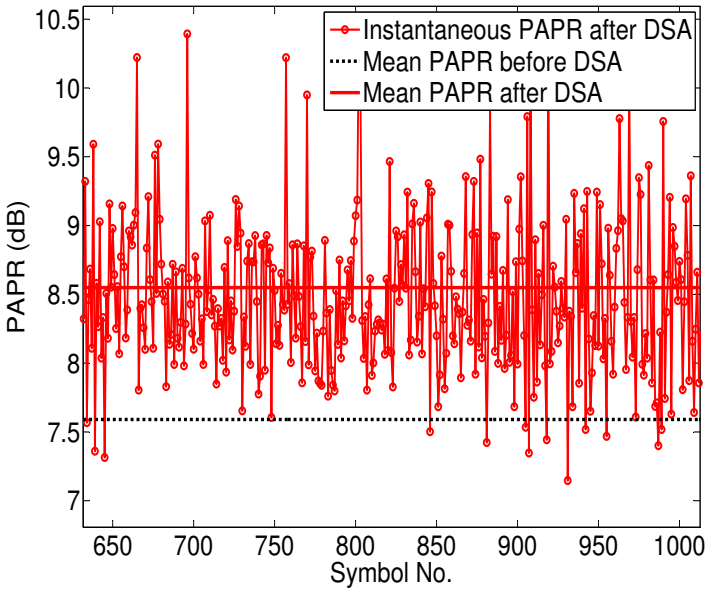

Figure 6.4: Instantaneous PAPR values before and after spectrum access with primary data fixed.

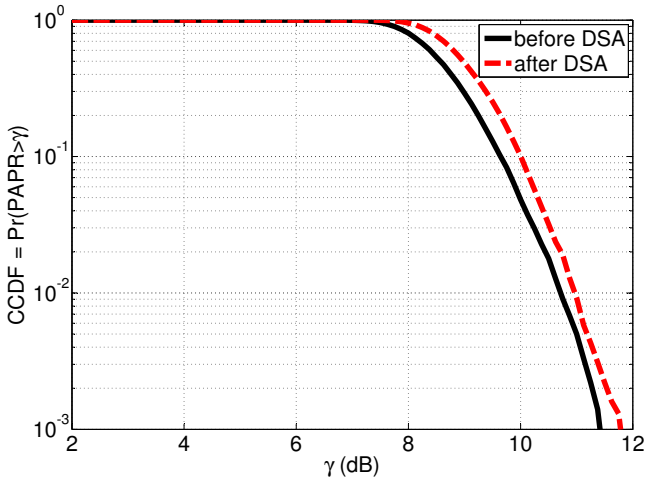

Figure 6.5: CCDF before and after spectrum access with random primary data.

Therefore, irrespective of the fact whether PAPR increases or decreases for a specific CR symbol, PAPR reduction must be performed to keep the peak power under control and avoid PA non-linearity.

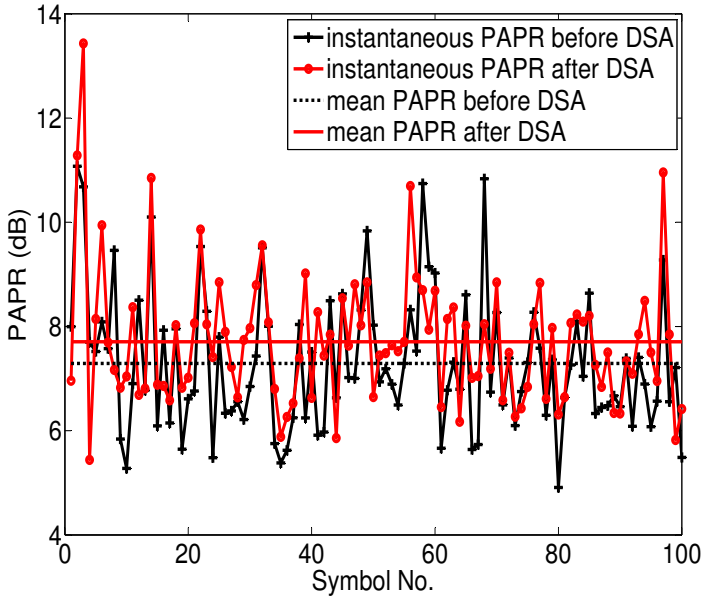

Figure 6.6: Instantaneous PAPR values before and after spectrum access with random primary data.

Now we shall present an upper bound on PARP after spectrum access and finally we shall deal with PAPR reduction by proposing a new DSA strategy.

6.6 PAPR variations on spectrum access: proposed mathematical developments

An initial study on the PAPR variation due to spectrum access is carried out and mathematically formulated. Let $PAPR_{new}$ be the PAPR after spectrum access. It can be upper bounded by the sum of initial PAPR of the primary users' signal before spectrum access $PAPR_p$ given by Eq.3.32 and the influence of the secondary users' signal on PAPR, to be given after mathematical developments.

Consider the case of a CR signal, where different standards occupy their specific bandwidths while the free bandwidth is used by the secondary users. Transforming the temporal CR signal into the frequency domain following the carrier per carrier vision presented above. Let the signal be divided in to N_S symbols and N be frequencies of the whole spectrum. Out of these N frequencies, N_p are the primary user frequencies and $N_s = N - N_p$ be the frequencies that are used by secondary users. Here the hypothesis is made that the spectrum occupied by secondary users is very small compared to primary users' spectral occupancy i-e $N_s << N_p$ and also $P_m(p) + P_m(s) \approx P_m(p)$ due to the fact that the

secondary signal mean power $P_m(s)$ is negligible compared to primary user mean power $P_m(p)$.

Now recalling from Eq. 3.18 that a signal sample $s_{j,k}$ can be written as,

$$s_{j,k} = \sum_{c=0}^{N-1} C_{j,c} e^{i2\pi kc/N}, \tag{6.3}$$

where $j \in [1, N_S]$, $k \in [0, N-1]$. Also $c \in [0, N-1]$ is the number of carriers, i-e size of c is the sum of N_p and N_s. Now following the above equation

$$|s_{j,k}|^2 = |\sum_{c=0}^{N-1} C_{j,c} e^{i2\pi kc/N}|^2. \tag{6.4}$$

Dividing the carriers in to primary and secondary user carriers,

$$|s_{j,k}|^2 = |\sum_{p\in P} C_{j,p} e^{i2\pi kp/N} + \sum_{s\in S} C_{j,s} e^{i2\pi ks/N}|^2. \tag{6.5}$$

Here P and S are the index sets of primary and secondary user frequencies respectively. Now following the inequality which stats; for complex vectors a and b,

$$|a+b| \leq |a| + |b|,$$

and consequently

$$(|a+b|)^2 \leq (|a| + |b|)^2. \tag{6.6}$$

Thus Eq. 6.5 becomes,

$$|s_{j,k}|^2 \leq (|\sum_{p\in P} C_{j,p} e^{i2\pi kp/N}| + |\sum_{s\in S} C_{j,s} e^{i2\pi ks/N}|)^2, \tag{6.7}$$

and

$$|s_{j,k}|^2 \leq |\sum_{p\in P} C_{j,p} e^{i2\pi kp/N}|^2 + |\sum_{s\in S} C_{j,s} e^{i2\pi ks/N}|^2 + 2|\sum_{p\in P} C_{j,p} e^{i2\pi kp/N}||\sum_{s\in S} C_{j,s} e^{i2\pi ks/N}|. \tag{6.8}$$

Let

$$\zeta_{j,k} = |\sum_{p\in P} C_{j,p} e^{i2\pi kp/N}|^2 + |\sum_{s\in S} C_{j,s} e^{i2\pi ks/N}|^2 + 2|\sum_{p\in P} C_{j,p} e^{i2\pi kp/N}||\sum_{s\in S} C_{j,s} e^{i2\pi ks/N}|. \tag{6.9}$$

Now following Eq. 3.29,

$$PAPR_{N_s}(S(n)) \leq \frac{\max_{k\in K}(\max_{j\in J}(\zeta_{j,k}))}{\sum_{k=1}^{N} P_m(k)}. \tag{6.10}$$

And thus the above equation can be written as,

$$PAPR_{N_s}(S(n)) \leq PAPR_p + \delta. \tag{6.11}$$

Here $PAPR_p$ is the PAPR contribution because of primary user's carriers i-e,

$$PAPR_p \approx \frac{\max_{k\in K}(\max_{j\in J}(|\sum_{p\in P} C_{j,p}e^{i2\pi kp/N}|^2))}{\sum_{k=1}^{N} P_m(k)}. \tag{6.12}$$

And δ is the amount of variation in the initial PAPR, $PAPR_p$, because of dynamic spectrum access. The factor δ can be written as,

$$\delta = \delta_s + \delta_m, \tag{6.13}$$

where

$$\begin{aligned}\delta_s &\approx \frac{\max_{k\in K}(\max_{j\in J}(|\sum_{s\in S} C_{j,s}e^{i2\pi ks/N}|^2))}{\sum_{k=1}^{N} P_m(k)} \\ &= \frac{\sum_{s\in S} P_m(s)}{\sum_{p\in P} P_m(p)}.PAPR_s.\end{aligned} \tag{6.14}$$

In Eq. 6.14, the factor $\frac{\sum_{s\in S} P_m(s)}{\sum_{p\in P} P_m(p)}$ is the ratio of secondary user's mean power to the primary user's mean power which is quite small and that's why the factor δ_s does not contribute much to the PAPR variations. Also $PAPR_s$ is the secondary user PAPR in frequency domain, i-e,

$$PAPR_s = \frac{\max_{k\in K}(\max_{j\in J}(|\sum_{s\in S} C_{j,s}e^{i2\pi ks/N}|^2))}{\sum_{s\in S} P_m(s)}. \tag{6.15}$$

And

$$\begin{aligned}\delta_m \approx \frac{1}{\sum_{k=1}^{N} P_m(k)}[&\max_{k\in K}(\max_{j\in J}(2|\sum_{p\in P} C_{j,p}e^{i2\pi kp/N}| \\ &.|\sum_{s\in S} C_{j,s}e^{i2\pi ks/N}|))].\end{aligned} \tag{6.16}$$

Here δ_m is the contribution because of the mutual correlation of the primary and secondary user carriers. It should be noted that the influence on PAPR due to spectrum access can be calculated with the help of spectral information of the primary and secondary signal. This vision facilitates the spectrum access phenomenon in the context of CR by directly relating the effect on PAPR with the spectral information of signal.

This formulation is applied on aforementioned bi-standard SWR signal. QPSK modulated 10 carriers are added on free bands in between these two standards and their effect on PAPR is demonstrated in Fig. 6.7.

6.7 Joint spectrum access methodology to reduce PAPR

In this section we shall present a novel spectrum access methodology which not only permits to transmit secondary data but also keeps the CR signal PAPR under control. The basic ideology is shown in Fig. 6.8. Generally spectrum is accessed dynamically using opportunistic approach for non-licensed users' data transmission. We reserve here, a very small percentage of that accessed spectrum for PAPR reduction of the overall CR signal.

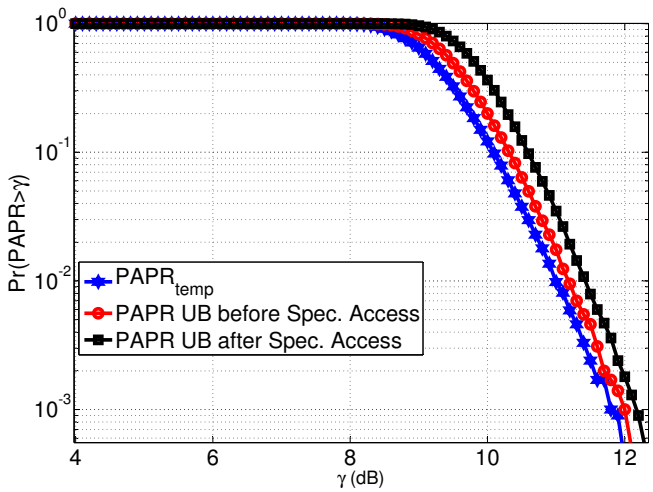

Figure 6.7: PAPR Upper bound is modified after spectrum access.

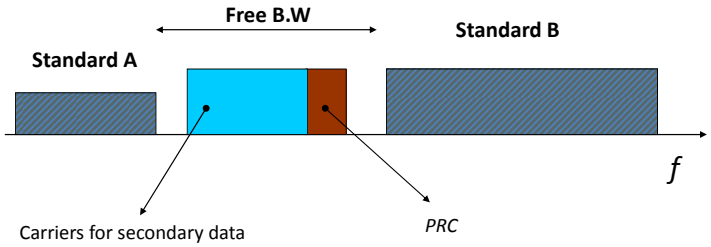

Figure 6.8: Joint spectrum access methodology for PAPR reduction.

For a bi-standard SWR system whose inter-standard band is accessed dynamically, we transmit secondary data on a considerably high percentage of accessed band. The rest of the band is used to generate *PRC*'s. Fig. 6.9 shows that original PAPR was varied on spectrum access but it was reduced using TR-SOCP. In our case we use 90% of the free spectrum for secondary data transmission while the rest of 10% is used for PAPR reduction.

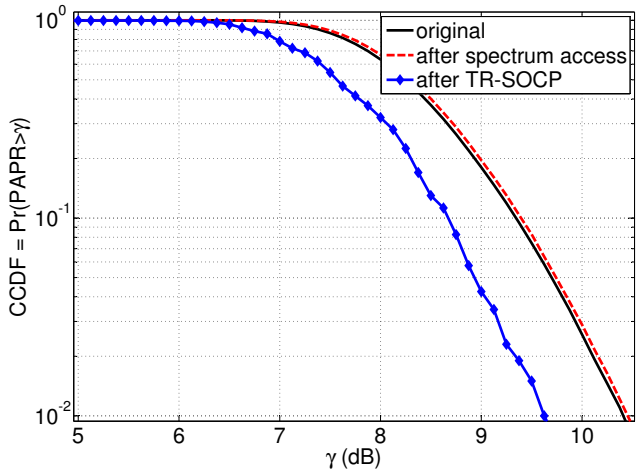

Figure 6.9: PAPR reduction using joint spectrum access methodology.

6.8 Conclusion

This chapter explored the PAPR issues in SWR based CR systems in the spectrum access scenario. High PAPR being a major problem in multi carrier communications and CR signal being a multi carrier signal suffers the same problem. Spectrum access in the CR context is about using the free spectrum under certain constraints like QoS maintenance of the primary users. Another constraint for spectrum access was discussed in this chapter which is PAPR as high PAPR affects transmitter specifications. The effects of spectrum access on PAPR were discussed in detail which show that PAPR is varied randomly on spectrum access resulting in the increase in mean PAPR value. An upper bound was given for PAPR after spectrum access which is based on the spectral knowledge of primary and secondary users. Thus this upper bound associated PAPR with spectrum. This spectral knowledge based PAPR upper bound helped in spectrum access by providing PAPR information about available bandwidths. The process of spectrum access under PAPR metric constraint was facilitated with this frequency vision of the signal as PAPR reduction methods like TR can be applied to CR signals. Consequently, a joint spectrum access scheme was presented according to which spectrum is accessed to transmit secondary data as well as some special carriers (*PRC*s). The use of *PRC*s helped reduce the global PAPR of CR signal and therefore keeps the spectrum access under PAPR constraints.

General Conclusion and Perspectives

This thesis presents a part of research work done in SCEE team at Supélec, Rennes campus on the analysis and reduction of PAPR in the context of SWR and Cognitive Radio signals.

General conclusions

Starting with the basic concepts of multi carrier transmission and its PAPR analysis, the details were extending to multi standard systems and its PAPR analysis and reduction. In **Chapter 1** a global picture of the thesis was presented. Initially the basic principles of OFDM were highlighted and it was found that with the evolution of technology, the study is not limited to multi-carrier signals but is extended to multiplex of standard systems called SWR. Further the integration of 'brain' in SWR has opened a new research domain known as Cognitive Radio. On one side where these systems try to fulfill the need of high data rate with reliable transmission under 'universal' terminal notion, they pose many implementation problems on the other side. One of these problems is due to the non linear amplifier characteristics which come into play because of the large power fluctuations i-e high PAPR of these signals.

At the very first step these power fluctuations were analyzed statistically for one of the basic multi carrier modulation schemes (OFDM) in **Chapter 2**. PAPR being a random variable is generally measured by its distribution function (CCDF) as the deterministic PAPR study does not lead to realistic PAPR measurements. Starting from an already existing theoretical based CCDF expression for continuous OFDM signals, a new CCDF expression was developed for a continuous OFDM signal which matches the already developed simulation based CCDF expression. Thus the correctness of simulation based expression is verified theoretically. This CCDF expression can be helpful in estimating the PAPR distribution of continuous signals whether OFDM or SWR.

Following on, in **Chapter 3** PAPR analysis was extended to SWR signals. SWR signal is a multi standard, multi modulation signal and thus a multi carrier signal like OFDM. Analytical and Gaussian equivalence was proved between OFDM and SWR signals. Then the PAPR analysis was performed for mono standard and multi standard SWR signals. The CCDF plots show that OFDM and SWR signal share the same PAPR distribution. A new frequency domain PAPR definition was provided to align the SWR spectrum concept with that of PAPR. This definition associates spectral information with PAPR. This new PAPR formulation along with OFDM-SWR analogies is an important result as it meant that some of the OFDM PAPR reduction methods could be applied to SWR signal to reduce its PAPR.

After discussing that SWR systems suffer from same high PAPR problem as OFDM, now it was time to reduce SWR signal PAPR which is performed in **Chapter 4**. Out of several OFDM PAPR reduction methods, TR was selected which is about reserving certain tones to reduce original signal peak. The main advantages of this method are downward compatibility when the peak reducing carriers are transmitted over unused carriers of the standards, no BER degradation, no SI transmission etc. A convex optimization technique called SOCP is used to optimize the reserved tones which when added to original tones results in the reduced peak signal. Working step wise, initially the influence of peak reducing carriers parameters on PAPR reduction in mono-band OFDM was discussed. These parameters include bandwidth, position and power of reserved carriers. Then the study was extended to multi-band OFDM and finally to bi-standard SWR signal. Multi-channel GSM case was also studied and peak reducing carriers were transmitted over unused GSM channels in a GSM base station to reduce its PAPR under mask and C/I constraints. For a bi-standard SWR system, out of band free carriers were used along with standard's unused carriers. The affect of the out of band parameters like power, position and bandwidth on PAPR reduction performance was also discussed here. It was demonstrated that the application of TR-SOCP method does neither degrade BER nor creates out of band interference and the power spectral masks of each standard is respected under constrained optimization of reserved carriers.

In **Chapter 5** TR-SOCP was compared with some other TR implementation schemes like TR-Gradient and TR-Geometric. The idea was to look for a PAPR reduction performance and complexity trade-off. Initially the three schemes were compared for WLAN standard and then for multi-channel GSM and a bi-standard SWR system under similar simulation parameters and constraints for all the three methods. It was found out that TR-SOCP is the most efficient PAPR reduction scheme among the three but most computationally exhaustive at the same time. Thus in order to reduce its complexity a Truncated IDFT algorithm was used which calculates the peak of IFFT output with much reduced complexity ($O(N)$) than that of classical IFFT algorithm $O(N \log_2(N))$.

Finally in **Chapter 6** the discussion was extended to Cognitive Radio systems in the spectrum access scenario. The problem of non linearity becomes even grave in Cognitive Radio systems when spectrum is dynamically accessed without taking care of PAPR constraints. The non linearity issues in SWR based Cognitive Radio systems was explored in the spectrum access scenario by exploiting the frequency vision of PAPR. The importance of this issue can be estimated by a simple fact that reduced PAPR would result in higher PA efficiency and in turns reduced energy consumption which is closely related to 'Green communication' concept [122]. Also the problem is addressed at the receiver end on Low Noise Amplifier (LNA) [123]. With the help of frequency PAPR vision, a new upper bound was developed to formulate PAPR variations on spectrum access. This spectral vision not only reduces the complexity of certain PAPR reduction methods but also aligns the concept of spectrum access with PAPR constraint and thus helps in spectrum access under PAPR bounds. Finally, a joint spectrum access methodology was presented which not only lets the secondary user transmit its information but also keep the PAPR under control.

Research Contributions

The main research contributions of this thesis are briefly highlighted in this section.

- **Continuous OFDM signal's PAPR distribution function [25]:** With the help of two already given PAPR distribution functions for continuous OFDM signal, a new distribution function is developed which agrees with the previous work and can be considered quite handy for the estimation of continuous signals whether OFDM or SWR.
- **SWR signal's PAPR behavior [26] & Frequency Domain PAPR vision[27]:** Analogies are drawn between SWR and OFDM signal. SWR signal's PAPR is demonstrated to have Gaussian distribution which means SWR signal inherits high PAPR. With a help of a new frequency domain PAPR vision it is concluded that some of the OFDM PAPR reduction methods could be applied to reduce SWR signal's PAPR as well.
- **SWR signal's PAPR reduction [29]:** Considering different cases of SWR signal, its PAPR is reduced. Tested SWR signal cases include i) a bi-standard signal which is composed of two OFDM based hypothetical standards and ii) a multi-channel GSM standard. SWR signal PAPR is reduced with the help of an OFDM PAPR reduction method called 'Tone Reservation' which is about reserving a set of sub-carriers for peak reduction. The influence on PAPR reduction performance due to the different parameters related to these reserved carriers are discussed in detail.
- **Comparison of different PAPR reduction schemes [30] & their complexity reduction algorithm [31]:** There are different schemes to implement Tone Reservation. Few of them are discussed and compared in terms of PAPR reduction performance and computational complexity for SWR signals. It turns out that most efficient PAPR reduction scheme happens to be most computationally complex. A truncated IDFT algorithm is used to reduce this complexity.
- **Formulation of PAPR variations due to Dynamic Spectrum Access [32, 27] & PAPR reduction in the Cognitive Radio context:** Finally the effects on PAPR due to dynamic spectrum access are observed and formulated in Cognitive Radio systems with the help of already developed Frequency Domain vision. It is noted that spectrum access must be performed under PAPR metric constraints to avoid PA non-linearity. Thus a joint spectrum access scheme is presented which uses the free spectrum for secondary data transmission and peak reducing carriers to keep the PAPR under specific limits.

Future perspectives

Some of the thesis perspectives could be,

- The relationship between PAPR reduction gain (in turns PA OBO decrement) and PA efficiency gain for SWR systems can be formulated. This would mean the development of a formula which provides terminal's power consumption for different values of PAPR reduction gains.

- It would be interesting to see the effect on PAPR reduction performance when *PRC* are placed inside the useful band as suggested in DVB-T2 specifications. A post-doc at SCEE team is currently investigating the very topic.
- For MC-GSM scenario, more PAPR reduction efficient and less complex algorithms might be explored along with the complete link budget when all the neighboring cells use TR for PAPR reduction.
- PAPR reduction performance of TR methods should be explored in the CR context when *PRC* are dynamically allocated depending upon the channel conditions and bandwidth availability.
- Truncated IFFT algorithm branch selection criterion should be improved and a statistical analysis for error probability should be provided.
- SOCP implementation using frequency domain PAPR interpretation instead of classical time domain PAPR definition might be studied.
- Like PAPR frequency vision in the CR context, ACPR might be defined in same context to establish a relationship between out of band channel interference and bandwidth occupation.
- PAPR frequency vision might help in investigation the filtering effects on signal PAPR. A master internship was carried out on the same subject at SCEE team.
- A study can be done on the effects of frequency selective channel on frequency domain PAPR view due to DSA.
- The PAPR reduction study could be performed for SWR signals from practical standards like LTE/LTE-A, WLAN and WiMAX standards etc.

In short, this thesis can be considered as one of the very initial studies on PA nonlinear distortions in the context of SWR and CR systems. Still there are certain dimensions which should be explored in future.

Appendix

Appendix A

PAPR reduction methods for OFDM signal

Some of the OFDM signal PAPR reduction techniques shall be discussed here and finally a classification of these techniques shall be presented.

A.1 Clipping and Filtering

The simplest method to reduce PAPR is to clip the multi carrier signal deliberately [80]. This reduces the PAPR to the desired level which is set by the help of predetermined clipping threshold. Let A be the threshold value for a signal x, then the clipped version $\widetilde{x}$ would be,

$$\widetilde{x} = \begin{cases} x & \text{if} \quad |x| \leq A \\ Ae^{j\phi(x)} & \text{if} \quad |x| > A \end{cases}, \tag{A.1}$$

Here $\phi(x)$ is the phase of x. The process of clipping being non linear in nature, leads to in-band and out-of-band distortions. In-band distortions degrade BER while out-of-band distortions reduce spectral efficiency.

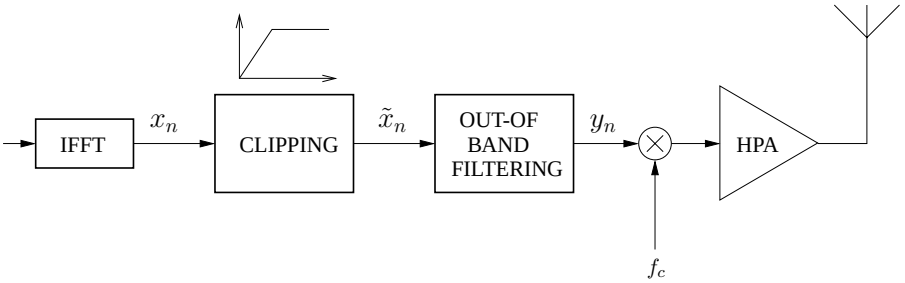

Figure A.1: Process of clipping and filtering to reduce PAPR.

Filtering is performed after clipping [6, 81] to reduce the out-of band radiations as shown in Fig. A.1 where signal $\mathbf{x}$ is clipping according to Eq. A.1 to get the clipped

signal $\widetilde{\mathbf{x}}$. This clipped signal is then filtered to nullify out-of-band radiations. Noting that filtering can not reduce in-band interference. The process of clipping and filtering results in peak regrowths which is tackled with repeated clipping and filtering [6, 81].

A.2 Selective Mapping (SLM)

In SLM, one favorable signal (with lowest PAPR) is selected from a set of signals in which each signal basically represents the same information [82, 83]. A block diagram of the SLM technique is shown in Fig. A.2. As it could be seen that each data block is multiplied by U different phase sequences where each of these phase sequences has length N, the data block size. After the multiplication we have U modified data blocks, X^u where $u = 1, 2, 3, ..., U$. Applying IFFT to all the U blocks we get U different signals x^u with $u = 1, 2, 3, ..., U$. The signal with least PAPR is selected among these signals.

Side information (SI) about the selected phase sequence needs to be transmitted for the receiver to properly extract the original information. Also the reverse operation is performed at the receiver. Although no interference is generated, the transmission of SI and receiver modifications are the flaws associated to this method.

The PAPR reduction techniques called Interleaving [84, 85, 86] is almost the same as SLM where a set of interleavers is used instead of set of phase sequence multipliers.

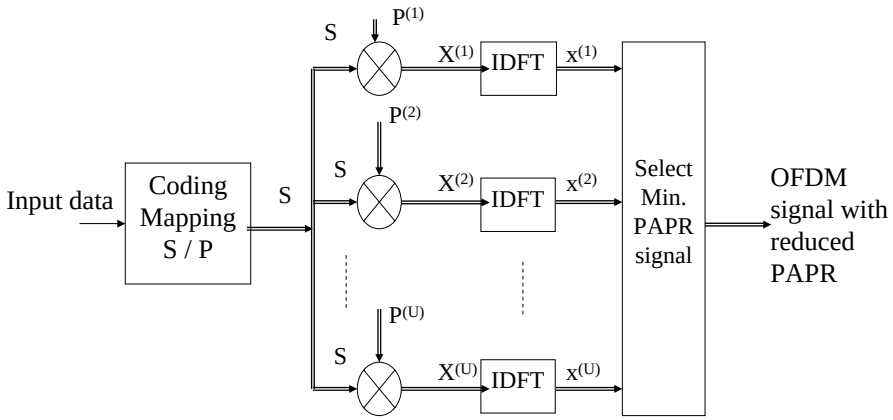

Figure A.2: Block diagram for SLM technique.

A.3 Partial Transmit Sequence

PTS method [7] consists of partitioning the incoming data vector S into a number of disjoint sub-blocks V. As shown in Fig. A.3, after IDFT, each of these sub-blocks is weighted by a phase factor P^j and optimized in such a way that the sum of these weighted blocks results in a signal with reduced PAPR.

Depending on the sub-block number V the optimized set of phase factors is searched at a high complexity cost. Like the SLM method presented before, implementation of a PTS method requires receiver modifications to recover the useful data. Further, the transmission of SI results in data rate loss.

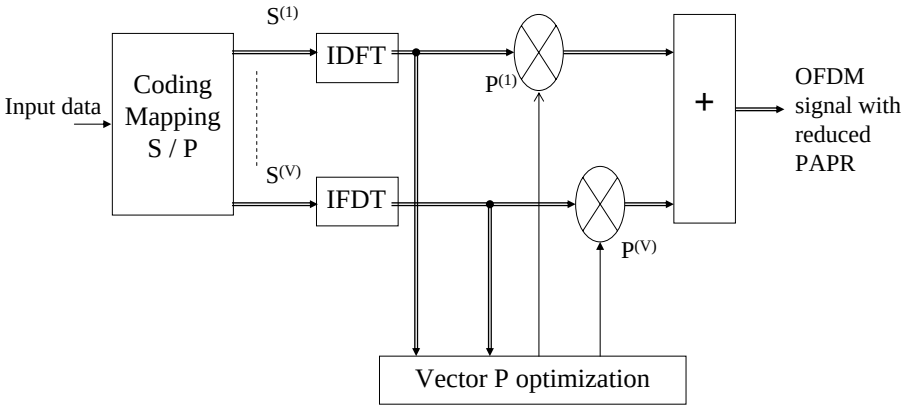

Figure A.3: Block diagram for PTS technique.

A.4 Tone Injection

The basic idea of TI is to increase the constellation size. In this way each of the points in the basic constellation can be mapped into several equivalent points in the expanded constellation [9]. As each constellation point can be mapped to a larger constellation scenario, the extra degree of freedom can be exploited for PAPR reduction. The method is called Tone Injection because substituting a point in the basic constellation for a new point in the larger constellation is equivalent to injecting a tone of the appropriate frequency and phase in the multi carrier signal. Mathematically speaking, let $x = \sum_{k=0}^{N-1} X_k e^{2\pi ikt}$ be a multi carrier signal with X_k being the values from original constellation with d being the minimal distance between the constellation points. Now the signal can be modified to,

$$\hat{x} = \sum_{k=0}^{N-1} (X_k + C_k) e^{2\pi ikt}. \tag{A.2}$$

Here $C_k = Dp_k + iDq_k$ and $p_k, q_k \in Z$. D is a positive real number known at the receiver. For an M-ary modulation scheme, the value of D should be at least $d\sqrt{M}$ in order not to increase BER [9]. Also $\hat{x}$ is the tone injected version of x. Making a simple choice by assigning p and q from a set $[0, \pm 1]$ would change a 16 QAM constellation to the one presented in Fig. A.4. Choosing non zero p_k, q_k coefficients would not create any ambiguity at the receiver since the coordinates of the detected constellation point can be reduced, modulo D. This means that the standard receiver needs to be modified to perform modulo-D operation after symbol decision.

There is another method called Active Constellation Extension (ACE) [87] which resembles TI. In this technique, some of the outer signal constellation points in the data block are dynamically extended toward the outside of the original constellation in order to reduce PAPR. Again the details of the method are not provided here.

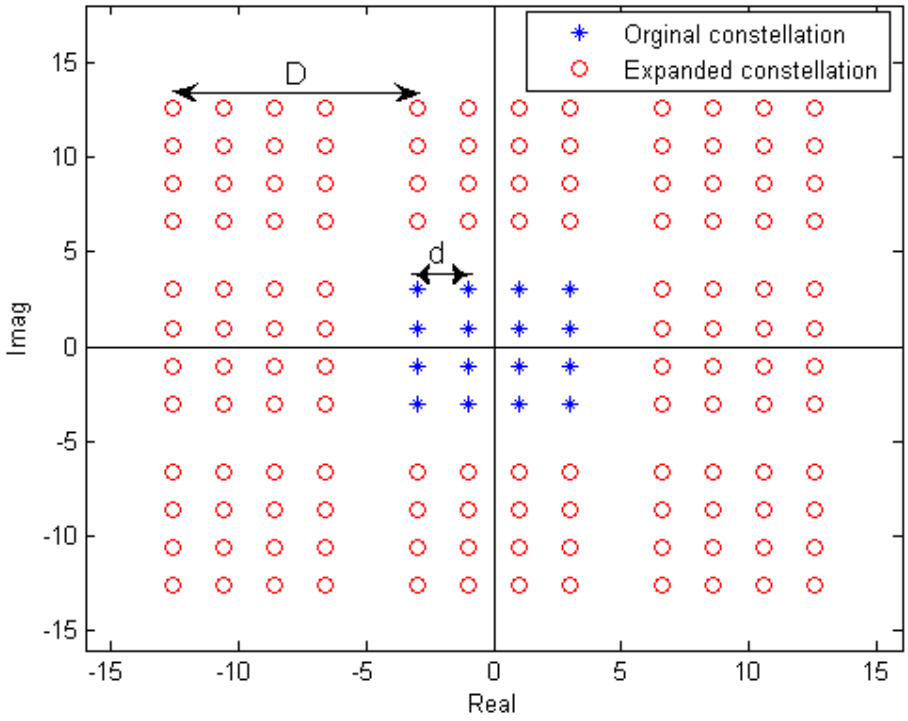

Figure A.4: Constellation for 16 QAM with TI.

A.5 Classification of PAPR reduction methods

We shall now present a classification of PAPR reduction methods which has been proposed in [5]. It mainly concerns OFDM PAPR reduction but some methods can be applied to any modulation scheme. The idea behind this classification is to gather the methods with similar characteristics into clusters and facilitate the selection of PAPR reduction method depending upon system requirements. There are different criteria to differentiate between existing PAPR reduction methods. Few of them are outlined below:

- Downward compatibility (DC): A method is called downward compatible if it does not imply any receiver change. When downward compatible, the PAPR reduction is implemented only at the transmitter meaning that the input data is manipulated to generate low PAPR. In that case BER needs to be investigated. Thus we have two subclasses when the method is downward compatible.
  - Cluster 1 : DC without BER degradation (e-g Active Constellation Extension)
  - Cluster 2 : DC with BER degradation (e-g Clipping, Peak windowing)
- If there is no DC, PAPR reduction method is implemented on both transmitter and receiver (the function and its 'inverse') and theoretically BER remains unchanged. In this case data rate loss has to be investigated.
  - Cluster 3 : no DC without date rate loss (e-g Pulse shaping, Tone Injection)

– Cluster 4 : no DC with date rate loss degradation (e-g Coding, Tone Reservation, Partial Transit Sequences)

These are the few examples given to illustrate the classification. The complete tree diagram of method classification is given in Fig. A.5. The classification presented also refers to linearization methods which do not take into account the PAPR reduction techniques.

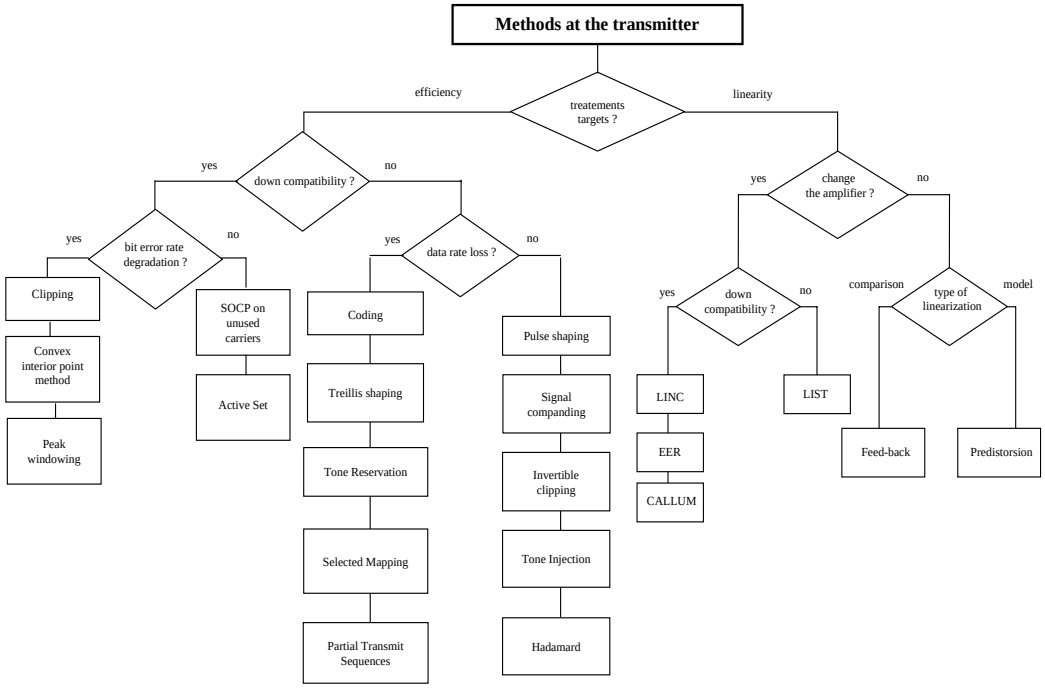

Figure A.5: classification of PAPR reduction methods.

Appendix B

TR-Geometric method

TR-Geometric method uses a geometric approach to calculate peak reducing signal. Here the details of this geometric method shall be discussed.

B.1 Principle of PAPR Reduction

Let us consider $x(t)$ be an OFDM baseband complex signal defined in Eq.(B.1).

$$x(t) = \frac{1}{\sqrt{N}} \sum_{k=0}^{N-1} X_k e^{j2\pi f_k t}, \quad 0 \leq t \leq T_s \ , \tag{B.1}$$

where N data symbols X_k form an OFDM symbol $\mathbf{X} = [X_0, \cdots, X_{N-1}]$, $f_k = \frac{k}{T_s}$, and T_s is the time duration of the OFDM symbol.

It can be expressed below as:

$$x(t) = I(t) + jQ(t), \tag{B.2}$$

where $I(t)$ is the inphase signal and $Q(t)$ the quadrature phase signal. According to Eq.(B.2), the complex envelope signal related to the OFDM signal $x(t)$ is given by:

$$r(t) = \sqrt{I^2(t) + Q^2(t)}. \tag{B.3}$$

Let us suppose that the artificial signal $a(t)$ in the continuous time-domain is written as

$$a(t) = I_a(t) + jQ_a(t). \tag{B.4}$$

The principle of the PAPR reduction is as follow:
Let A be the maximum permissible magnitude (magnitude threshold).

(i) If $r(t) \geq A$, the artificial signal $a(t)$ is generated so that

$$|x(t) + a(t)|^2 = A^2. \tag{B.5}$$

(ii) On the contrary, i.e. when $r(t) < A$, the artificial signal $a(t)$ is equal to zero.

Let us consider a time t such as: $r(t) \geq A$, we seek the parameters $I_a(t)$ and $Q_a(t)$ which validates Eq.(B.5).

Developing Eq.(B.5), we obtain:

$$[I(t) + I_a(t)]^2 + [Q(t) + Q_a(t)]^2 = A^2. \tag{B.6}$$

Note that Eq.(B.6) can be solved geometrically which is described in the next section.

B.2 Geometric approach based problem solution

Let us suppose that $r(t) \geq A$, where $0 \leq t \leq T_s$. Let (I/Q) be the plan defined as shown in Fig. B.1 by:

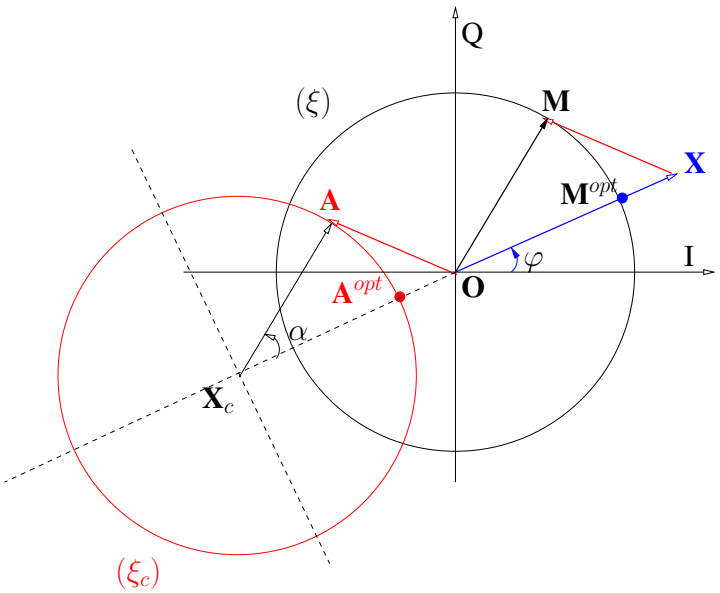

Figure B.1: Geometric approach based problem solution.

(i) (ξ), the circle of center **O** and radius A

(ii) $\overrightarrow{\mathbf{OX}}$ is associated with $Z_X = re^{j\varphi} = I + jQ$
$\overrightarrow{\mathbf{OM}}$ is associated with $Z_M = Ce^{j(\alpha+\varphi)}$
$\overrightarrow{\mathbf{OA}}$ is associated with $Z_A = I_a + jQ_a$

(iii) $\mathbf{X}_c$ is the **X** central symmetry compared to **O**.

(iv) (ξ_C), the circle of center $\mathbf{X}_c$ and radius A

(v) $\varphi = \left(\overrightarrow{\mathbf{OI}}, \overrightarrow{\mathbf{OX}} \right)$ and $\alpha = \left(\overrightarrow{\mathbf{OX}}, \overrightarrow{\mathbf{OM}} \right)$.

Solving Eq.(B.6) consists to find $\mathbf{A} \in (I/Q)$ such as

$$\begin{array}{c} \left|\overrightarrow{\mathbf{OX}} + \overrightarrow{\mathbf{OA}}\right|^2 = A^2 \\ \Updownarrow \\ (I + I_a)^2 + (Q + Q_a)^2 = A^2 \end{array} . \tag{B.7}$$

From Eq.(B.7), the points $\mathbf{A}$ of coordinates $\begin{bmatrix} I_a \\ Q_a \end{bmatrix}$ describe the circle (ξ_c). In the following, we will determine the analytical expressions of I_a and Q_a.

From the relation $\overrightarrow{\mathbf{OA}} = \overrightarrow{\mathbf{OM}} - \overrightarrow{\mathbf{OX}}$, we deduce that:

$$Z_A = Z_M - Z_X. \tag{B.8}$$

Let us note that :

$$Z_M = Ae^{j(\alpha+\varphi)} = \frac{A}{r}e^{j\alpha}Z_X. \tag{B.9}$$

Substituting Eq.(B.9) into Eq.(B.8), we obtain:

$$Z_A = \left\{\frac{A}{r}e^{j\alpha} - 1\right\} Z_X. \tag{B.10}$$

Referring to Eq.(B.10), there are an infinite number of solutions to the problem related to the choice of α. One constraint of our method is to provide the solution with the least additional power. It is obvious that $\alpha = 0$ is the solution which gives the least additional power. Indeed,

$$\forall \alpha \in [0, 2\pi[\,, \quad |Z_A| \;\geq \left|\frac{A}{r} - 1\right| |Z_X|\,.$$

So, the solution with the least additional power is expressed as

$$Z_A^{(opt)} = \left\{\frac{A}{r} - 1\right\} Z_X. \tag{B.11}$$

The expressions of I_a and Q_a are obtained by taking the real part and imaginary part of Z_A in Eq. (B.11) and they are given by Eq.(B.12).

$$\begin{bmatrix} I_a^{(opt)} \\ Q_a^{(opt)} \end{bmatrix} = \left(\frac{A}{r} - 1\right) \begin{bmatrix} I \\ Q \end{bmatrix}. \tag{B.12}$$

In conclusion, the intermediate signal $\tilde{a}(t)$ is expressed as:

$$\begin{aligned} \tilde{a}\,(t) &= a^{(opt)}\,(t)\, e^{2j\pi\Delta f t}, \\ &= \left[I_a^{(opt)}\,(t) + jQ_a^{(opt)}\right] e^{2j\pi\Delta f t}, \end{aligned}$$

where I_a and Q_a are expressed in Eq.(B.12).

B.3 Principle of the filter-based FFT/IFFT

The PAPR-reduction scheme in Fig.5.1 shows that the intermediate signal $\tilde{a}_n$ is followed by a filter-based FFT/IFFT. This filter consists of a FFT followed by an IFFT operation as shown in Fig.B.2.

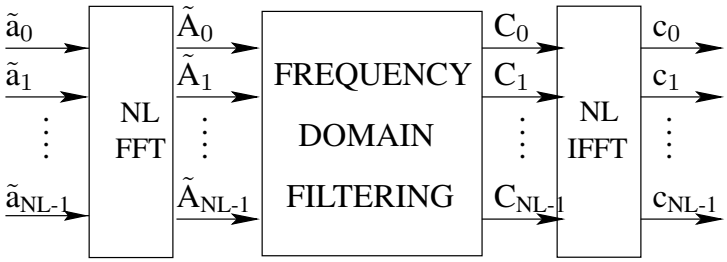

Figure B.2: Digital filtering-based FFT/IFFT.

The forward FFT transforms $\tilde{a}_n$ back to the frequency-domain. The discrete frequency components of $\tilde{a}_n$ on the unused subcarriers $\mathcal{R}$ are passed unchanged while the data subcarriers $\mathcal{R}^c$ and the OOB components $\mathcal{O}$ are set to zero, i.e,

$$C_k = \begin{cases} \tilde{A}_k, & k \in \mathcal{R} \\ 0, & k \in (\mathcal{R}^c \cup \mathcal{O}) \end{cases}, \tag{B.13}$$

where, $\mathcal{R} = \{i_0, \cdots, i_{N_r-1}\}$ is the locations of the unused subcarriers, $\mathcal{R}^c$ is the complement of $\mathcal{R}$ in $\mathcal{I}$ where $\mathcal{I}$ is the set of in-band carriers.

The IFFT operation transforms C_k, $k = 0, \ldots, NL-1$ back to the time domain. This results in the peak canceling signal c_n at the output of the filter-based FFT/IFFT. Because of $\mathcal{R} \cap (\mathcal{R}^c \cup \mathcal{O}) = \emptyset$, the BER of data subcarriers with TR-Geometric technique is the same as that of the original OFDM system.

B.4 Peak regrowths in TR-Geometric methods

TR-Geometric method is a sort of clipping method where a corrective signal is added to original signal to reduce PAPR. Corrective signal is carried by carriers orthogonal to data carriers and therefore no BER degradation occurs.

Anyhow, it is important to see the effects on PAPR reduction performance when the distance between original and added carriers varies on the frequency axis. Let Δf be the frequency gap between data carriers and PRCs. Also let BW be the bandwidth of a multi carrier signal e-g OFDM. Defining a factor $\alpha = \Delta f/BW$ to represent the frequency gap we see its effects on peak of the signal after addition of corrective signal. In Fig. B.3, it could be seen that the addition of corrective signal reduces the peak when $\alpha = 0.25$.

Contrary when $\alpha = 4.0$ is used peak regrowths occur as shown in Fig. B.4. Note that the value of α greater than 1 mean that the frequency gap between original and added carriers is more than the bandwidth of the original signal.

The variations in PAPR reduction ($\Delta PAPR$=PAPR after TR-Geometric-PAPR before TR-Geometric) are plotted in Fig. B.5 as a function of α. It could be noted that PAPR

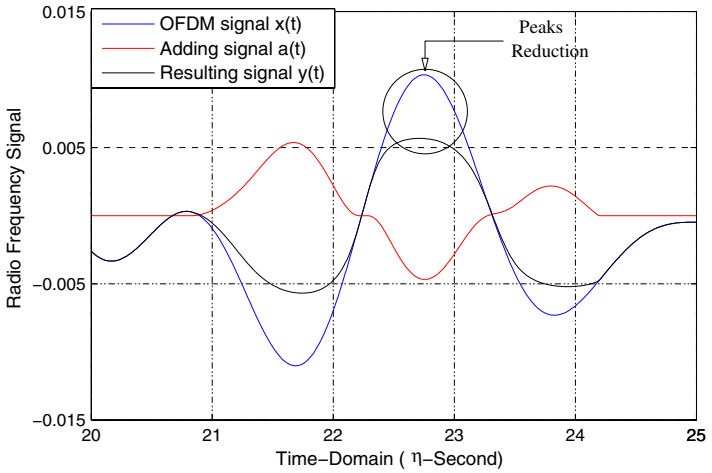

Figure B.3: Peak reduction: OFDM, adding and resulting signal at $\alpha = 0.25$.

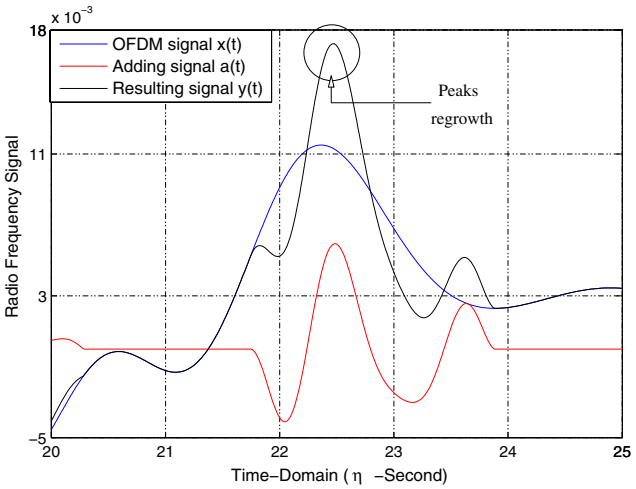

Figure B.4: Peak regrowth: OFDM, adding and resulting signal at $\alpha = 4$.

reduction is maximum when α and in turns Δf is equal to zero i-e the PRCs are placed adjacent to the original carriers. As the value of Δf increases, PAPR reduction becomes smaller and smaller before reaching the negative values. The negative value of $\Delta PAPR$ mean that peak regrowths occur and PAPR is increased instead of decreasing.

There is an iterative version of TR-Geometric method which encounters the problems of peak regrowth.

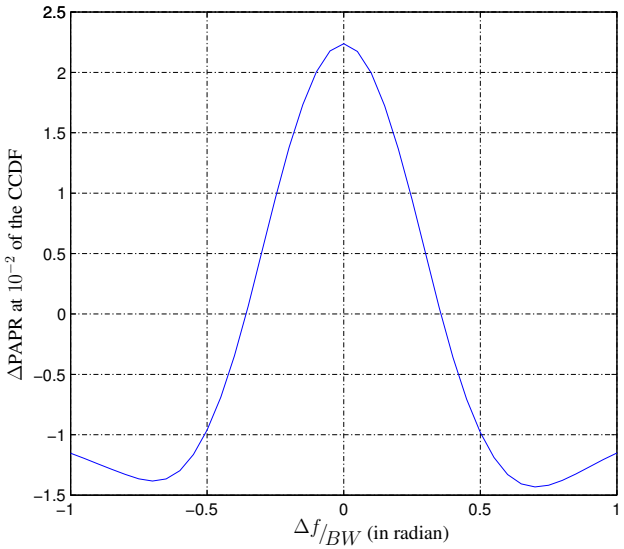

Figure B.5: PAPR reduction performance as a function of $\alpha = \Delta f/BW$ in TR-Geometric method.

List of Figures

List of Tables

Bibliography

[1] S.B. Weinstein and P.M. Ebert, "Data transmission by frequency division multiplexing using the Discrete Fourier Transform," *IEEE Trans. Commun. Technol.*, vol. 19, no. 5, October 1971.

[2] J. Mitola, "Software Radios : Survey, Critical Evaluation and Future Directions," in *National Telesystems Conference: IEEE Press*, (NY), May 1992.

[3] J. Mitola III, "Cognitive Radio: An Integrated Agent Architecture for Software Defined Radio," *Royal Institute of Technology (KTH) Stockholm, Sweden*, May 2000.

[4] S. H. Han and J. H. Lee, "An overview of peak-to-average power ratio reduction techniques for multicarrier transmission," *IEEE Wireless Communications Magazine*, vol. 12, pp. 56–65, April 2005.

[5] Y. Louet and J. Palicot, "A classification of methods for efficient power amplification of signals," *Annals of Telecom*, vol. 63, pp. 351–368, July/August 2008.

[6] X. Li, and L. Cimini, Jr., "Effects of clipping and filtering on the performance of OFDM," *IEEE Communications Letters*, vol. 2, pp. 131–133, May 1998.

[7] S. H. Müller and J.B. Huber, "OFDM with reduce peak to average power ratio by optimum combination of partial transmit sequences," *Electronics Letters*, vol. 33, no. 5, pp. 368–369, February 1997.

[8] R. W. Bauml, R. F. H. Fischer, and J. B. Huber, "Reducing the peak-to-average power ratio of multicarrier modulation by selected mapping," *Electronics Letters*, vol. 32, no. 22, pp. 2056–2057, 1996.

[9] J. Tellado-Mourelo, *Peak to Average Power Ratio Reduction for multicarrier modulation.* PhD thesis, Stanford University, September 1999.

[10] D. Guel, Y. Louet, and J. Palicot, "A Geometric Method for Papr Reduction in a Signal Adding Context for OFDM Signals," in *Proc. 15th International Conference on Digital Signal Processing*, (Cardiff, UK), pp. 347–350, 1–4 July 2007.

[11] H. Ochiai and H. Imai, "Peak-Power Reduction schemes in OFDM systems : a review," in *International Symposium on Wireless Personal Multimedia Communications, Yokosuka Research Park*, pp. 247–252, November 1998.

[12] R. van Nee and A. de Wild, "Reducing the peak-to-average power ratio of OFDM," in *Proc. 48th IEEE Vehicular Technology Conference VTC 98*, vol. 3, (Ottawa, Canada), pp. 2072–2076, 18–21 May 1998.

[13] X. Zhou, and J. Caffery, Jr., "A new distribution bound and reduction scheme for OFDM PAPR," in *Proc. 5th International Symposium on Wireless Personal Multimedia Communications*, vol. 1, (Honolulu, Hawaii), pp. 158–162, 27–30 Oct. 2002.

[14] H. Ochiai and H. Imai, "On the distribution of the peak-to-average power ratio in OFDM signals," *IEEE Transactions on Communications*, vol. 49, pp. 282–289, Feb 2001.

[15] M. Lobo, L. Vandenberghe, S. Boyd, and H. Lebret, "Applications of second order cone programming," *Linear Algebra and its Applications, Special Issue on Linear Algebra in Control, Signals and Image Processing*, pp. 193–228, November 1998.

[16] S. Zabre, J. Palicot, Y. Louet, and C. Lereau, "SOCP Approach for OFDM Peak-to-Average Power Ratio Reduction in the Signal Adding Context," in *Proc. IEEE International Symposium on Signal Processing and Information Technology*, (Vancouver, Canada), pp. 834–839, Aug. 2006.

[17] S. Litsyn, *Peak Power Control in Multicarrier Communications*. Cambridge University Press, 2007.

[18] D. Cabric, "Cognitive Radio Research," tech. rep., University of California, Berkeley, Summer Retreat 2006.

[19] C. Bremenson et al., "Linearizing TWT Amplifiers in Satellite Transponders, Systems Aspects and Practical Implementation," in *AIAA 8th Communications Satellite System Conference*, (Orlando, Fla.), pp. 80–89, April 1980.

[20] J. Steck, and D. Pham, "A New TWT Linearizer for Satellite-Communications Transmitters," *Microwave System News and Communications Technology*, vol. 17, no. 9, pp. 28–42, June 1987.

[21] S.H. Han, and J.H. Lee, "An overview of peak to average power ratio reduction techniques for multi carrier transmission," *IEEE Wireless Communications*, pp. 56–65, April 2005.

[22] J. Macleod, M. Beach et al., "IST-TRUST, 1999-12070, D3.1.1," tech. rep., European Project, Septembre 2000.

[23] H. H. Lee, D. N. Liu, W. Zhu, M. P. Fitz, "Peak power reduction using a unitary rotation in multiple transmit antennas," in *IEEE International Conference on Communication*, vol. 4, pp. 2407–2411, May 2005.

[24] M. Tan, Z. Latinovic and Y. Bar-Ness, "STBC MIMO-OFDM Peak-to-Average Power Ratio Reduction by Cross-Antenna Rotation and Inversion," *IEEE Communication Letters*, vol. 9, no. 7, July 2005.

[25] Y. Louet and S. Hussain, "Peak-to-Mean Envelope Power Ratio Statistical Analysis of Continuous OFDM Signal," in *Proc. IEEE Vehicular Technology Conference VTC Spring 2008*, (Singapore), pp. 1681–1685, 11–14 May 2008.

[26] S. Hussain and Y. Louet, "Peak to Average Power Ratio Analysis of Multi-carrier and Multi-standard Signals in Software Radio Context," in *Proc. 3rd International Conference on Information and Communication Technologies: From Theory to Applications ICTTA 2008*, pp. 1–5, 7–11 April 2008.

[27] S. Hussain, J. Palicot, Y. Louet, and S. Zabre, "Frequency Domain Interpretation of Power Ratio Metric for Cognitive Radio Systems," *Proceedings of IET Communications Journal*, vol. 2, pp. 783–793, July 2008.

[28] S. Hussain, and Y. Louet, "Peak to Average Power Ratio Reduction for Multi-Band OFDM System using Tone Reservation," in *URSI General Assembly*, August 2008.

[29] S. Hussain and Y. Louet, "PAPR reduction of Software Radio signals using PRC method," in *Proc. IEEE Sarnoff Symposium SARNOFF '09*, (Princeton, NJ.), pp. 1–6, March 30 2009–April 1 2009.

[30] S. Hussain, D. Guel, Y. Louet, and J. Palicot , "Performance comparison of PRC based PAPR reduction schemes for WiLAN systems," in *European Wireless*, (Aalborg, Denmark.), May 2009.

[31] S. Hussain, and Y. Louet , "Tone Reservation's complexity reduction using fast calculation of maximal IDFT element," in *IEEE/ACM IWCMC*, (Crete, Greece.), August 2008.

[32] S. Hussain, Y. Louet, and J. Palicot , "PAPR variations on Dynamic Spectrum Access in Cognitive Radio systems," in *IEEE Wireless VITAE*, (Aalborg, Denmark.), May 2009.

[33] R. W. Chang, "Synthesis of Band Limited Orthogonal Signals for Multi-channel Data Transmission," *Bell System Technical Journal*, vol. 45, pp. 1775–1796, Dec. 1966.

[34] L. Hanzo and T. Keller, *OFDM and MC-CDMA: A Primer.* Wiley-IEEE Press, April 2006.

[35] B. Saltzberg, "Performance of an Efficient Parallel Data Transmission System," *IEEE Transactions on Communication Technology*, vol. 15, pp. 805–811, December 1967.

[36] R. W. Chang, "Orthogonal Frequency Division Multiplexing," *US Patent No. 3,488,445*, January 6, 1970.

[37] B. Hirosaki, "An Analysis of Automatic Equalizers for Orthogonally Multiplexed QAM Systems," *IEEE Transactions on Communications*, vol. 28, pp. 73–83, Jan 1980.

[38] W. E. Keasler, D. L. Bitzer, and P. T. Tucker, "High-speed Modem Suitable for Operating with a Switched Network," *Patent No. 4,206,320*, June 3, 1980.

[39] L. Cimini, Jr., "Analysis and Simulation of a Digital Mobile Channel Using Orthogonal Frequency Division Multiplexing," *IEEE Transactions on Communications*, vol. 33, pp. 665–675, Jul 1985.

[40] M. Alard and R. Lassalle, "Principles of modulation and channel coding for digital broadcasting for mobile receivers," Tech. Rep. 224, EBU Technical Review, August 1987.

[41] J. M. Cioffi, "A Multicarrier Primer," Tech. Rep. T1E1.4/91-157, ANSI, November 1991.

[42] ANSI Committee T1-Telecommunications, "A Technical Report on High-Bit-Rate Digital Subscriber Lines (HDSL)," Tech. Rep. 28, February 1994.

[43] "Digital Audio Broadcasting (DAB); DAB to mobile, portable and fixed Receivers," Tech. Rep. ETSI ETS 300 401 ed.1, European Telecommunication Standard Institute, February 1995.

[44] "Radio Equipment and Systems (RES); HIgh PErformance Radio Local Area Network (HIPERLAN) Type 1; Functional specification," Tech. Rep. ETSI ETS 300 652 ed.1, European Telecommunication Standard Institute, October 1996.

[45] "Digital Video Broadcasting (DVB); Framing structure, channel coding and modulation for digital terrestrial television (DVB-T)," Tech. Rep. ETSI ETS 300 744 ed.1, European Telecommunication Standard Institute, March 1997.

[46] "Very-high-speed Digital Subscriber Lines: System Requirements," Tech. Rep. T1E1.4 VDSL SR: 98-043R5, ANSI, September 1998.

[47] "Transmission and Multiplexing (TM); Access transmission systems on metallic access cables; Very high speed Digital Subscriber Line (VDSL); Part 1: Functional requirements," Tech. Rep. ETSI TS 101 270-1 V1.1.2, European Telecommunication Standard Institute, June 1998.

[48] "Broadband Radio Access Networks (BRAN); Inventory of broadband radio technologies and techniques," Tech. Rep. ETSI TR 101 173 V1.1.1, European Telecommunication Standard Institute, May 1998.

[49] "IEEE Standard 802.11a: Wireless LAN Medium Access Control (MAC) and Physical Layer (PHY) specifications: high speed physical layer in the 5 GHz band," 1999.

[50] "IEEE Standard 802.11g: Wireless LAN Medium Access Control (MAC) and Physical Layer (PHY) specifications," 2003.

[51] "ETSI standard:Digital Video Broadcasting (DVB); Transmission System for Handheld Terminals (DVB-H)," November 2004.

[52] "IEEE Standard 802.16: Air Interface for Fixed Broadband Wireless Access Systems," 2004.

[53] "IEEE Candidate Standard 802.11n: Wireless LAN Medium Access Control (MAC) and Physical Layer (PHY) specifications," 2004.

[54] "IEEE Candidate Standard 802.15.3a: Wireless Medium Access Control (MAC) and Physical Layer (PHY) specifications for high rate Wireless Personal Area Networks (WPANs) involving imaging and multimedia," 2004.

[55] M. Yabusaki, "Asia Pacific Viewpoint and Activities: Introduction," in *4G Forum*, (London, UK.), 27 May 2003.

[56] "ETSI standard: Framing structure, channel coding and modulation for second generation digital terrestrial television broadcasting system (DVB-T2)," June 2008.

[57] P. Cruz and N. B. Carvalho, "Characterization of a SDR Front-End Receiver with Mutlisine Excitations," in *7th Conference on Telecommunications*, (Santa Maria de Feira, Portugal), May 2009.

[58] R. I. Lackey and D. W. Upmal, "Speakeasy: the military software radio," *IEEE Communications Magazine*, vol. 33, pp. 56–61, May 1995.

[59] C. Roland, *Etude d'un recpteur Universel Auto-adaptatif pour les transmissions sans fil.* PhD thesis, CNAM, October 2001.

[60] "AS37 Action Spécifique 37 Radio Logicielle," *web.univ-ubs.fr/lester/~boutillon/AS_Radio_Logicielle/AS_RL_Equipes.pdf*, .

[61] C. Shannon, "A Mathematical Theory of Communication," *Bell System Technical Journal*, vol. 27, pp. 379–423 and 623–656, July and October 1948.

[62] C. Shannon, "Communication Theory of Secrecy Systems," *Bell System Technical Journal*, vol. 28, pp. 656–715, 1949.

[63] C. Shannon, "Programming a Computer for Playing Chess," *Philosophical Magazine Series 7*, vol. 41, no. 314, pp. 256–275, March 1950.

[64] http://www.fcc.gov/oet/cognitiveradio/.

[65] "Facilitating Opportunities for Flexible, Efficient, and Reliable Spectrum Use Employing Cognitive Radio Technologies," *http://hraunfoss.fcc.gov/edocs_public/attachmatch/FCC-03-322A1.pdf*, 2003.

[66] http://www.fcc.gov/oet/sptf/.

[67] http://www.sharedspectrum.com/.

[68] Q. Zhao, and A. Swami, "A survey of Dynamic spectrum access signal processing and networking perspectives," in *ICASSP*, vol. 4, pp. 1349–1352, April 2007.

[69] http://www.cttc.es/resources/doc/090420-ws-wwebb-150409-63657.ppt/.

[70] A. Guy, *Etude, conception et réalisation d'un système de linéarisation d'amplificateurs de puissance à état solide pour des applications spatiales.* PhD thesis, Université Paul Sabatier de Toulouse, May 2000.

[71] H. Abdulkader, *Application de réseaux de neurones à des chaînes de transmission numérique par satellite - gradient naturel.* PhD thesis, Institut National Polytechnique de Toulouse, June 2003.

[72] S. Bouchired, *Equalization of time-varying non-linear channels using neural networks : Application to the satellite mobile channel.* PhD thesis, Institut national polytechnique de Toulouse, 1999.

[73] A. A. M. Saleh, "Frequency independent and frequency dependent nonlinear model of TWT amplifiers," *IEEE Transactions on Communications*, vol. COM-29, pp. 1715–1720, November 1981.

[74] C. Rapp, "Effects of HPA-nonlinearity on a 4-DPSK/OFDM-signal for a digitial sound broadcasting system," in *Second European Conference on Satellite Communications*, (Liege, Belgium), pp. 179–184, October 1991.

[75] F. Launey, *Contribution à la modélisation comportementale des amplificateurs de puissance.* PhD thesis, Université de Nantes, Septembre 2003.

[76] S. C. Cripps, *RF Power Amplifiers for Wireless Communications.* Artech House, April 1999.

[77] S. Ragusa, *Ecrêtage Inversible pour l'Amplification Non-Linéaire des Signaux OFDM dans les Terminaux Mobiles.* PhD thesis, Université Joseph FOURIER, Grenoble, June 2006.

[78] A. Chaker, *Influence de l'amplificateur de puissance sur une chaîne de transmission multiporteuses :prise en compte de l'effet mémoire.* PhD thesis, Université Cergy-Pontoise, July 2004.

[79] E. Costa and S. Pupolin, "QAM-m-OFDM System Performance in the Presence of a non-linear Amplifier and Phase Noise," *IEEE Transactions on Communications*, vol. 50, no. 3, March 2002.

[80] R. O'Neill and L. B. Lopes, "Envelope variations and spectral splatter in clipped multicarrier signals," in *Proc. Sixth IEEE International Symposium on Personal, Indoor and Mobile Radio Communications PIMRC'95. 'Wireless: Merging onto the Information Superhighway'*, vol. 1, pp. 71–75, 27–29 Sept. 1995.

[81] J. Armstrong, "Peak-to-average power reduction for OFDM by repeated clipping and frequency domain filtering," *Electronics Letters*, vol. 38, pp. 246–247, February 2002.

[82] S. H. Muller and J. B. Huber, "A comparison of peak power reduction schemes for OFDM," in *Proc. IEEE Global Telecommunications Conference GLOBECOM '97*, vol. 1, (Phoenix, Arizona), pp. 1–5, 3–8 Nov. 1997.

[83] H. Breiling, S. H. Muller-Weinfurtner, and J. B. Huber, "SLM peak-power reduction without explicit side information," *IEEE Communications Letters*, vol. 5, pp. 239–241, June 2001.

[84] A. D. S. Jayalath and C. Tellambura, "Reducing the peak-to-average power ratio of orthogonal frequency division multiplexing signal through bit or symbol interleaving," *Electronics Letters*, vol. 36, pp. 1161–1163, June 2000.

[85] G. R. Hill, M. Faulkner, and J. Singh, "Reducing the peak-to-average power ratio in OFDM by cyclically shifting partial transmit sequences," *Electronics Letters*, vol. 36, pp. 560–561, March 2000.

[86] P. Van Eetvelt, G. Wade, and M. Tomlinson, "Peak to average power reduction for OFDM schemes by selective scrambling," *Electronics Letters*, vol. 32, pp. 1963–1964, October 1996.

[87] B. S. Krongold and D. L. Jones, "PAR reduction in OFDM via active constellation extension," *IEEE Transactions on Broadcasting*, vol. 49, pp. 258–268, Sept. 2003.

[88] T. A. Wilkinson and A. E. Jones, "Minimisation of the peak to mean envelope power ratio of multicarrier transmission schemes by block coding," in *Proc. IEEE 45th Vehicular Technology Conference*, vol. 2, (Chicago, IL.), pp. 825–829, 25–28 July 1995.

[89] T. Jiang, Y. Yang, and Y. H. Song, "Exponential companding technique for PAPR reduction in OFDM systems," *IEEE Transactions on Broadcasting*, vol. 51, pp. 244–248, June 2005.

[90] T. Jiang, and Y. Wu, "An Overview: Peak-to-Average Power Ratio Reduction Techniques for OFDM Signals," *IEEE Transactions on Broadcasting*, vol. 54, pp. 257–268, June 2008.

[91] Y. Louët, and J. Palicot, "Synthèse de la notion de facteur de crête et application aux modulations monoporteuse," in *GRETSI 2005*, (Louvain La Neuve, Belgium), September 2005.

[92] M. Friese, "Multitone signals with low crest factor," *IEEE Transactions on Communications*, vol. 45, pp. 1338–1344, Oct. 1997.

[93] M. Friese, "Multicarrier modulation with low peak-to-average power ratio," *Electronics Letters*, vol. 32, pp. 713–714, April 1996.

[94] J. Palicot, and Y. Louët, "Power Ratio definitions and analysis in single carrier modulation," in *EUSIPCO 05*, (Antalya, Turkey), September 2005.

[95] N. Dinur and D. Wulich, "Peak-to-average power ratio in high-order OFDM," *IEEE Transactions on Communications*, vol. 49, pp. 1063–1072, June 2001.

[96] C. Tellambura, "Computation of the Continuous-Time PAP of an OFDM Signal with BPSK Subcarriers," *IEEE Communications letters*, vol. 5, no. 5, May 2001.

[97] R. Van Nee and R. Prasad, *OFDM for wirelless multimedia communications*. Artech House, January 2000.

[98] A. D. S. Jayalath and C. R. N. Athaudage, "On the PAR reduction of OFDM signals using multiple signal representation," *IEEE Communications Letters*, vol. 8, pp. 425–427, July 2004.

[99] M. Sharif, M. Gharavi-Alkhansari, and B. H. Khalaj, "On the peak-to-average power of OFDM signals based on oversampling," *IEEE Transactions on Communications*, vol. 51, pp. 72–78, Jan. 2003.

[100] M. Branch, T. Coleman, and Y. Li, "A Subspace, Interior, and Conjugate Gradient Method for Large-Scale Bound-Constrained Minimization Problems," *SIAM Journal on Scientific Computing*, vol. 21, no. 1, pp. 1–23, 1999.

[101] A. Fasbender, F. Reichert, E. Geulen, J. Hjelm, and T. Wierlemann, "Any network, any terminal, anywhere [cellular radio]," *IEEE Personal Communications*, vol. 6, pp. 22–30, April 1999.

[102] H.G. Ryu, N. T. Hieu and D. Tien, "A PAPR Reduction of MC-DS-CDMA Signal by Spectrum Phase Control (SPC) Method," in *IEEE International Conference of Communication*, June, 2006.

[103] O. Vaananen, J. Vankka, and K. Halonen, "Reducing the peak to average ratio of multicarrier GSM and edge signals," in *Proc. 13th IEEE International Symposium on Personal, Indoor and Mobile Radio Communications*, vol. 1, (Lisbon, Portugal), pp. 115–119, 15–18 Sept. 2002.

[104] S. Zabre, and J. Palicot, "PAPR Analysis of a multiplex of modulated carriers in a Software Radio context," in *5th Karlsruhe Workshop on Software Radio*, February 2004.

[105] C. Roland, J. Palicot, "A Self Adaptive Universal Receiver," *Annals of Telecom*, vol. 57, pp. 5–6, May and June 2002.

[106] S. Daumont, B. Rihawi, and Y. Louet, "Root Raised Cosine filter influences on PAPR distribution of single carrier signals," in *IEEE ISCCSP 08*, (Malta), March 08.

[107] P. Cruz and N. B. Carvalho, "PAPR Evaluation in Multi-Mode SDR Transceivers," in *Proc. 38th European Microwave Conference EuMC 2008*, pp. 1354 –1357, October 2008.

[108] C. L. Wang, Y. Ouyang and H. C. Chen, "A Low-Complexity Peak-to-Average Power Ratio Reduction Technique for OFDM-Based Systems," in *IEEE Vehicular Technology Conference*, (Milan, Italy), May 2004.

[109] A. Aggarwal and T. H. Meng, "A convex interior-point method for optimal OFDM PAR reduction," in *Proc. IEEE International Conference on Communications ICC 2005*, vol. 3, (Seoul, Korea), pp. 1985–1990, 16–20 May 2005.

[110] B. Rihawi and Y. Louet, "PAPR reduction scheme with SOCP for MIMO-OFDM systems," *International Journal of Communications, Network and System Sciences*, vol. 1, no. 1, pp. 29–35, 2008.

[111] S. Zabre, J. Palicot, Y. Louet, and C. Lereau, "Reduction of OFDM Peak to Mean Envelope Power Ratio using Ghost Carriers," in *Proc. 3rd IEEE International Conference on Wireless and Mobile Communications 2007*, (Guadeloupe, French Caribbean), 4–9 March 2007.

[112] P. Cruz and N. B. Carvalho, "Multi-Mode Receiver for Software Defined Radio," in *2nd Congress of Portuguese Committee of URSI*, (Lisbon, Portugal), November 2008.

[113] H. G. Bae, M. Helaoui, S. Boumaiza, and F. M. Ghannouchi, "Peak-to-Average Power Ratio Reduction for SDR Transmitters," in *Practical Real World Technologies for Communications and Embedded Platforms Conference*, (Banff, Canada), pp. 33–34, May 2006.

[114] U. Reimers, "Digital Video Broadcasting," *IEEE Communications Magazine*, vol. 36, pp. 104–110, June 1998.

[115] L. Wang, and C. Tellambura, "Analysis of Clipping Noise and Tone-Reservation Algorithms for Peak Reduction in OFDM Systems," *IEEE Transactions on Vehicular Technology*, vol. 57, pp. 1675–1694, May 2008.

[116] "IEEE 802.11g-2003: Further Higher Data Rate Extension in the 2.4 GHz Band," October 2003.

[117] K.C. Toh, M.J. Todd, and R.H. Tutuncu, "SDPT3 — a Matlab software package for semidefinite programming," *Optimization Methods and Software*, vol. 11, pp. 545–581, 1999.

[118] S. Boyd, and L. Vandenberghe, *Convex Optimization.* Cambridge University Press, 2004.

[119] R. Blahut, *Fast Algorithms for Digital Signal Processing.* Addison-Wesley, 1985.

[120] D. Guel, J. Palicot, and J.-J. Bellanger, "Frequency based asymptotic distribution of the PAPR for geometric adding signal approach in OFDM signals context," in *SPAWC*, July 2008.

[121] R. Hachemani, J. Palicot, and C. Moy, "A New Standard Recognition Sensor for Cognitive Radio Terminals," in *EUSIPCO*, (Poznan, Poland), September 2007.

[122] http://www.ieee-icc.org/workshops.html#GreenComm.

[123] P. F. Marshall, "Cognitive Radio as a mechanism to manage front end linearity and dynamic range," *IEEE Communications Magazine*, pp. 81–87, March 2009.

Personal Publications

Journals

- Sajjad Hussain, Jacques Palicot, Yves Louet, Sidkieta Zabre "Frequency Domain Interpretation of Power Ratio Metric for Cognitive Radio Systems", Proceedings of IET Communications Journal, Volume 2, Issue 6, July 2008 Page(s):783 - 793.

Book Chapters

- Jacques Palicot, Yves Louët, Sajjad Hussain, "Power Amplification issues related to Dynamic Spectrum Access in the Cognitive Radio Systems", in the book "Cognitive Radio Systems", ISBN 978-953-7619-25-1.

International Conferences

- Sajjad Hussain, Désiré Guel, Yves Louët, Jacques Palicot, "Performance comparison of PRC based PAPR reduction schemes for WiLAN systems", European Wireless, Aalborg Denmark, May 09.
- Sajjad Hussain, Yves Louët, Jacques Palicot, "PAPR variations on dynamic spectrum access in Cognitive Radio systems", IEEE Wireless VITAE, Aalborg Denmark, May 09.
- Sajjad Hussain, Yves Louët, "PAPR reduction of Software Radio signals using PRC method", IEEE Sarnoff Symposium, NJ USA, March 09.
- Sajjad Hussain, Yves Louët, "Peak to Average Power Ratio Reduction for Multi-band OFDM System using Tone Reservation", URSI General Assembly 08, Chicago USA, Aug 08.
- Sajjad Hussain, Yves Louët, "Tone Reservation's complexity reduction using fast calculation of maximal IDFT element", IEEE/ACM IWCMC 08, Crete, Greece, August 08.
- Yves Louët, Sajjad Hussain, "Peak to Mean Power Ratio Statistical Analysis of continuous OFDM signals", IEEE VTC 08, Singapore, May 08.
- Sajjad Hussain, Yves Louët, "Peak to Average Power Ratio Analysis of Multi-carrier and Multi-standard signals in software radio context" IEEE ICTTA 08, Damas, Syria, April 08.

Seminar

- Sajjad Hussain, "PAPR variations due to dynamic spectrum access in the context of Cognitive Radio", Seminar SCEE, 13 November 2008, Supélec, Rennes Campus.

Divers

- Sajjad Hussain, "PAPR reduction of SWR signals", Brittany Doctoral 2008, Brest-Rennes (France), 16-21 November 2008.
- Sajjad Hussain, "PAPR and non-linearity issues in the context of multi carrier signals", Ph.D. students Day 2007, Rennes (France), 20 June 2007.